Department of Spatial Sciences

An examination of the Australian Height Datum

Michael Shaun Filmer

This thesis is presented for the degree of
Doctor of Philosophy
of
Curtin University of Technology

December 2010

Declaration

To the best of my knowledge and belief this thesis contains no material previously published by any other person except where due acknowledgement has been made.

This thesis contains no material which has been accepted for the award of any other degree or diploma in any university.

Signature: .....

Date: .....

ABSTRACT

The Australian Height Datum (AHD) was established in 1971, and is the basis for all physical heights in Australia. However, a complete revision of the AHD has never occurred, despite problems that, although not always obvious to surveyors at the local level, have come to prominence through the introduction of Global Navigation Satellite Systems (GNSS) and gravimetric quasi/geoid models. Improvements in GNSS, quasi/geoid and sea surface topography (SSTop) models, plus moderate upgrades to the Australian Levelling Network (ANLN) since 1971 now allow a meaningful revision of the AHD to be made. This thesis first conducts an investigation of AHD/ANLN errors, culminating in the realisation of an Australian Experimental Vertical Datum (AEVD).

An assessment of 1366 ANLN loops reveals 15−20 misclosures >0.5 m (up to 0.93 m), situated primarily in the interior of the continent. GNSS−quasi/geoid information was included in a second loop-based assessment, adding redundancy in an attempt to isolate errors within the levelling sections. These assessments indicate that the ANLN database requires corrections and updating by State and Territory geodetic agencies, including the replacement of average two-way levelled height differences between benchmarks (BMs) currently in the database with forward and reverse levelled height differences. A simulation of the effects of refraction on the AHD and ANLN suggest that height errors of up to 0.4 m in central Australia may result from neglecting to apply refraction corrections to the ANLN. However, the metadata required to properly correct the ANLN for refraction is not currently available.

A major objective of this thesis is to identify the causes of the north-south slope observed in the AHD when compared with geoid models. The CARS2006 climatology (oceanographic) and Rio05 combined mean dynamic topography (geodetic and oceanographic) SSTop models along with the EGM2008 and gravimetric component of AUSGeoid09 (AGQG09) SSTop estimates at tide-gauges are shown to effectively remove the

north-south slope. This indicates that the north-south AHD slope was caused solely by fixing the Australian levelling survey to mean sea level (MSL) at 30 mainland tide-gauges. In addition, it was found that the vertical offset between mainland AHD and Tasmanian AHD (vertical datums separated by the sea) is negligible. The CARS2006 SSTop model provided the best estimates of SSTop at tide-gauges and was used in the final realisation of the AEVD as an SSTop correction when the AEVD is constrained to 32 AHD tide-gauges, also unifying the mainland and Tasmanian levelling networks.

To determine the height system best suited to the AEVD, gravity at ANLN BMs was computed from EGM2008 and also from terrestrial gravity held in the Australian National Gravity Database (ANGD). Despite problems with both, 'reconstructed' BM gravity from EGM2008 demonstrated the best results and is used for gravimetric height corrections applied to the ANLN. Differences between Helmert orthometric and normal-orthometric heights (used for the AHD) were up to 0.44 m at heights >2,000 m in the Australian Alps. However, differences between normal and normal-orthometric heights were <30 mm across most of Australia, but reached 0.17 m in the Australian Alps. Normal heights were considered most appropriate for the AEVD because of the sensitivity of Helmert orthometric heights to the poor quality of ANGD- and EGM2008-derived gravity, and normal-orthometric heights being inconsistent with quasigeoid models, particularly at elevations >1,000 m.

A combined least-squares adjustment (CLSA) of the ANLN (with normal height corrections applied to the levelling) was conducted using MSL + CARS2006 at 32 AHD tide-gauges and GNSS−AGQG09 at 277 GNSS stations as weighted constraints to realise the AEVD. An outlier detection process was undertaken first, to attempt to identify the problem levelling sections of the ANLN and re-weight them so they have less influence in the CLSA. Validation of the AEVD used GNSS−AGQG09 at 765 GNSS stations not used in the CLSA. RMS of the differences at the 765 GNSS stations between the AEVD and GNSS−AGQG09 were ±0.098 m (considered external accuracy), compared to an RMS of ±0.207 m for differences between the AHD and GNSS−AGQG09, indicating an improvement of the AEVD over the AHD.

ACKNOWLEDGEMENTS

Firstly, I would like to thank my supervisor, Will Featherstone, for initially encouraging me to undertake a PhD and for his guidance, advice and encouragement throughout this project. I am also grateful to my co-supervisor, Michael Kuhn, particularly for discussions on technical issues. I acknowledge scholarship funding from an Australian Postgraduate Award, The Institute for Geoscience Research, and the Cooperative Research Council for Spatial Information.

Thanks also to David Bruce and John Gilliland (Univ S Aust) for their advice and support when I was deciding whether to undertake a PhD. Other people at Curtin who have all helped me in some way during this project are: Jon Kirby, Sten Claessens, David Belton, Ira Anjasmara, Bernie Klingseissen, Lennard Huisman, and Christian Hirt. In general I would like to thank all staff at the Department of Spatial Sciences, who have contributed to the enjoyable working environment.

I would also like to thank Xiaoli Deng (Univ Newcastle), Gary Johnston, Jim Steed (ret) and Nick Brown (GA), Linda Morgan and Graeme Holloway (Landgate), Steve Turner (LSG), Peter Morgan (Univ Canb), Dru Smith (NOAA/NGS), Richard Coleman (formerly UTas, now ARC), Bill Kearsley and Jean Rüeger (UNSW), Zarina Jayaswal (AHO), Tony Lamberto (WA Gov), and Paul Davill (NTC) who have all contributed data or advice at some stage during this project. I also appreciate the constructive comments from the two examiners of this thesis.

Finally, I would like to thank my wife Dianne for her love and support that has made it possible for me to undertake this PhD. I am also grateful to our two children, Wil and Asha for their love and patience, particularly at times when I have been unable to spend as much time with them as I would like. I am indebted to my parents Ian and Helen, for their support and practical assistance over the last four years.

TABLE OF CONTENTS

LIST OF FIGURES

LIST OF TABLES

LIST OF ACRONYMS AND ABBREVIATIONS

AAGD07	Australian Absolute Gravity Datum 2007
ACT	Australian Capital Territory
AEVD	Australian Experimental Vertical Datum
AG98	AUSGeoid98
AGD66	Australian Geodetic Datum 1966
AGQG09	Gravimetric-only component of AUSGeoid09
AHO	Australian Hydrographic Office
AHD	Australian Height Datum
AHD(mainland)	Australian Height Datum on mainland Australia
AHD(Tas)	Australian Height Datum on Tasmania
ALS	Australian Levelling Survey
ANGD	Australian National Gravity Database
ANLN	Australian National Levelling Network
AUSPOS	Geoscience Australia's online GPS processing service
AVD	Australian Vertical Datum
BAR	Barrier adjusted relief
BM	Benchmark
BM1	Benchmark at the start of a levelling section
BM2	Benchmark at the end of a levelling section
BP	Bouguer plate
BS	Backsight
CARS2006	CSIRO Atlas of Regional Seas 2006
CGVD1928	Canadian Geodetic Vertical Datum of 1928
CLSA	Combined least-squares adjustment
CMDT	Combined mean dynamic topography
CSIRO	Australian Commonwealth Scientific and Research Organisation
CV	Critical value
DNSC08 MDT	Danish National Space Centre 2008 mean dynamic topography

DNSC08 MSS	Danish National Space Centre 2008 mean sea surface
EGM2008	Earth Gravitational Model 2008
FCA	Free-convection approximation
FS	Foresight
GA	Geoscience Australia
GDA94	Geocentric Datum of Australia 1994
GIA	Glacial isostatic adjustment
GMT	Generic Mapping Tools
GNSS	Global Navigation Satellite Systems
GPS	Global Positioning System
GRACE	Gravity Recovery and Climate Experiment
GRS80	Geodetic Reference System 1980
GVD	Global Vertical Datum
HC	Height correction
IB	Inverse barometer
ICSM	Inter-governmental Committee for Surveying and Mapping
IE1924	International (Hayford) ellipsoid 1924
IGF1930	International gravity formula 1930
IGSN71	International Gravity Standardisation Network 1971
ITRF	International Terrestrial Reference Frame
JP	Junction point
JPL	Jet Propulsion Laboratory
LINZ	Land Information New Zealand
LSA	Least-squares adjustment
MC	Minimally constrained
MCLSA	Minimally constrained least-squares adjustment
MDB	Minimal detectable bias
MDE	Marginal detectable error
MDT	Mean dynamic topography
MSL	Mean sea level
MSLD1929	Mean Sea Level Datum of 1929
MSS	Mean sea surface

NAVD88	North American Vertical Datum 1988
NGVD29	National Geodetic Vertical Datum of 1929
NIB	No inverse barometer
NMC	National Mapping Council of Australia
NSW	New South Wales
NT	Northern Territory
NTC	National Tidal Centre
NZVD2009	New Zealand Vertical Datum 2009
NZGeoid2009	New Zealand Quasigeoid 2009
OD	Outlier detection
ODRW	Outlier detection and re-weighting process
OW	One-way levelling section
PSMSL	Permanent Service for Mean Sea Level
Qld	Queensland
RMS	Root mean square
RTM	Residual terrain model
SA	South Australia
SB	Spherical Bouguer shell
SLA	Sea level anomaly
SNAP	Survey Network Adjustment Program
SPP	Simple Poincaré-Prey gravity reduction
SR	Standardised residual
SRTM	Shuttle Radar Topography Mission
SSH	Sea surface height
SSTop	Sea surface topography
SSTM	Sea surface topography model
STD	Standard deviation
TAR	Topographic adjusted relief
Tas	Tasmania
TC	Terrain correction
TGBM	Tide-gauge benchmark
T/P	TOPEX/Poseidon

TW	Two-way levelling section (undefined order)
UK	United Kingdom
UO	Undefined order
URE	Unequal refraction error
US	United States
VFR	Variance factor ratio
Vic	Victoria
WA	Western Australia
WGS84	World Geodetic System 1984

LIST OF SYMBOLS

a	Semi-major axis of an ellipsoid
a_k	Constant from the Kukkamäki (1938) temperature function
a_t	Half the number of hours between sunrise and sunset
$\mathbf{A}$	Design matrix
AHD_0	AHD zero-reference
b	Length of the semi-minor axis of an ellipsoid
b_a	Bottom layer of the atmosphere
b_k	Constant from the Kukkamäki (1938) temperature function
b_t	Difference in time between when radiation is zero with respect to sunrise and sunset
B_0	Incidence angle between the Sun's rays and a level surface
B_1	Incidence angle between the Sun's rays and the ground surface
c	Unit rejection criterion for different levelling orders
c_{GL}	Estimate of unit standard deviation derived from GNSS-ANLN loop misclosures
c_k	Constant from the Kukkamäki (1938) temperature function
c_L	Estimate of unit standard deviation derived from ANLN loop misclosures (computed c)
C	Geopotential number
C_f	Cloud cover factor
C^N	Normal geopotential number
C_p	Specific heat of air at constant pressure
$\mathbf{C}\nabla$	Least-squares model error
d	Distance of levelling run or loop
d_k	Change in refractive index per 1°C change in temperature
d_3	Constant term in the NOC_R
D_F	Degrees of freedom
D_{sub}	Sub-section distance (km)

$D\{\underline{\mathbf{y}}\}$	Dispersion or variance of a vector of observables
DC	Dynamic height correction
$\hat{e}_i$	Least-squares residual for the i^{th} observation
e^2	Square of the first numerical eccentricity of an ellipsoid
E	Evaporation rate
$E\{\underline{\mathbf{y}}\}$	Expectation or mean of a vector of observables
f	Geometric flattening of the reference ellipsoid
g	Magnitude of gravity
$\mathbf{g}$	Gravity vector
$\bar{g}$	Integral mean gravity along the plumbline between the topographic surface and the geoid
g_{BM}	Gravity at a benchmark
$\bar{g}_s$	Mean gravity on the topographic surface between BM1 and BM2
g'_0	Dimensional constant for the NOAA et al. (1976) equation for the lapse rate of atmospheric pressure
g_{obs}	Gravity observation
G	Universal gravitational constant
G_F	Heat flux into the ground
GM	Product of the Earth's mass and universal gravitational constant
h	Ellipsoidal height
h_D	Derived ellipsoidal height
h_P	Ellipsoidal height at point P on the terrain surface
h_{TG}	Ellipsoidal height of MSL at a tide-gauge
h_{TGBM}	Ellipsoidal height at a tide-gauge benchmark
$\bar{H}$	Mean height between benchmarks
H_A	Alternative hypothesis
H_{AG98}	GNSS ellipsoidal height minus AUSGeoid98 height anomaly
H_{AG09}	GNSS ellipsoidal height minus AGQG09 height anomaly
H_B	Bias between CARS2006 and GNSS ellipsoidal height minus AGQG09 height anomaly
H_{CARS}	CARS2006 SSTop height
$\hat{H}_{CARS}$	ANLN JP heights from fixed LSA of the ANLN

H^D	Dynamic height
H_{EGM08}	GNSS ellipsoidal height minus EGM08 height anomaly
H_F	Heat flux
H'_F	Heat flux on an inclined surface
$H_{ISS(t)}$	Instantaneous sea surface height at time (t)
H_{M,b_a}	Mean sea level height (zero) in NOAA et al. (1976)
$H_{MSL(t)}$	Height of mean sea level at time (t)
H^{MC}_{TG}	Height at a tide-gauge from a minimally constrained least-squares adjustment of the ANLN
H^N	Normal height
$\hat{H}^N$	Australian Experimental Vertical Datum normal heights
H^N_{CLSA}	Normal height from a combined least squares-adjustment
H^N_{MC}	Normal heights from a minimally constrained least-squares adjustment of the ANLN
H^N_P	Normal height at point P on the terrain surface
$H^{N\text{-}O}$	Normal-orthometric height
$H^{N\text{-}O}_{BM}$	AHD normal-orthometric height at a benchmark
$H^{N\text{-}O}_{g_{obs}}$	AHD normal-orthometric height at a gravity observation
H^O	Orthometric height
H^O_P	Orthometric height at point P on the terrain surface
H_{TGBM}	AHD height at a tide-gauge benchmark
H_0	Null hypothesis
HOC	Helmert orthometric correction
k_{vk}	von Kármán's constant
L	Length scale from the Obukhov (1971) similarity theory
L_{M,b_a}	Vertical temperature gradient in NOAA et al. (1976)
n_{obs}	Number of FS and BS observations in a levelling sub-section
n_r	Refractive index
$n_{\Delta H}$	Sum of the number of FS and BS observations in a levelling sub-section
m	Geodetic parameter (ratio of gravitational and centrifugal forces at the equator)

m_c	Coefficient dependent on the portion of the sky covered by clouds
M_0	Mean molecular weight of air at mean sea level
MC_B	MCLSA of the ANLN basic network
MC_{H_F}	MCLSA of the ANLN with Angus-Leppan (1979) refraction correction applied using H_F
$\mathrm{MC}_{H'_F}$	MCLSA of the ANLN with Angus-Leppan (1979) refraction correction applied using H'_F
MC_{HOC}	MCLSA of the ANLN with Helmert orthometric corrections applied
MC_{NC}	MCLSA of the ANLN with normal corrections applied
MC_{NOC_R}	MCLSA of the ANLN with Rapp's normal-orthometric correction applied
MC_R	MCLSA of the ALS basic network by Roelse et al. (1971)
MC_{SB}	MCLSA of the ANLN supplementary and basic network
N	Geoid height
N_{TG}	Geoid height at a tide-gauge
N_{TGBM}	Geoid height at a tide-gauge benchmark
NC	Normal correction
NOC	Normal-orthometric correction
NOC_B	Bomford (1971) normal-orthometric correction
NOC_H	Heck (1995) normal-orthometric correction
NOC_{NZ}	New Zealand normal-orthometric correction
NOC_R	Rapp (1961) normal-orthometric correction
O_{Tas}	Datum offset between AHD(mainland) and AHD(Tas)
O_{TG}	Local offset between AHD zero-reference and the geoid at a tide-gauge
O_{TGBM}	Local offset between AHD zero-reference and the geoid at a tide-gauge benchmark
OC	Orthometric correction
P_a	Atmospheric pressure
P_{M,b_a}	Atmospheric pressure at mean sea level in NOAA et al. (1976)
P_0	Intersection of the geoid and plumbline also passing through

	point P on the terrain surface
Q^N	Intersection point of the normal plumbline and the telluroid
Q^O	Approximate midpoint along the plumbline between the terrain surface and the geoid
$\mathbf{Q_y}$	Variance matrix
Q_0	Zero-reference for ellipsoid heights
r_a	Reflectivity (albedo)
r_{BM}	Geocentric radius to a benchmark
r_i	i^{th} local redundancy number
r_m	Maximum allowable levelling misclose
$r_{m_{GL}}$	Maximum allowable GNSS-ANLN loop misclose
R	Earth radius
R_B	Back-sight refraction error
R_F	Fore-sight refraction error
R^*	Gas constant
RC	Refraction correction
$RC_{A\text{-}L}$	Angus-Leppan (1979) refraction correction
$RC^b_{A\text{-}L}$	Angus-Leppan (1979) refraction correction (balanced sight)
$RC^s_{A\text{-}L}$	Angus-Leppan (1979) refraction correction (single sight)
S_ℓ	Maximum levelling sight length
$S_{\ell R}$	Levelling sight length reduced for refraction simulation
$S_{\ell M}$	Levelling sight length maximum for refraction simulation
S_n	Net solar radiation
S_r	Solar radiation
S'_r	Instantaneous solar radiation on a horizontal surface
S''_r	Instantaneous solar radiation on an inclined surface
$S(t)$	Meteorological surge component of instantaneous sea level
SSTop_{TG}	Sea surface topography at a tide-gauge
SSTop^G_{TG}	Sea surface topography height at a tide-gauge from GNSS h and a geoid model
SSTop^L_{TG}	Sea surface topography height at a tide-gauge from MCLSA of the ANLN

SSTop_{TG}^{M}	Sea surface topography height at a tide-gauge from a SSTop model
t_s	Sun's hour angle
t_2	Constant term in the NOC_R
t_3	Constant term in the NOC_R
t_4	Constant term in the NOC_R
T	Tension factor in **surface** function of Generic Mapping Tools
T_a	Air temperature
T_{BM}	Disturbing potential at a benchmark
T_{M,b_a}	Mean sea level temperature gradient in NOAA et al. (1976)
$T(t)$	Tidal surge component of instantaneous sea level
T_*	Temperature scale from the Shaw and Smietana (1983) refraction correction
u_*	Velocity scale from the Shaw and Smietana (1983) refraction correction
U	Normal gravity potential
$U_{N\text{-}O}$	Normal gravity potential on $H^{N\text{-}O}$ zero-reference
U_P	Normal gravity potential at a point on the topographic surface
U_{Q^N}	Normal gravity potential at the intersection of the normal plumbline and the telluroid
U_R	Normal gravity potential at the intersection of the normal plumbline and the quasigeoid
U_0	Normal gravity potential on the surface of the reference ellipsoid
w_i	w-test of the i^{th} observation
W	Gravity potential
W_f	Surface wetness factor
W_P	Gravity potential at a point on the topographic surface
W_0	Gravity potential at the geoid
$\mathbf{x}$	Unknown parameter vector
$\underline{\hat{\mathbf{x}}}$	Least-squares estimate of the parameter vector
x_1	Stability factor for uphill sighting in Shaw and Smietana (1983) refraction correction
x_2	Stability factor for downhill sighting in Shaw and Smietana (1983)

	refraction correction
y	Stability factor in Shaw and Smietana (1983) refraction correction
Z_B	Backsight staff reading
Z_F	Foresight staff reading
Z_i	Instrument height
Z_ℓ	Staff reading
$Z_{i,\ell}$	Height factor in Angus-Leppan (1979) refraction correction
Z_{i,ℓ_B}	Height factor of the backsight observation in the Angus-Leppan (1979) refraction correction
Z_{i,ℓ_F}	Height factor of the foresight observation in the Angus-Leppan (1979) refraction correction
$\lvert\nabla_i\rvert$	Minimal detectable bias of the i^{th} observation
α	Probability of a Type I error occurring in a statistical test
α_s	Sun's azimuth
α_{V}	Geodetic azimuth computed using Vincenty (1975)
α'	Constant term in the NOC_R
β	Gravity flattening of the reference ellipsoid
β_t	Probability of a Type II error occurring in a statistical test
γ	Normal gravity computed on the ellipsoid surface
$\boldsymbol{\gamma}$	Normal gravity vector
$\bar{\gamma}$	Integral mean of normal gravity along the normal plumbline between the telluroid and the ellipsoid
γ_{BM}	Normal gravity at a benchmark
γ_e	Normal gravity at the equator
γ_L	Azimuth of the levelling sub-section
γ_p	Normal gravity at the poles
γ_P	Power of a statistical test
γ_{ρ_T}	Azimuth of the terrain slope
γ_0	The value of normal gravity at 45° latitude
δg_{AC}	Atmospheric correction
δg_{F2}	Second order free-air correction
δg_{BM}	Scalar gravity disturbance at a benchmark

δg_{BP}	Gravitational attraction of the Bouguer plate
δg_{SB}	Gravitational attraction of the spherical Bouguer shell
δg^T	Terrain correction applied in Niethammer and Mader orthometric corrections
$\delta \bar{g}^T$	Integral mean terrain correction between the topographic surface and the geoid in the Niethammer orthometric correction
δg_0^T	Terrain correction applied on the geoid in the Mader orthometric correction
δg_{TOP}	Gravitational attraction of the topographic masses
δ_{PTC}	Planar terrain correction
δ_s	Sun's declination
δ_{STC}	Spherical terrain correction
δU	The unknown normal potential difference between U_R and $U_{N\text{-}O}$
$\delta \rho$	Topographic mass variation
Δg_F	Free air gravity anomaly
Δg_B	Bouguer anomaly
Δg_{CPB}	Complete planar Bouguer anomaly
Δg_{SPB}	Simple planar Bouguer anomaly
Δg_{CSB}	Complete spherical Bouguer anomaly
Δn	Levelled height difference between benchmarks
Δn_F	Height difference of a forward levelling run
Δn_B	Height difference of a backward levelling run
Δn_o	Observed height difference between foresight and backsight
Δh	Ellipsoidal height difference
ΔH	Height difference
ΔH_{AG98}	Difference between GNSS ellipsoidal height minus AGQG09 height anomaly at two benchmarks
ΔH^N	Normal height difference
$\Delta H^{N\text{-}O}$	Normal-orthometric height difference
ΔH_{RF}	Refraction-free height difference
ΔH_{S_ℓ}	Height difference over one sight length
ΔH_{sub}	Height difference for the levelling sub-section

ΔH_{URE}	Height difference contaminated by unequal refraction error
Δ E	Easting difference (m)
Δ N	Northing difference (m)
ΔT_a	Observed vertical temperature difference
$\Delta\zeta$	Height anomaly difference
$\Delta\zeta_{AG98}$	AUSGeoid98 height anomaly difference
$\Delta\phi$	Latitude difference
$\Delta\lambda$	Longitude difference
ε_{GL}	GNSS-ANLN loop misclosure
ε_L	Levelling loop misclosure
$\varepsilon_{\Delta\zeta}$	Relative AUSGeoid98 error
ζ	Height anomaly
ζ_{AG98}	AUSGeoid98 height anomaly
ζ_{AG09}	AGQG09 height anomaly
ζ_{BM}	Height anomaly at a benchmark
ζ_{EGM08}	EGM2008 height anomaly
ζ_s	Sun's zenith distance
ζ_{TG}	Height anomaly at a tide-gauge
ζ_{TGBM}	Height anomaly at a tide-gauge benchmark
θ_{BM}	Geocentric co-latitude in spherical polar coordinates at a benchmark
$\bar{\theta}_{BM}$	Geocentric latitude in spherical polar coordinates at a benchmark
ν	Prime vertical radius of curvature
κ	Constant term in the NOC_R
λ	Longitude
λ_{BM}	ANLN benchmark longitude
$\lambda_{g_{obs}}$	Longitude of gravity observation
λ_H	Latent heat of vaporisation of water
λ_p	Non-centrality parameter in least-squares
λ_{TG}	Tide-gauge longitude
σ	Standard deviation
σ_A	ANLN *a priori* standard deviation used in the combined LSA

σ_{AG09}	Standard deviation of AGQG09 height anomaly
σ_c	Standard deviation of levelling derived from ICSM (2007) c
σ_{CARS}	Standard deviation of CARS2006
$\sigma_{\hat{e}_i}$	Standard deviation of the least-squares residual
σ_h	Standard deviation of the ellipsoid height
$\sigma_{\hat{H}^N}$	Combined LSA *a posteriori* standard deviation
σ_L	Standard deviation of a two-way levelling misclose
σ_{obs}	Standard deviation of a single levelling run
σ_{RW}	Re-weighted *a priori* STD
σ_{ST}	Steed (2006) *a priori* STD
σ_{TG}	Standard deviation of MSL at tide-gauges
σ_{US}	Empirically determined *a priori* STD for US levelling
σ_{y_i}	*a priori* STD of the i^{th} observation
$\sigma^2_{y_i}$	*a priori* variance of the i^{th} observation
$\sigma^2_{\hat{y}_i}$	*a posteriori* variance of the i^{th} observation
σ_1	Unit standard deviation for levelling
$\hat{\sigma}^2$	*a posteriori* variance factor
σ^2	*a priori* variance factor of unit weight
$\sigma_{\Delta h}$	Standard deviation of the ellipsoid height difference
$\sigma_{\Delta n}$	Standard deviation of the levelled height difference
ρ	Average density of the Earth
ρ_A	Air density
ρ_T	Terrain slope
τ	Turbulent sheer stress
ϕ	Geodetic latitude
$\bar{\phi}$	Mid-latitude between two benchmarks
ϕ_{BM}	Geodetic latitude of an ANLN benchmark
$\phi_{g_{obs}}$	Geodetic latitude of a gravity observation
ϕ_{TG}	Geodetic latitude of a tide-gauge
$\phi_{1\text{-}2}$	Geodetic latitude difference between two benchmarks
χ^2_α	Chi-square distribution with α the chosen significance level
ω	Angular velocity of the Earth's rotation

Ω_{BM}	ANLN benchmark position (ϕ, λ)
$\Omega_{g_{obs}}$	ANGD gravity observation position (ϕ, λ)
Ω_{TG}	Tide-gauge benchmark position (ϕ, λ)

1. INTRODUCTION

Although serving Australia well since its inception in 1971, the Australian Height Datum (AHD; Roelse et al., 1971, 1975; Granger, 1972) no longer meets all the requirements of a modern vertical datum (e.g., Holloway, 1988; Morgan, 1992; Kearsley et al., 1993a; Featherstone, 1998, 2002b, 2004, 2006, 2008; Featherstone and Dent, 2002; Featherstone and Kuhn, 2006; Featherstone and Sproule, 2006; Featherstone and Filmer, 2008). This is primarily because the north-south slope and other distortions in the AHD (see Section 1.2 for details) make it inconsistent with heights from Global Navigation Satellite Systems (GNSS; e.g., Global Positioning System; GPS) and gravimetric geoid models (note that in this Chapter, the term geoid will be used to generally refer to both the geoid and quasigeoid). In addition, the AHD has deficiencies when used for regional and global scientific studies such as monitoring vertical crustal movement or sea-level change, and for testing new global and regional datasets or models (oceanographic or space-based) (e.g., Claessens et al., 2009; Featherstone et al., 2011).

However, a redefinition of the AHD, although often discussed (e.g., Kearsley et al., 1988; Morgan, 1992; Kearsley et al., 1993a; Featherstone, 1998, 2002b), has never eventuated, although Steed (2006, unpublished) conducted experimental least-squares adjustments (LSAs) of the Australian National Levelling Network (ANLN; ANLN dataset provided by Geoscience Australia; G. Johnston 2007, pers. comm.; also see Sections 1.2.1 and 2.3). This thesis investigates the problems that affect the AHD, attempting to quantify the errors, while also implementing methods to improve or upgrade the datum, culminating in a 'first iteration' of an Australian Experimental Vertical Datum (AEVD).

1.1 Background

This section provides a background on vertical datums, their definition, a brief history of heights in Australia, and international continent-wide vertical datums and their development. Comparing other continent-wide vertical datums not only puts the methods used to implement the AHD into context, but also demonstrates the options currently available to redefine the the AHD.

1.1.1 Vertical datums and height systems

A vertical datum is a 1D coordinate system consisting of heights referred to a zero-reference. Vaníček (1991) describes three different types of zero-references used in geodesy (cf. Jekeli, 2000; Rummel and Teunissen, 1988): the geoid, which is the zero-reference for orthometric and dynamic heights (H^O and H^D respectively); the quasi-geoid, which is the zero-reference for normal heights (H^N); and the reference ellipsoid, which is the zero-reference for ellipsoidal heights (Chapter 7). Height systems using the geoid or quasigeoid are referred to as physical (or natural) heights, as they better indicate the direction of fluid flow (Section 6.1.1). The geoid is the equipotential surface (upon which the Earth's gravity potential is constant), that provides a 'best fit' to mean sea level (MSL) on a global scale. On the other hand, the quasigeoid is not an equipotential surface (therefore not describing fluid flow), although it coincides with the geoid over the oceans, but diverges from the geoid over land.

Ellipsoidal heights (h) can be determined by GNSS. However, because they have no direct relation to gravity, they cannot determine the direction of fluid flow, and are therefore of limited practical use in most cases (Vaníček, 1988). In addition, the distance between the geoid and the ellipsoid (geoid height; N) reaches 110 m for geocentrically positioned ellipsoids (e.g., Jekeli, 2000). Thus, the physical vertical datum can be indirectly accessed (to a theoretical accuracy of <1 mm; Jekeli, 2000, 15) by $H^O = h - N$ (Section 2.5.1; Figure 7.1), with N computed through a gravimetric geoid model. However, in practice, distortions and errors in vertical datums and geoid mod-

els mean that N-transformed H^O is usually an imperfect realisation of the physical height defined by the vertical datum (Kotsakis and Sideris, 1999; Fotopolous, 2005; Featherstone, 2008).

Because the geoid and quasigeoid approximate MSL, which can be directly measured by tide-gauges, the zero-reference for levelling-based physical vertical datums is usually local MSL (Vaníček, 1991; Jekeli, 2000). A levelling network is connected to MSL, so as to carry heights relative to the zero-reference inland. However, MSL departs from the geoid by a spatially variable magnitude (about ± 1 m globally; Torge, 2001, 78) known as sea surface topography (SSTop), so MSL observations at a specific tide-gauge are only an approximation of the geoid (Vaníček, 1991). There are a number of ways to define the zero-reference for a levelling network. The choices considered are (cf. Vaníček, 1991):

1. adopt MSL (or SSTop-corrected MSL) as the zero-reference at one tide-gauge;
2. adopt MSL as the zero-reference at multiple tide-gauges (ignoring the effects of SSTop at the different tide-gauges);
3. adopt SSTop-corrected MSL at multiple tide-gauges;
4. constrain the levelling network to both SSTop-corrected MSL at multiple tide-gauges, and $h - N$ (using appropriate error estimates for the different measurement types).

Hence, the geoid can be directly (but approximately) accessed through MSL, but also indirectly (and imperfectly) through GNSS h and gravimetric N (cf. Vaníček, 1991).

1.1.2 Heights in Australia

Geologically, Australia is a very old continent, with mostly benign topography (minimum height -16 m at Lake Eyre; maximum 2228 m at Mt Kosciuszco; Figure 1.1) and is generally tectonically stable (Johnson, 2009, Chapter 1), despite seismic activity

occurring in several regions in Australia (e.g., the Southwest Seismic Zone in Western Australia (WA); Dentith and Featherstone, 2003).

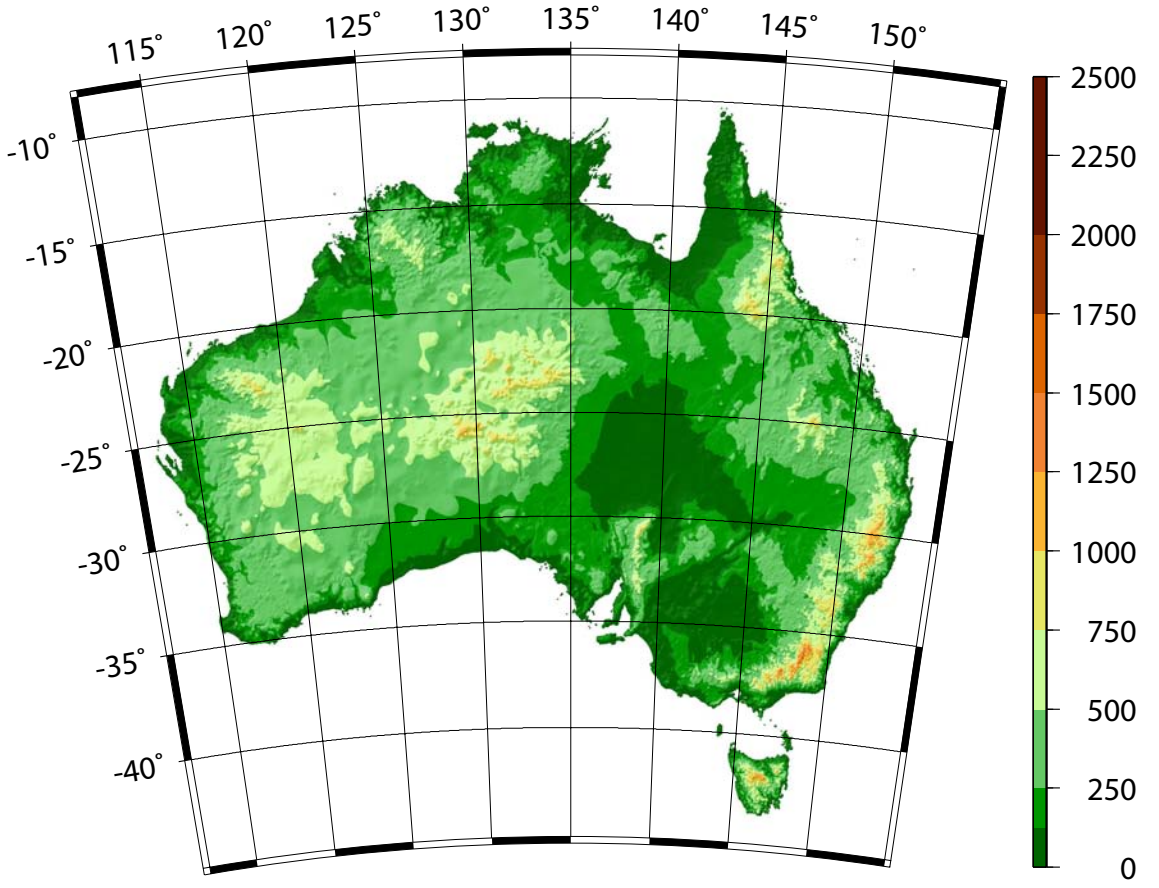

Figure 1.1: Australian terrain. Data from 9 arc-sec by 9 arc-sec GEODATA v2.1 DEM (Hutchinson, 2001). Lambert projection, units are in metres. From Kuhn et al. (2009).

The concept of a national vertical datum for Australia had been advocated since 1893, but it was not until immediately after 1945 that coordinated progress began (Lines, 1992, 238-239). Post-1945, the Australian Levelling Survey (ALS; Section 2.2.1) slowly took shape, with the predominately third-order network (Section 2.3.5) rapidly expanding after 1959, due to requirements for heights across the country to support gravity surveys conducted for mineral and petroleum exploration, and for national topographic mapping (Lines, 1992, 241-242).

The AHD was realised in 1971 from a national adjustment of the ALS, with MSL at 30 mainland tide-gauges defining the zero-reference for the AHD (option 2 in Section 1.1.1). The Tasmanian levelling network was adjusted independently in 1983, using MSL at two Tasmanian tide-gauges forming the zero-reference for the Tasma-

nian AHD (ICSM, 2006). The normal-orthometric correction (NOC) of Rapp (1961), was applied to the ALS, making the AHD a normal-orthometric height system ($H^{N\text{-}O}$; Holloway, 1988; Featherstone and Kuhn, 2006). The AHD has remained largely unchanged since 1971 (cf. Holloway, 1988; Morgan, 1992), with the exception of some 'infill' or correction by State and Territory geodetic agencies, although not all of these updates have been included in the ANLN (cf. Section 2.3.2; Steed, 2006; Filmer and Featherstone, 2009).

1.1.3 International continent-wide vertical datums

The United States (US) and Canada have the most comparable experiences to Australia with respect to national vertical datums, primarily because of their continental extent bounded by oceans. The Mean Sea Level Datum of 1929 (MSLD1929; referred to since 1973 as the National Geodetic Vertical Datum of 1929; NGVD29; Lachapelle and Gareau, 1980), was a general adjustment of the US and Canadian levelling networks, adopting MSL (tide-gauge observation epoch unknown) as the zero-reference at 26 tide-gauges (21 US; five Canadian; option 2 in Section 1.1.1; Zilkoski et al., 1992). Canada did not adopt the MSLD1929, instead retaining previously published heights from the Canadian Geodetic Vertical Datum of 1928 (CGVD1928), which adopted MSL as the zero-reference at five tide-gauges (Lachapelle and Gareau, 1980).

New levelling and gravity surveys, and readjustment programs began in the US and Canada in 1977 (Whalen, 1980b; Boal et al., 1985), resulting in the North American Vertical Datum 1988 (NAVD88; Zilkoski et al., 1992). However, Canada chose not to adopt NAVD88 due to unexplained discrepancies between the east and west coasts, and despite research into these problems (e.g. Carrera, 1984; Vaníček et al., 1985), are currently developing a new vertical datum based on a gravimetric geoid model (Section 1.3.3; Véronneau et al., 2006). NAVD88 uses the Helmert orthometric height system (Helmert, 1890) and is referenced to MSL at a single tide-gauge (option 1 in Section 1.1.1) located at Father Point/Rimouski (Canada), at the mouth of the St. Lawrence River (Zilkoski et al., 1992).

Discrepancies between NGVD29 and NAVD88 were found to be between −0.40 m and +1.50 m, which could be due to systematic levelling errors and the corrections applied (cf. Balazs and Young, 1982), time-dependent topographic surface motion (e.g. Carrera, 1984; Chi and Reilinger, 1984) and levelling-MSL discrepancies (Sturges, 1967, 1974; Balasz and Douglas, 1979) caused by the multiple MSL constraints used for NGVD29 (Zilkoski et al., 1992). Incompatibility between $h - N$ derived heights and NAVD88 H^O ranging between ±1.50 m led to a solution (Milbert, 1995; Smith and Milbert, 1999; Smith and Roman, 2001) where a gravimetric geoid was 'fitted' to the NAVD88 at 2951 GNSS/levelling points to provide a 'product' (cf. Vermeer, 1998; Iliffe et al., 2003; Featherstone and Sproule, 2006; Featherstone et al., 2011) that would enable users to directly realise NAVD88 H^O from GNSS h. The US is, like Canada (cf. Véronneau et al., 2006), developing a new geoid-only vertical datum (Section 1.3.3).

European vertical datums have been characterised by separate (usually national) levelling networks using different height systems and tide-gauges to define MSL (e.g., Marti and Schlatter, 2002; Christie, 1994). Moves to unify the European vertical datums through a combination of levelling networks, tide-gauge records, gravity measurements and GNSS observed h are described in Ihde and Sánchez (2005), but this unification is not yet complete. The European approach using levelling networks referenced to MSL at tide-gauges, but underpinned by a GNSS-derived network of h and a gravimetric quasigeoid (Ihde et al., 2002), differs from the geoid-only approach of the US and Canada to vertical datum re-definition (cf. Véronneau et al., 2006).

Ihde and Sánchez (2005) propose that the European approach be adopted to connect separate national vertical datums in South America. South American national vertical datums have been established as separate levelling networks using local MSL as their zero-reference, but usually adopting normal-orthometric height systems due to the unavailability of observed gravity (Sánchez, 2002; Luz et al., 2002b; de Freitas et al., 2002). The connection between the national levelling datums is to be via the South American geocentric reference system (SIRGAS) and a quasigeoid model (Luz et al., 2002a). African vertical datums appear to also be a collection of separate levelling networks with local MSL as their zero-references (Merry, 2003), although there is lim-

ited information regarding the status of these various African vertical datums. Merry (2003) discusses proposals for the unification of African vertical datums, but at this stage GNSS/levelling points are only publicly available in Algeria, Egypt and South Africa.

1.2 Problem definition

Many of the AHD's problems have remained largely hidden to land surveyors observing relative height differences over small areas with conventional surveying instruments, hence the lack of calls for a new datum (cf. Kearsley et al., 1988). However, the introduction of GNSS and gravimetric geoid models (e.g., Featherstone, 2008) have further exposed the deficiencies in the AHD (e.g., Featherstone, 2002b). Indeed, discrepancies of >1 m (Featherstone et al., 2011) between the AHD and $h-$AUSGeoid98 (AG98; Featherstone et al., 2001) have been found when using single-receiver GNSS positioning (relative to continually operating GNSS reference stations spread sparsely across Australia) processed using Geoscience Australia's (GA's) AUSPOS online GNSS data processing service (e.g., Featherstone and Dent, 2002).

While 'fitting' a gravimetric geoid to the vertical datum minimises the discrepancy between the vertical datum and $h-N$ derived height (e.g., Vermeer, 1998; Smith and Milbert, 1999; Smith and Roman, 2001; Iliffe et al., 2003; Featherstone and Sproule, 2006; Featherstone et al., 2011), it should only be considered an interim solution, as the errors in the vertical datum still exist. This 'solution', although resulting in a product that is acceptable to most 'users', merely hides the problems in the vertical datum and cannot be considered a long term alternative to re-defining the vertical datum. Thus, the real long-term driver to redefine the AHD is to provide a physical vertical datum for industry and research with a zero-reference that correctly coincides with a global geoid, to which the appropriate height system is accurately referred. The most significant problems in the AHD are described in the following sections.

1.2.1 Australian National Levelling Network

The decision to use third-order levelling rather than first-order standards as used in other countries (cf. Zilkoski et al., 1992; Yang et al., 2003; Amos and Featherstone, 2009; Ses and Mohamed, 2009) was taken so that the large distances could be covered more quickly and because third-order levelling was considered sufficient for mapping and geophysical exploration (Granger, 1972). However, this decision has resulted in a lower quality levelling network, despite plans at that time to expand the first-order network with a view to future re-adjustment (Lambert and Leppert, 1975; Leppert et al., 1975), which has not yet eventuated. Although the ANLN has had some updates and corrections (e.g., Wellman and Tracey, 1987; Morgan, 1992), it is essentially the same levelling data that defined the AHD.

The most serious issues are the gross errors (blunders) and systematic errors in the ANLN (e.g., Chapter 2; Morgan, 1992; Filmer and Featherstone, 2009). Gross errors have been discovered in one-way sections found mostly in Queensland, but also the interior of Western Australia and Northern Territory. Multiple systematic errors are also likely to affect the ANLN (Table 2.1). However, these are difficult to detect (cf. Entin, 1959; Strange, 1981; Craymer and Vaníček, 1986) and are often only revealed at continental scales when connected at tide-gauges (e.g., Roelse et al., 1971; Zilkoski et al., 1992).

Two-way levelling observations are necessary to help detect systematic errors, but the ANLN contains only the average of the two-way observations, making analysis of systematic levelling errors in the ANLN virtually impossible. The lack of additional information such as date and time of survey and weather conditions, also hinder attempts to correct systematic errors in the ANLN. Scaling benchmark (BM) positions (latitude and longitude; ϕ, λ) to the nearest arc-minute on 1:250,000 maps (Roelse et al., 1971, 40), has caused uncertainty of $\pm$30 arc-seconds ($\sim$900 m) in the BM positions, although approximate plotting on maps and other approximations/errors may result in the real BM positional uncertainty being larger than this.

1.2.2 North-south slope in the AHD

Fixing the ALS to local MSL (adopted as the AHD zero-reference; AHD_0) at multiple tide-gauges (option 1 in Section 1.1.1) has been a contentious decision (e.g., Morgan, 1992; Stewart, 1998; Featherstone, 2002b). However, it has been justified on the basis of allowing the different States and Territories to use local MSL as their AHD_0 (Roelse et al., 1971; Granger, 1972; Lines, 1992). Investigations over a number of years indicate that SSTop at the AHD tide-gauges have caused the north-south slope in the AHD (e.g., Hamon and Greig, 1972; Featherstone, 2004, 2006). However, it has been difficult to verify whether SSTop is the sole cause of the AHD slope because of uncertainty over the reliability of the levelling at continental scales (e.g., Coleman et al., 1979; Vaníček et al., 1980; Castle and Elliot, 1982). Thus, the issue is yet to be fully resolved (cf. Chapter 5).

1.2.3 AHD Tasmania−mainland offset

The mainland levelling network was fixed to MSL (observed between 1966 and 1968 for 29 tide-gauges, but 1957 to 1960 at Karumba) at 30 mainland tide-gauges to realise AHD(mainland) in 1971, whereas AHD(Tas) used the Tasmanian component of the ANLN fixed to MSL (observed during 1972) at two Tasmanian tide-gauges (NMC, 1979). Because of this, it is believed that an offset (variously estimated at between 0.10 m and 0.33 m; Rizos et al., 1991; Rapp, 1994; Featherstone, 2000, 2002a) exists between AHD(mainland) and AHD(Tas). Unification of these two datums (cf. Amos and Featherstone, 2009; Rummel and Teunissen, 1988; Zhang et al., 2009; Poutanen, 1999) is an additional issue that needs resolving (see Section 5.8) in the development of any new Australian vertical datum (AVD).

1.2.4 Height system

Lack of sufficient gravity observations in Australia in 1971 resulted in the AHD using a normal-orthometric height system (Holloway, 1988, 16), through the implementation of a truncated version of the Rapp (1961) normal-orthometric correction. Normal-orthometric corrections use normal gravity rather than observed gravity, which is required for H^O or H^N.

The effect on AHD heights of using normal-orthometric corrections instead of normal or orthometric height corrections is not well known, despite Mitchell (1973a) computing geopotential numbers across Australia, but only to establish that the use of normal-orthometric corrections were not the cause of the AHD's north-south slope (cf. Section 1.2.2). Allister and Featherstone (2001) computed Helmert H^O over a short section of the Darling Scarp in WA, suggesting the difference with $H^{N\text{-}O}$ was only a few mm in this area, but this was at heights <200 m, where the effects of different height systems are usually small (see Chapter 7).

The compatibility of AHD $H^{N\text{-}O}$ with gravimetric geoid or quasigeoid models is also uncertain. Featherstone and Kirby (1998) computed approximate differences (up to 0.15 m) between the geoid and quasigeoid over Australia, but this was affected by averaging gravity observations in the Australian Alps. It was also assumed that the quasigeoid was suitable for use with AHD $H^{N\text{-}O}$, but this is questionable for higher elevations (cf. Sections 7.8.2 and 7.9.5; Filmer et al., 2010; Kao et al., 2000).

1.2.5 AHD adjustment strategy

The AHD was least-squares adjusted in five regions rather than a simultaneous national adjustment, which, although a further potential source of error, was necessary due to the lack of available computing power at that time. This resulted in the LSA of the basic network defining the AHD, with the supplementary network subsequently adjusted onto the fixed basic junction points (JPs; Roelse et al., 1971, 45; also see

Section 2.2.3). In addition, new or corrected levelling added to the ANLN has been incorporated into the AHD by holding the junction points fixed, rather than allowing a complete readjustment (Morgan, 1992; Holloway, 1988). For comparisons between a complete readjustment and the staged AHD adjustment see Section 2.3.8 (Figure 2.3; also see Chapter 8).

1.3 Methods for vertical datum realisation

Levelling networks have traditionally formed the backbone of national vertical datums (e.g., Roelse et al., 1971; Zilkoski et al., 1992; Christie, 1994; Ihde et al., 2002; Yang et al., 2003; Amos and Featherstone, 2009; Ses and Mohamed, 2009; Abeyratne et al., 2010). However, the introduction of GNSS, gravimetric geoid models and SSTop models have provided alternative methods of defining and realising national vertical datums. The three options presented here for any new AVD are a levelling-only vertical datum, a 'combined' vertical datum (e.g., Kearsley et al., 1993a; Balasubramania, 1994; Hwang, 1997) and a geoid-only datum (cf. Véronneau et al., 2006; Amos and Featherstone, 2009). These three types of vertical datums are defined, and the advantages and disadvantages for each are presented and discussed.

1.3.1 Levelling-only vertical datums

A national levelling network constrained to MSL in a national adjustment at one or multiple tide-gauges defines most national vertical datums currently in operation (e.g., Roelse et al., 1971; Zilkoski et al., 1992; Christie, 1994; Ihde et al., 2002; Ses and Mohamed, 2009; Abeyratne et al., 2010). A levelling-only datum is defined here as a national levelling network constrained at one or more tide-gauges, with the zero reference defined by MSL-only or SSTop corrected MSL (options 1, 2 or 3 in Section 1.1.1). The advantages of a levelling-only vertical datum are:

1. The vertical datum is independent of GNSS and gravimetric geoid models, so can be used to validate global and regional geoid models (and *vice versa*);

2. BMs with heights directly related to the vertical datum are available for users; users can access the heights without GNSS technology;

3. High local precision from levelling, whereas GNSS is less accurate in the height component.

The disadvantages of a levelling-only vertical datum are:

1. Long-wavelength systematic and gross levelling errors, plus the 'noisy' nature of ANLN third-order levelling, make it difficult to accurately realise the vertical datum from GNSS h and gravimetric N (h and N errors notwithstanding);

2. A levelling network needs at least a partial upgrade in problem areas, plus ongoing maintenance.

Fixing a levelling-only vertical datum to MSL (with or without SSTop corrections) at one tide-gauge (option 1 in Section 1.1.1) could be effective with a high quality levelling network of limited extent. However, for large levelling networks covering entire continents such as Australia, it has been shown that systematic levelling errors accumulating over long distances and/or gross errors in poorly-checked sections (Chapters 2, 3 and 4) can degrade the resulting heights (e.g., Morgan, 1992; Filmer and Featherstone, 2009). Where levelling errors at tide-gauges become larger than MSL and SSTop errors at those tide-gauges, as shown for the ANLN in Chapter 5, fixing the levelling network at only one tide-gauge becomes a less attractive option.

On the other hand, adopting local MSL (with no SSTop corrections) at multiple tide-gauges (option 2; e.g., Roelse et al., 1971; Vaníček, 1991; Zilkoski et al., 1992) remains an option, but experience with the AHD (and demonstrated in Chapter 5) suggests that this option will result in the vertical datum not being aligned with the geoid. The extent of this non-alignment with the geoid depends on the variation of SSTop at the

different tide-gauges used to fix the levelling network, but this option is not considered appropriate for any new Australian vertical datum. Provided SSTop corrections of sufficient accuracy can be realised (cf. Merry and Vaníček, 1983), option 3 (Section 1.1.1) is the most attractive option for a levelling-only datum. However, although there are advantages for using a levelling-only vertical datum, these are overshadowed by the high costs of upgrading and maintaining the levelling network (Véronneau et al., 2006).

1.3.2 Combined vertical datums

A combined vertical datum is defined here as a vertical datum that combines the influence of SSTop-corrected MSL observed at multiple tide-gauges and $h-N$ to define the zero-reference, but relies on the levelling network (constrained to $h-N$ and SSTop-corrected MSL; option 4 in Section 1.1.1) to propagate the heights through the network. Kearsley et al. (1993a) and Hwang (1997) have discussed the concept of a combined vertical datum (cf. Milbert, 1988), but the author is not aware of a current national vertical datum that has employed this concept. Australia is well placed to consider this option, given access to tide-gauges along its entire coastline (Figures 2.1 and 2.2), the recent availability of the gravimetric-only component of AUSGeoid09 (AGQG09; Featherstone et al., 2011), and the increasing number of GNSS observations across the continent. Advantages in adopting this approach are:

1. BMs with heights directly related to the vertical datum are available for users; users can access the heights without access to GNSS technology;

2. High local precision from levelling;

3. Long-wavelength systematic and gross levelling errors, plus the 'noisy' nature of ANLN third-order levelling can be controlled by $h - N$ and SSTop + MSL constraints to improve accuracy of the transformation to the vertical datum from h using gravimetric N. Therefore, there may be less need to update the levelling network than for a levelling-only vertical datum.

Despite advantages over levelling-only vertical datums, the combined vertical datum does have some disadvantages:

1. The vertical datum will not be independent of GNSS h and gravimetric N as these observations are used as constraints, so a combined vertical datum cannot be used to validate global and regional geoid models (and *vice versa*);
2. The combined vertical datum can be more accurately realised from $h - N$ observations (compared to the levelling-only vertical datum). However, unresolved residuals between H and $h - N$ will remain, due to levelling, SSTop + MSL and $h - N$ errors;
3. The levelling network needs to be upgraded and maintained, although there will be less need for new levelling than for the levelling-only datum (dependent on land subsidence or uplift and loss of BMs).
4. The local zero-reference will no longer be local MSL, which is often required by engineers for design purposes (e.g., local coastal drainage, or flood mitigation control), although local offsets between a combined vertical datum and MSL can be made available for these specific purposes.

The major advantage of the combined vertical datum compared to levelling-only vertical datums are the $h - N$ constraints that allow the long-wavelength levelling errors to be reduced (assuming that there are smaller long-wavelength errors in the geoid model). However, they are not completely removed (depending on error estimates for each data set), and in addition, the combined model can no longer be used for independent validation of geoid models.

1.3.3 Geoid-only vertical datums

A geoid-only datum is defined here as being determined solely by a specified geoid model and ellipsoidal heights referred to a specific geodetic datum, or reference frame at the stations of the regional GNSS network. It is envisioned that such a vertical

datum would not contain officially maintained BMs or levelling, but that datum 'in-fill' would consist of continuously operating GNSS reference stations (CORS). The improvement (and further anticipated improvement) in accuracy of gravimetric geoid models through dedicated satellite gravimetry missions (e.g., Arabelos and Tscherning, 2001; Featherstone, 2003) has prompted discussion and development in the area of geoid-only vertical datums (e.g., Véronneau et al., 2006). This is particularly attractive because:

1. Geoid-only vertical datums can avoid the expense and associated problems of maintaining and upgrading levelling networks (e.g., Véronneau et al., 2006; Christie, 1994);

2. Users can directly access the vertical datum using GNSS technology.

Disadvantages of a geoid-only vertical datum are:

1. Published heights related to the geoid-only vertical datum will not be available at BMs unless the BM has observed GNSS h. Thus, users without access to GNSS technology may not be able to fully access the vertical datum;

2. Although considered inexpensive to maintain, to achieve adequate local precision, the terrestrial gravity database will need to be improved. This will be at considerable expense, even if provided/supplemented by airborne gravimetry;

3. Local relative precision (subject to h and N errors) is not likely to be as high as that provided by levelling, because levelling is more precise than $h-N$ over short distances. It is not yet known if airborne and satellite gravimetry will provide the required level of accuracy for a vertical datum that is equivalent to third-order standard (or better), particularly in mountainous and coastal regions (cf. Hwang et al., 2007; Serpas and Jekeli, 2005);

4. Geoid-only vertical datums cannot (unlike high quality levelling-only vertical datums) independently validate new global and regional geoid models.

5. The local zero-reference will no longer be local MSL, which is often required by engineers for design purposes (e.g., local coastal drainage, or flood mitigation control), although local offsets between a combined vertical datum and MSL can be made available for these specific purposes.

While development of geoid-only vertical datums is progressing, there are no geoid-only vertical datums (as defined here) in operation yet. New Zealand Vertical Datum 2009 (NZVD2009) uses the New Zealand Quasigeoid 2009 (NZGeoid2009; Claessens et al., 2011) as its zero-reference. However, NZVD2009 is used in conjunction with levelling-based local vertical datums using the normal-orthometric height system (Amos and Featherstone, 2009) and cannot be considered a geoid-only vertical datum under the definition used here.

It is likely that some of the disadvantages listed here will be overcome sometime in the future (the US and Canada are working towards geoid-only datums), and although Australia could develop a geoid-only datum using currently available data, it is questionable whether its accuracy would be as good as a combined vertical datum at this time. Thus, geoid-only datums will not be discussed further, and the focus of this thesis will be on levelling-only and combined vertical datums for Australia.

1.4 Research objectives

A primary objective of this thesis is to produce a rigorous revision of the AHD, that could could eventually lead to a new AVD. Regardless of any new AVD, a full investigation into the current AHD is warranted, not only to fully identify the problems in the data sets used for the AHD, but also the data sets that will be used for any new AVD. The research objectives for this thesis are described in Section 1.4.1 to Section 1.4.4 .

1.4.1 Investigation into the ANLN

Gross levelling errors in the ANLN are suspected of causing regional distortions in the AHD (Morgan, 1992; Holloway, 1988), so identifying levelling sections containing blunders is a priority. Loop-based investigations (Sections 2.4 and 2.5; Filmer and Featherstone, 2009) and statistical outlier detection methods (e.g., Section 8.4; Baarda, 1968; Schwarz and Kok, 1993; Teunissen, 2006c,b) are employed to identify such errors. Due to insufficient information in the ANLN, meaningful analysis of systematic levelling errors is difficult (cf. Entin, 1959; Angus-Leppan, 1975). However, a simulated estimate using assumed data (Chapter 4) of the effects of atmospheric refraction on levelled heights (cf. Holdahl, 1981; Strange, 1981; Mark et al., 1987) is conducted using the refraction correction of Angus-Leppan (1979).

1.4.2 Identification and correction of the north-south slope in the AHD using SSTop models

The strategy of selecting MSL at 30 mainland (and two Tasmanian) tide-gauges and its consequences have been discussed often (e.g., Roelse et al., 1971; Hamon and Greig, 1972; Mitchell, 1973b; Fischer, 1975; Leppert et al., 1975; Coleman et al., 1979; Macleod et al., 1988; Featherstone and Stewart, 1998; Featherstone, 2004, 2006; Featherstone and Filmer, 2008). However, it has not yet been determined if all of the AHD north-south slope is attributable to fixing the ALS to MSL, or whether other factors affecting the levelling network contribute to the slope. The aim in this thesis is to determine the factors causing the slope, and find methods to correct this problem. Five different SSTop models (SSTMs) will be tested and used for this objective, assisted by $h-$AGQG09 (H_{AG09}), to determine their suitability and effectiveness as constraints for a 'level' vertical datum.

1.4.3 Test gravimetric height corrections

The effects of gravimetric height corrections (orthometric and normal) on the ANLN compared to the Rapp (1961) normal-orthometric corrections applied for the AHD (Roelse et al., 1971, 65) are unknown (cf. Mitchell, 1973a; Allister and Featherstone, 2001). The aim here is to first test and compare these height corrections (Chapter 7; Filmer et al., 2010), then select one as the most suitable to be used in any new AVD. Because gravity has only been directly observed at ∼9500 out of ∼90,000 BMs, the most challenging component of implementing gravimetric height corrections is realising gravity values at ANLN BMs. Two approaches are taken, with BM gravity computed from i) the Earth Gravity Model 2008 (EGM2008; Pavlis et al., 2008); and ii) the GA Australian National Gravity Database 2007 (ANGD2007; Murray, 1997; Tracey et al., 2007).

1.4.4 Adjustment of the ANLN using SSTop at tide-gauges and $h - N$ as weighted constraints

The culmination of this assessment of the AHD is an 'experimental' vertical datum (cf. Section 1.3.2) using the ANLN, but constrained at tide-gauges using SSTop corrections to MSL, and H_{AG09} through the interior of the country (e.g., Chapter 8; Kearsley et al., 1993a). This solution ideally uses the local accuracy of levelling, but aims to restrict the propagation of levelling errors through the adjusted vertical datum heights (cf. Milbert, 1988). By using MSL + SSTop at tide-gauges, and H_{AG09} as weighted constraints rather than 'fixing' in the adjustment, the errors in levelling, SSTop, MSL, GNSS h and AGQG09 are treated more appropriately than fixing them (e.g., Ahmad et al., 1993; Kearsley et al., 1993a). The weighting of constraints with respect to their individual errors is also described by Jiang and Duquenne (1996), Kotsakis and Sideris (1999), Kotsakis et al. (2002) and Fotopolous (2005), but in the context of 'fitting' a geoid model to the existing vertical datum.

1.5 Thesis outline

This thesis comprises nine chapters. Chapter 2 describes the background to the AHD and the evolution of the ALS into the present ANLN. A loop closure-based investigation identifies numerous loops with above-tolerance misclosures, but also provides estimates of the precision of the different ANLN levelling orders. A second component of Chapter 2 introduces GNSS h and AG98 as additional pseudo-observations to attempt to isolate errors in specific levelling sections. The work in Chapter 2 has been published in the Australian Journal of Earth Sciences (Filmer and Featherstone, 2009).

Investigations into the effect of atmospheric refraction are described in Chapters 3 and 4. A review of available refraction corrections, followed by a sensitivity analysis for input data in the Angus-Leppan (1979) refraction correction is contained in Chapter 3, identifying input data errors that could result in above-tolerance levelling misclosures. A short note was published in the Journal of Spatial Science (Filmer et al., 2009) for a correction to the Angus-Leppan (1979) refraction correction. A simulation was conducted in Chapter 4, where assumed input data was used (because the information is not available in the ANLN) to apply refraction corrections to the ANLN. The height differences resulting from two minimally constrained adjustments of the ANLN (one with refraction corrections and one without) provided a crude estimate of refraction effects on the AHD.

The significant issue of the adoption of MSL at multiple tide-gauges as the AHD_0 is addressed in Chapter 5. Methods of computing SSTop heights at tide-gauges is described, followed by a comparison among five (geodetic and oceanographic) SSTop models at Australian tide-gauges. Further comparisons are among the SSTop model heights, ANLN- and $h-$geoid-implied SSTop heights at Australian tide-gauges, demonstrating that the AHD slope is solely attributable to the adoption of MSL as the AHD_0. It is shown how sea surface slope effects can be removed from the AHD (or any new AVD) using the CARS2006 (Ridgway et al., 2002) climatological model of SSTop at tide-gauges. In addition, a revised estimate for the vertical datum offset between mainland Australia and Tasmania using five SSTMs and H_{AG09} is made (cf. Rizos et al., 1991;

Rapp, 1994; Featherstone, 2002a, 2000).

The application and testing of gravimetric height corrections is covered in Chapters 6 and 7, with a paper published in the Journal of Geodesy (Filmer et al., 2010). The methods used to compute gravity at BMs (using ANGD2007 and EGM2008) and the validation of these values are described in Chapter 6. The different types of height corrections are introduced in Chapter 7, with a sensitivity analysis of the orthometric, normal and normal-orthometric corrections indicating the effects of input data error on the different height corrections. A manuscript on the effects of input data errors on these three different height corrections has been accepted for publication in the Journal of Spatial Science. The differences among heights from ANLN adjustments with Helmert orthometric, normal and normal-orthometric corrections applied are also shown in Chapter 7, indicating the full effects of gravimetric height corrections on the ANLN.

The final stage of the thesis is the combined adjustment of the ANLN, MSL + SSTop at tide-gauges, and H_{AG09}, which is detailed in Chapter 8. Statistical outlier detection methods (e.g., Baarda, 1968; Schwarz and Kok, 1993) are employed to identify levelling sections with errors, which are then re-weighted to reduce their influence on the adjustment. The final combined adjustment of the ANLN, MSL + SSTop at tide-gauges and H_{AG09} realises the AEVD. Chapter 9 concludes the thesis, containing a summary of the research, plus conclusions and recommendations for future work. Appendix A contains weather station information and Appendix B contains meteorological information used for refraction corrections in Chapter 4.

2. INVESTIGATION OF LEVELLING ERRORS IN THE AUSTRALIAN NATIONAL LEVELLING NETWORK

The Australian Height Datum (AHD) is based on the Australian Levelling Survey (ALS; Roelse et al., 1971). However, the ALS (now called the Australian National Levelling Network; ANLN; e.g., Steed, 2006) has been investigated many times due to the assumption that it contains errors that contribute to problems in the AHD (e.g., Angus-Leppan, 1975; Leppert et al., 1975; Lambert and Leppert, 1975; Coleman et al., 1979; Holloway, 1988; Kearsley et al., 1993a; Morgan, 1992; Featherstone and Stewart, 1998; Filmer and Featherstone, 2009). This Chapter introduces differential levelling and its associated errors, and describes the current ANLN (provided by Geoscience Australia; GA; G. Johnston 2007, pers. comm.).

A loop-closure-based investigation into levelling errors is then conducted; first using only the ANLN, then the ANLN augmented by Global Navigation Satellite Systems (GNSS; e.g., Global Positioning System; GPS) minus AUSGeoid98 (AG98; Featherstone et al., 2001) height differences (cf. Filmer and Featherstone, 2009). It is shown that the GNSS-AG98 height differences add redundancy, which can be used to identify problem sections in above-tolerance levelling loops, making it easier for State and Territory geodetic agencies to identify and correct office transcription errors, or to locate and re-survey levelling (or transcription) errors made in the field. The use of GNSS-AG98 height differences as pseudo-observations is necessary because i) the ANLN contains only averaged height differences (not two-way levelling observations), ii) additional levelling data held by State and Territory geodetic agencies is not currently available for this study, and iii) the ANLN contains large loops with poor redundancy (see Section 2.3.2).

2.1 Background

2.1.1 Levelling procedure

Differential levelling is a simple and inherently precise method of measuring height differences between two points (Vaníček et al., 1980). The levelling instrument is set up (line of collimation orthogonal to the plumbline passing through the instrument) at the midpoint between two graduated staves, both held upright and tangent to their local plumblines. The maximum distance between instrument and staves is determined by the required precision of the survey (see Tables 2.2 and 2.3; also ICSM, 2007, A-13), but also by the steepness of the terrain along the levelling line and atmospheric conditions (e.g., Mark et al., 1987). The observer reads the back-sight (BS) to the staff in the reverse direction of the survey, then the fore-sight (FS) to the staff in the forward direction of the survey.

The arithmetic difference between the FS reading (Z_F) and back-sight reading (Z_B) is the observed height difference Δn_o. By reading a series of Δn_o between two benchmarks (BMs; usually several km apart), $\sum_{BM1}^{BM2} \Delta n_o$ provides Δn between BM1 and BM2 (e.g., Schomaker and Berry, 1981). Here, levelling between two BMs is defined as a sub-section (e.g., Morgan, 1992), with multiple sub-sections called sections, where the start and end BM of the section connect to other sections and are referred to as junction points (JPs). Multiple levelling sections develop into a levelling network, which can be expanded to continental extents. For a full treatment of levelling, see Bomford (1971, Section 3.2), Vaníček et al. (1980), Schomaker and Berry (1981), Rappleye (1948), or Gareau (1986).

Due to the lack of redundancy that is inherent in levelling measurements, levelling sub-sections should comprise two-way levelling (Bomford, 1971, 243). Indeed, two-way levelling is required to conform to most levelling specifications (e.g., ICSM, 2007, B-11). Two-way levelling comprises a forward run, which is levelling from the start point of the sub-section (BM1), to the terminal point of the sub-section (BM2), with the backward run being the return levelling from BM2 back to BM1. Two-way levelling should

identify gross errors (Vaníček et al., 1980), while the redundancy enables assessment of systematic and random errors in the network (e.g., Morgan, 1992).

2.1.2 Levelling instruments

Differential levelling instruments (or levels) have made significant technological advances in recent decades, although the procedure (Section 2.1.1) has remained essentially unchanged (Vaníček et al., 1980). There are two types of optical levelling instruments: spirit-levels and automatic compensating levels (Schomaker and Berry, 1981, 3-11). Digital levels, which do not require the staff to be read manually, became available in the early 1990s (Rüeger, 2003, 27). Spirit-levels (or tilting levels), are approximately levelled with a small circular bubble, but rely on the main bubble in the long level vial situated on top of the instrument in the line of the telescope. This main bubble is centred with the tilting screw before each reading, hence making the line of sight parallel with the local equipotential surface (Bomford, 1971, 233).

Automatic compensating levels were introduced in 1950 (Torge, 2001, 207). A small circular bubble is also used for approximate levelling of the automatic instrument, but rather than a second bubble, an automatic compensating mechanism comprising a system of reflecting mirrors and prisms, suspended inside the instrument is used to remove the residual dislevellment (Bomford, 1971, 234). Automatic levels provide time savings, as the requirement to precisely set (and reset) the main bubble is avoided, while Schomaker and Berry (1981) suggest that automatic levels provide improved precision over spirit levels. However, Torge (2001, 207) considers spirit-levels to be superior to automatic levels when high frequency oscillations such as traffic or wind are present, due to better damping of the main spirit-level bubble. For further information on optical levelling instruments, see Schomaker and Berry (1981, Section 3.3), Bomford (1971, Section 3.04), and Clendinning and Olliver (1969).

Digital levelling instruments read staves with barcode graduations. They provide considerable advantages over optical levels, such as not having to optically read the staff and electronic data recording of the observation. Digital level errors are similar to

those of automatic levels (Rüeger, 2003, 27, 40), and generally use the same compensating system as optical automatic levels (Rüeger, 2003, 30). For further details, see Rüeger (2003, Section 3.1). Most levelling conducted these days uses optical or digital automatic levels.

Levelling staves (or rods), are generally about three metres long and can be of various design, manufacture or composition. High precision levelling requires rigid staves constructed of invar (e.g., Schomaker and Berry, 1981, 3-41), although folding or telescopic staves constructed of wood, fibreglass and aluminium can be used for low precision levelling (e.g., ICSM, 2007, B-9). For a comparison of the effects of graduation and expansion errors in wood, fibreglass or aluminium levelling staves, see Rüeger (1997). Levelling staves, also require accurate calibration and maintenance (e.g., Schlemmer, 1985; Thwait, 1966). For further details on levelling staves, see Schomaker and Berry (1981, Section 3.4), Rappleye (1948, 21-23), or Bomford (1971, 236).

2.1.3 Random levelling errors

Vaníček et al. (1980) groups levelling errors into random, systematic (Section 2.1.4), or gross (blunders; Section 2.1.5) errors. Random errors are caused by inaccurate observation, small instrumental errors (non-systematic) and high frequency variations in atmospheric conditions (Vaníček et al., 1980). Although random errors cannot be eliminated, they can be minimised by good survey procedure, representing the 'noise level' that limits the precision of the levelling (Schomaker and Berry, 1981, 3-1).

The standard deviation (STD; 1σ) between BM1 and BM2 is generally proportional to $\sqrt{d}$, where d is the distance of the levelling run between BM1 and BM2 (Vaníček et al., 1980). The STD of Δn ($\sigma_{\Delta n}$) is (Vaníček and Krakiwsky, 1982, 431)

$$\sigma_{\Delta n} = \sigma_1 \sqrt{d} \tag{2.1}$$

where σ_1 is the unit STD (usually over 1 km). Equation (2.1) is sometimes called the square root law, which only applies when the errors are statistically independent (cf. Lucht, 1971), which is not usually the case for levelling observations. However, this

is usually ignored and statistical independence is assumed for levelling networks (cf. Vaníček et al., 1980).

As a quality control measure, Equation (2.1) can be modified to determine acceptable closures of levelling sub-sections and loops as (ICSM, 2007, A-12)

$$r_m = c\sqrt{d} \tag{2.2}$$

where r_m is the maximum allowable misclose in mm, c (mm) is an empirically derived unit value that determines r_m for different standards of levelling. σ_1 can be estimated from two-way levelling at the sub-section or section level (cf. Morgan, 1992; Zilkoski et al., 1992), from loop closures (e.g., Section 2.4; Filmer and Featherstone, 2009; Lambert and Leppert, 1975), or, more crudely, from c (e.g., Sections 2.3.8 and 8.3.2; Kearsley et al., 1993a; Steed, 2006). Note that values for c for different levelling orders in Australia (Table 2.3) may vary for different countries.

2.1.4 Systematic levelling errors

There are many different sources of systematic error in levelling observations. Systematic errors are often difficult to detect, as they are generally small and can randomise under certain circumstances (Angus-Leppan, 1975). Thus, systematic errors may only become apparent over long distances, or even continental scales and are not always revealed in network closures (Vaníček et al., 1980). Table 2.1 lists the major sources of systematic error in levelling. The systematic effects on levelling due to variations in the Earth's gravity field are described in Chapters 6 and 7.

Atmospheric refraction is often considered the most significant source of systematic error in levelling (cf. Section 3.3.1; Strange, 1981, 1983; Castle et al., 1983; Craymer and Vaníček, 1986; Mark et al., 1987; Craymer and Vaníček, 1989; Stein et al., 1989). Refraction error will not be discussed here, as Chapters 3 and 4 provide a fuller treatment of this problem. The rising or sinking of the staff and tripod is a potentially significant error (e.g., Craymer and Vaníček, 1986; Angus-Leppan, 1975), but is dependent on the time taken for observation, the type of ground mark supporting the staff, and type

of surface along the level run (Entin, 1959). However, Angus-Leppan (1975) suggests that two-way levelling in opposite directions using the same procedure (observation sequence for FS/BS), will cancel this error (cf. Section 2.3.7).

Error	Reference
Atmospheric refraction	Angus-Leppan (1979), Angus-Leppan (1980), Craymer and Vaníček (1986), Holdahl (1981), Kukkamäki (1938), Kukkamäki (1939), Remmer (1980), Mark et al. (1987), Shaw and Smietana (1983), Stein et al. (1986), Strange (1981) Also see Chapters 3 and 4
Rising or sinking of staff and instrument	Entin (1959), Angus-Leppan (1975) Craymer and Vaníček (1986)
Staff expansion	Rüeger (1997)
Magnetic effects on automatic levels	Strange (1985), Rüeger (2003, 45)
Staff calibration	Craymer and Vaníček (1986), Craymer et al. (1995)
Earth tides and ocean loading	Vaníček and Krakiwsky (1982, 594), Bretreger (1986), Heck (1993)
Under- or over-compensation in automatic levels	Angus-Leppan (1975) Bomford (1971, 235)
Collimation	Angus-Leppan (1975), Bomford (1971, 236)
Hysteresis	Angus-Leppan (1975)

Table 2.1: List of principal systematic errors that can effect optical levelling (and some associated references). For information on systematic errors specific to digital levelling, see Rüeger (2003, Section 3.1).

Staff expansion is dependent on temperature variation and staff composition, and is correlated with height (Rüeger, 1997). The error has opposite signs for forward and backward runs (and is thus hidden), but will result in errors in heights adjusted from the levelled height differences. Regular staff calibration should minimise staff calibration error, although some residual error may be present, with Craymer and Vaníček (1986) suggesting that staff graduation may vary between staves calibrated in a horizontal position and in their vertical observation position. In addition, scale errors between staff pairs can also affect levelled height differences (Craymer et al., 1995).

Early models of automatic levels were affected by the Earth's magnetic field because the compensator was constructed of materials that were attracted by magnetic forces.

Rüeger (2003, 45) suggests potentially large errors of up to 2.2 mm per km due to magnetic field effects, although since 1982, manufacturers have reduced instrument susceptibility to magnetic effects. A correction for magnetic error is developed by Strange (1985). However, difficulties were found in correctly representing the Earth's magnetic field, the empirically derived field values for the compensator's unique proportionality constant differed from laboratory tests, and finally, the compensator constant could be large and highly variable within instruments of the same type.

Earth tide effects on levelling are small, generally in the order of a few mm per 100 km (Vaníček and Krakiwsky, 1982, 594), but are systematic and accumulate primarily in the north-south direction. Ocean loading effects are somewhat more complex, due to difficulties modelling ocean tides in coastal regions, but could reach one order of magnitude larger than Earth tide effects (Bretreger, 1986).

Under- or over-compensation of the automatic level's compensator is caused by slight imperfections in the compensator. Hysteresis (e.g., Angus-Leppan, 1975) is the error in the final position of the compensator due to damping and friction in the mechanism and the direction and speed at which it comes to rest. Correct handling procedure by the observer will minimise hysteresis (cf. Roelse et al., 1971, 54-55). These two compensator-related errors will cancel in the mean of the backward and forward runnings under similar procedures, but will generally not accumulate over longer distances, even when the procedure is different (Angus-Leppan, 1975). Collimation error is cancelled when the distance from the level to the BS is the same as the distance to the FS, and can be identified by a two-peg test (Bomford, 1971, 236).

2.1.5 Gross levelling errors

Gross errors (blunders) are caused by mistakes such as incorrectly reading the staff (e.g., reading stadia cross hair) or incorrectly recording the observation in the field book (Schomaker and Berry, 1981, 3-6). In addition to field blunders, gross errors can also occur during the office processing, where transcription or calculation errors can occur. Gross levelling errors are usually detected by sub-section closures in two-way

levelling, or in loop closures (Vaníček et al., 1980). The sub-section and loop closures are expected to close within a tolerance which is a function of the square root of the distance levelled (Equation (2.2)), and depends on the order of the levelling (e.g., ICSM, 2007, A-13; also see Tables 2.2 and 2.3).

While gross levelling errors are usually detected by closure checks, there are situations where undetected errors may remain hidden in a levelling network. Compensating errors are when two gross errors of similar magnitude, but opposite sign are contained within a sub-section, or loop, so that the overall closure is within tolerance (Holloway, 1988). In addition, large levelling loops of low-quality levelling have large r_m (computed using Equation (2.2)), allowing gross errors to remain in the loop if they are $<r_m$. However, double-graduated staves (metres and feet), good procedures and vigilant checks should enable gross errors to be avoided (Schomaker and Berry, 1981, 3-5).

2.2 Background to the Australian Height Datum

2.2.1 The Australian Levelling Survey

The creation of the National Mapping Council (NMC) in 1945 began the process towards a national Australian vertical datum (Roelse et al., 1971, 2). By 1950, the then-ALS consisted of 4,800 km of levelling. An additional 16,000 km was levelled between 1956 and 1960, which up until then had been conducted only by State, Territory and Federal authorities. After 1961, private contract surveyors conducted most of the levelling (under the control and supervision of State, Territory and Federal authorities), so that by the end of 1970, the ALS consisted of 161,000 km of levelling (Roelse et al., 1971, 2), of which 97,320 km was deemed the 'primary' network (Figure 2.1), with the remainder referred to as the 'supplementary' network (Roelse et al., 1971, 11; cf. Figure 2.2).

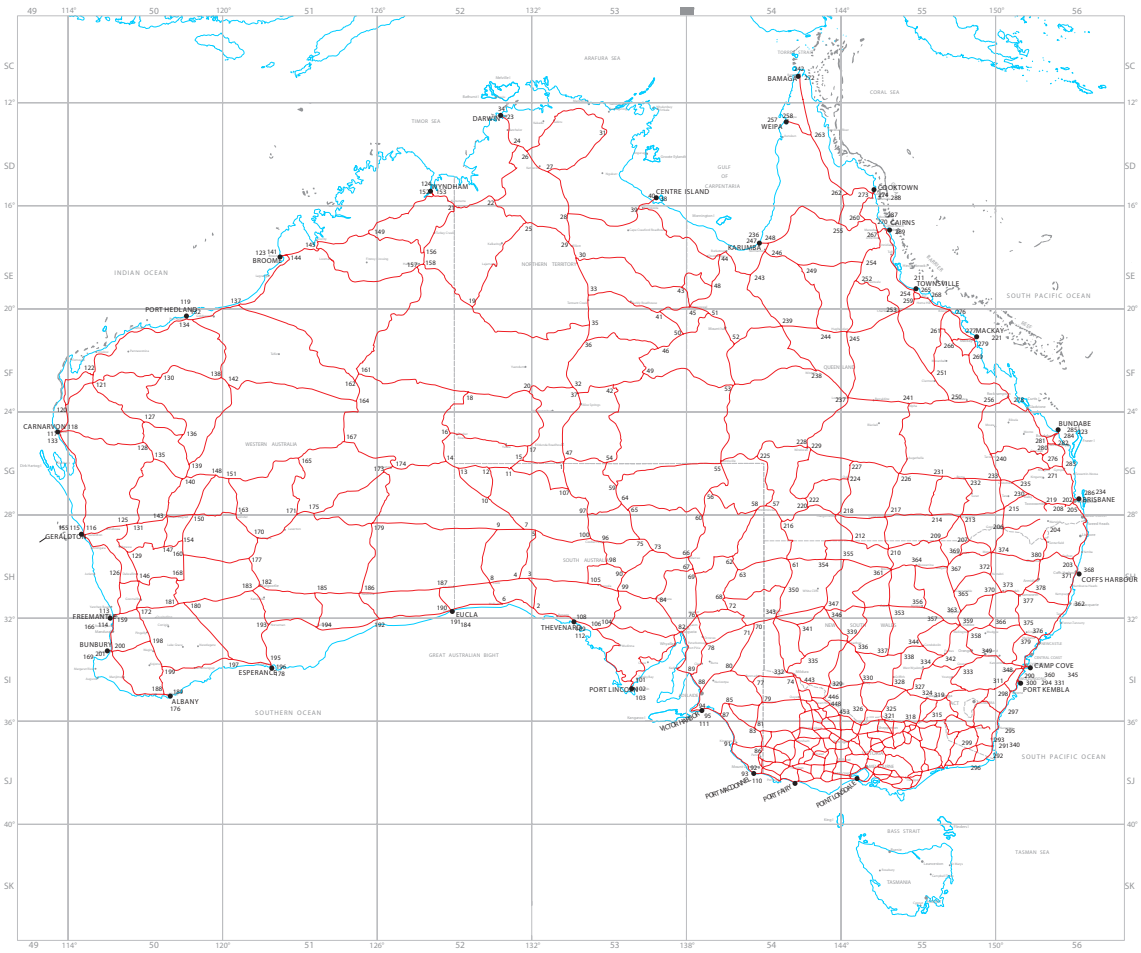

Figure 2.1: ALS primary network used for the AHD in 1971. Levelling lines are in red, and tide-gauges are black dots (cf. Figure 2.2). Image courtesy of Gary Johnston (Geoscience Australia).

2.2.2 Quality control and data preparation

It was not until 1966 that uniform national specifications for levelling were established (Roelse et al., 1971, 9). At this stage, ∼129,000 km had been levelled, much of it in remote Queensland (Qld) and Northern Territory (NT), adding to the non-uniform nature of the ALS (Mitchell, 1990, 33). The NMC (1966) standard specifications are reproduced from Roelse et al. (1971) in Table 2.2. For description of the different orders of levelling in Australia, see Sections 2.3.3 to 2.3.7 (also Figure 2.2).

Following data preparation (Roelse et al., 1971, Section 5), Rapp (1961) normal-orthometric height corrections (Section 7.2.1) were applied to 757 sections of the primary network that were then formed into 261 loops (Figure 2.1), which were checked

for above-tolerance loop closure (see Equation (2.2) and Table 2.2; Roelse et al., 1971, Annex B).

Order	Max. allowable misclose		Max. sight length	
	c (feet; d in miles)	c (mm; d in km)	feet	metres
First	0.017	4.0	132	40
Second	0.035	8.4	NA	NA
Third	0.050	12.0	300	91

Table 2.2: NMC (1966) standard specifications for levelling. From Roelse et al. (1971). Although fourth-order levelling is cited in Roelse et al. (1971), there are no defined specifications; also, there is no stated maximum sight length for second-order.

2.2.3 Least-squares adjustment of the ALS

Five regional least-squares adjustments (LSAs) were initially undertaken, as computing power was not available at that time to simultaneously adjust the entire primary network (Roelse et al., 1971, 45). A national minimally constrained LSA (MCLSA) of the five regions fixed at Johnston Origin in central Australia (25°56′55″S, 133°12′30″E; AHD height 566.300 m; Roelse et al., 1971, 16-20) was then conducted. This was followed by a second LSA of the (regionally adjusted) primary network fixed to Mean Sea Level (MSL; MSL = zero) at 30 tide-gauges around Australia (see Section 5.1.2; Figures 2.1 and 2.2), forming the AHD (Roelse et al., 1971, 48). The supplementary sections were subsequently adjusted onto the primary JPs, which were held fixed at their new AHD heights (Roelse et al., 1971, 52).

The Tasmanian levelling network was adjusted in 1983, held fixed to MSL (MSL = zero) at two Tasmanian tide-gauges (ICSM, 2006, 41; also see Figure 2.2). AHD on the Australian mainland (AHD(mainland)) is considered a separate vertical datum to the AHD in Tasmania (AHD(Tas)), as it has previously been shown that there is an offset of $\sim 0.10 - 0.30$ m between AHD(mainland) and AHD(Tas) (cf. Rizos et al., 1991; Rapp, 1994; Featherstone, 2000, 2002a). However, this is revised in Section 5.8.

2.2.4 ALS - MSL discrepancies along northern east coast of Australia

A notable feature of the MCLSA of the then-ALS was the differences with the MSL-fixed adjusted heights of the AHD (Roelse et al., 1971, Annex C; cf. Figure 2.3(b)). Neglecting the effects of sea surface topography (SSTop) at the tide-gauges contributed to much of the observed north-south separation (see Chapter 5). However, some MCLSA-AHD discrepancies exceeded estimates of sea surface slope in Australian seas (e.g., Hamon and Greig, 1972), particularly a ∼1.7 m difference between Coffs Harbour on the New South Wales coast (NSW; 30°11′S; see Figures 2.1 and 2.2 for tide-gauge location) and Bamaga at the tip of Cape York (10°54′S; Angus-Leppan, 1975).

These discrepancies remained unexplained despite numerous studies (e.g., Hamon and Greig, 1972; Angus-Leppan, 1975; Mitchell, 1973b,c; Leppert et al., 1975; Coleman et al., 1979). However, a re-levelling survey along the coast between Coffs Harbour and Cairns (16°55′S; for details of the re-levelling survey, see Morgan, 1992) identified gross errors between Rockhampton and Mackay (∼0.7 m) and between Bowen and Ayr (∼0.5 m). Both these sections had been levelled one-way (third-order) in 1962, with a second one-way (third-order) validation run in 1964 (Morgan, 1992). In addition, unexplained differences between the pre-1971 levelling and the 1975-76 re-levelling were identified by Morgan (1992), indicating systematic levelling errors (see Section 2.1.4) in either the old or new levelling (or both).

A limited re-adjustment of the AHD along the Qld coast to incorporate the new levelling (holding inland JPs fixed, rather than a full network re-adjustment; Morgan, 1992) decreased the Coffs Harbour to Bamaga MCLSA-AHD slope (Section 2.3.8; Figure 2.3), but excessively steep slopes remain in places along this coast (Figure 5.7). Holloway (1988, 20) also notes that when the new levelling was incorporated, there was little effect in the recomputed loop closures, suggesting that gross compensating errors remain within some of these loops.

2.3 The Australian National Levelling Network

The ANLN (previously ALS) digital data file (**Australia.lin**; plotted in Figure 2.2) has received some data updates since 1971 (e.g., Morgan, 1992), and an unpublished evaluation by Steed (2006) at GA. Although considered a third-order levelling network (Morgan, 1992), the ANLN comprises a number of different orders of levelling. Figure 2.2 shows the different levelling orders and their location, with the number of sections for each levelling type in Table 2.3.

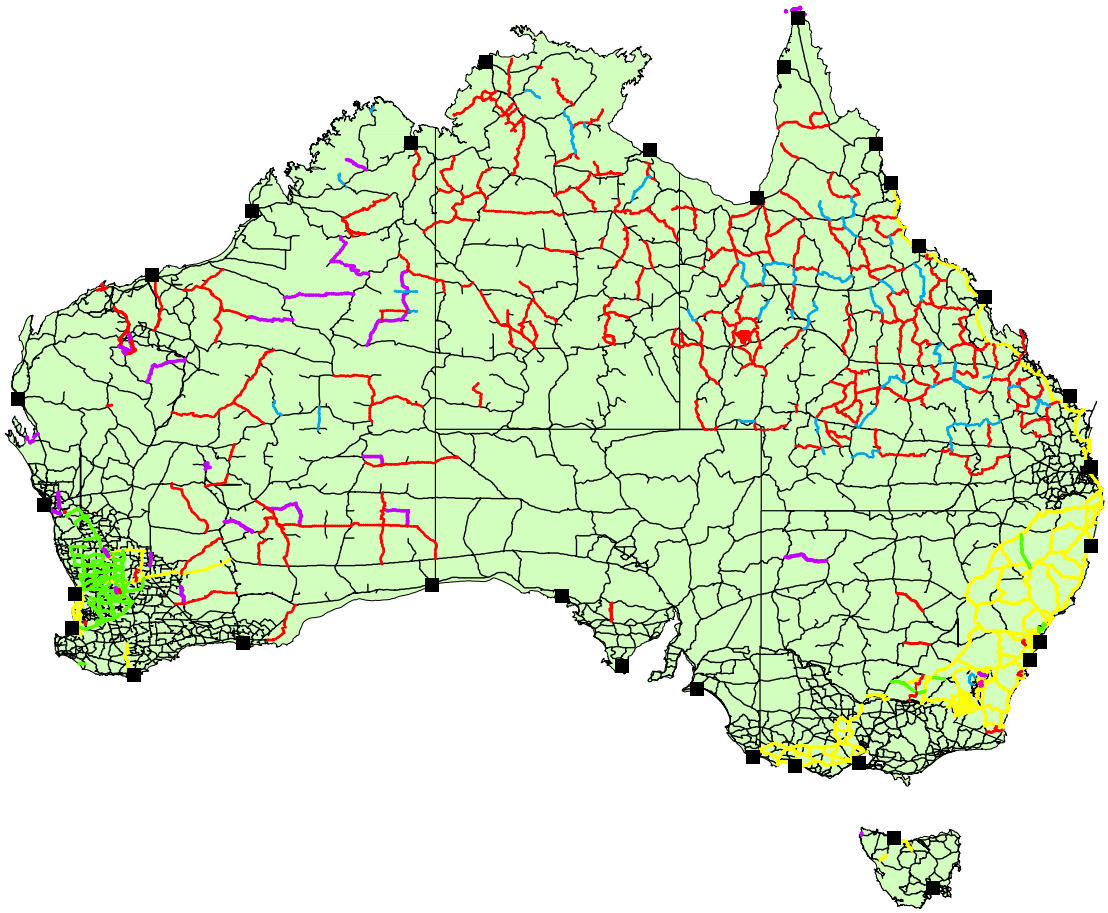

Figure 2.2: ANLN levelling sections; first-order levelling is represented by yellow, second-order is green, third-order is black, fourth-order is purple, one-way (OW) sections are red and two-way (TW; order undefined) sections are blue. AHD tide-gauges are black squares. Mercator projection. ANLN provided by Geoscience Australia.

2.3.1 Data format of the ANLN

The ANLN digital data file (hereafter simply referred to as the ANLN) holds Australian levelling information (ASCII text format) at the sub-section level. The data is arranged in individual sections, which comprises one sub-section per line, with a header record for each section. Information in the section header includes: the start and terminal JPs, the State or Territory that the section is in, section order, whether the section is part of the basic (also referred to as primary) or supplementary network and the number of records in the section. One record for each sub-section follows the section header containing (from left to right): BM name, distance from previous BM (km), observed height difference (averaged for two-way levelling), normal orthometric height correction for the sub-section, BM latitude, BM longitude, comments (often referring to location), and official AHD height. The first sub-section in each section contains the start BM (JP) and the last contains the terminal BM (JP). The file contains 94,186 records.

2.3.2 Problems with the ANLN

A number of problems have been identified in the ANLN (Figure 2.2), with respect to the currency and completeness of the data. Firstly, and most seriously, only average Δn are provided for two-way levelling sub-sections. While this is adequate for adjustment purposes, a full analysis of the levelling network requires the observed forward and backward Δn for each sub-section (cf. Section 2.1.5). This allows a better estimate of levelling precision than from loop closures (e.g., Filmer and Featherstone, 2009), and treatment of systematic errors in the network (e.g., Morgan, 1992). In addition, two-way Δn assist identification of gross levelling errors (cf. Section 2.1.5). Lack of date and time of levelling (and comments on atmospheric and ground conditions) makes the rigorous application of corrections for systematic errors such as refraction (cf. Chapter 3 and 4) or Earth tides impossible.

Uncertainty in BM position (latitude and longitude; ϕ_{BM}, λ_{BM}) is also an issue when interpolating gravity values to BMs (Section 6.5.6). ANLN BM positions are assumed to be on the Australian Geodetic Datum 1966 (AGD66; G. Holloway 2009, pers. comm.) which results in a horizontal error of ∼190 m (Section 6.5.1; Featherstone, 1995) compared to Australia's current Geocentric Datum of Australia 1994 (GDA94), which is used with AUSGeoid98 (Featherstone et al., 2001), and now AUSGeoid09 (Featherstone et al., 2011). The (systematic) ∼190 m error caused by AGD66 − GDA94 differences is subsumed by the ∼±1 km positional uncertainty of ANLN BM's caused by scaling to the nearest arc-minute (see Section 1.2.1).

Currency and completeness of the ANLN is also an issue. Steed (2006, 2) states that levelling updates made by some State and Territory authorities have not been forwarded to GA for inclusion in the ANLN. For example, a visit by the author to Land Services Group at Netley, South Australia (SA) in February 2008, revealed roughly 100 levelling sections (S. Turner 2009, pers. comm.) in hardcopy form in the Netley archives that were not in the ANLN. The value of including this additional data is highlighted by levelling loop #890 (third-order) on the Eyre Peninsula in SA that has a (well-above maximum allowable) misclosure of 0.45 m ($r_m = 0.17$ m; from Equation (2.2)). In the SA records, this loop has a misclosure well within tolerance, with a number of updated sub-sections (numerous new BMs placed), suggesting that this error has been found and corrected, or is a typographic error in the ANLN. It is likely there are numerous similar examples in other States/Territories, but this has not been verified due to the size and complexity of the task involved in searching all (hardcopy) archives, assuming they still exist.

2.3.3 First-order levelling

Details for first-order levelling in the pre-1971 ANLN can be found in Roelse et al. (1971, Annex H), with $c = 0.017$ feet (Equation (2.2); for d in miles; or converted to 4 mm when d is in km), with maximum sight length (S_ℓ) 132 feet (∼40 m; Table 2.2). First-order levelling is now referred to as class LA (ICSM, 2007, A-13), but with unchanged

c (converted to metric units) and S_ℓ (Table 2.3; ICSM, 2007, A-13), with further information on requirements found in ICSM (2007, B-8 - B-12). First-order levelling in the ANLN is confined mostly to eastern NSW and the Australian Capital Territory (ACT), along the Great Dividing Range, south western Victoria (Vic) and south west Western Australia (WA) (yellow lines in Figure 2.2). The first-order levelling along the Qld coast is the 1975-76 re-levelling survey described in Morgan (1992). However, first-order levelling in the ANLN has been found to be of a lesser precision than is expected for first-order levelling (Section 2.4.3).

ANLN Order	ICSM Class	# ANLN Sections	Steed c mm	ICSM c mm	FF c mm	ICSM S_ℓ metres
First	LA	346	4	4	4	40
Second	LB	167	8	8	8	60
Third	LC	3505	12	12	12	80
Fourth	LE	52	18	18	18	100
First OW	NA	9	12	NA	4	NA
Third OW	NA	323	36	NA	12	NA
Two-way	NA	54	36	NA	12	NA

Table 2.3: Number of ANLN sections for each ANLN order with equivalent ICSM (2007) class. Comparisons are shown among ICSM (2007), Steed (2006, Steed in table) and Filmer and Featherstone (2009, FF in table; also see Section 2.4) c (Equation (2.2)), with maximum ICSM (2007) sight length (S_ℓ). *OW* indicates one-way levelled sections.

2.3.4 Second-order levelling

There does not appear to be any second-order levelling in the pre-1971 ANLN. The only details on second-order c are given in (Roelse et al., 1971, Annex H), which give c as 0.035 feet (for d in miles; converted to 8.4 mm when d is in km; Table 2.2), but no S_ℓ is given in Roelse et al. (1971, Annex H). c is rounded to 8 mm for the equivalent ICSM (2007, A-13) class LB in (Table 2.3), with a S_ℓ of 60 m. Second-order levelling is primarily found in the south west of WA (green lines in Figure 2.2) which was re-levelled between 1981 and 1984 following several earthquakes in this region (Wellman and Tracey, 1987).

2.3.5 Third-order levelling

The ANLN comprises mostly of third-order levelling (Table 2.3; black lines in Figure 2.2), and is essentially a third-order vertical datum (Morgan, 1992), meaning that it generally complies with Australian third-order levelling precision specifications. Standards for pre-1971 third-order levelling are in Roelse et al. (1971, Annex H), and reproduced in Table 2.2, where c is 0.05 feet (for d in miles; converted to 12 mm when d is in km). S_ℓ is 300 feet, or ∼91 m. Third-order is the equivalent of class LC in ICSM (2007, B-8 - B-12), with c still 12 mm, but S_ℓ is now 80 m (Table 2.3).

2.3.6 Fourth-order levelling

Fourth-order levelling does not appear in the pre-1971 ALS (Roelse et al., 1971, Annex B5). The specifications for fourth-order levelling in Roelse et al. (1971, Annex H) do not give c or S_ℓ, suggesting that fourth-order levelling was not a well-defined levelling type at that time. The current equivalent to fourth-order levelling is class LD (ICSM, 2007, B-8 - B-12), with c = 18 mm, and S_ℓ 100 m (Table 2.3), although this can be compared to NMC (1981, 27), which allows S_ℓ of 200 m. Figure 2.2 (purple lines) shows that there are only a handful of fourth-order sections in the ANLN, mostly in the interior of WA.

2.3.7 One-way and two-way levelling

Figure 2.2 shows most one-way (OW) levelling (red lines) to be in Qld, NT and WA. A considerable amount of this levelling was done prior to 1970 (Roelse et al., 1971, Annex B5), although when compared to Figure 2.2, it appears that some have been re-levelled to form two-way third-order levelling, while some have been removed from the ANLN.

Roelse et al. (1971, 14) states that >25% of the primary network was originally levelled OW by the Department of the Interior (using automatic levels and reversible foot staves to third-order specifications; Roelse et al., 1971, 2), which was later re-levelled to form two-way levelling. The OW re-levelling adhered to specific standards for OW levelling (Roelse et al., 1971, 15), where foot-metric staves were to be used. These staves had graduations in feet on one side and metres on the other, with Δn_o (in feet) to be converted to metres for a check against Δn_o (in metres), which were required to agree to third-order r_m (Table 2.2). However, the third-order re-levelling misclosure with the original levelling only needed to be below $0.075\sqrt{d}$ feet (d in miles; $18\sqrt{d}$ mm; with d in km).

It is not clear where the levelling referred to as OW in the ANLN (Steed, 2006) has come from (cf. Roelse et al., 1971, 38); it is assumed here that it is OW third-order levelling that did not receive check levelling (to form two-way levelling). However, NMC (1981, 4) indicates that for metric-foot levelling, the feet and metre results should agree to fourth-order specification ($18\sqrt{d}$ mm; with d in km), while fourth-order loop closures for any OW levelling should not exceed $36\sqrt{d}$ mm; with d in km. The two-way levelling (TW; undefined order) specifications in the ANLN are also not stated in Steed (2006); it is assumed that these are two separate OW levelling that do not reach third-order standards (blue lines in Figure 2.2).

Assigning c to these latter two levelling orders is therefore rather problematic (cf. Sections 2.3.8 and 8.3.2). Steed (2006) assigns NMC (1981, 4) c of 36 mm for OW and TW loops. Given that Roelse et al. (1971) indicates that much of the OW levelling may be foot-metric (or reversible foot staff) levelling, which uses third-order specifications, class LC (Table 2.3) is adopted for ANLN OW levelling for the loop closure analysis in Section 2.4 (also for Filmer and Featherstone, 2009). It is acknowledged that this may be too low in some cases, due to the (probable) variable quality of the OW and TW levelling. However, $c = 36$ mm seems too high for calculating r_m for OW third-order levelling, assuming third-order observing standards were adhered to. The use of $c = 36$ mm should be considered more of an acceptance that the OW levelling contains gross errors, due to the absence of a second check levelling run (cf. Morgan, 1992), rather

than an accurate reflection of precision.

2.3.8 Differences between the AHD and a re-adjustment of the current ANLN

Comparisons are made here between LSAs of the (current) ANLN and AHD heights (cf. Roelse et al., 1971). Two LSAs of the ANLN are conducted for comparison with the AHD: i) fixed to the same 32 tide-gauges as the AHD, with MSL held at zero (partially recreating the AHD), and ii) minimally constrained (MC) at Albany tide-gauge (35°02′S, 117°53′S; for AHD(mainland)) and Hobart tide-gauge (42°52′S, 147°20′S; for AHD(Tas)), partially replicating Roelse et al. (1971, Annex C). Differences are computed at 4,247 supplementary and primary JPs.

Steed (2006) suggests *a priori* STD (1σ; σ_1 in Equation (2.1)) estimates based on c being 2σ (cf. Schomaker and Berry, 1981, 3-6) where c for each levelling order (Table 2.3) can thus be related to σ_1 by dividing by two (ICSM, 2007, A-19), so that $\sigma_1 = c/2$. However, this can be compared to Kearsley et al. (1993a), who suggest that most rejection criterion are normally 3σ (cf. Zilkoski et al., 1992) and can be divided by three (cf. Section 8.3.2; $\sigma_1 = c/3$).

The overall precision of the Roelse et al. (1971) MCLSA of the ALS was $\pm 8.1\sqrt{d}$ mm for the primary network (cf. $\pm 7\sqrt{d}$ mm from Lambert and Leppert, 1975), suggesting a scale factor of 1.481 (12/8.1; Roelse et al., 1971) to 1.714 (12/7; Lambert and Leppert, 1975) to relate c to σ_1, for the (mostly) third-order primary network. ICSM (2007) states that c is at 1σ, but this is unlikely to be correct if the maximum allowable misclosure is considered a measure defining outliers, which is usually 2σ to 3σ (cf. Teunissen, 2006c, 67).

Here, the estimates of Steed (2006) were adopted for the LSA of the ANLN in Figure 2.3, because they produced the best fit to the data in the LSA (variance factor ratio close to one, but ignoring outliers; see Section 2.4). However, the rather problematic issue of selecting *a priori* STD estimates are considered further in Section 8.4, before the final LSA. The LSA software used for this project is Survey Network Adjustment

Program (SNAP; http://www.linz.govt.nz/geodetic /software-downloads) developed at Land Information New Zealand (LINZ). Normal-orthometric height corrections from the ANLN were applied prior to the LSA in Figure 2.3.

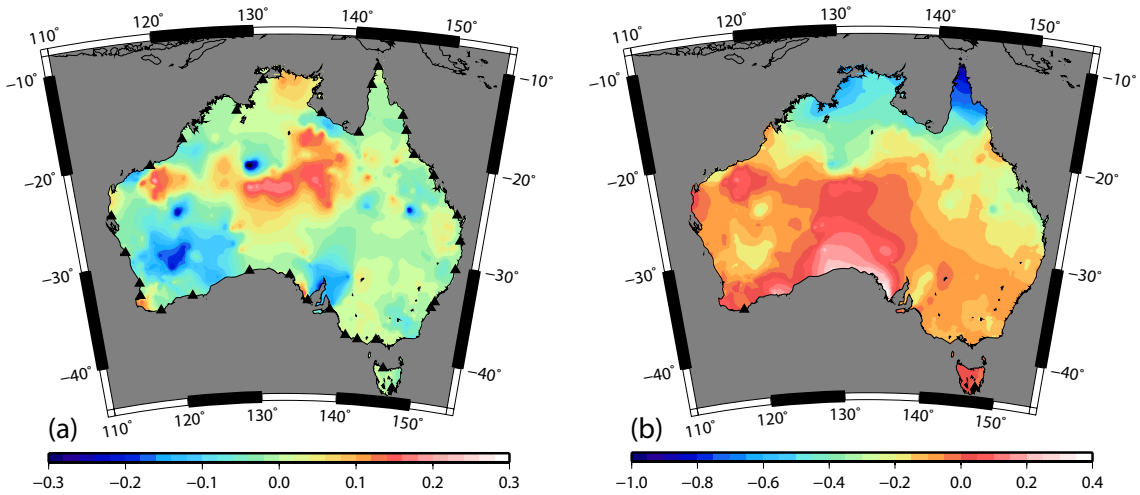

Figure 2.3: Difference between (a) AHD minus LSA ANLN fixed at 32 AHD tide-gauges to MSL (where MSL = zero); and (b) AHD minus MCLSA of the ANLN fixed at Albany tide-gauge (35°02′S, 117°53′S; mainland) and Hobart tide-gauge (42°52′S, 147°20′S; Tasmania) at 4,247 JPs. Tide-gauges are black triangles, Lambert projection, units in metres.

Differences between the AHD and the fixed LSA of the current ANLN are shown in Figure 2.3(a). AHD minus fixed LSA ANLN differences are caused by several factors. New data has been added to the ANLN since the original AHD adjustment in 1971, and although some of this has been included in the AHD (Holloway, 1988, 20), it has been incorporated through a local LSA, holding surrounding JPs fixed. The tide-gauge fixed ANLN LSA allows this new levelling to propagate further inland through the network. This is also the case for the supplementary network, which in 1971 was adjusted to fixed AHD JPs after the primary network LSA. Here, in the fixed ANLN LSA, all of the supplementary and primary network is combined in one simultaneous adjustment, compared to the staged LSA for the AHD.

Figure 2.3(b) shows differences between AHD heights and the MCLSA of the ANLN. The most prominent feature is the north-south slope (cf. Fischer, 1975), which reaches ∼1 m (see Chapter 5). The decrease in the difference between Coffs Harbour (30°11′S) and Cairns (16°55′S) from ∼1 m (Roelse et al., 1971, Annex C) to ∼0.08 m (Figure 2.3(b)) indicates the addition of the 1975-76 levelling along the Qld coast described in Morgan (1992). However, ∼0.7 m still remains between Cairns and Bamaga

(10°54′S; this section of the coast was not re-levelled in 1975-76), which is similar to that identified in (Roelse et al., 1971, Annex C).

2.4 ANLN loop closure analysis

2.4.1 Assigning order to ANLN loops

The variable quality of ANLN levelling (Table 2.3) requires a method for determining r_m for each loop so that gross errors can be identified. Although the term class is used in current specifications (ICSM, 2007), the term order will continue to be used to define levelling types, as this is the terminology used in the ANLN. Here, Equation (2.2) is used to determine r_m, where the loop closure (ε_L) must be $<r_m$, or the loop is rejected.

STD (1σ) for each loop can be estimated by rearranging Equation (2.2) to yield a value that is referred to here as 'computed' c (c_L; cf. Section 2.7). Substituting ε_L for r_m, c_L (in mm per unit km, which is propagated over distances >1 km through $\sqrt{d}$, with d in km) is considered a similar value to σ_1 (Equation (2.1)), but derived from ANLN levelling loops as

$$c_L = \frac{\varepsilon_L}{\sqrt{d}} \tag{2.3}$$

where ε_L is the ANLN levelling loop misclosure (cf. Equation (2.8)).

The values for c adopted for first- to fourth-order levelling to determine whether a loop is $<r_m$, are those of Filmer and Featherstone (2009, FF c in Table 2.3), and are the same for class LA to LD in ICSM (2007). Assignment of order (and thus c) to each loop is rather problematic. A simple solution was used, where the order of a loop is defined by the lowest quality levelling order contained within that loop. Thus, for a loop to be assigned first-order, the entire loop must comprise first-order levelling. However, this solution may cause c_L to be over-optimistic, because, for example, loops defined as OW may contain a large proportion of third-order (or better) levelling, which will improve c_L for that particular loop (cf. Table 2.4). Figure 2.2 shows that there are numerous loops comprising just third-order levelling, with a handful of first-order and

second-order loops, but there are many mixed loops.

A FORTRAN95 script was written to reformat the ANLN into 1,366 unique loops (Figure 2.2) comprising 126 primary and 1,240 supplementary loops, then compute ε_L and determine if $\varepsilon_L < r$. c_L for each loop was also evaluated in this program. Primary loops are defined in this analysis as original loops from the 1971 primary network LSA (Roelse et al., 1971, 261 loops; Annex B1-B3) that exist unaltered in the ANLN, with supplementary loops being any loops that fully or partially comprise supplementary levelling. Some very small loops were excluded (mostly in the Brisbane (Qld) metropolitan area) because they would not significantly contribute to the results, but were time consuming to include, due to numerous sub-km sections.

Considerable manual preparatory work was required for the computation. The loops were allocated a unique identifier, and a control file was built to hold JPs for each loop in the correct sequence to sum the section in the correct direction (all summed clockwise) to yield loop closures.

2.4.2 Results of loop closure analysis

Table 2.4 shows that 117 of the 1,366 loops (8.6%) comprising the ANLN were rejected using Equation (2.2) with c from Filmer and Featherstone (2009) (FF in Table 2.4). This is broken down into the different levelling orders, with low rejection percentages for second-order loops (5.0%), third-order loops (3.1%), and fourth-order loops (2.7%) compared to first-order loops (14.3%), third-order OW (27.7%), TW (37.5%), and third-order OW/fourth-order combined loops (21.4%). c_L (Equation (2.3)) for all 1,366 loops is ±5.2 mm (Table 2.4) which is less than ±7 mm for Lambert and Leppert (1975) and ±8.1 mm for Roelse et al. (1971), although these latter estimates only include the primary network.

Figure 2.4 indicates that c_L are not normally distributed. This supports Morgan (1992) in his analysis of the 1975-76 first-order re-levelling along the north eastern coast of Australia, where subsection closures of these observations were also found to not be

normally distributed. Morgan (1992) suggested that the 1975 re-levelling misclosures were best represented by Weibull (Weibull, 1951) or triangular distributions, which strongly resemble Figure 2.4. Maximum ε_L for the ANLN analysis was 0.93 m (loop #826; on the WA-NT border), with the STD of all ε_L ∼0.14 m (loop misclosures are normally distributed).

Loop order	# Loops	Rejected	% Rej.	FF c	c_L
All	1366	117	8.6	-	5.217
First	56	8	14.3	4	2.431
Second	20	1	5.0	8	2.831
Third	975	30	3.1	12	4.222
Fourth	37	1	2.7	18	6.321
Third OW	256	71	27.7	12	9.201
Two-way	8	3	37.5	12	10.649
Third OW/Fourth	14	3	21.4	18	10.178

Table 2.4: Analysis of ANLN loops. FF c is used for loop closures in Filmer and Featherstone (2009). Units for c and c_L are mm.

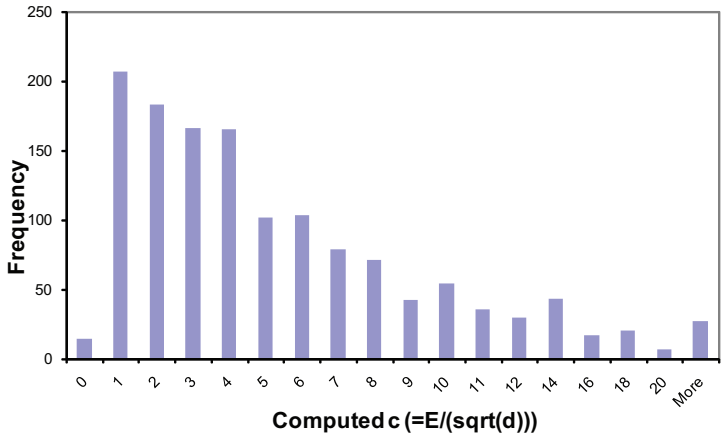

Figure 2.4: Histogram of c_L (computed c in the graph; in mm) for the ANLN loop analysis.

2.4.3 Discussion of results

Second-, third- and fourth-order c_L (Table 2.4) support the assumption of Kearsley et al. (1993a) that c is 3σ, because dividing c by c_L gives scale factors of 2.826 (second-order), 2.842 (third-order), and 2.848 (fourth-order), which are closer to three than two (cf. Section 8.3.2; Steed, 2006). Comparisons of MCLSAs of the ANLN using the different scale factors indicate a height difference of ∼0.30 m between MCLSAs

using Steed's (2006) scale factor of two and the empirically derived c_L in Table 2.4, with differences of $\sim$0.05$-$0.10 m between MCLSAs using c_L and STD derived from $c/3$. However, first-order c_L (2.431 mm) suggests that some of this levelling is not to first-order standard (cf. Section 2.3.3). Assuming the same scale factor of 2.8 between first-order c and c_L as for second-, third- and fourth-order, first-order c_L should be 1.429 mm, which is considerably less than the first-order c_L obtained from the ANLN (cf. Table 8.1). TW and third-order OW/fourth-order loops are small samples that may not provide meaningful results and are therefore not discussed.

The high rejection rate and high c_L for the third-order OW and TW loops are prominent in Table 2.4, suggesting that using $c = 12$ mm may be too small. However, many OW and TW loops comprise a large proportion of third-order levelling, indicating that the high c_L for OW and TW loops is caused by gross levelling errors (cf. Morgan, 1992), rather than very low precision in the observations. This hypothesis is supported by an examination of the magnitude of third-order OW loop misclosures. Arbitrarily adopting $c = 20$ mm (considered a large misclosure e.g., 0.45 m misclose for a 500 km loop compared to 0.27 m for $c = 12$ mm), 29 third-order OW loops were rejected (11.3%), but only one third-order loop was rejected. This reflects the lack of checks in the OW levelling.

2.5 Detecting gross levelling errors in the ANLN using GNSS and a gravimetric quasigeoid

Although above-tolerance loop closures were identified in Section 2.4, the specific section in the loop containing the error is not uniquely identified. To isolate the problem section, redundant observations are required (cf. Section 8.4). Since additional levelling is not available at this time (Section 2.3.2), height differences derived from GNSS (where available) and AG98 are used here as pseudo-observations to add redundancy that assists in the identification of problem sections. Isolating sections containing gross errors assist State and Territory geodetic agencies to locate and correct these errors.

2.5.1 GNSS levelling

GNSS has introduced an alternative method to differential levelling for measuring Δn (e.g., Kearsley, 1988; Gilliland, 1986; Mitchell, 1988, 1990; Featherstone et al., 1998; Collier and Croft, 1997a,b; Macleod et al., 1988; Stewart, 1998). However, GNSS heights are measured above the ellipsoid (along the straight ellipsoidal normal; see Section 7.1.1), and do not have any physical meaning (so cannot determine the direction of unrestricted fluid flow). GNSS-derived ellipsoidal heights (h) are transformed to physical heights through the geoid height (N), which is the separation between the geoid and ellipsoid (realising orthometric heights; H^O) or the height anomaly (ζ), which is the separation between the quasigeoid and ellipsoid (realising normal heights; H^N; see Figure 7.1).

N is provided by a gravimetric geoid model (e.g., Marti and Schlatter, 2002), while ζ is realised from a gravimetric quasigeoid model (e.g., Featherstone et al., 2011). To transform h to H^N,

$$H^N = h - \zeta \tag{2.4}$$

To determine the normal height difference ΔH^N, which is equivalent to spirit-levelled height differences (Section 2.1.1) with the normal correction applied (NC; Section 7.6; Molodensky et al., 1962), Equation (2.4) becomes (cf. Kearsley, 1988)

$$\Delta H^N = \Delta h - \Delta\zeta \tag{2.5}$$

where Δh is the ellipsoidal height difference between BM1 and BM2, and $\Delta\zeta$ is the difference between the height anomaly at BM1 and BM2.

Although the AHD is a normal-orthometric height system (e.g., Holloway, 1988), ζ is a reasonable approximation (to <30 mm over most of Australia) to transform h to normal-orthometric heights ($H^{N\text{-}O}$; cf. Filmer et al., 2010). Thus, the quasigeoid model AG98 (see Section 2.5.3) can be used to compute approximate normal-orthometric height differences $\Delta H^{N\text{-}O}$, using Equation (2.5).

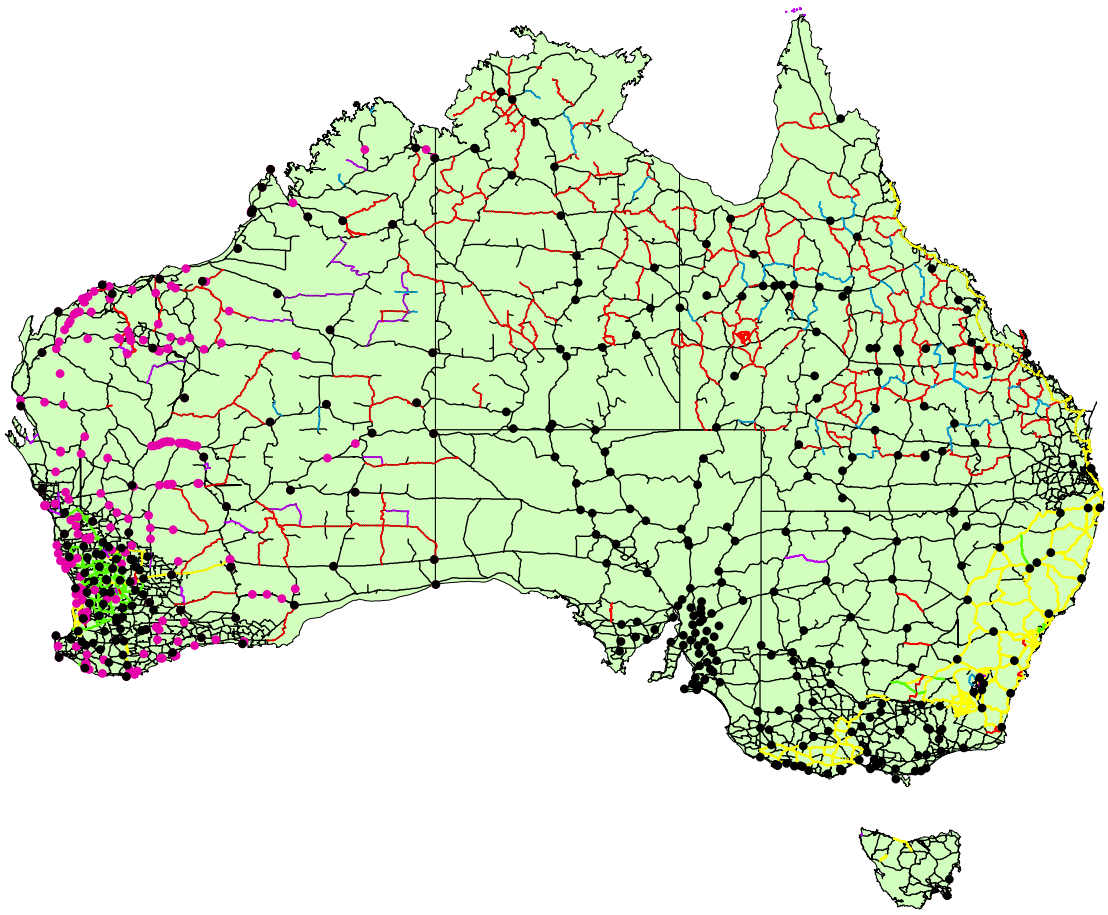

Figure 2.5: 3D GNSS coordinates used in GNSS-levelling loops for this study. 354 GNSS points processed in ITRF2000 from GA are shown as solid black circles, and 243 GNSS points processed in ITRF2005 from Landgate are shown as solid pink circles, plotted with the ANLN (cf. Figure 2.2).

2.5.2 GNSS data used

The GNSS data set used for this study is combined from several different sources; 354 3D GNSS coordinates from GA (G. Johnston 2007, pers. comm.), and 243 WA 3D GNSS coordinates from Landgate (L. Morgan 2007, pers. comm.). A total of 586 GNSS-derived h were available after 11 duplicate points were removed (Figure 2.5). Most of the 354 GA 3D GNSS coordinates are in ITRF2000 (Altamimi et al., 2002) at epoch 2000 (although this information is not provided for all points; Steed, 2006), with the 243 3D GNSS coordinates from Landgate processed using Bernese v5.0 software (Dach et al., 2007) in ITRF2005 (Altamimi et al., 2007) at epoch 2000 (Hu, 2007). An updated set of GNSS data in ITRF2005 became available after this study was completed (used for the final combined adjustment in Chapter 8; Section 8.2), but

were not used to repeat this experiment.

The 243 WA points have a mean precision for heights (1σ) of $\sim$20 mm, (Featherstone and Filmer, 2008), while Luton (2000) reported the precision (preliminary results) for the 1999/2000 GNSS tide-gauge survey to be generally better than 20 mm. Stewart (1998) suggests the estimated mean error of the WA STATEFIX network (Stewart et al., 1997) is smaller than the $\pm$50 mm quoted error (95% confidence) for the Australian National GPS Network (ANN), with $\pm$35 mm considered a more likely value. However, the small vertical bias between ITRF2000 and ITRF2005 points will introduce further uncertainty, although this will amount to only a few cm for points processed at epoch 2000.0, because ITRF2000 and and ITRF2005 are very closely aligned at this epoch (Altamimi et al., 2007). In addition, this difference will only occur when ITRF2000 and ITRF2005 points are used in the same baseline.

Taking these various estimates into account, absolute mean h error (σ_h; 1σ) of 30 mm for all GNSS points is assumed. From this absolute estimate, the relative error for Δh ($\sigma_{\Delta h}$; 1σ) can be approximated (because correlation information is not available) using the linear propagation of variances (e.g., Lyons, 1991)

$$\sigma_{\Delta h} = \sqrt{\sigma_{\Delta h_1}^2 + \sigma_{\Delta h_2}^2} \tag{2.6}$$

where $\sigma_{\Delta h_1}$ and $\sigma_{\Delta h_2}$ are $\sigma_{\Delta h}$ at BM1 and BM2 respectively. Assuming constant σ_h of 30 mm, $\sigma_{\Delta h}$ is 42 mm.

2.5.3 AUSGeoid98

AUSGeoid98 has been the standard quasigeoid model for (approximate) transformation of GNSS h to the AHD in Australia (Featherstone, 2008), although since the time of this study, it has been superseded by AUSGeoid09 (Featherstone et al., 2011). AG98 ζ (ζ_{AG98}) were computed at all 586 GNSS sites using GA's online 'compute an N-value service' (http://www.ga.gov.au/geodesy/ausgeoid/nvalcomp.jsp), which is based on GA's **Winter** interpolation software. **Winter** uses bi-cubic interpolation from the AG98 2 $\times$ 2 arc-minute grid (cf. Featherstone, 2001).

Estimating errors for AG98 is more difficult than for h; Featherstone and Filmer (2008) cautiously 'guesstimate' an absolute error of $\sim$0.10$-$0.20 m, but it is possible that this value is exceeded in certain areas. Featherstone and Guo (2001) develop an approximate method to estimate relative AG98 ($\Delta\zeta_{AG98}$) errors based on the general equation for an asymptotic function. Least-squares regression were used to determine the constants in the equation (Featherstone and Guo, 2001)

$$ppm = \frac{13.539}{(km)^{0.6261}} \tag{2.7}$$

where ppm is mean relative AG98 error (mm/km) and km is the distance over which the relative error is computed. Equation (2.7) is used to compute relative errors for $\Delta\zeta_{AG98}$ over specified distances (Table 2.5), which provides an estimate of the AG98 error budget for a baseline between two GNSS stations.

km	ppm	$\varepsilon_{\Delta\zeta}$ (m)
100	0.76	0.076
500	0.28	0.138
1000	0.18	0.179
1500	0.14	0.209
2000	0.12	0.232

Table 2.5: Relative AG98 error estimates (from Equation (2.7)). ppm is relative error in mm/km, and $\varepsilon_{\Delta\zeta}$ is ppm over different distances (km).

Table 2.5 shows that for baselines of 1,000 km between two GNSS stations, $\Delta\zeta_{AG98}$ error is $\sim$0.18 m, decreasing to $\sim$0.14 m over 500 km. The relative Δh error estimate of 42 mm (Equation (2.6)) can be added to the $\Delta\zeta_{AG98}$ error estimate, providing an indication of combined (Δh and $\Delta\zeta_{AG98}$) baseline error. However, the numerical derivation of Equation (2.7) uses 1013 Australian GNSS/AHD points, some of which have since been found to be derived h from AHD heights and a geoid model, not observed h (Claessens et al., 2009). In addition, Equation (2.7) has been derived from the fit of these 1013 GNSS points to the AHD, so errors in the distortions in the AHD (e.g., Filmer and Featherstone, 2009), will also affect the estimates in Table 2.5. Therefore, although these are the best error estimates for AG98 available at the time of the study, it is acknowledged that they should be treated with some caution. However, the relative AG98 error estimates are only used to crudely test the significance of GNSS-AG98-ANLN loop closures, so more rigorous error estimates are not justified.

2.6 Method for identifying errors in the ANLN using GNSS and AG98

Here, a methodology is described that attempts to identify errors in the ANLN using $h - \zeta_{AG98}$ (referred to here as H_{AG98}) as pseudo-observations (cf. Poutanen, 1999). This adds redundancy to existing ANLN levelling sections and partially overcomes the problem of the ANLN having average Δn for each sub-section, rather than the two-way levelling runs. However, this method assumes that $\Delta h - \Delta\zeta_{AG98}$ (ΔH_{AG98}) baselines are more accurate than the levelled Δn against which they are compared. The error estimates in Table 2.5, will therefore be used as a guide to indicate the significance of the misclosures between H_{AG98} and levelled Δn.

Re-arranging Equation (2.5) gives

$$\varepsilon_{GL} = (\Delta h - \Delta\zeta_{AG98}) - \Delta n \tag{2.8}$$

where ε_{GL} is the residual misclosure for the GNSS-ANLN loop defined by the ΔH_{AG98} pseudo-observation between BM1 and BM2 and levelled Δn (usually multiple ANLN sections) between BM1 and BM2.

2.6.1 GNSS-ANLN levelling connections

Levelled connections between the GNSS stations and the ANLN JPs were necessary to compute the misclose between ΔH_{AG98} and Δn. State and Territory geodetic agencies (responsible for GNSS observations and levelling Δn connection to ANLN JPs) provided GA with the reduced AHD height of the GNSS station, rather than the two-way levelling observations used to compute the AHD height. However, a single height (rather than two-way observed Δn) is susceptible to transcription or reduction errors during processing (e.g., Section 2.7.2), which cannot be checked without the original levelling observations.

Of the 430 GNSS stations used in this study, 84 were co-located on the ANLN JP which makes a levelled connection unnecessary, which is the preferred situation. These co-located GNSS/ANLN JPs are mostly in the eastern states, particularly Qld. Very few

co-located GNSS/ANLN JPs exist in WA due to the large size of the State, as the practice is to observe the closest BM (L. Morgan 2007, pers. comm.). No distances were provided for the GNSS-ANLN JP connections or between the two GNSS stations (needed for c_{GL}; computed c for GNSS-ANLN loops), so the distance was computed using GA's approximate ellipsoidal distance formula (http://www.ga.gov.au/geodesy/datums/ distance.jsp#spheroidal), which approximates the distance along the geodesic.

The approximate ellipsoidal formula used here is accurate to ∼1 km at the maximum distance between GNSS stations of 813 km (Table 2.6), or accurate to ∼200 m at the average distance between GNSS stations of 172 km (see error estimates at http://www.ga.gov.au/geodesy/datums/distance.jsp#spheroidal). Assuming a distance error of ∼1 km in the largest GNSS-ANLN loop (1,743 km; Table 2.6), would cause an error in the maximum allowable misclosure for GNSS-ANLN loops ($r_{m_{GL}}$; for third-order; $12\sqrt{d}$) of 0.14 mm. Here, an error in $r_{m_{GL}}$ for the GNSS-ANLN loop (to determine whether the loop is rejected) of <1 mm is negligible, justifying the choice of an approximate formula.

2.6.2 GNSS-ANLN loops

GNSS-ANLN loops were formed from a single ΔH_{AG98}, and connected ANLN levelling sections. GNSS-ANLN loops were generally formed onto ANLN levelling loops where $\varepsilon_L > r_m$, so that the ANLN section with the error could be identified. However, the existing location of the GNSS points determine the GNSS-ANLN loop location, so many ANLN loops with large misclosures could not be investigated effectively because there were insufficient well-located GNSS points. An additional 313 GNSS-ANLN loops were formed, adding redundancy (increase loop numbers by 23%) to the existing levelling-only network.

Statistics for the GNSS-GNSS station and GNSS-ANLN JP connection Δn and distances are shown in Table 2.6. The estimated error for $\Delta\zeta_{AG98}$ (for mean distance GNSS-GNSS of 172 km; using Table 2.5) is around 93 mm, which combined with the GNSS relative error (42 mm; Equation (2.6)) is 102 mm ($\sqrt{93^2 + 42^2}$). The maximum

GNSS-ANLN connection is 187.9 km, but the mean is 12.9 km (co-located GNSS BMs removed), with the minimum 0.0 km (not a co-located point, caused by ∼1 arc-minute uncertainty in BM position).

Statistic	GNSS-GNSS		GNSS-ANLN	
	Δh (m)	Distance (km)	Δn (m)	Distance (km)
Max	1824.000	812.6	300.367	187.9
Min	−1542.960	19.1	−594.705	0.0
Mean	−1.287	172.2	−43.902	12.9

Table 2.6: Height differences and distances between GNSS stations (GNSS-GNSS) and connections between GNSS stations and ANLN JPs (GNSS-ANLN) used in GNSS-ANLN loops.

2.7 Results of GNSS-ANLN loop analysis

Third-order r_m ($12\sqrt{d}$) was used to determine above-tolerance GNSS-ANLN loops. This found 90 rejected GNSS-ANLN loops (28.8%), but it should be remembered that GNSS-ANLN loops were deliberately formed in areas where there were known to be problems in the ANLN. Table 2.7 shows the GNSS-ANLN loop statistics. The maximum and minimum loop misclosures indicate the largest errors to be around 1 m. The direction of loop summation was not consistent (cf. clockwise summation of ANLN loops) due to the irregular GNSS-ANLN loop shapes where the ANLN section and GNSS baseline would often intersect each other. Therefore, the sign of mean, maximum and minimum ε_L should not be considered significant.

Stat	ε_{GL} (m)	d (km)	Third-order r_m (m)	c_{GL} (mm)
Min	−0.887	44.2	0.080	0.0
Max	1.245	1743.1	0.501	46.9
Mean	0.024	498.1	0.268	9.6
STD	±0.303	-	-	-

Table 2.7: Statistics for GNSS-ANLN loops. Third-order r_m is maximum allowable misclose for minimum, maximum and mean GNSS-ANLN loop distance in metres. GNSS-ANLN loop distance and c_{GL} are not normally distributed, so STD is only given for misclose (ε_{GL}).

The STD of the GNSS-ANLN loop misclosures (the misclosures are normally distributed) is ±0.30 m (cf. ∼0.14 m for ANLN loops). The average c_{GL} is 9.6 mm (cf. Table 2.4), indicating that although there were many loops rejected at third-order level, there were numerous GNSS-ANLN loops with small misclosures. Like the ANLN loops, c_{GL} are not normally distributed (cf. Figure 2.4; Morgan, 1992) so STD is not shown.

The maximum c_{GL} is 46.9 mm (Table 2.7) indicating the presence of a gross error (or errors) in this ANLN levelling section (loop 3171; NT). Loop 3171 contains a large proportion of OW levelling, with loop 3172 (c_{GL} = 46.9 mm) adjoining it along three OW sections. Here, there is considerable evidence that a gross levelling error (field or office) is located in one of these three OW sections. There are 34 GNSS-ANLN loops (10.9%) with c_{GL} >20 mm, which was suggested in Section 2.4.3 as a threshold for a large gross levelling error.

2.7.1 Case studies of error detection using GNSS-ANLN loops

ANLN loop 821 (Figure 2.6(a)) has ε_{GL} of 0.45 m, a loop distance of 1,202 km and c_{GL} is 13.1 mm. Three GNSS stations (6172, 6062, 6712) are reasonably evenly distributed around the loop, allowing three GNSS-ANLN loops to be formed (Table 2.8). Two loops (3069; 3070) reveal very low c_{GL} (<1.0 mm), but one has c_{GL} of 20.9 mm (misclose 0.46 m), strongly indicating the gross levelling error to be between ANLN JPs 165 and 167.

Figure 2.6(b) shows ANLN loop 54 (ε_{GL} is 0.33 m; d is 895 km; c_{GL} is ∼11 mm), which has GNSS points located at each ANLN JP, so has good redundancy to identify ANLN sections containing errors. Table 2.8 provides details of the seven GNSS-ANLN loops formed along the perimeter of ANLN loop 54. Only one GNSS-ANLN loop has ε_{GL} greater than third-order r_m (GNSS-ANLN loop 3103; c_{GL} = 30.8 mm) indicating a large error in the ANLN section between JPs 54 and 59. All other GNSS-ANLN c_{GL} were <12 mm, although there were several with c_{GL} >8 mm, indicating either 'noisy' levelling observations, systematic errors (e.g., refraction or staff settlement;

Section 2.1.4), or lower-magnitude blunders (or $\Delta\zeta_{AG98}$ and/or Δh errors).

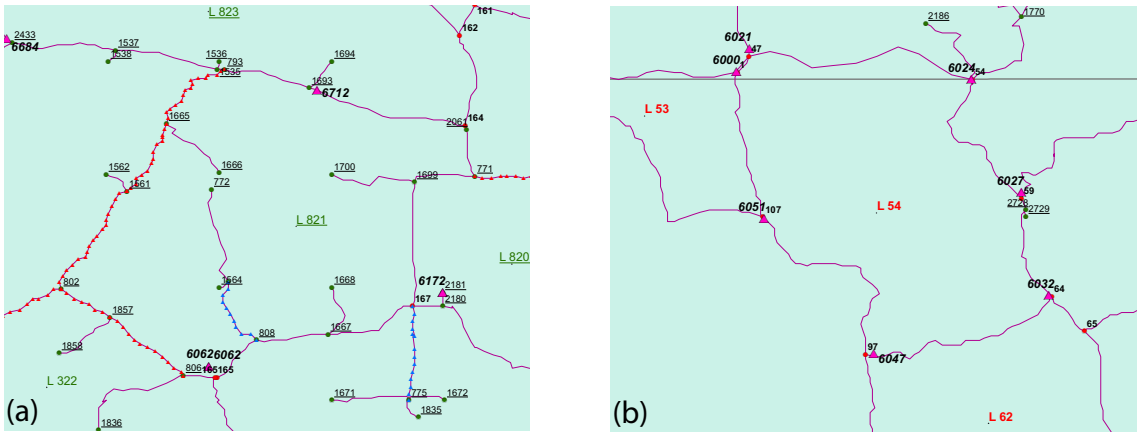

Figure 2.6: Supplementary loop 821 (a) in central WA and basic loop 54 (b), on the SA-NT border. The GPS JPs are pink triangles, numbered in bold italic black (6000 range), the ANLN basic JPs are red circles (numbered in black), the ANLN supplementary green circles (numbered in underlined black). The supplementary loop numbers are in green, basic in red.

ANLN Loop #	GNSS/ANLN Loop #	From GNSS	To GNSS	d (km)	ε_{GL} (m)	c_{GL} (mm)
54	3103	6024	6027	232	0.47	30.8
54	3104	6027	6032	178	-0.05	3.7
54	3105	6032	6047	300	-0.09	5.2
54	3106	6047	6051	326	0.15	8.3
54	3107	6051	6000	248	0.10	6.4
54	3108	6000	6021	44	-0.06	9.0
54	3109	6021	6024	355	-0.18	9.6
821	3068	6172	6062	484	-0.46	20.9
821	3069	6062	6712	914	-0.02	0.7
821	3070	6712	6172	664	0.02	0.8

Table 2.8: GNSS-ANLN loop statistics for ANLN loop 54 and 821 (Figure 2.6). Large GNSS-ANLN loop c_{GL} and ε_{GL} indicates gross errors in the ANLN levelling section.

2.7.2 Discussion of GNSS-ANLN loop misclosures

There are numerous more case studies than those shown here. Some clearly identify the ANLN levelling section in error, but others are inconclusive. The disadvantages of this technique are the reliance on AG98 errors being small, and the location of the existing GNSS observations. In areas where GNSS points are sparse, multiple ANLN sections are required to form a GNSS-ANLN loop, so that even when a large error

is identified, the specific section cannot be determined. However, the availability of new data sets (e.g., ∼1,000 GNSS points processed in ITRF2005, N. Brown 2009, pers. comm.; AGQG09, Featherstone et al., 2011) may improve the results from this method.

The capabilities of this method (using 586 mostly ITRF2000 GNSS points and AG98) is highlighted by the example where a 1 m error in the AHD height of the Karratha GNSS site (∼117°06′S, ∼20°59′; north west WA) was detected. The misclose was traced back to a typographic error in the GA MS Excel spreadsheet used to hold the GNSS data. If two-way levelling connections between GNSS sites and ANLN JPs were provided, rather than a single AHD height at the GNSS site, this error could have been identified more easily. Furthermore, it demonstrates that this technique can only be effective if the levelling connections between GNSS sites and ANLN JPs are correct (smaller connection errors may not be identified by this method).

Based on this study, four major recommendations are made, which would result in a complete update of the ANLN:

1. A national audit of existing levelling observations held by State and Territory geodetic agencies that are not currently in the ANLN (including corrections to existing ANLN data), should be conducted. This would identify how much data is available and the time and funding required to manually enter the data (probably all in hardcopy form) into the ANLN file (**Australia.lin**);

2. All levelling observations connecting the ANLN to GNSS points need to be entered into the ANLN. Ideally, all future GNSS observations should be on JPs;

3. Two-way levelling observations (if available) should be entered into the ANLN to replace the average of the two-way height differences that are currently in the ANLN. Additional metadata such as date and time of observations should also be entered into the ANLN (an investigation into the availability of this information could be conducted with the audit described in 1.);

4. All suspected gross errors detected in this study should be investigated by State and Territory geodetic agencies, firstly by examining field books to identify whether errors are caused by transcription mistakes, and if not found to be office errors, then field investigation should follow.

Note that it is not possible for gross errors to be removed as per point 4 for this project, because it is a large task and is the responsibility of the appropriate State and Territory geodetic agencies.

2.8 Summary

This Chapter begins with a brief review of levelling methods, instruments and errors, leading to a description of the AHD and the data and processes used in its realisation. The vast distances levelled across Australia have resulted in lower-quality levelling than is preferable (also due to the NMC's urgent requirements for heights across Australia), which have led to problems such as a large discrepancy with SSTop along the NSW-Qld coast that was only partially resolved by the discovery of gross levelling errors. The ANLN in its current form is plagued by a number of problems that need addressing, most notably the currency and completeness of the levelling data, and the uncertainty of horizontal BM locations.

Minimally and fully constrained LSAs of the ANLN reveal differences to the AHD that can most likely be attributed to the addition of new levelling data, different adjustment strategies and a north-south slope apparently caused by using MSL constraints in the AHD (cf. Chapter 5). A loop closure-based analysis of the ANLN indicated that although much of the ANLN is broadly satisfactory to third-order standards, numerous gross errors exist in the network ($\sim$100 identified). These could be transcription errors made when processing or entering data into electronic files, or field errors made during the survey. The loop closure analysis identifies loops with above-tolerance misclosure, but redundant observations provided by GNSS observations and AG98 are able to detect errors in individual levelling sections if sufficient well-placed GNSS points are

available. Four main recommendations are made that would result in the full update of the ANLN, but these would require significant input from all State and Territory geodetic agencies. Some of these results in this Chapter have been published in the Australian Journal of Earth Sciences (Filmer and Featherstone, 2009)

3. REVIEW OF REFRACTION CORRECTIONS AND SENSITIVITY ANALYSIS OF ANGUS-LEPPAN'S EQUATIONS

Atmospheric refraction is a major source of systematic error in geodetic levelling (e.g., Bomford, 1971, 240). Although procedures were in place to minimise refraction effects in the Australian Levelling Survey (ALS) (e.g., minimum staff reading of 0.3 m; Roelse et al., 1971, Annex H) refraction corrections (*RC*s) were never applied to the ALS prior to the realisation of the AHD. ICSM (2007) requires temperature to be taken for class LA, LB and LC levelling (equivalent to first- second- and third-order), but does not require *RC*s to be applied. An investigation into the effects of not applying *RC*s to the ANLN is thus warranted.

This Chapter first lists different *RC*s available, presents and reviews *RC*s most relevant to the ANLN, then conducts a sensitivity analysis on the Angus-Leppan (1979) *RC* ($RC_{A\text{-}L}$), which could be applied retrospectively to the ANLN. However, the current ANLN file **Australia.lin** does not contain the information required to apply the $RC_{A\text{-}L}$ (date and time of observation; atmospheric and ground conditions) because this information was either never collected, or not transferred from field books to **Australia.lin**. Thus, a simulation of the effects of refraction on the ANLN (and subsequently the AHD) is conducted in Chapter 4 using assumed survey and meteorological information (cf. Holdahl, 1981).

3.1 Atmospheric refraction error in levelling

The line of sight through the atmosphere of an optical levelling observation can deviate from a straight line due to changes in the vertical gradient of the refractive index ($d\mathrm{n}_r/dz$; n_r is the refractive index) close to the heated ground surface (Shaw and Smietana, 1983). $d\mathrm{n}_r/dz$ is assumed to be the same at the back-sight (BS) and fore-

sight (FS), resulting in stratified temperature layers roughly parallel to the Earth's topographic surface. Figure 3.1 shows the dashed (straight) line of sight from the telescope to the staves as the true staff reading, with the solid (curved) line from the telescope to the staves representing the refraction contaminated staff reading actually observed. The difference between the true and observed staff reading is the refraction error.

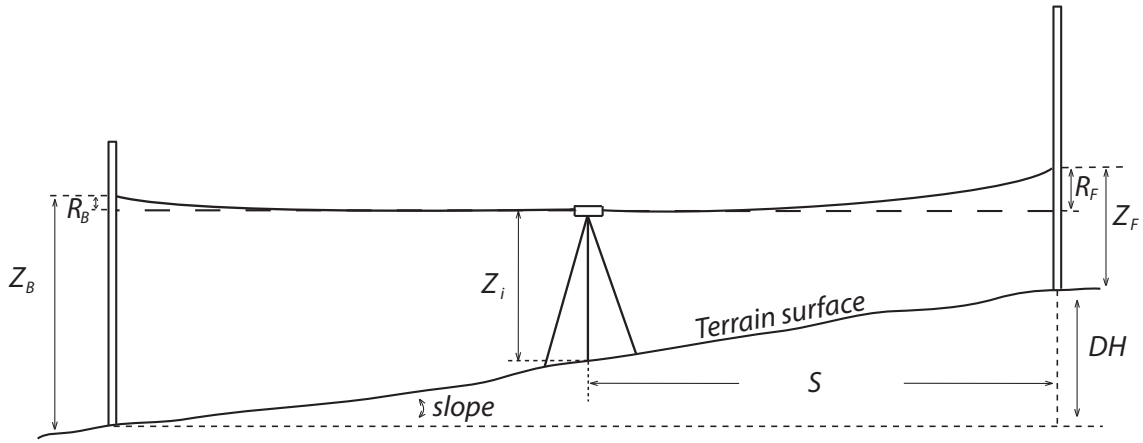

Figure 3.1: Levelling setup on a slope (instrument positioned mid-way between the FS and BS staves) illustrating the effects of unequal refraction error (URE) (exaggerated for illustrative purposes). R_F is the FS refraction error and R_B the BS refraction error. Slope is the gradient of the terrain along the levelling line, Z_i is the instrument height, Z_F the FS and Z_B the BS staff reading (contaminated by refraction), DH the height difference (ΔH) between staves and S_ℓ is the sight length (S in diagram).

3.1.1 Unequal refraction error (URE)

FS refraction error (R_F) will be equal to the BS refraction error (R_B; cf. Figure 3.1) when levelling on flat ground, as both BS and FS observations are parallel to the ground and assumed to be influenced by the same $d\mathrm{n}_r/dz$. However, when levelling up- or down-hill, the effects do not cancel (Bomford, 1971, 240), as the BS and FS observations pass through air with different $d\mathrm{n}_r/dz$, so that R_F is larger than R_B (Figure 3.1), resulting in unequal refraction error (URE; Mark et al., 1987). The magnitude of the imbalance between R_F and R_B depends on a number of parameters, particularly sight length (S_ℓ), terrain slope (ρ_T), instrument height (Z_i) and heat flux (H_F).

3.1.2 Unstable, stable and neutral atmospheric conditions

Unstable atmospheric conditions exist when H_F (units in W/m^2) rises upwards in eddies (H_F is positive) from the heated surface of the Earth on a clear day, causing the gradient of potential temperature ($\partial\theta_T/\partial z$) to become negative, or lapse (Webb, 1968). Shaw and Smietana (1983) define potential temperature (θ_T) as the temperature that a parcel of air would achieve if brought dry adiabatically to a pressure of 10^5 Pa. The difference between θ_T and the actual temperature is small but constant (Webb, 1968). H_F is subject to random fluctuations, wind-shear and thermal buoyancy effects (Webb, 1968), thus the lowest layer of the atmosphere is rather complex and in a continuous state of turbulence (e.g., Shaw and Smietana, 1983). However, these random fluctuations are over small time- and distance-scales, such that the time-averaged properties of the surface layer of the atmosphere are reasonably well behaved (Shaw and Smietana, 1983).

Stable conditions occur during clear nights when the ground cools, causing an inversion (positive $\partial\theta_T/\partial z$) with H_F negative (directed downward) (Webb, 1968). When $\partial\theta_T/\partial z$ is zero, a neutral condition exists (Webb, 1968) and H_F is also zero, which may occur during heavily overcast days (Angus-Leppan, 1979). Different RC formula are required for stable conditions (e.g., Angus-Leppan, 1980), although the literature does not comment on the transitional period between stable-neutral-unstable conditions, or if any lag-time occurs. However, refraction effects are considered small (and negligible compared to large variations during the day; cf. Figure 3.3) through the sunset/sunrise transition period when conditions are assumed to be close to neutral. Stable conditions are not discussed further, as levelling is not usually conducted during the night.

3.2 Refraction corrections to levelling

There have been numerous investigations that have sought to model and remove URE from geodetic levelling, with many (but not all) examples listed in Table 3.1. Only RCs most relevant to the ANLN will be described and discussed. Note that Whalen

(1980a) and Holdahl (1981) give predictions of the temperature gradient $\partial T_a/\partial z$ (or more accurately a prediction of the observed temperature difference ΔT_a at different heights), and use different *RC*s (usually Kukkamäki (1939)).

Correction	Symbol
Kukkamäki (1938, 1939)	RC_K
Brocks (1948)	RC_{BR}
Reissman (1954)	RC_{RE}
Mozzuchin (1977)	RC_M
Garfinkel (1978, 1979)	RC_G
Angus-Leppan (1979, 1980)	$RC_{A\text{-}L}$
Remmer (1980)	RC_R
Whalen (1980a)	ΔT_W
Fawaz (1981)	RC_F
Holdahl (1981)	ΔT_H
Pelzer (1982)	RC_P
Shaw and Smietana (1983)	RC_{SS}
Heer (1984)	RC_H
Kharaghani (1987)	RC_{KH}
Rüeger (1997)	RC_{RG}
Chrzanowski (1999)	RC_C
Skeivalas (2005)	RC_S

Table 3.1: Refraction corrections developed to reduce the effect of URE. This list is not exhaustive, but includes *RC*s that may be relevant to the ANLN.

The Kukkamäki (1938) *RC* (RC_K) is seminal with regard to refraction in levelling and will be described, as will the Holdahl (1981) temperature stratification model designed to predict ΔT_a for retrospective application to levelling data. The *RC* of Angus-Leppan (1979) ($RC_{A\text{-}L}$) is also presented as an *RC* that does not require observed temperatures at the time of survey. It can be used to retrospectively apply *RC* to levelling that does not have observed ΔT_a (cf. Chapter 4; Holdahl, 1981).

A more rigorous *RC* is introduced by Shaw and Smietana (1983) that accounts for buoyantly driven convective turbulence and shear-induced mixing as the air travels over a rough surface within the framework of the Monin-Obukhov similarity (Obukhov, 1971). This is described as a comparison to the free-convection approximations of the Angus-Leppan (1979) and Holdahl (1981) models that Shaw and Smietana (1983) claim do not account for air movement or surface roughness (cf. Webb, 1968).

3.2.1 Kukkamäki's *RC*

The single setup *RC* of Kukkamäki (1938) (RC_{K1}) is (Angus-Leppan, 1984)

$$RC_{K1} = -d_k \frac{S_\ell^2 b_k}{(Z_B - Z_F)^2} \left[\frac{1}{c_k + 1} \left(Z_B^{c_k+1} - Z_F^{c_k+1} \right) - Z_i^{c_k} \left(Z_B - Z_F \right) \right] \tag{3.1}$$

where d_k is the change in refractive index n_r for a change of 1° in temperature (T_a), computed as $d_k = -10^{-6}(0.933 - 0.0064(T_a - 20))P_a/1013$ (P_a is atmospheric pressure in mb), S_ℓ is the sight length (m), Z_i is the height of the instrument (m), with Z_F the FS and Z_B the BS staff reading (m). The constants a_k, b_k and c_k come from the temperature function of (Kukkamäki, 1938), which is (Angus-Leppan, 1984)

$$T_a = a_k + b_k z^{c_k} \tag{3.2}$$

where T_a is assumed to be in K, (although not stated by Angus-Leppan, 1984), z is the height of the T_a measurement above the ground, while b_k and c_k can be computed from observed T_a (Angus-Leppan, 1984).

A form of RC_{K1} more convenient for computation (Kukkamäki, 1939) (referred to as RC_{K2}) is presented in Holdahl (1981) as

$$RC_{K2} = -10^{-6} A_k \left(\frac{S_\ell}{50} \right)^2 \Delta H \Delta T \tag{3.3}$$

where ΔH (m) is the measured difference in elevation for a single setup, but can be extended over a levelling section between benchmarks (BMs) (cf. Balazs and Young, 1982), ΔT_a is the difference in air temperature between two temperature observations (T_1, T_2) taken at different heights z_1 and z_2, usually 0.5 m and 2.5 m respectively (Holdahl, 1981). A_k can be assumed constant and is calculated using (Holdahl, 1981)

$$A_k = \frac{1190}{z_2^{c_k} - z_1^{c_k}} \left[\frac{1}{c_k + 1} \left(Z_B^{c_k+1} - Z_F^{c_k+1} \right) - Z_i^{c_k} \left(Z_B - Z_F \right) \right] \tag{3.4}$$

Ideally, the value of ΔT_a is measured, but it can be predicted empirically from T_a measurements (Best, 1935), from models based on records of average monthly meteorological data (Section 3.2.2; Holdahl, 1981), or from observation of cloud and wetness conditions at the time of survey (Section 3.2.3; Angus-Leppan, 1979).

3.2.2 Holdahl's temperature stratification model

The temperature stratification model of Holdahl (1981) (ΔT_H) was constructed for the purpose of retrospectively removing refraction from levelling data in the US. It was also an attempt to avoid observing vertical temperature profiles for current levelling surveys (cf. Angus-Leppan, 1979). RC_{K2} (Equation (3.3); Kukkamäki, 1939) is used with the Holdahl (1981) model used to predict values for ΔT_a.

The formula used to compute ΔT_a in unstable conditions is (Holdahl, 1981)

$$\Delta T_a = T_2 - T_1 = 3\left[\frac{H_F^2\, T_0}{(C_p\,\rho_A)^2\, g}\right]^{1/3}\left(z_2^{-1/3} - z_1^{-1/3}\right) - 0.0098(z_2 - z_1) \tag{3.5}$$

where T_0 is T_a at height z_0 (usually 1.5 m) in K, C_p is specific heat of the air at constant pressure, ρ_A is air density ($C_p\,\rho_A = 1200$ J m^{-3} K^{-1} for Holdahl, 1981) and g is the acceleration due to gravity (ms^{-2}). H_F is (Holdahl, 1981)

$$H_F = S_n - G_F - \lambda_H E \text{ cal cm}^{-2}\,\text{min}^{-1} \tag{3.6}$$

where S_n is net solar radiation, G_F is heat flux into the ground, E is evaporation rate and λ_H is the latent heat of vaporisation of water. $\lambda_H E$ depends on the amount of water in the soil and is highly correlated with S_n.

The value for S_n was taken from a model constructed from mean daily totals of solar radiation (S_r) for each month over a period averaging 30 years at 192 weather stations across the US. S_r is converted to instantaneous solar radiation on a horizontal surface S_r' (Holdahl, 1981)

$$S_r' = \frac{\pi S_r}{4(a_t - b_t)}\sin\left[\frac{(t_s + a_t - b_t)\pi}{2(a_t - b_t)}\right] \tag{3.7}$$

where t_s is the Sun's hour angle (in minutes), b_t is the difference in time between when radiation is zero with respect to sunrise and sunset (here, $b_t = 30$ minutes). a_t is half the number of minutes between sunrise and sunset. S_r' is then converted to instantaneous solar radiation received on an inclined surface (S_r'') (Holdahl, 1981)

$$S_r'' = \frac{S_r' \sin B_1}{\sin B_0} \tag{3.8}$$

where B_0 is the incidence angle between the Sun's rays and a level surface and B_1 the incidence angle between the Sun's rays and the ground surface.

S_n is then computed as (Holdahl, 1981)

$$S_n = (1 - r_a - m_c)S_r'' + q \tag{3.9}$$

with q a regression coefficient assigned the value -0.037 cal cm^{-2} min^{-1} and r_a the reflectivity (albedo), which was taken from the Kung et al. (1964) model across the US that accounts for diurnal, spatial and seasonal variations. m_c is an empirically estimated coefficient dependent on the portion of the sky covered by clouds (in tenths) which was also modelled across the US by Holdahl (1981).

For a discussion of ΔT_H evaluations and comparison with other RCs, see Section 3.3.

3.2.3 Angus-Leppan (1979) *RC*

The vertical temperature gradient $\partial T_a/\partial z$ can be related to the potential temperature gradient $\partial \theta_T/\partial z$ as (Angus-Leppan, 1979), (cf. Shaw and Smietana, 1983)

$$\frac{\partial T_a}{\partial z} = \frac{\partial \theta_T}{\partial z} - 0.01 \tag{3.10}$$

For unstable conditions, Angus-Leppan (1979) simplifies $\partial \theta_T/\partial z$ based on Priestley (1959) and Webb (1965)

$$\frac{\partial \theta_T}{\partial z} = -0.027 H_F^{2/3}\, z^{-4/3} \tag{3.11}$$

Equation (3.11) is a free-convection approximation (FCA) of the temperature profile which neglects the mechanically induced mixing of the air layers by the wind (cf. Shaw and Smietana, 1983).

The single sight $RC_{A\text{-}L}$ ($RC^s_{A\text{-}L}$), in metres is (Angus-Leppan, 1979)

$$RC^s_{A\text{-}L} = 10^{-6}\, \frac{P_a S_\ell^2}{T_a^2} \left\{ 1 - 3.3 H_F^{2/3}\, Z_{i,\ell} \right\} \tag{3.12}$$

where P_a is in millibars (mb), T_a is in K, S_ℓ is in m, H_F is in W/m^2 and $Z_{i,\ell}$ is the height factor which is a function of instrument height Z_i and staff reading Z_ℓ (m). Equation (3.12) can be developed into a balanced sight equation (BS/FS; $RC^b_{A\text{-}L}$)

$$RC^b_{A\text{-}L} = \left(10^{-6}\, \frac{P_a S_\ell^2}{T_a^2} \left\{ 1 - 3.3 H_F^{2/3}\, Z_{i,\ell_B} \right\} \right) - \left(10^{-6}\, \frac{P_a S_\ell^2}{T_a^2} \left\{ 1 - 3.3 H_F^{2/3}\, Z_{i,\ell_F} \right\} \right) \tag{3.13}$$

where Z_{i,ℓ_B} is the height factor for the BS observation and Z_{i,ℓ_F} is the height factor for the FS observation.

The height factor $Z_{i,\ell}$, expresses the height dependence of $RC^{b}_{A\text{-}L}$ as (Angus-Leppan, 1979)

$$Z_{i,\ell} = \left\{ Z_i^{2/3} + 2Z_i^{-1/3}\, Z_\ell - 3Z_\ell^{2/3} \right\} (Z_i - Z_\ell)^{-2} \tag{3.14}$$

Equation (3.14) can be developed into two equations to calculate the height factor for the BS Z_{i,ℓ_B}

$$Z_{i,\ell_B} = \left\{ Z_i^{2/3} + 2Z_i^{-1/3}\, Z_B - 3Z_B^{2/3} \right\} (Z_i - Z_B)^{-2} \tag{3.15}$$

and FS Z_{i,ℓ_F}

$$Z_{i,\ell_F} = \left\{ Z_i^{2/3} + 2Z_i^{-1/3}\, Z_F - 3Z_F^{2/3} \right\} (Z_i - Z_F)^{-2} \tag{3.16}$$

3.2.4 Estimation of H_F for $RC_{A\text{-}L}$

Angus-Leppan (1979) directly estimates H_F (cf. Holdahl, 1981) for use in Equation (3.13) as

$$H_F = 450\, C_f\, W_f\, \cos\zeta_s \tag{3.17}$$

where C_f is a factor accounting for cloud cover, W_f is a factor accounting for surface wetness, both evaluated using Figure 3.2. ζ_s is the Sun's zenith distance, with $\cos\zeta_s$ (Angus-Leppan, 1979)

$$\cos\zeta_s = \sin\phi\, \sin\delta_s + \cos\phi\, \cos\delta_s\, \cos t_s \tag{3.18}$$

where ϕ (latitude of observation) and δ_s (Sun's declination) are positive if north, negative if south.

A similar equation is derived by Angus-Leppan (1979) to estimate H_F as it varies due to the slope and aspect of the surface

$$\cos\zeta_s' = \cos\rho_T\, \cos\zeta_s + \sin\rho_T\, \sin\zeta_s\, \cos(\gamma_{\rho_T} - \alpha_s) \tag{3.19}$$

where ρ_T is the slope of the terrain, γ_{ρ_T} is the azimuth of ρ_T (e.g., when $\gamma_{\rho_T} = 180°$, the terrain slopes down to the south), α_s is the Sun's azimuth, which is (Angus-Leppan,

1979)

$$\cot \alpha_s = \sin \phi \, \cot t_s \, - \, \frac{\cos \phi \, \tan \delta_s}{\sin t_s} \tag{3.20}$$

H'_F is H_F on an inclined surface (Angus-Leppan, 1979)

$$H'_F = H_F(\cos \rho_T + \sin \rho_T \tan \zeta_s \cos(\gamma_L - \alpha_s)) \tag{3.21}$$

where γ_L is the azimuth of the levelling sub-section used in place of γ_{ρ_T}, which is unknown. Equation (17) in Angus-Leppan (1979) is incorrect, but Equation (3.21) shown here is correct as re-derived in Filmer et al. (2009).

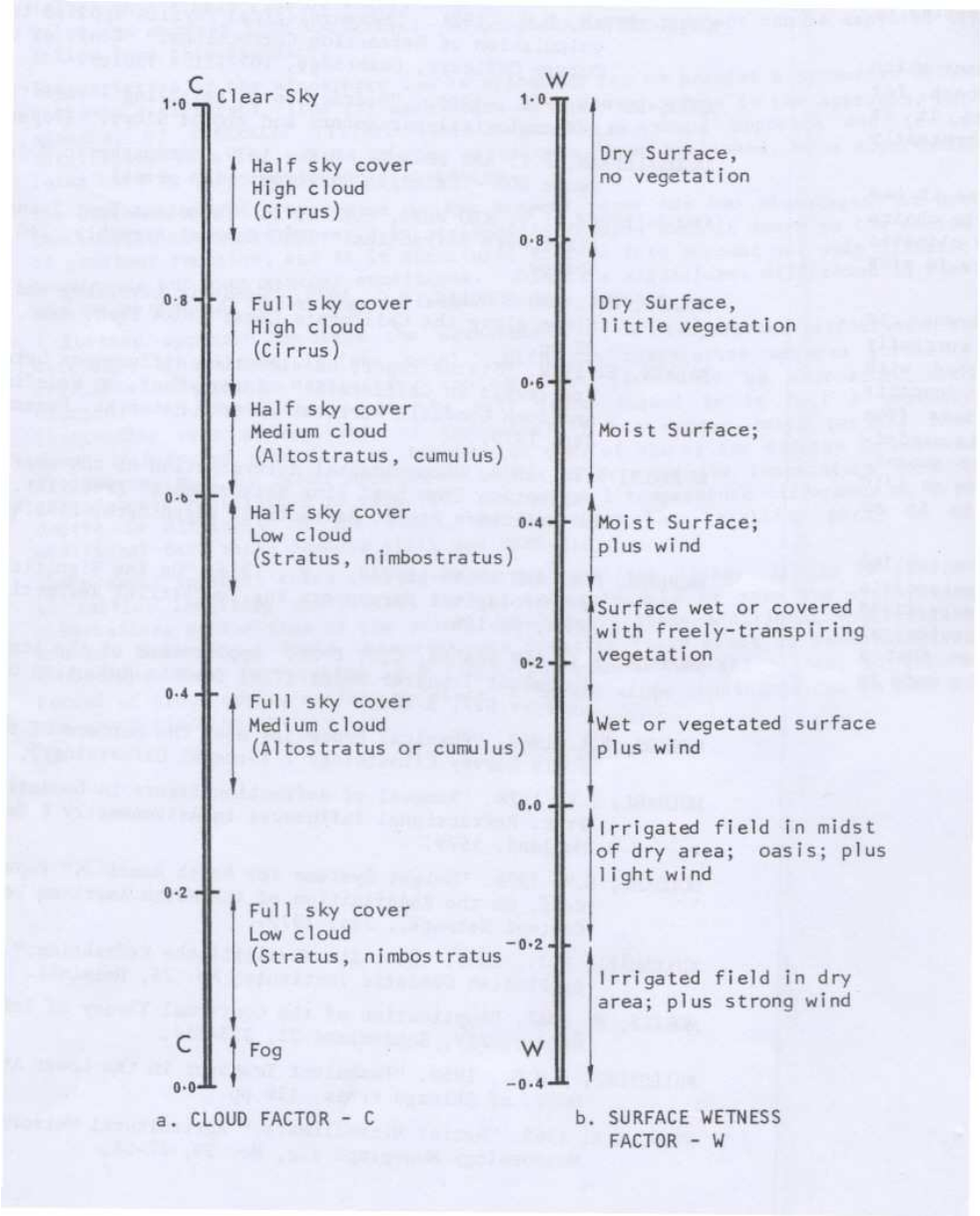

Figure 3.2: Diagram from Angus-Leppan (1979) for estimating parameters C_f and W_f

Angus-Leppan (1979) postulated that H'_F was significantly larger on slopes facing the Sun than those facing away from the Sun, as they would receive higher S_r and therefore higher H_F. The effect in the north-south direction when levelling towards the equator would be to define the zero level too low, thus creating the appearance of the sea sloping upwards towards the equator (cf. Chapter 5; Hamon and Greig, 1972; Fischer, 1975; Coleman et al., 1979). This magnitude was estimated by Angus-Leppan (1984) as between 0.05 m and 1 m per 1,000 km (cf. Section 4.2.3), being quite variable depending on ρ_T, climate, season and ϕ. A discussion of $RC_{A\text{-}L}$ is in Section 3.3.

3.2.5 Shaw and Smietana (1983) *RC*

Rather than use the free convection model to obtain the relationship between the height of the line of sight and $\partial T_a/\partial z$, Shaw and Smietana (1983) obtain a more general treatment within the Monin-Obukhov similarity theory (Obukhov, 1971).

The balanced RC equation of Shaw and Smietana (1983) (RC_{SS}) is

$$RC^b_{SS} = \frac{10^{-6}\, A_s\, P_a\, T_*}{\rho_T^2\, T_a^2\, k_{vk}} \left\{ (Z_i + \rho_T\, S_\ell) \ln \left[\left(\frac{x_2+1}{x_2+1} \right) \left(\frac{y-1}{y+1} \right) \right] - (Z_i - \rho_T\, S_\ell) \ln \left[\left(\frac{x_1+1}{x_1-1} \right) \left(\frac{y-1}{y+1} \right) \right] - \frac{L}{8}(x_2 - x_1) \right\} \tag{3.22}$$

with A_s a constant (taken as 0.79 K Pa^{-1}), P_a in pascals (Pa), T_a in K, k_{vk} is von Kármán's constant (dimensionless; 0.4 used by Shaw and Smietana (1983)) and T_* a temperature scale where Shaw and Smietana (1983),

$$T_* = -\frac{H_F}{\rho_A C_p u_*} \tag{3.23}$$

with u_* a velocity scale. u_* is Shaw and Smietana (1983)

$$u_* = \left(\frac{\tau}{\rho} \right)^{\frac{1}{2}} \tag{3.24}$$

where τ is not defined in Shaw and Smietana (1983), but is assumed to be turbulent sheer stress (Obukhov, 1971). L is a length scale from Monin-Obukuv similarity theory and is computed as Shaw and Smietana (1983)

$$L = -\frac{u_*^3\, T_a\, \rho_A\, C_p}{k\, g\, H_F} \tag{3.25}$$

y, x_1 and x_2 are stability factors defined as

$$y = \left[1 - \frac{16Z_i}{L}\right]^{\frac{1}{2}} \tag{3.26}$$

with x_1 for uphill sighting

$$x_1 = \left[1 - \frac{16(Z_i - \rho_T\, S_\ell)}{L}\right]^{\frac{1}{2}} \tag{3.27}$$

and x_2 for downhill sighting

$$x_2 = \left[1 - \frac{16(Z_i + \rho_T\, S_\ell)}{L}\right]^{\frac{1}{2}} \tag{3.28}$$

3.3 Discussion of *RC*s

Numerous field tests and critical analyses of various refraction models/corrections were conducted during the 1980's, leading up to the re-adjustment of the North American levelling network to realise the North American Vertical Datum 1988 (NAVD88; Zilkoski et al., 1992).

3.3.1 Comparison of predicted and observed temperature gradient

Field tests in the US (Whalen, 1980a) used levelling lines with very short S_ℓ (generally <13 m) to get a 'refraction free' height difference (ΔH_{RF}) at Gaithersburg, Maryland (July-September 1979 and March 1980; 26 km line) and Tucson, Arizona (April 1980; 29 km line). Tucson is hotter and dryer than Gaithersburg, with higher S_r, thus providing different environments to test the *RC*. Re-levelling using $S_\ell = 60$ m obtained a height difference assumed to contain URE (ΔH_{URE}). $\Delta H_{URE} - \Delta H_{RF}$ accumulated to -0.065 m (Gaithersburg) and -0.159 m (Tucson) with the difference ($\delta\Delta H_{URE}$) assumed to be entirely URE.

Whalen (1980a, 772) indicates that RC_K and RC_G (Garfinkel, 1978, 1979, see Table 3.1) removed between 82% and 100% of $\delta\Delta H_{URE}$ using observed ΔT_a at both Gaithersburg and Tucson. Predicted ΔT_a (ΔT_H and ΔT_W) using RC_K or RC_G removed 102% to

106% of $\delta\Delta H_{URE}$ at Gaithersburg, but at Tucson where S_r is higher, ΔT_H over-corrects by 34% using RC_K, but ΔT_W under-corrects by 35% using RC_K and by 46% using RC_G. The Best (1935) ΔT_a (ΔT_B) based on observations in southern England are found to be inadequate, under-correcting by 55% (Gaithersburg) and 65% (Tuscon).

Strange (1981) and Holdahl (1982) both applied predicted ΔT_a to historical levelling data at two different sites in California where differences between repeated levellings had been interpreted as uplift resulting from vertical crustal motion (Castle et al., 1976). However, there was debate over the large magnitude of the uplift identified by the repeat levelling (e.g., Kerr, 1981). Holdahl (1982) applied ΔT_H with RC_{K2} retrospectively to repeat levelling lines, reducing the apparent uplift from 0.35 m to 0.075±0.040 m, while Strange (1981) used ΔT_B (doubled to allow for higher S_r in California) with RC_K, also reducing apparent uplift from 0.25−0.35 m to 0.05−0.10 m. Strange (1981) and Holdahl (1982) both concluded that the uplift interpreted by Castle et al. (1976), was caused by URE in the original levelling, but reduced in subsequent surveys when S_ℓ was reduced (cf. Section 3.5.6). Re-levelling of one of the California levelling lines by Stein et al. (1986) using $S_\ell = 42$ m and $S_\ell = 22$ m also found differences of six times the expected random error between the two lines. After applying RC using both observed and predicted ΔT_a, the difference between levelling runs complied with first order (US) levelling standards (see Schomaker and Berry, 1981, 3-7).

Heer and Neimeier (1985) tested $RC_{A\text{-}L}$ using C_f and W_f estimated by the observer, finding that $RC_{A\text{-}L}$ reduced levelled elevation differences (from 55 levelling runs conducted over seven years) by about one third. When $RC_{A\text{-}L}$ was applied to the Californian levelling line (with 13 other RCs) used by Strange (1981) and Stein et al. (1986), Heer and Neimeier (1985) found that all RCs reduced the discrepancies to within the range of expected random error. However, most appeared to over-correct, with $RC_{A\text{-}L}$ second worst (after Mozzuchin, 1977) in this respect.

Castle et al. (1983) and Mark et al. (1987) claim that errors caused by URE are overstated, thereby challenging the results of Strange (1981), Holdahl (1982) and Stein

et al. (1986). However, applications of RCs to levelling using observed ΔT_a (e.g., Heroux et al., 1985; Heer and Neimeier, 1985; Stein et al., 1986) appear to improve levelling results (cf. Calvert and Dodson, 1985). The results of Strange (1981), Whalen (1980a), Holdahl (1982) and Heer and Neimeier (1985) also suggest that predicted ΔT_a (combined with some estimations) can retrospectively reduce the effects of URE (cf. Heroux et al., 1985). However, using predicted ΔT_a is somewhat problematic as it is dependent on the required information being recorded at the time of observation; if the information is unavailable, assumptions are made instead (e.g., Strange, 1981), significantly reducing the rigour with which retrospective RCs can be applied. In addition, the true magnitude of URE (and hence, the improvement resulting from applying RCs) is difficult to estimate due to contamination of levelling by other small systematic errors (Section 2.1.4).

3.3.2 Comparison of FCA and RC_{SS}

The differences among RC_{SS} (Equation (3.22)), $RC_{A\text{-}L}$ (Equation (3.13)) and RC_K (Equations (3.1) and (3.3)) are the inclusion of wind speed and a surface roughness factor. Shaw and Smietana (1983) contend that the inclusion of these factors will result in a refraction estimate that is more accurate than using a simple FCA, which assumes that mechanically induced mixing of the air layers by the wind does not have an important effect on the vertical temperature gradient (cf. Webb, 1968). Experiments by Shaw and Smietana (1983) indicate that FCA of RC is an upper bound for URE, whereby FCA generally over-estimate URE (cf. Heer and Neimeier, 1985).

Shaw and Smietana (1983) also applied RC_{SS} to the Californian levelling line examined by Holdahl (1982), Stein et al. (1986) and Craymer and Vaníček (1986) using Equation (3.22), although assumptions had to be made to compute wind speed and the surface roughness factor. Compared to RC_{SS}, a FCA RC over-estimated refraction errors by between 9% and 53% (compared to Equation (3.22)). The difference between the accumulated difference between the short (average 24.8 m) and long (average 41.8 m) S_ℓ over the $\sim$50 km levelling line was between 13% (60.0 mm compared to 53.2

mm) and 42% (69.5 mm compared to 48.8 mm) more for the FCA RC.

3.4 Meteorological data for sensitivity analysis of $RC_{A\text{-}L}$

The $RC_{A\text{-}L}$ was selected to simulate the effect of retrospectively applying RCs to the ANLN because of its relatively small number of input parameters and apparent adequacy, despite the suggestion that it tends to over-correct (e.g., Heer and Neimeier, 1985; Shaw and Smietana, 1983). There is little point using a more rigorous RC for the simulation when the effectiveness of the simulation will be determined by the accuracy of the approximated assumptions used for input data (described in this Section and Chapter 4), which are not currently available in the ANLN. A sensitivity analysis of $RC_{A\text{-}L}$ is undertaken in Section 3.5 to evaluate the effectiveness of the simulation with regard to the accuracy of the assumptions.

Meteorological input data for Austral summer (January) and winter (July) (July and January averages from the full record of each weather station) to quantify the seasonal and diurnal variation of H_F (Section 3.5.1) at four selected mainland Australian weather stations (Table 3.2), is contained in Table 3.3, which was obtained from the Australian Bureau of Meteorology at http://www.bom.gov.au/climate/averages/. The four stations were selected so as to demonstrate the variability of meteorological conditions both spatially and temporally within Australia.

The average meteorological information in Table 3.3 is used to estimate C_f and W_f from Figure 3.2. Note that P_a is given at MSL. The formula for computing P_a at the height of each station is (NOAA et al., 1976)

$$P_a = P_{M,b_a}\left[\frac{T_{M,b_a}}{T_{M,b_a} + L_{M,b_a}(H - H_{M,b_a})}\right]^{\left[\frac{g_0' M_0}{R^* L_{M,b_a}}\right]} \tag{3.29}$$

where the subscript b_a indicates the bottom layer of atmosphere, between 0 km (MSL) and 11 km, g_0' is a dimensional constant (9.80665), M_0 is the mean molecular weight of air at MSL (28.9644 kg/kmol), R^* is the gas constant (8.31432×10^3 N$\cdot$ m/(kmol$\cdot$ K), L_{M,b_a} is dT/dH (-0.0065 K/m), H_{M,b_a} is MSL height (zero), T_{M,b_a} is temperature

(288.15 K), P_{M,b_a} is MSL pressure (using Table 3.3) and H is height of the station.

Site	State	Lat°S	Lon°E	Elev (m)	Opened
Bathurst	NSW	33.43	149.56	713	1908
Birdsville	QLD	25.90	139.35	47	1892
Weipa	QLD	12.63	141.88	11	1914
Bridgetown	WA	33.96	116.14	150	1887

Table 3.2: Location, heights and length of data record (from opening date) for weather stations used to estimate realistic input parameters for sensitivity analysis of $RC_{A\text{-}L}$. Data from the Australian Bureau of Meteorology.

Site		CLR		CDY		PREC		MT		MP		WS	
		W	S	W	S	W	S	W	S	W	S	W	S
Bathurst	BATH	10	6	8	11	69	44	28	12	1011	1017	9	6
Birdsville	BIRD	17	21	5	4	25	10	39	22	1005	1020	13	8
Weipa	WEIP	1	5	19	7	447	2	32	31	1005	1014	9	6
Bridgetown	BRID	14	3	6	14	14	146	30	17	1014	1021	8	6

Table 3.3: Meteorological parameters from four selected weather stations. Averages for summer (S) or winter (W) for: number of clear days (CLR) and cloudy days (CDY), precipitation (PREC) in mm, maximum daily temperature (MT) in °C, maximum daily atmospheric pressure (MP) in millibars at MSL, and wind speed (WS) in km/hour. Data from the Australian Bureau of Meteorology.

Set	H_F (W/m^2)	P_a (mb)	S_ℓ (m)	T_a (K)	ΔH (m)
A	50	1010	90	300	50
B	200	1010	90	300	50
C	300	1010	90	300	50
D	400	1010	90	300	50

Table 3.4: Data sets A-D containing input values for the sensitivity analysis of $RC_{A\text{-}L}$.

To assess the sensitivity of $RC_{A\text{-}L}$ under a range of Australian conditions, four sets of input parameters were prepared (A-D; Table 3.4). All values were constant, except for H_F, which was given values between 50 W/m^2 and 400 W/m^2 which is a realistic range for unstable conditions in Australia (cf. Figures 3.3). $\Delta H = 50$ m is the assumed height difference over a 5 km levelling section. This value was selected as it is an example of a long steady gradient where maximum third-order S_ℓ (90 m; NMC, 1966) can be used while maintaining staff readings of at least 0.5 m above the ground (cf. ICSM, 2007), thus simulating conditions where $RC^b_{A\text{-}L}$ may be large (e.g., Angus-Leppan, 1979). The

resultant FS staff readings per setup (Z_i =1.65 m) are 1.05 m for S_ℓ =60 m and 0.75 m for S_ℓ =90 m; BS staff readings are 2.25 m for S_ℓ =60 m and 2.55 m for S_ℓ =90 assuming constant ρ_T.

It is important to clarify here that class LC levelling in ICSM (2007) has maximum S_ℓ of 80 m. Third-order maximum S_ℓ of 90 m from NMC (1966) is used for this Chapter and Chapter 4 because the investigation is primarily focussed on the possible errors in the AHD, and the ALS used for the AHD would have been observed to NMC (1966) specifications (Roelse et al., 1971). However, maximum allowable misclosure (r_m; determined by c; Section 2.1.3) for NMC (1966) third-order are the same as ICSM (2007) class LC ($c = 12$; Table 2.3), with c for NMC (1966) first-, second- ($c = 8$ mm is adopted here for the ANLN; cf. Table 2.2) and fourth-order the same as ICSM (2007) class LA, LB and LD respectively.

3.5 Sensitivity analysis of $RC_{A\text{-}L}$

To apply the $RC_{A\text{-}L}$ retrospectively requires assumptions about the meteorological conditions at the time of survey and the S_ℓ and ΔH of the individual observations. Here, the effects of these assumptions on the computed $RC_{A\text{-}L}$ are tested, indicating the confidence with which the simulated application of $RC_{A\text{-}L}$ to the entire ANLN can be viewed.

These tests are also significant in relation to the way that the $RC_{A\text{-}L}$ appears to currently be used. Rather than direct computation of Equation (3.13), the constant (seasonal) values of $RC_{A\text{-}L}$ per 100 m ΔH (Angus-Leppan, 1979, Table V) have been adopted in recent Australian studies of total station and differential levelling (Johnston et al., 2002; Robertson, 2003; Robertson and Snow, 2005). This appears to be based on Kearsley et al. (1993b) and Kearsley and Ahmad (1993), despite the equations necessary to compute $RC_{A\text{-}L}$ being provided in addition to Table V from Angus-Leppan (1979). Sensitivity of $RC_{A\text{-}L}$ to variations within a season (see Section 3.5.1) suggests that $RC_{A\text{-}L}$ should be rigorously re-computed using Equation (3.13) using meteorolog-

ical conditions observed during the survey.

3.5.1 Diurnal and seasonal variations in H_F

Estimates of average H_F at the four locations in Table 3.2 for Austral summer (January) and winter (July) are made using values of C_f and W_f estimated from Tables 3.2 and 3.3, Figure 3.2 and Equation (3.17). Equation (3.18) is used to compute ζ_s, with changing t_s simulating the average variation in H_F during the day; e.g., $t_s = 0$ hours (midday, sun is on the meridian), $t_s = 1$ hour (11 am or 1 pm; hour angle = 15°). The variation in H_F is evaluated up to $t_s = 5$ hours (7 am or 5 pm; hour angle = 75°).

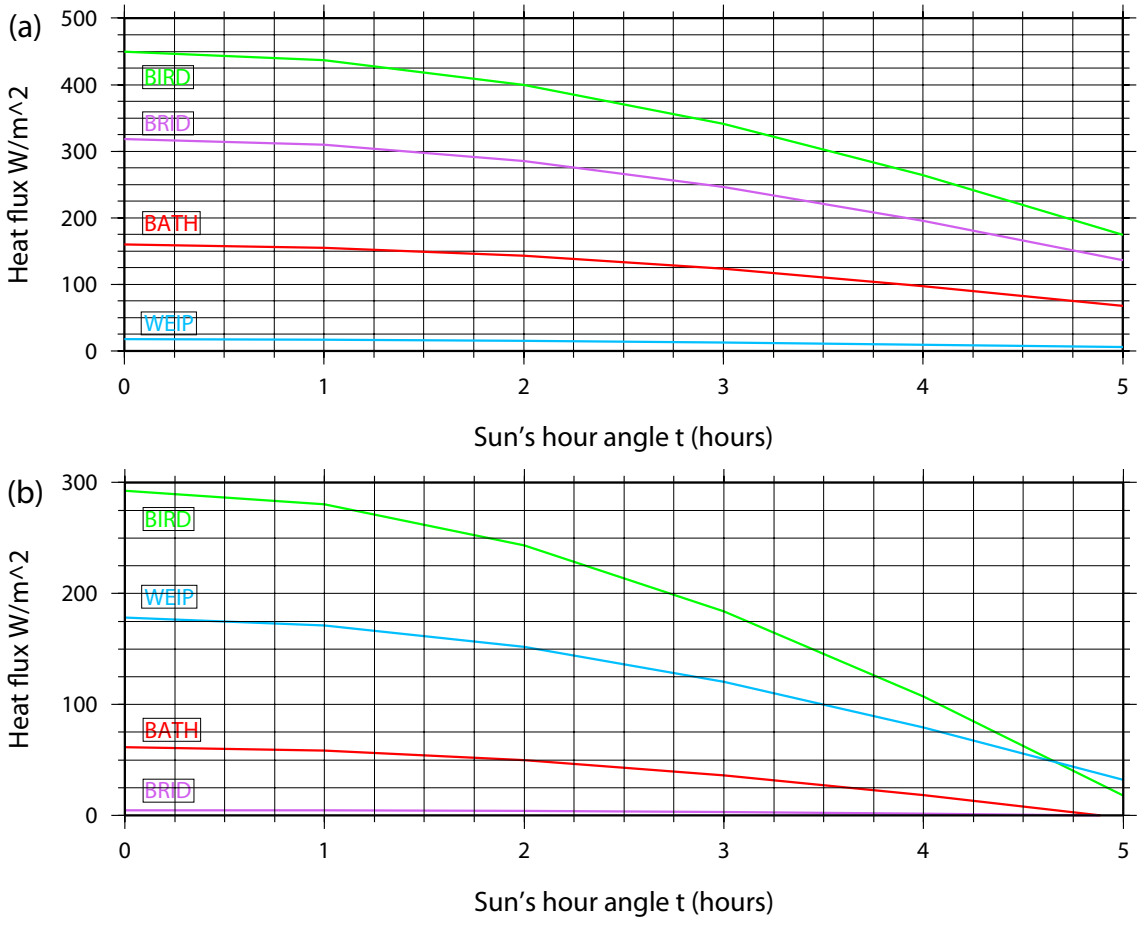

Figure 3.3: Diurnal changes in the value of H_F in the 5 hours before and after midday (symmetrical around midday) at Bathurst (BATH; red), Birdsville (BIRD; green), Weipa (WEIP; blue), and Bridgetown (BRID; purple) during (a) summer (January); and (b) winter (July).

The average diurnal variation in H_F between 7 am and 5 pm (cf. Holdahl, 1981) at the four locations are shown in Figure 3.3(a) and Figure 3.3(b). The maximum diurnal variation in H_F is almost 200 W/m^2 for Birdsville in summer (Figure 3.3(a)), but reaches almost 300 W/m^2 at Birdsville in winter (Figure 3.3(b)). Bridgetown has a diurnal variation in H_F of just over 100 W/m^2 in summer, with H_F varying diurnally by about 100 W/m^2 at Weipa in winter. H_F changes diurnally by about 50 W/m^2 at Bathurst during both summer and winter. The diurnal variation in H_F at Weipa in summer and Bridgetown in winter is negligible. This is due to the cool cloudy and wet conditions in Bridgetown in winter and the very cloudy and wet conditions (monsoonal) in Weipa during summer. Note that H_F at both Bathurst and Bridgetown become negative in July (Figure 3.3(b)) before 5 pm and remaining so until after 7 am the next morning, thus creating neutral or stable atmospheres (see Section 3.1.2).

3.5.2 Sensitivity of H_F to C_f and W_f

The diurnal variations in H_F presented in Figures 3.3(a) and 3.3(b) assume constant values for C_f and W_f. Changes in the actual meteorological conditions at the site during the day such as cloud cover, wind speed or rain would result in C_f and W_f also varying. The sensitivity of H_F to variations or errors in C_f (δC_f) and W_f (δW_f) values is tested here.

For a sensitivity analysis, the partial differentials of C_f and W_f are evaluated as

$$\frac{\partial H_F}{\partial C_f} = 450 W_f \cos\zeta_s \tag{3.30}$$

$$\frac{\partial H_F}{\partial W_f} = 450 C_f \cos\zeta_s \tag{3.31}$$

Equations (3.30) and (3.31) are evaluated using $t_s = 2$ hours (30°), $\delta_s = +23.5°$ in winter and $-23.5°$ for summer, $\phi = 25.0°$S and W_f and C_f =0.4, 0.6 and 0.8. Using δC_f and δW_f of 0.0−0.8, δH_F resulting from δC_f is

$$\delta H_F = \frac{\partial H_F}{\partial C_f}\delta C_f \tag{3.32}$$

and from δW_f

$$\delta H_F = \frac{\partial H_F}{\partial C_f}\delta C_f \tag{3.33}$$

The effects of δW_f and δC_f on δH_F are identical, as shown in Figure 3.4(a) for summer (January) and Figure 3.4(b) for winter (July).

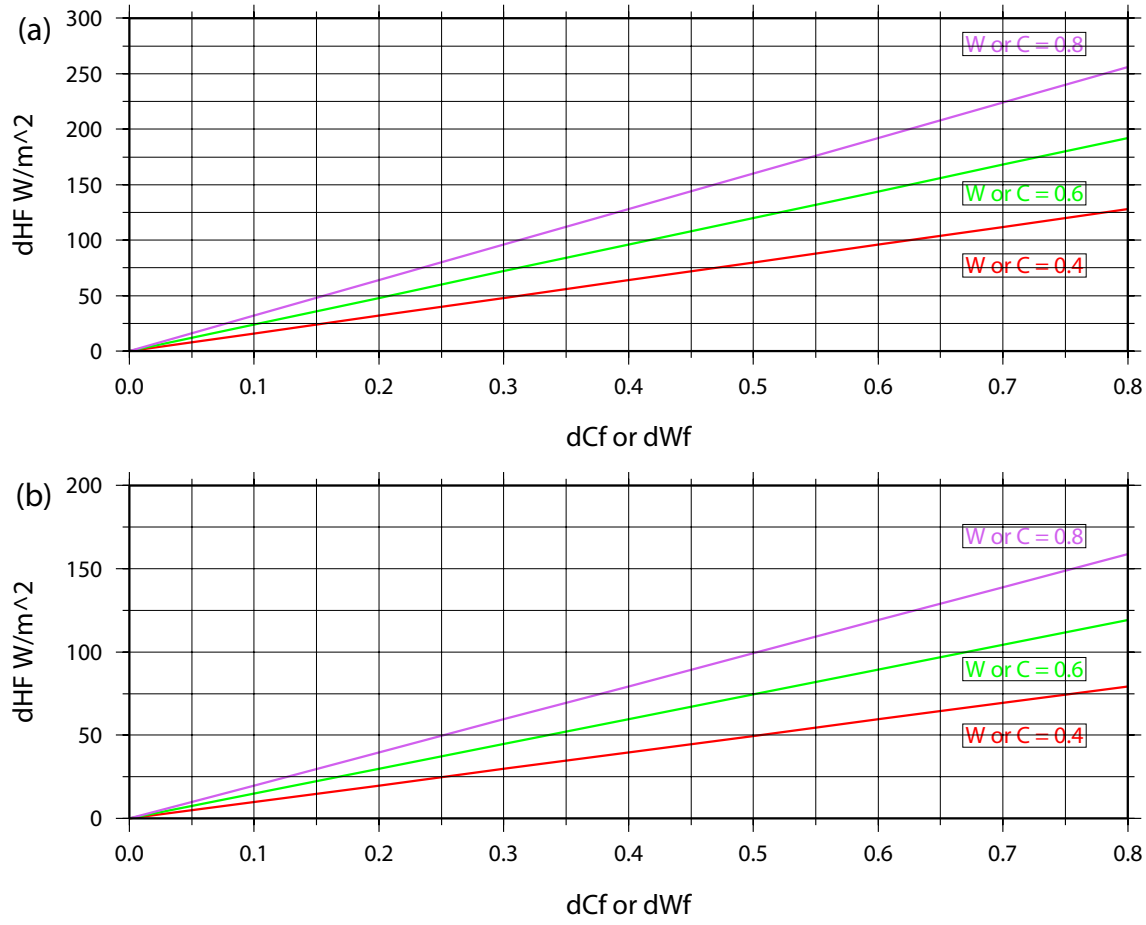

Figure 3.4: Changes in the value of H_F (dHF; δH_F) resulting from δC_f or δW_f (dCf and dWf) for different values of C_f and W_f during (a) summer (January); and (b) winter (July).

δH_F due to δC_f and δW_f is larger in summer (Figure 3.4(a)), increasing as δC_f and δW_f increase, with H_F more sensitive to δC_f and δW_f when C_f and W_f are large. When δC_f or δW_f are 0.3, and C_f or W_f are 0.8, δH_F could be up to 100 W/m^2 in summer (Figure 3.4(a)), or 60 W/m^2 in winter (Figure 3.4(b)). If weather conditions are recorded at the time of survey, it is likely that C_f and W_f could be estimated with errors of $<$0.2, but when there is no information about when the survey is conducted, the possibility of winter conditions assumed for a summer survey (e.g., Section 4.1.1) could cause δC_f and δW_f to be as large as 0.6$-$0.8. This could cause δH_F to be $>$200 W/m^2, which would lead to large errors in $RC_{A\text{-}L}$. The maximum effects of diurnal- or seasonal-related errors in H_F therefore have the potential to reduce the effectiveness of $RC_{A\text{-}L}$. See Section 3.5.5 for the possible effects of δH_F on $RC_{A\text{-}L}$.

3.5.3 Partial differentiation of $RC_{A\text{-}L}$

Error propagation (e.g., Lyons, 1991) is used here to test the sensitivity of each parameter in $RC_{A\text{-}L}$ to errors in the input values. The constant 10^{-6} in Equation (3.12) is changed to 10^{-3} (Equations (3.34) to (3.38)) so that output units are in mm rather than metres (e.g., Angus-Leppan, 1984). The partial derivatives for Equation (3.12) with respect to each parameter are

$$\frac{\partial RC^{s}_{A\text{-}L}}{\partial H_F} = 10^{-6}\,\frac{P_a S_\ell^2}{T_a^2}\left\{-2.2 H_F^{-1/3}\,Z_{i,\ell}\right\} \tag{3.34}$$

$$\frac{\partial RC^{s}_{A\text{-}L}}{\partial P_a} = 10^{-6}\,\frac{S_\ell^2}{T_a^2}\left\{1 - 3.3 H_F^{2/3}\,Z_{i,\ell}\right\} \tag{3.35}$$

$$\frac{\partial RC^{s}_{A\text{-}L}}{\partial S_\ell} = 20^{-6}\,\frac{P_a S_\ell}{T_a^2}\left\{1 - 3.3 H_F^{2/3}\,Z_{i,\ell}\right\} \tag{3.36}$$

$$\frac{\partial RC^{s}_{A\text{-}L}}{\partial T_a} = -20^{-6}\,\frac{P_a S_\ell^2}{T_a^3}\left\{1 - 3.3 H_F^{2/3}\,Z_{i,\ell}\right\} \tag{3.37}$$

$$\frac{\partial RC^{s}_{A\text{-}L}}{\partial Z_{i,\ell}} = 10^{-6}\,\frac{P_a S_\ell^2}{T_a^2}\left\{1 - 3.3 H_F^{2/3}\right\} \tag{3.38}$$

Equations (3.34) to (3.38) use Equation (3.13) and input values from Table 3.4 to numerically evaluate the partial differentials for both BS and FS. In Equation (3.38), $Z_{i,\ell}$ drops out of the partial differential, thus the numerical partial derivatives for the BS and FS cancel. The sensitivity of $RC^{b}_{A\text{-}L}$ to $\delta Z_{i,\ell}$ is investigated separately in Section 3.5.6.

3.5.4 Total differential of $RC^{b}_{A\text{-}L}$

The evaluated partial derivatives are substituted into the total derivative for the error in $RC^{b}_{A\text{-}L}$ ($\delta RC^{b}_{A\text{-}L}$),

$$\delta RC^{b}_{A\text{-}L} = \frac{\partial RC^{b}_{A\text{-}L}}{\partial P_a}\delta P_a \;+\; \frac{\partial RC^{b}_{A\text{-}L}}{\partial S}\delta S_\ell \;+\; \frac{\partial RC^{b}_{A\text{-}L}}{\partial T_a}\delta T_a \;+\; \frac{\partial RC^{b}_{A\text{-}L}}{\partial H}\delta H_F \tag{3.39}$$

$(\partial RC^{b}_{A\text{-}L}/\partial Z_{i,\ell})\delta Z_{i,\ell}$ is equal to zero.

The sensitivity of $RC^b_{A\text{-}L}$ to errors in the input values for each parameter is reflected in the error $\delta RC^b_{A\text{-}L}$, which is evaluated for data set A (see Table 3.4 for data sets A-D),

$$\delta RC^b_{A\text{-}L} = 0.005126\,\delta H_F \,+\, 0.000381\,\delta P_a \,+\, 0.000534\,\delta S_\ell \,-\, 0.000160\,\delta T_a \qquad (3.40)$$

data set B

$$\delta RC^b_{A\text{-}L} = 0.003229\,\delta H_F \,+\, 0.000959\,\delta P_a \,+\, 0.001346\,\delta S_\ell \,-\, 0.000404\,\delta T_a \qquad (3.41)$$

data set C

$$\delta RC^b_{A\text{-}L} = 0.002821\,\delta H_F \,+\, 0.001257\,\delta P_a \,+\, 0.001763\,\delta S_\ell \,-\, 0.000529\,\delta T_a \qquad (3.42)$$

data set D

$$\delta RC^b_{A\text{-}L} = 0.002563\,\delta H_F \,+\, 0.001523\,\delta P_a \,+\, 0.002136\,\delta S_\ell \,-\, 0.000641\,\delta T_a \qquad (3.43)$$

Equations (3.40) to (3.41) indicate that $\delta RC^b_{A\text{-}L}$ is most sensitive to δH_F, although less so as H_F increases. After H_F, $\delta RC^b_{A\text{-}L}$ is most sensitive to errors in input values for S_ℓ, P_a and T_a in this order. This sensitivity increases as the input value for H_F increases (see Table 3.4).

3.5.5 Effect of δH_F on $\delta RC^b_{A\text{-}L}$

The effects of increasing δH_F on $\delta RC^b_{A\text{-}L}$ are presented in Figure 3.5 (solid colour lines), showing the results of the computations in Section 3.5.3 and Section 3.5.4 using the data sets A-D in Table 3.4. These results are computed for a 5 km levelling section, with ΔH_F =50 m for the section (constant gradient assumed). Figure 3.5(a) uses S_ℓ = 90 m and Figure 3.5(b) S_ℓ = 60 m in Equations (3.34) - (3.38). The change in S_ℓ results in $RC^b_{A\text{-}L}$ over the 5 km section (dashed coloured lines; red = set A, green = B, purple = C, light blue = D) more than doubling. However, this is more the result of changing S_ℓ affecting $Z_{i,\ell}$ (cf. Sections 3.5.6 and 3.5.7).

The increase in $\delta RC^b_{A\text{-}L}$ is considerably larger when H_F is small (Figure 3.5; set A, solid red line) indicating that $\delta RC^b_{A\text{-}L}$ is less sensitive to δH_F when values of H_F are large

(approximately H_F >100). The effects of δH_F on $\delta RC^b_{A\text{-}L}$ (solid colour lines) appears inversely proportional to $RC^b_{A\text{-}L}$ over the 5 km section (dashed colour lines) for data sets A-D (Figures 3.5(a) and 3.5(b)). An error of ~72 W/m^2 or more in the estimation of H_F (using set A) will result in $\delta RC^b_{A\text{-}L} = RC^b_{A\text{-}L}$ over the 5 km levelling section (for both $S_\ell = 60$ m and $S_\ell = 90$ m; winter and summer). This can be compared to set B ($H_F = 200$ W/m^2) where δH_F would need to be 300 W/m^2 for $\delta RC^b_{A\text{-}L} = RC^b_{A\text{-}L}$ for the section. Although $\delta RC^b_{A\text{-}L}$ is large for sets C and D when $\delta H = 300$ W/m^2 (24 mm and 22 mm respectively for $S_\ell = 90$ m; Figure 3.5(a); 10 mm and 9 mm respectively for $S_\ell = 60$ m; Figure 3.5(b)), they do not exceed $RC^b_{A\text{-}L}$ for the section.

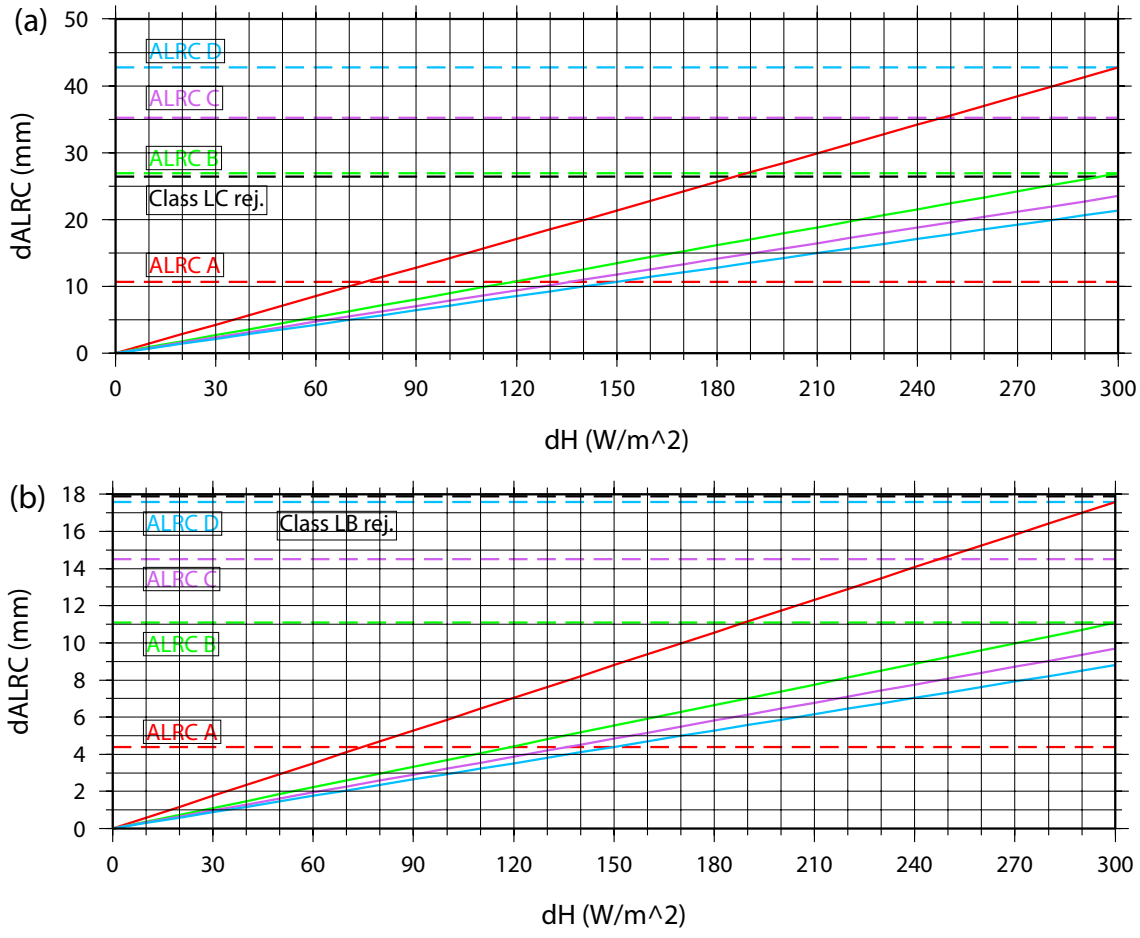

Figure 3.5: The effect on $\delta RC^b_{A\text{-}L}$ (dALRC in mm) of increasing δH_F (dH) when extrapolated over a 5 km levelling sub-section (solid colour lines). The different data sets used are (see Table 3.4) red for set A, green for set B, purple for set C and blue for set D. The dashed colour lines represent the $\delta RC^b_{A\text{-}L}$ computed using each data set (A, B, C, D) over the 5 km levelling section. Figure(a) uses $S_\ell = 90$ m (third-order maximum), with third-order (labelled class LC) r_m for 5 km represented by dashed black line; and Figure (b) uses $S_\ell = 60$ m (second-order maximum), with second-order (labelled class LB) r_m for 5 km represented by dashed black line).

Here, it is important to note that $RC^{b}_{A\text{-}L}$ does not exceed second-order (ICSM (2007) class LB; S_ℓ = 60 m; Figure 3.5(b)) r_m (black dashed line) of 17.89 mm ($8\sqrt{d}$; see Table 2.3) for 5 km. However, sets A, B and C are significant in terms of the *a priori* STD estimation of 8.94 mm ($4\sqrt{d}$) over 5 km (Section 2.3.8; Steed, 2006) and 6.26 mm ($2.8\sqrt{d}$) over 5 km (Table 2.4; Filmer and Featherstone, 2009).

When S_ℓ = 90 m (Figure 3.5(b)), sets B, C and D all exceed third-order (ICSM (2007) class LC) r_m (black dashed line) of 26.83 mm ($12\sqrt{d}$; see Table 2.3) for 5 km. Sets A, B and C are significant in terms of the *a priori* STD estimates of 13.42 mm ($6\sqrt{d}$) over 5 km (Section 2.3.8; Steed, 2006), with all sets significant to 9.39 mm ($4.2\sqrt{d}$) over 5 km (Table 2.4; Filmer and Featherstone, 2009). Here, for example, where $RC^{b}_{A\text{-}L}$ = 43 mm (Figure 3.5(a); set D) URE is 86 mm per 100 m of ΔH (cf. Section 4.2.1; Angus-Leppan, 1979; Kearsley et al., 1993b; Rüeger, 1997).

Although this simulation uses assumed values that are conducive to large URE (and acknowledging that $RC_{A\text{-}L}$ can over-correct in some conditions), it demonstrates that parts of the ALS/ANLN are likely to be contaminated with systematic errors caused by URE that have propagated into the AHD. The tests also indicate that RC should be applied to current levelling observations, particularly ICSM (2007) class LC and LD. Because the lower quality levelling types (class LC and LD) are allowed longer S_ℓ, they are much more susceptible to URE, despite their larger r_m. In addition, large errors/variations in H_F ($>\sim$30 W/m^2; cf. Section 3.5.1) will potentially degrade the accuracy of $RC^{b}_{A\text{-}L}$.

3.5.6 Effect of $\delta Z_{i,\ell}$ on $\delta RC^{b}_{A\text{-}L}$

Evaluating the sensitivity of $RC^{b}_{A\text{-}L}$ to errors in $Z_{i,\ell}$ is somewhat problematic because $Z_{i,\ell}$ is a function of S_ℓ, ΔH and Z_i. To best present the sensitivity of $RC^{b}_{A\text{-}L}$ to errors in $Z_{i,\ell}$, simulated changes to $RC^{b}_{A\text{-}L}$ resulting from variations in S_ℓ, ΔH and Z_i changing $Z_{i\ell}$ are conducted.

Re-computing $RC^b_{A\text{-}L}$ using data set D, but varying S_ℓ between 40 m (maximum S_ℓ for first-order), and $S_\ell = 90$ m (maximum S_ℓ for third-order) demonstrates the change in $RC^b_{A\text{-}L}$ over a 5 km section (Figure 3.6). Using the refraction-conducive conditions of data set D ($H_F = 400$ W/m^2; $\Delta H = 50$ m), Figure 3.6 shows $RC^b_{A\text{-}L}$ to be approximately the same as r_m at maximum S_ℓ for first- and second-order (labelled class LA and LB respectively; second-order $S_\ell = 60$ m), but considerably above r_m for third-order at maximum S_ℓ (labelled class LC). The effect of changing Z_i from 1.65 m to 1.50 m is also shown, with a lower Z_i increasing the effects of URE.

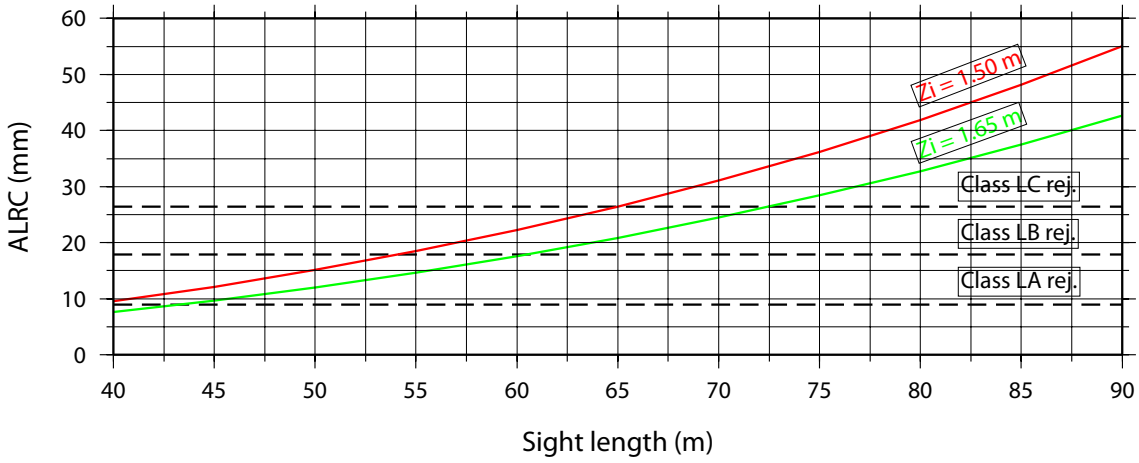

Figure 3.6: $RC^b_{A\text{-}L}$ (ALRC in mm) over a 5 km levelling section using different sight length (S_ℓ) and data set D. The large changes in $RC^b_{A\text{-}L}$ are primarily the effect on Z_{i,ℓ_B} and Z_{i,ℓ_F} of changing S_ℓ. Change of Z_i can also be seen. First-, second- and third-order r_m for 5 km are labelled as class LA, LB, and LC respectively.

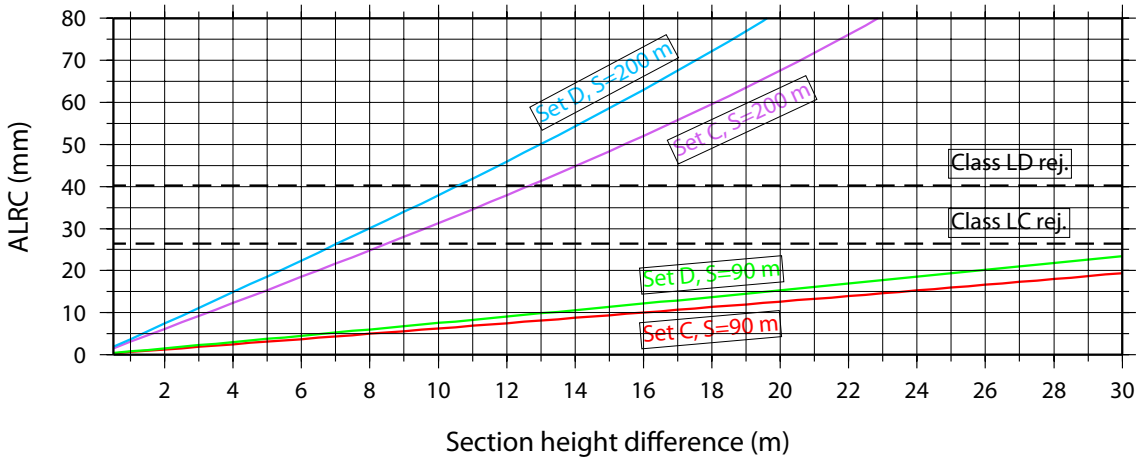

Figure 3.7: $RC^b_{A\text{-}L}$ (ALRC in mm) over a 5 km levelling section for 0.5 m $< \Delta H <$ 50 m (changing Z_ℓ). Sets C and D are used in this example (using $S_\ell = 90$ m, and $S_\ell = 200$ m) where the difference between Z_{i,ℓ_F} and Z_{i,ℓ_B} decreases as ΔH decreases. Third- and fourth-order r_m for 5 km are labelled as class LC and LD respectively

Figure 3.7 shows ΔH varying from 0.5 m to 30 m and the effects on $RC^{b}_{A\text{-}L}$ over a 5 km section. Different ΔH over 5 km will result in variations in Z_ℓ. Using data set C and D with $S_\ell = 90$ m, Figure 3.7 (red and green solid lines respectively) shows that for a 5 km section, ΔH <30 m results in $RC^{b}_{A\text{-}L}$ staying below class LC r_m. By contrast, using maximum S_ℓ for NMC (1981) fourth-order ($S_\ell = 200$ m; solid blue and purple lines), causes very large $RC^{b}_{A\text{-}L}$, well above fourth-order (class LD) r_m where ΔH >∼12 m. Note that NMC (1981) fourth-order S_ℓ of 200 m is now 100 m under ICSM (2007) class LD standards (see Section 2.3), although r_m is $18\sqrt{d}$ for both. NMC (1981) fourth-order S_ℓ is used here to demonstrate maximum possible errors, as it is assumed that fourth-order levelling in the ANLN was conducted to NMC (1981) standards.

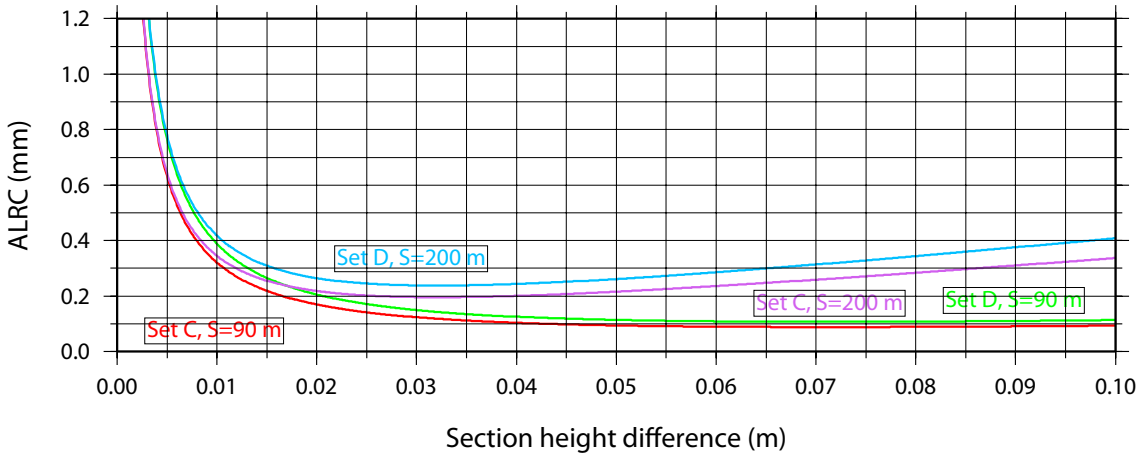

Figure 3.8: $RC^{b}_{A\text{-}L}$ (ALRC in mm) over a 5 km levelling section for 0.0001 m < ΔH < 0.2 m, showing the behaviour of $RC^{b}_{A\text{-}L}$ as $\Delta H \to 0$. Sets C and D are used in this example (using $S_\ell = 90$ m, and $S_\ell = 200$ m) where the difference between Z_{i,ℓ_F} and Z_{i,ℓ_B} decreases as ΔH decreases.

Figure 3.7 starts at $\Delta H = 0.5$ m because Equation (3.14) shows that when Z_i and Z_ℓ are equal $RC^{b}_{A\text{-}L}$ is undefined. Figure 3.8 shows the behaviour of Equation (3.14), where $RC^{b}_{A\text{-}L}$ becomes very large as $\lim_{(Z_i - Z_\ell)\to 0}$. Identification of the inflection point is necessary, so that when ΔH becomes small, the point at which $RC^{b}_{A\text{-}L}$ should be considered zero is known. This point appears to be as large as 0.08−0.09 m when S_ℓ = 90 m, but closer to 0.03−0.04 m when S_ℓ = 200 m. When ΔH is 0.0001 m (the smallest possible in the ANLN), $RC^{b}_{A\text{-}L}$ is 38 mm for set D and 31 mm for set C (for both S_ℓ = 90 m and 200 m). For ΔH <0.1 m, it is suggested that $RC^{b}_{A\text{-}L}$ should be considered zero (see Chapter 4).

3.5.7 Effect of δS_ℓ, δP_a and δT_a on $\delta RC^b_{A\text{-}L}$

$RC^b_{A\text{-}L}$ is less sensitive to changes in S_ℓ, P_a and T_a than to changes in H_F or $Z_{i,\ell}$. Here, set D (see Table 3.4; $H_F = 400$ W/m^2) is used to estimate maximum $\delta RC^b_{A\text{-}L}$ for errors/variations in input values for S_ℓ (δS_ℓ), P_a (δP_a) and T_a (δT_a). When $\delta S_\ell = 40$ m, $\delta RC^b_{A\text{-}L}$ increases to almost 2.5 mm over the 5 km levelling section. The sensitivity of $\delta RC^b_{A\text{-}L}$ to S_ℓ is not fully revealed here, as a change in S_ℓ will also result in a change to $Z_{i,\ell}$, which has more influence on $\delta RC^b_{A\text{-}L}$ (see Section 3.5.6).

When δP_a is 35 mb, $\delta RC^b_{A\text{-}L}$ increases to 1.5 mm over the 5 km section and when $\delta T_a = 30°$ K, $\delta RC^b_{A\text{-}L}$ reaches a maximum magnitude of -0.55 mm. $\delta RC^b_{A\text{-}L}$ is more sensitive to δS_ℓ, δP_a and δT_a when H_F is larger, but even using maximum values, $\delta RC^b_{A\text{-}L}$ is well below third-order r_m for the 5 km section (26.83 mm) and is also not significant in terms of estimated STD from either Steed (2006) or Filmer and Featherstone (2009) (cf. Section 3.5.5). $RC^b_{A\text{-}L}$ is therefore considered to be virtually unaffected by errors or large variations in S_ℓ, P_a and T_a.

3.5.8 Discussion of results

Levelling sections using long S_ℓ (e.g., 90 m, which is ANLN third-order) that run up or down moderate gradients where maximum S_ℓ could still be used are most susceptible to URE (cf. Strange, 1981). High H_F in these conditions will cause $RC_{A\text{-}L}$ to be >40 mm over 5 km levelling runs, which is larger than third-order/class LC r_m over this distance (26.83 mm), suggesting that refraction may contribute significantly to errors and distortions in the AHD. It appears that RC should be applied to all levelling where the necessary input atmospheric data is available, but particularly to ICSM (2007) class LC/ANLN third-order or lower quality levelling because of the detrimental effects that long S_ℓ have in regard to URE.

$RC_{A\text{-}L}$ is shown to be more sensitive to errors or variations in some variables than others. $RC_{A\text{-}L}$ is most sensitive to errors or variations in H_F when H_F is low ($<\sim$100 W/m^2); when H_F is 50 W/m^2, an error/variation of $\sim$72 W/m^2 in the H_F input value

will cause an error in $RC_{A\text{-}L}$ the same magnitude of $RC_{A\text{-}L}$ itself. However, although H_F can vary by up to 300 W/m^2 at Birdsville (in winter; Figure 3.3(b)), $RC_{A\text{-}L}$ is much less sensitive to variation when H_F is high. The effect of retrospectively approximating H_F (without knowing the time of year the observations took place) for input into $RC_{A\text{-}L}$, in addition to the use of average H_F for an entire day (i.e., ignoring diurnal variations), will degrade the accuracy of simulated $RC_{A\text{-}L}$ (in an extreme example, an error the size of the RC itself could occur). The ANLN cannot be currently rigorously retrospectively corrected for refraction because there is insufficient information available for accurate estimation of input data.

Changes to S_ℓ impact on $Z_{i,\ell}$, indicating that in conditions conducive to URE, S_ℓ should not exceed 50 m (or possibly less), especially if RC are not applied. However, although these tests indicate errors caused by URE can exceed r_m, they will possibly not be detectable in the field, because the effects are terrain dependent, assuming that S_ℓ and H_F remain constant (which is often not the case). Thus, forward and backward levelling runs up and down a steady gradient will contain the same magnitude of URE, but with opposite signs, resulting in satisfactory closure (cf. Angus-Leppan, 1984). However, the full refraction error will remain in the mean height difference for the two-way levelling, making the magnitude of the mean height difference less than it should be. In this way, URE can remain hidden.

3.6 Summary

A review of attempts to retrospectively correct for URE reveal numerous versions of RC that have been applied with varying success. A difference of views emerged in the 1980s as to whether refraction has a significant effect on levelling. However, there is sufficient evidence that refraction does affect levelling, but the variable nature of refraction and difficulties in measuring or predicting the temperature gradient cause difficulties in accurately reducing URE in levelling observations. The ANLN cannot be rigorously corrected for URE at this stage, because insufficient information is available in the ANLN (it is assumed that some or all of this metadata exists elsewhere in

hardcopy format), but the $RC_{A\text{-}L}$ can be used to retrospectively simulate RC in the ANLN. A combination of average meteorological data at four sites across Australia and assumed input data was used to conduct a sensitivity test for the $RC_{A\text{-}L}$ to assess the effects of assumptions made for unavailable input data.

Diurnal and seasonal variations in H_F can be large, with H_F also sensitive to errors in estimates of C_f and W_f. An error in C_f or W_f of 0.3 can cause an error in H_F of 50−100 W/m^2, depending on the input value of C_f and W_f. The error analysis showed that $RC_{A\text{-}L}$ is most sensitive to errors in H_F, particularly when H_F is low (<100 W/m^2), and less sensitive when H_F is high. Separate tests also demonstrate that $RC_{A\text{-}L}$ is sensitive to changes in $Z_{i,\ell}$ which itself is a function of S_ℓ, Z_i and ΔH. However, $RC^b_{A\text{-}L}$ appears relatively insensitive to errors/variations in the remaining input parameters S_ℓ, P_a and T_a. Under conditions conducive to high URE, simulations suggest that $RC^b_{A\text{-}L}$ can exceed ICSM (2007) r_m, particularly for third-order/class LC and fourth-order/class LD levelling, primarily because of longer maximum S_ℓ. Thus, it is likely that because the ANLN comprises mostly third-order levelling (S_ℓ of 90 m), URE is probably contributing to the large errors and distortions identified in the AHD and ANLN, in addition to the gross errors identified in Chapter 2. It is an open question as to whether URE can be effectively reduced in the ANLN by applying RCs, and can only be answered by testing when the necessary metadata becomes available, or new data is collected specifically to test this.

4. SIMULATED APPLICATION OF ANGUS-LEPPAN (1979) REFRACTION CORRECTIONS TO THE ANLN

The absence of atmospheric and time/date of survey information in the Australian National Levelling Network (ANLN) metadata places considerable limitations on any attempt to retrospectively apply refraction corrections (RC) to ANLN levelling observations. However, an approximation of the effect on adjusted heights of applying Angus-Leppan (1979) RC ($RC_{A\text{-}L}$) to the ANLN can be made through a simulation, where assumed information is used in place of unavailable metadata. Thus, identifying the possible effects of refraction on AHD heights (of which no estimate currently exists) is the primary objective of this Chapter. This is important to gauge the significance of refraction in the ANLN, which may provide justification for extracting metadata (now in hardcopy format) into the ANLN file so that attempts can be made to reduce actual unequal refraction error (URE) in the ANLN.

4.1 Assumed data and computation methods

4.1.1 Estimates of C_f and W_f

Details of cloud cover are required to estimate C_f (factor accounting for cloud cover), while wind speed and surface moisture are needed to estimate W_f (factor accounting for surface wetness; both evaluated using Figure 3.2), which are required to compute heat flux (H_F) using Equation (3.17). This information (or the information with which to derive it) is not available in the ANLN metadata, so estimates are made from average meteorological conditions at different locations. Weather station location and elevation (e.g., Table 3.2) and average meteorological observations (e.g., Table 3.3), like those used in Section 3.4) were compiled for 53 weather stations across Australia (data from the Australian Bureau of Meteorology, http://www.bom.gov.au/climate/averages/; see Appendices A and B). The location of these stations are shown in Figure 4.1. These

data (maximum temperature, wind speed, precipitation and cloudy/clear days) were used to estimate C_f and W_f (from Figure 3.2) at each station and assumed to be representative of local conditions for a particular month.

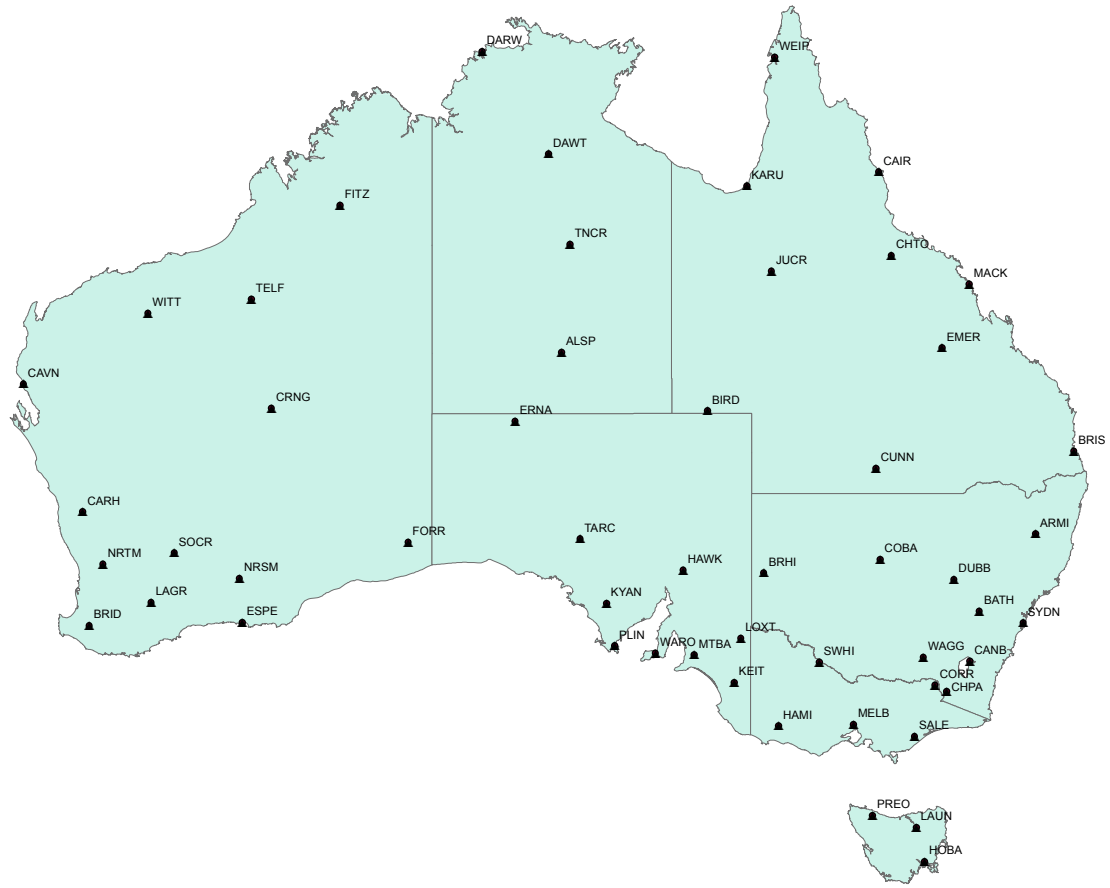

Figure 4.1: The 53 Australian weather stations (see Appendices A and B) from which average July meteorological data were used to estimate C_f and W_f. These stations also provided values for T_a and P_a. Mercator projection, map produced in ESRI arcGIS. Data from the Australian Bureau of Meteorology.

Average values for July (Australian winter) were used on the assumption that most of Australia (particularly the hot interior and north) was surveyed in the cooler (and dryer in the case of the tropical north) months of the year. However, it is acknowledged that levelling for the ALS could have been conducted at all times of the year. These assumptions were required because the date of observation is not available for ANLN sections. Although the assumption that all surveys are conducted in winter will introduce errors, it was considered preferable to under-correct summer observations than over-correcting winter observations, thus over-stating the effect on the AHD of not applying RCs.

The data for each station includes the input meteorological parameters required for $RC_{A\text{-}L}$: temperature (T_a), air pressure (P_a), C_f and W_f (Appendix B). Two sets of values for C_f and W_f were prepared and tested in the simulation, to account for the uncertainty in the C_f and W_f estimates (for levelling on a particular day) that would result from using average winter meteorological data. The initial estimates of C_f and W_f are referred to as meteorological data set 1 (met1), while the second set is meteorological data set 2 (met2). The difference between met 1 and met 2 is that C_f and W_f values for met 2 were slightly less because heavier clouds for cloudy days and higher moisture retention in the soil at each weather station is assumed for met 2 (cf. Figure 3.2). However, it is impossible to gauge which interpretation is closest to the 'truth', particularly as the variation from average values encountered within a season, and also during a day can both vary by up to 300 W/m^2 in extreme conditions (Section 3.5.1).

Values for T_a, P_a, C_f and W_f at each of the 53 stations located across Australia were spline-interpolated onto a 0.5° grid using the **surface** subroutine in Generic Mapping Tools (GMT) version 4.2.0 (Wessel and Smith, 2007). **Surface** is a continuous curvature surface gridding algorithm (Smith and Wessel, 1990) with an adjustable tension factor T where $1 \geqslant \mathrm{T} \geqslant 0$. A value of $\mathrm{T} = 0.25$ is used here as recommended by Wessel and Smith (2007) for smooth surfaces. These grids provided input T_a, P_a, C_f and W_f to compute $RC_{A\text{-}L}$ dependent upon the spatial location of each ANLN sub-section.

Figure 4.2 shows C_f and W_f interpolated from the 53 weather stations. The cool and wet conditions in southern Australia contrast with warm and dry conditions in central and northern areas during July. The differences between C_f and W_f from met1 (Figures 4.2(a) and 4.2(c)) and met2 (Figures 4.2(b) and 4.2(d)) appears to be $\sim 0.1-0.2$ (C_f and W_f were estimated to the nearest 0.1 at the weather stations; Appendix B). The effects of errors/variations in C_f and W_f on H_F is investigated in Section 3.5.2, which show that variations of 0.2 in C_f or W_f can cause errors of up to 70 W/m^2, but more typically <50 W/m^2 (see Figures 3.4(a) and 3.4(b)).

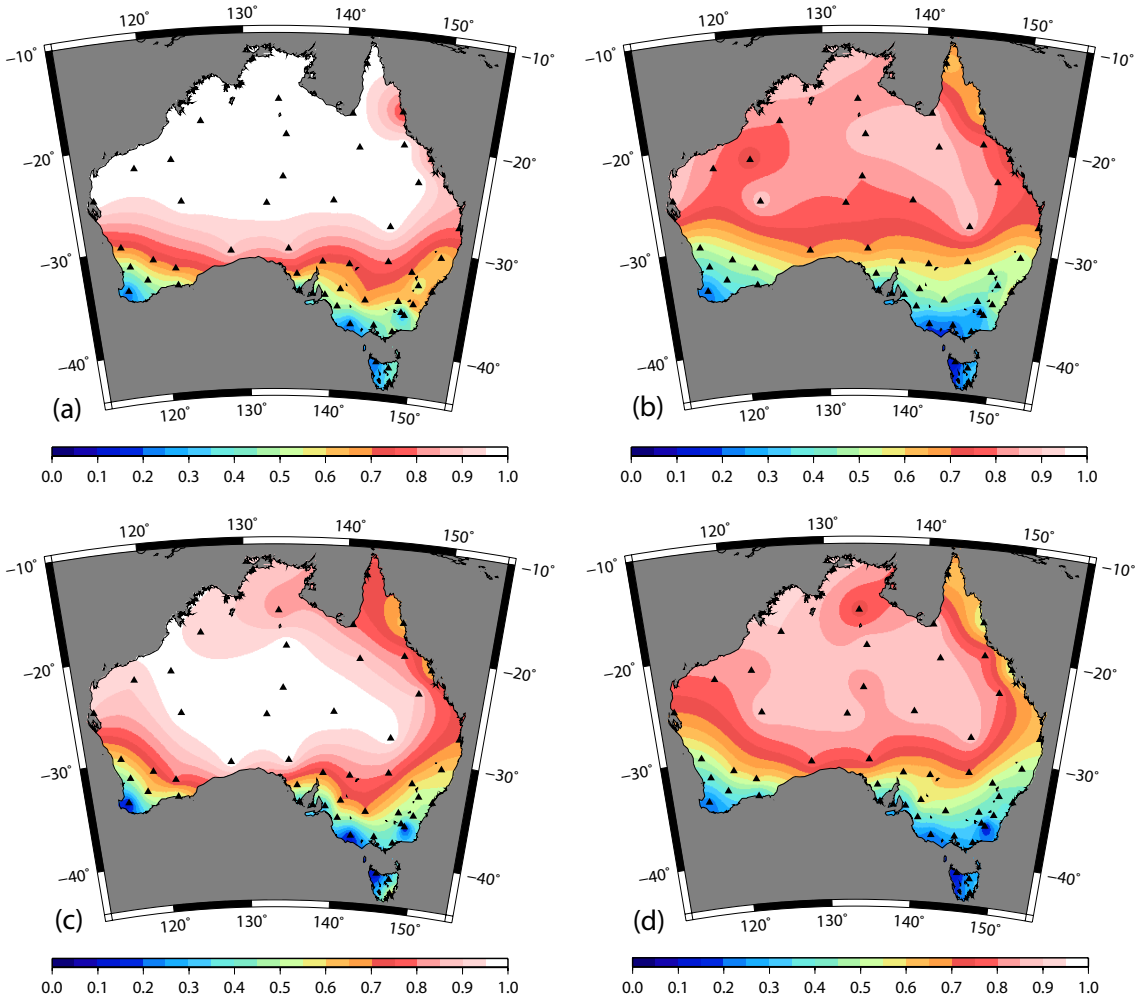

Figure 4.2: C_f and W_f values over Australia spline-interpolated from 53 weather stations (black triangles). (a) is C_f using met1, (b) is C_f using met2, (c) is W_f using met1, and (d) is W_f using met2. Lambert projection, C_f and W_f are dimensionless. Data from the Australian Bureau of Meteorology.

4.1.2 Computation of H_F and H'_F

Equation (3.17) was used to compute H_F, with C_f and W_f values read from the gridded files (Figure 4.2) at the latitude (ϕ_{BM}) and longitude (λ_{BM}) of the terminal benchmark (BM) for the ANLN subsection. The uncertainty in ANLN ϕ_{BM} (∼1.8 km) and λ_{BM} (∼1.8 km; see Section 2.3.2) is not significant when C_f and W_f are interpolated from a 0.5° (∼55 km) grid.

Equation (3.18) was used to determine $\cos\zeta_s$ (ζ_s is the Sun's zenith distance), with the latitude of observation (ϕ) = ϕ_{BM} at the terminal BM of the ANLN subsection, hour angle (t_s) set at two hours or 30° of arc (10 am or 2 pm) and the Sun's declination (δ_s)

set at +23.5°, which is the maximum value during the Southern Hemisphere winter (winter solstice, June 21). The value of H_F on an inclined surface (H'_F) is computed using Equation (3.21), but first requires the slope of the terrain surface (ρ_T), azimuth of the terrain slope (γ_{ρ_T}; i.e. aspect), and the Sun's azimuth α_s to be computed (details to follow).

4.1.3 Azimuth of slope γ_{ρ_T}

The assumption made here is that γ_{ρ_T} is the same as the azimuth of the levelling γ_L (see later for a discussion on this assumption). Note that when $\gamma_{\rho_T} = 180°$, the slope is downwards towards the south; $\gamma_{\rho_T} = 0°$ indicates the terrain slopes downwards towards north (Angus-Leppan, 1979). γ_L is computed using ϕ_{BM1} and λ_{BM1} (Ω_{BM1}) of the starting BM and ϕ_{BM2} and λ_{BM2} (Ω_{BM2}) of the terminal BM of each sub-section. While a precise equation to compute the azimuth could be used (e.g., Vincenty, 1975), the accuracy of ($\Omega_{BM1}, \Omega_{BM2}$) are only ∼1 arc minute (Section 2.3.2). The inverse formula of Vincenty (1975) required here has a sub-mm accuracy for distances up to 18,000 km (Thomas and Featherstone, 2005), but is considered unnecessary here, because of the low positional accuracy of Ω_{BM} (1 arc minute or ∼1.8 km).

The method adopted here to compute γ_L uses the length of an arc on a sphere to compute latitude and longitude differences between Ω_{BM1} and Ω_{BM2} ($\Delta\phi = \phi_{BM2} - \phi_{BM1}$ and $\Delta\lambda = \lambda_{BM2} - \lambda_{BM1}$ respectively) in metres (ΔE, ΔN)

$$\Delta E = R(\Delta\lambda)\cos\phi_{BM1} \tag{4.1}$$

$$\Delta N = R(\Delta\phi). \tag{4.2}$$

Here, $\Delta\phi$ and $\Delta\lambda$ are in radians and R is the mean radius of the GRS80 ellipsoid (6,371 km; Torge, 2001, 99). Although the Gaussian radius of curvature at ϕ_{BM1} and ϕ_{BM2} would provide a better local approximation of R (e.g., Torge, 2001, 98), Equations (4.1) and (4.2) are relatively insensitive to large changes in R (only a few arc-seconds difference in azimuth resulted from testing different values of R), indicating that using $R = 6371$ km is satisfactory for determining γ_L. The term $\cos\phi_{BM1}$ in

Equation (4.1) was applied to compensate for the convergence of the meridians as the latitude increases.

ΔE and ΔN are now assumed to be on a plane rectangular grid (suitable for distances <10 km; see Table 4.1 for likely errors). The following formulas were used to compute γ_L for each sub-section, conditional on the quadrant in which the azimuth was located (determined by the signs of ΔE and ΔN)

$$\gamma_L = 360^\circ + \arctan\left(\frac{\Delta E}{\Delta N}\right) \begin{cases} \Delta E < 0 \\ \Delta N > 0 \end{cases} \tag{4.3}$$

$$\gamma_L = 180^\circ + \arctan\left(\frac{\Delta E}{\Delta N}\right) \{\Delta N < 0 \tag{4.4}$$

$$\gamma_L = \arctan\left(\frac{\Delta E}{\Delta N}\right) \begin{cases} \Delta E > 0 \\ \Delta N > 0 \end{cases} \tag{4.5}$$

Further conditions were imposed to avoid computational problems when ΔE or ΔN (or both) were zero. When the section is short and $\Delta\phi$ and $\Delta\lambda$ (and therefore also ΔN and ΔE) both round to zero, γ_L is indeterminate. In this case, the value of H_F is adopted as a close approximation of H'_F. When the denominator ΔN or ΔE is zero, conditions were imposed to assign the correct azimuth (i.e., 0°, 90°, 180° or 270°). If the sub-section height difference (ΔH_{sub}) is positive in the direction of γ_L, the azimuth is reversed (±180°; considered adequate where distances <10 km) to maintain the condition that γ_L points downhill.

α_{V}	ϕ_{BM1}	λ_{BM1}	D_{km}	$\delta\gamma_L$ (DMS)	$\delta\gamma_L$ (m)
90° 01′ 13″	-23° 45′	118° 05′	10.2	-1′ 13″	3.6
162° 57′ 12″	-23° 45′	118° 05′	8.7	4′ 50″	12.2
180° 00′ 00″	-23° 45′	118° 05′	6.5	0′ 00″	0.0
222° 36′ 13″	-23° 45′	118° 11′	11.3	-8′ 14″	27.1
305° 55′ 31″	-23° 50′	118° 07′	3.1	9′ 36″	8.7
137° 22′ 41″	-23° 45′	118° 05′	2.5	9′ 20″	6.8
137° 11′ 28″	-42° 19′	146° 39′	10.1	3′ 43″	10.9
222° 48′ 59″	-42° 18′	146° 46′	10.1	3′ 42″	10.9
143° 25′ 41″	-42° 19′	146° 39′	2.3	5′ 29″	3.7

Table 4.1: Errors in γ_L ($\delta\gamma_L$) in DMS and in metres at distance D_{km} compared to the azimuth computed using the Vincenty (1975) inverse solution (α_{V}).

Differences between γ_L ($\delta\gamma_L$) computed using Equations (4.1) to (4.5) and Vincenty (1975) were computed to demonstrate that the method used here is adequate for this purpose, given the positional accuracy of ANLN Ω_{BM}. A sample of Ω_{BM1} (shown in Table 4.1) and Ω_{BM2} within Australia were compiled for the test. The Vincenty (1975) inverse formula, was then used to compute azimuth (α_{V}) and distance (D_{km}) between the same positions (using GA's online program http://www.ga.gov.au/geodesy/ datums/vincenty_inverse.jsp). α_{V} is assumed to be the 'correct' azimuth for the purpose of this test.

The difference between γ_L and α_{V} is $\delta\gamma_L$. Values for $\delta\gamma_L$ in DMS are in Table 4.1, which are converted to a distance (in metres) over D_{km} for easier assessment, where $\delta\gamma_L(\mathrm{m}) = \tan^{-1}(\delta\gamma_L\ (\mathrm{DMS}))\ D_{km}$. Table 4.1 shows that maximum $\delta\gamma_L$ (DMS) is $<10'$ (in azimuth), and $\delta\gamma_L$(m) is <30 m (in position). The typical length of an ANLN sub-section is ∼5 km. Considering that ANLN Ω_{BM} are accurate to the nearest 1 arc-minute (∼1.8 km in position) the error in the method adopted here can be considered negligible, because the accuracy of the (approximate) azimuth is considerably more accurate than the ϕ and λ used to compute it.

However, there are some problems associated with assuming that the levelling line runs in the same direction as ρ_T. There would undoubtedly be situations where the levelling line runs across the aspect, particularly in steep terrain where difference between H'_F and H_F is larger (cf. Angus-Leppan, 1979, Table V). The aspect could, for example, be facing north and therefore should have a higher value for H'_F, but the levelling line runs west, resulting in the the value for H'_F being virtually unchanged from H_F. In these circumstances, ΔH_{sub} will be used to compute ρ_T, when ΔH_{sub} is actually much smaller than ρ_T (cf. Section 4.1.4). However, given the inadequate ANLN metadata, there does not appear to be a realistic alterative to this method. High-resolution digital elevation models (DEMs) over Australia (e.g., Hirt et al., 2010b) may provide a solution in the future, but is not warranted for this simulation, given the numerous crude assumptions needed here, versus the additional computational complexity.

4.1.4 Slope of terrain ρ_T

Here, ρ_T is computed as

$$\rho_T = \text{abs}\left(\tan^{-1}\left[\frac{\Delta H_{sub}}{1000 \cdot D_{sub}}\right]\right) \tag{4.6}$$

where D_{sub} is the sub-section distance in km, provided in the ANLN to the nearest 0.1 km. Testing using the examples in Angus-Leppan (1979) demonstrate that ρ_T must be positive.

A problem was encountered on the occasions that ρ_T became so steep that H'_F computed using Equation (3.21) became negative. A stable atmosphere is implied by negative H_F (cf. Section 3.1.2; Angus-Leppan, 1980), but an unstable atmosphere is assumed for this simulation. Negative H'_F also results in Equation (3.13) being indeterminate. This was avoided by capping the value of ρ_T at 25°. ρ_T is >25° 16 times in the ANLN, in which case D_{sub} is generally <200 m and ΔH_{sub} >100 m, although ΔH_{sub} can reach ∼300 m.

Equation (3.20) is used to compute the Sun's azimuth α_s. However, when $t_s = 2$ (used to compute $\cos\zeta_s$ in Equation (3.18), and H_F in Equation (3.17); actual time of levelling is not provided in ANLN), α_s refers to 2 pm (not 10 am), which may bias the effect of the terrain aspect ($(\gamma_L - \alpha_s)$ term in Equation (3.21)). To attempt to minimise any bias, α_s is set to zero (midday in the Southern Hemisphere in winter, Sun is to the north). This avoids a morning/afternoon bias and also maximises the North-South effect and hence, the difference between H_F and H'_F.

4.1.5 Sight length S_ℓ

Any variation in sight length (S_ℓ) is usually due to S_ℓ needing to be made shorter when levelling directly up or down steep slopes. However, for third-order ANLN levelling, the 90 m S_ℓ may have been reduced when H_F is high, because poor observing conditions would make precise observations difficult (e.g., Mark et al., 1987; Rüeger, 1997). To account for the possibility that maximum S_ℓ was not always used, two sets of assumed

S_ℓ were adopted (Table 4.2) in an attempt to simulate the effect of using less-than-maximum S_ℓ.

	$S_{\ell R}$			$S_{\ell M}$		
Order	S1	S2	S3	S1	S2	S3
First	40	30	15	40	30	15
Second	50	30	15	60	40	20
Third	70	40	20	90	60	30
Fourth	100	50	30	150	80	40

Table 4.2: The two sets of sight length (S_ℓ) used; shortened (reduced) S_ℓ ($S_{\ell R}$) and maximum S_ℓ ($S_{\ell M}$). Up to two decreases were made from maximum S_ℓ (S1) to S2, and finally S3 if necessary to shorten S_ℓ on steep slopes. Units are in metres.

These two sets were referred to as reduced (shortened) sight length ($S_{\ell R}$) and maximum sight length ($S_{\ell M}$). $S_{\ell R}$ is (arbitrarily, as there is no other information) made slightly shorter (Table 4.2) from maximum allowable S_ℓ for the ANLN (see Roelse et al., 1971, Annex H), while $S_{\ell M}$ adopts the maximum allowable S_ℓ for the ANLN (Roelse et al., 1971). The very long maximum S_ℓ for fourth-order levelling (200 m; NMC, 1981) makes assumptions regarding the S_ℓ actually used rather problematic. Although ICSM (2007, Table 18, B-11) now states that fourth-order (class LD) maximum S_ℓ is 100 m, it is assumed that the fourth-order levelling in the ANLN was conducted under the NMC (1981) specifications (ANLN fourth-order levelling probably post-AHD). However, $S_{\ell M}$ = 200 m for fourth-order is reduced here to 150 m, on the assumption that 200 m would be rarely used due to difficulties sighting over this distance (cf. Rüeger, 1997).

An attempt was also made to simulate shortening S_ℓ as ρ_T increases, with a condition imposed that all staff readings (Z_ℓ) are to be >0.30 m (cf. Roelse et al., 1971, Annex H). Instrument height Z_i was assumed constant at 1.65 m, so maximum height difference between the instrument and FS staff is 1.35 m (when levelling uphill; if levelling downhill this applies to the BS). Thus, maximum staff readings were 3.00 m (BS levelling uphill; FS downhill) and minimum 0.30 m (FS levelling uphill; BS downhill). When the FS (uphill; BS downhill) staff reading in the simulation is <0.30 m, S_ℓ is shortened, maintaining a minimum staff reading of 0.30 m.

Table 4.2 shows how S_ℓ is shortened from maximum S_ℓ (S1) to S2 and S3 (if necessary) when the staff reading is <0.30 m. When S_ℓ <0.30 m, S1 is decreased to S2 S_ℓ, then Z_ℓ is re-computed; if S_ℓ is still <0.30 m, S3 S_ℓ is adopted. S3 is the minimum S_ℓ used, because for steeper ρ_T, it is assumed that the levelling line will zig-zag uphill (or obliquely) to allow Z_ℓ to be >0.30 m without needing to shorten S_ℓ. More iterations with smaller reductions could be made in this computation, but given the uncertainty associated with assumptions for S_ℓ, it is considered that further refinement is of little benefit to the simulation.

The number of FS and BS observations in a particular sub-section (n_{obs}) is

$$n_{obs} = \frac{1000 D_{sub}}{S_\ell} \tag{4.7}$$

where D_{sub} is in km. The number of individual height differences (BS−FS) for the sub-section ($n_{\Delta H}$) is

$$n_{\Delta H} = \frac{n_{obs}}{2} \tag{4.8}$$

with the height difference per S_ℓ (ΔH_{S_ℓ})

$$\Delta H_{S_\ell} = \frac{\Delta H_{sub}}{n_{obs}} \tag{4.9}$$

with ΔH_{sub} in metres.

4.1.6 Height factor $Z_{i,\ell}$

It was necessary to identify all sub-sections where ΔH_{sub} is close to zero due to the behaviour of Equations (3.15) to (3.16) when ΔH_{sub} approaches zero (see Figure 3.8). It is suggested in Section 3.5.6 (based on Figure 3.8), that when ΔH_{sub} <0.10 m (D_{sub} = 5 km), thus making ΔH_{S_ℓ} = 1.8 mm (for third-order S_ℓ of 90 m), $RC_{A\text{-}L}$ should be set to zero. To ensure a safety margin when ΔH_{sub} is small, $RC_{A\text{-}L}$ is set to 0.000 m when $|\Delta H_{S_\ell}|$<0.02 m.

Backsight and foresight readings (Z_B and Z_F respectively) for each set-up (constant for the subsection; Z_i = 1.65 m) were dependent on ΔH_{S_ℓ} (see Section 4.1.5). When

levelling uphill and $\Delta H_{S_\ell} > 0.02$ m,

$$Z_F = Z_i - |\Delta H_{S_\ell}| \tag{4.10}$$

$$Z_B = Z_i + |\Delta H_{S_\ell}| \tag{4.11}$$

when levelling downhill and $\Delta H_{S_\ell} < -0.02$ m,

$$Z_F = Z_i + |\Delta H_{S_\ell}| \tag{4.12}$$

$$Z_B = Z_i - |\Delta H_{S_\ell}| \tag{4.13}$$

Where Z_B >3.00 m and Z_F <0.30 m when levelling uphill (very steep slope, S_ℓ reduced to S3; see Section 4.1.5) $Z_B = 3.00$ m and $Z_F = 0.30$ m on the assumption that the levelling was conducted obliquely. The reverse applies for downhill levelling. Equations (3.15) to (3.16) are then used to compute the BS height factor (Z_{i,ℓ_B}) and FS height factor (Z_{i,ℓ_F}) respectively. $RC^b_{A\text{-}L}$ for the entire sub-section ($RC^b_{A\text{-}L}$(sub))is

$$RC^b_{A\text{-}L}(\text{sub}) = n_{\Delta H}(RC^b_{A\text{-}L}) \tag{4.14}$$

4.2 Simulation results

Results from the simulation are presented in terms of $RC_{A\text{-}L}$ per 10 m of height change (ΔH), because this is a common measure of URE, demonstrating correlation with increase in height (e.g., Bomford, 1971; Angus-Leppan, 1979; Rüeger, 1997). In addition, comparisons of loop misclosures (ε_L) before and after simulated $RC_{A\text{-}L}$ are applied to ANLN sub-sections are made, where smaller ε_L may suggest that the URE has been reduced. Differences between minimally constrained least-squares adjusted (MCLSA) heights (with and without $RC_{A\text{-}L}$) are also evaluated to simulate the magnitude of URE that may have propagated into the AHD, and could also propagate into any new levelling-based Australian vertical datum (AVD) if URE is not removed or minimised. However, it is difficult (or impossible) to assess whether the simulated $RC_{A\text{-}L}$ have 'improved' the accuracy of the heights, because the 'true' heights are not known.

4.2.1 Simulated $RC_{A\text{-}L}$ correlation with ΔH

Because URE accumulates with height, the magnitude of the RC can be calculated with respect to ΔH. Bomford (1971, 241) suggests a worst case error of 2 mm per 10 m ΔH. Rüeger (1997) estimates a maximum of 3 mm per 10 m ΔH on a sunny day in summer around noon, but with the assumption that Z_ℓ are >0.5 m (cf. Roelse et al., 1971) and maximum $S_\ell = 50$ m. Angus-Leppan (1979, Table V) also suggests maximum values of ∼25 mm per 100 m ΔH (maximum $S_\ell = 50$ m). The results from this simulation can be compared to these suggested values for RC by computing $RC_{A\text{-}L}$ per 10 m ΔH for each ANLN sub-section.

	$RC_{A\text{-}L}$ (mm per 10 m ΔH)	
Data set	Mean	Maximum
$S_M$met1	2.5	19.0
$S_M$met2	2.0	15.3
$S_R$met1	1.5	8.3
$S_R$met2	1.2	7.1

Table 4.3: Average and maximum (for all 89,607 ANLN sub-sections) simulated $RC_{A\text{-}L}$ corrections (mm per 10 m ΔH) for the four data sets.

The average simulated $RC_{A\text{-}L}$ computed from the 89,607 ANLN sub-sections are shown for each set of assumed information in Table 4.3. The average for $S_{\ell M}$met1 is 2.5 mm per 10 m ΔH (cf. Rüeger, 1997; Angus-Leppan, 1979, Table V), while the average for $S_{\ell M}$met2 is 2.0 mm per 10 m ΔH (cf. Bomford, 1971, 241). However, the simulated values here are for winter, while the estimates of Rüeger (1997) and Angus-Leppan (1979) are for summer. The differences can be explained by many areas of central Australia having conditions in winter that are similar to summer in more temperate regions. This will inflate the simulated values, but the differences are probably due more to the predominately third-order levelling of the ANLN having an allowable maximum S_ℓ of 90 m, while Rüeger (1997) and Angus-Leppan (1979) consider maximum S_ℓ of 50 m (cf. Figures 3.6 and 3.7). $S_{\ell R}$met1 (1.5 mm per 10 m ΔH) and $S_{\ell R}$met2 (1.2 mm per 10 m ΔH) are more comparable to the winter values of Rüeger (1997) and Angus-Leppan (1979), but are probably an under-estimation (for winter) for the mostly third-order ANLN with maximum $S_\ell = 90$ m.

The impact on height-correlated RC values of different maximum S_ℓ is indicated in Figure 4.3 by a histogram of the percentage of ANLN sub-sections within certain values (1 mm intervals) of height-correlated RC. Although Figure 4.3 represents the entire ANLN (89,607 sub-sections), a separate analysis of the different levelling orders reveal that ~80% of first-order levelling (11,742 sub-sections) have simulated $RC_{A\text{-}L}$ in the 0−1 mm per 10 m ΔH range for all four data sets, contributing to the high percentage of $RC_{A\text{-}L}$ in the 0−1 mm per 10 m ΔH range in Figure 4.3. About 15% of all sub-sections (for all four data sets) have $RC_{A\text{-}L}$ of 0.0 mm per 10 m ΔH, which also contribute to the high percentage in the 0−1 mm per 10 m ΔH range. The second-order levelling (3,309 sub-sections) generally fall in the $RC_{A\text{-}L}$ = 0−2 mm per 10 m ΔH range.

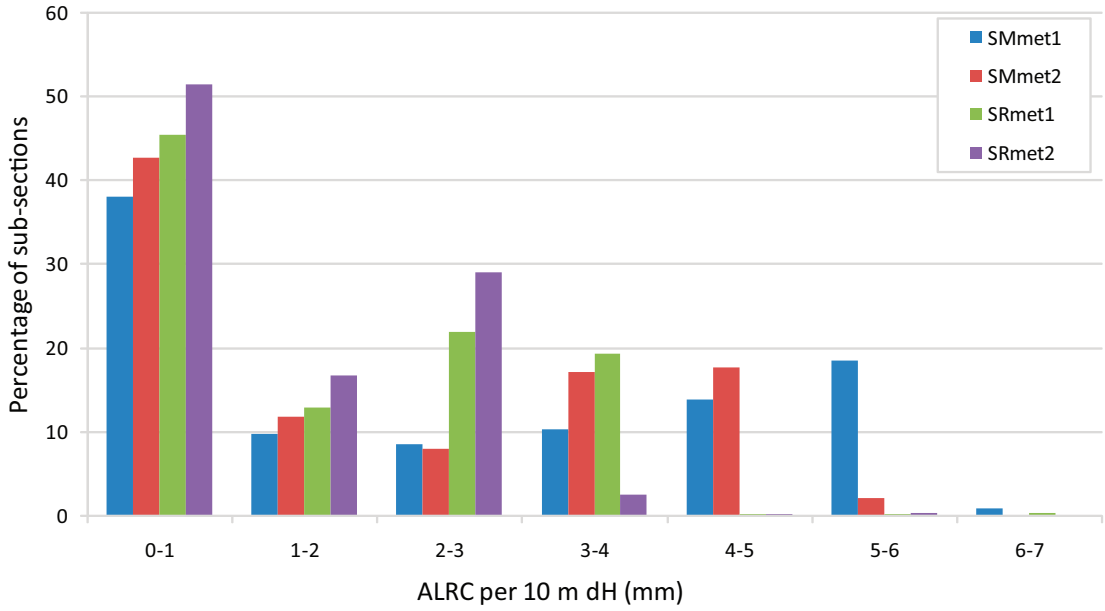

Figure 4.3: Histogram of simulated $RC_{A\text{-}L}$ (mm per 10 m of ΔH) for $S_{\ell M}$ (met1 and met2; $S_M$met1 (blue), $S_M$met2 (red)) and $S_{\ell R}$ (met1 and met2; $S_R$met1 (green), $S_R$met2 (purple)) (see Figure 4.2) and the percentage of ANLN sub-sections (89,607) at different rates of $RC_{A\text{-}L}$ (mm per 10 m of ΔH). Interval size is 1 mm.

However, the third-order levelling (57,736 sub-sections) are spread out over the $RC_{A\text{-}L}$ = 0−6 mm per 10 m ΔH range for $S_M$met1, reducing to $RC_{A\text{-}L}$ = 0−3 mm per 10 m ΔH range in $S_R$met2, but tend to 'spike' in a particular range. These are (Figure 4.3): $S_M$met1 at ~$RC_{A\text{-}L}$ = 5−6 mm per 10 m ΔH, $S_M$met2 at $RC_{A\text{-}L}$ = 3−5 mm per 10 m ΔH, $S_R$met1 at $RC_{A\text{-}L}$ = 2−4 mm per 10 m ΔH and $S_R$met2 at $RC_{A\text{-}L}$ = 2−3 mm per 10 m ΔH. Although the sample is small, and is not shown in Figure 4.3, 68.5% of

the fourth-order levelling (693 sub-sections) in $S_M$met1 have $RC_{A\text{-}L}$ >10 mm per 10 m ΔH and 53.8% >10 mm per 10 m ΔH in $S_M$met2. This decreases to $RC_{A\text{-}L} = 3{-}6$ mm per 10 m ΔH for 64% of fourth-order sub-sections in $S_R$met2.

The implication from these results is that the different levelling types (primarily differing by maximum S_ℓ) are affected differently by URE. Seventy-one percent of the ANLN comprise third-order levelling, which with maximum $S_\ell = 90$ m is very susceptible to URE and could contain systematic errors of up to 6 mm per 10 m ΔH in hot, sunny conditions, which are common in most parts of Australia.

4.2.2 Effect of simulated $RC_{A\text{-}L}$ on ANLN loop closures

It is contended that URE does not appear in ε_L (Angus-Leppan, 1984; Strange, 1981), under the assumption that the levelling comprising a loop is conducted under constant atmospheric conditions and terrain slope, thus cancelling residual URE. However, the likelihood of constant atmospheric conditions and symmetric terrain slope cannot be assumed for an entire loop (cf. Holdahl, 1980, 663), particularly for large loops covering many hundreds of km, as found in Australia (Figure 2.2). Due to time-variability of meteorological conditions and the spatial-variability of terrain slope (URE is dependent on both; see Section 3.5) it is likely that residual URE will often remain in ε_L (cf. Mark et al., 1987; Remmer, 1994).

ANLN ε_L with simulated $RC_{A\text{-}L}$ can be tested for any 'improvement' (i.e., decreases) in ε_L through computed c (c_L in mm; Equation (2.3); cf. Section 2.4.1). Given that rather broad assumptions have to be made to replace unavailable ANLN metadata for highly variable parameters, large decreases in ε_L are not anticipated. Furthermore, the acknowledged presence of other systematic errors in the ANLN could, in fact, cause the loop closures to appear worse, even if URE is effectively removed from the levelling observations (cf. Mark et al., 1987; Craymer and Vaníček, 1986).

Table 4.4 contains average c_L for the ANLN. When no RC is applied, c_L, and thus ε_L for all 1,366 ANLN loops generally appear smaller, although the increases when

simulated $RC_{A\text{-}L}$ is applied are relatively small (∼6% for $S_M$met1; <2% for $S_R$met2). There is a slight increase (1.4% to 2.3%) in c_L for first-order levelling for the four data sets, decreasing when using $S_{\ell R}$met2. Second-order loops indicate a slight decrease in c_L, while third-order loops show increases in c_L similar to those for all 1,366 loops.

Third-order c_L heavily influence the c_L for all 1,366 ANLN loops, as 975 of the 1,366 ANLN loops (71%) are third-order (Table 4.4). Third-order one-way (OW; here, third-order two-way levelling is referred to as third-order, and is considered a separate class to third-order OW) shows small c_L increases for $S_{\ell M}$ (both met1 and met2), but virtually no change for $S_{\ell R}$ (both met1 and met2). The fourth-order loops all display small increases in c_L, although $S_{\ell M}$met2 appears to give the closest result to no RC. Neither the two-way (undefined order; UO; Steed, 2006) and third-order OW/fourth-order mixed loops were included in this analysis due to their low quality and small sample sizes (see Table 2.4).

Order	No. of loops	No $RC_{A\text{-}L}$	met1		met2	
			$S_{\ell M}$	$S_{\ell R}$	$S_{\ell M}$	$S_{\ell R}$
All loops	1366	5.217	5.540	5.362	5.416	5.312
First	56	2.430	2.487	2.475	2.475	2.464
Second	20	2.835	2.730	2.750	2.755	2.770
Third	975	4.222	4.613	4.407	4.465	4.342
Third OW	256	9.202	9.354	9.209	9.301	9.210
Fourth	37	6.316	6.611	6.511	6.322	6.414

Table 4.4: Average c_L (mm) for 1,366 ANLN loops and main levelling types after simulated $RC_{A\text{-}L}$ is applied, compared to when no RC is applied. Third OW is one-way third-order levelling. Normal-orthometric height corrections have been applied to all sub-sections.

It is difficult to draw conclusions from Table 4.4 on the effectiveness (or otherwise) of the simulation. However, it is likely (although difficult to demonstrate) that gross and systematic errors (Sections 2.1.4 and 2.1.5) in the ANLN (e.g., Filmer and Featherstone, 2009; Morgan, 1992) may be masking any decrease in c_L due to $RC_{A\text{-}L}$ (cf. Craymer and Vaníček, 1986). For example, URE could be cancelling a systematic error of similar magnitude, but opposite sign. When URE is removed/reduced in the simulation by the application of $RC_{A\text{-}L}$, the remaining undetected systematic error could now make c_L larger. The other (more likely) reason for seeing no decrease in c_L is the

crude assumptions that have to be made because of the lack of ANLN metadata. The assumptions made for time and date of observation have a potentially large impact on the estimation of H_F which could result in an $RC_{A\text{-}L}$ error being nearly as large as the $RC_{A\text{-}L}$ itself (cf. Figure 3.5).

4.2.3 Difference between H_F and H'_F

Angus-Leppan (1979) predicted a north-south slope in the ANLN (possibly of decimetres; see Section 3.2.4) resulting from higher H_F on slopes with north-facing aspect (i.e., facing the Sun in the Southern Hemisphere) than on south-facing slopes. The computation of H'_F (Equation (3.19)) to replace H_F, takes the aspect of the terrain slope and the position of the Sun into account. H'_F was computed for this simulation (as per Section 4.1), as was H_F (required in Equation (3.19)). To test the postulate of Angus-Leppan (1979), $RC_{A\text{-}L}$ was computed separately using H'_F and H_F, with both applied to the ANLN (referred to as $\text{ANLN}_{H'_F}$ and ANLN_{H_F}).

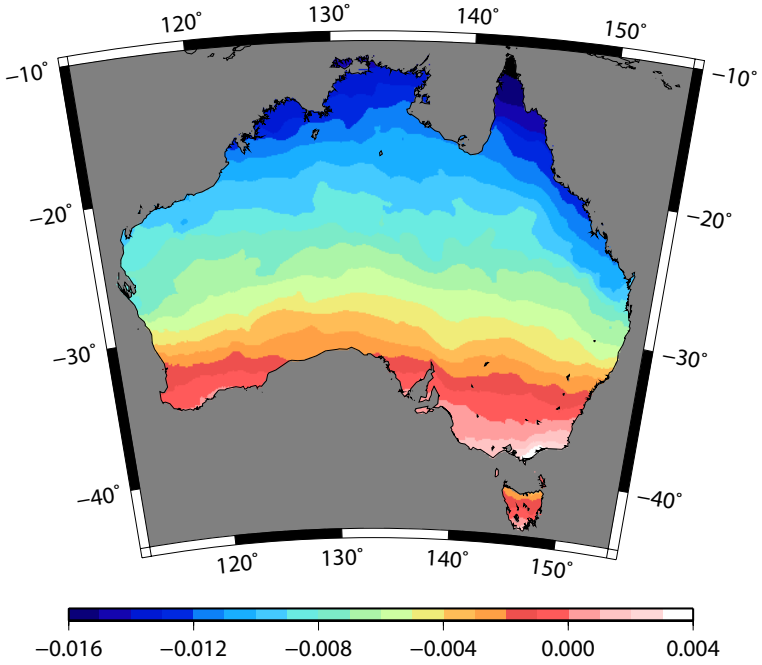

Figure 4.4: $\text{MC}_{H'_F} - \text{MC}_{H_F}$. Both MC ANLN fixed to MSL = zero at Albany tide-gauge (WA; JP 176) and Hobart tide-gauge (Tas; JP 3034). Units are in metres.

A MCLSA of the ANLN (MC ANLN; fixed to MSL = zero at Albany tide-gauge, JP 176, and Hobart tide-gauge, JP 3034, as was done in Section 2.3.8) was conducted for

$\text{ANLN}_{H'_F}$ ($\text{MC}_{H'_F}$) and ANLN_{H_F} (MC_{H_F}; normal-orthometric height correction applied to both MC ANLN). The difference between $\text{MC}_{H'_F}$ and MC_{H_F} is shown in Figure 4.4. A north-south trending-slope between $\text{MC}_{H'_F}$ and MC_{H_F} is apparent, but the range is only ∼20 mm, somewhat less than the 0.05 m to 1 m per 1000 km of north-south levelling predicted by Angus-Leppan (1984, 173). It therefore appears unlikely that the unequal heating of north-facing and south-facing terrain slopes contributes to a significant north-south trend (in terms of the ∼1 m AHD slope) in the ANLN (and thus the AHD). It will be shown in Chapter 5 that sea surface topography (SSTop) is the main cause of the north-south AHD slope.

4.2.4 Effect of simulated $RC_{A\text{-}L}$ on adjusted ANLN heights

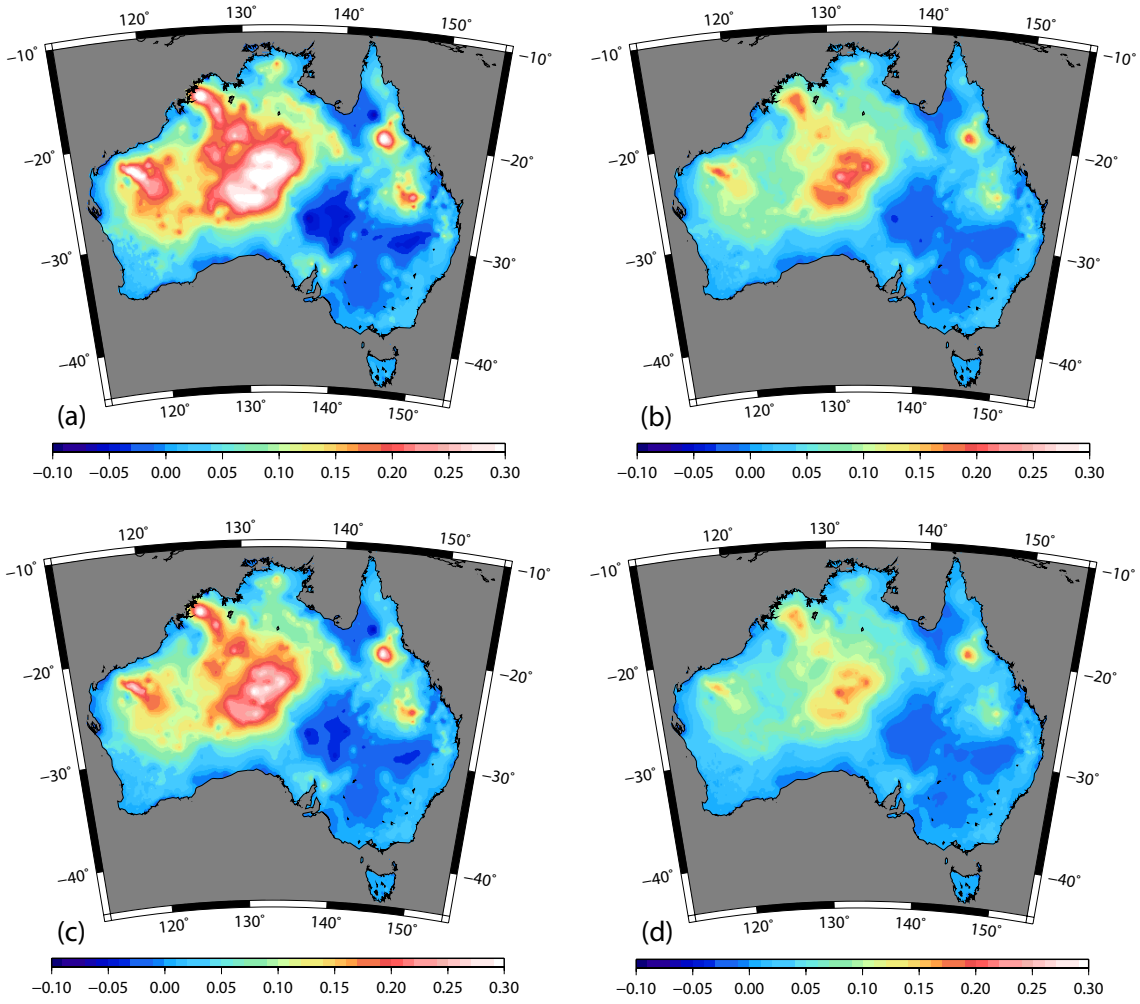

Figure 4.5: Fixed LSAs of the ANLN with $RC_{A\text{-}L}$ (fixANLN_{RC} (see text for adjustment details) minus fixANLN (no $RC_{A\text{-}L}$). Meteorological data for each fixANLN_{RC} are (a) $S_M$met1; (b) $S_R$met1; (c) $S_M$met2; and (d) $S_R$met2. Lambert projection, units are in metres.

To simulate the effect of not applying RC to the ANLN to remove (or reduce) URE, fixed LSAs of the ANLN (fixANLN) were compared with and without simulated $RC_{A\text{-}L}$. For all fixANLN, the ANLN was fixed to MSL + CSIRO Atlas of Regional Seas 2006 (CARS2006; Ridgway et al., 2002) SSTop heights (see Chapter 5) at 32 AHD tide-gauges with normal-orthometric height corrections applied to the ANLN in all adjustments (cf. Chapter 7). Comparisons of fixANLN with simulated $RC_{A\text{-}L}$ (using each of the four different datasets; fixANLN$_{RC}$) minus fixANLN (no RC) can be seen in Figure 4.5, which indicates the possible magnitude of error in AHD heights that could be caused by URE.

The maximum difference can be seen in Figure 4.5(a) ($RC_{A\text{-}L}$ using $S_M$met1). The prominent feature is large positive differences in central Australia where fixANLN$_{RC}$ is higher than fixANLN (no RC), with the differences strongly height-correlated (cf. Figure 1.1), particularly in the northern and central parts of Australia, where H_F is higher. Thus, the application of simulated RC causes high elevations to be higher by a few decimetres (cf. Angus-Leppan, 1984).

The maximum difference (Figure 4.5(a)) is 0.42 m (Table 4.5) in the MacDonnell Ranges (centred at 25°S, 130°E), but with differences >0.30 m in the Hammersley Range (centred at 23°S, 118°E), King Leopold Ranges (centred at 14°S, 125°E), and northern Great Dividing Range (centred at 19°S, 143°E). The reverse can be seen where the minimum of −0.07 m is located at Lake Eyre (−16 m AHD; centred at 28°S, 137°E) where fixANLN$_{RC}$ is lower than fixANLN (no RC). The RC therefore makes the terrain slope steeper, so that in addition to the high points being higher, the low points are also lower. Note that there is <0.05 m difference in the Australian Alps (centred at 37°S, 148°E), which contain the largest mountains in Australia. The very low H_F (winter conditions used in the simulation) is a contributing factor, plus the large amount of first-order levelling in this region (see Figure 2.2), which has shorter maximum S_ℓ (40 m) and thus smaller RC (cf. Figure 3.6).

Using $S_{\ell R}$ in place of $S_{\ell M}$ reduces the height differences resulting from the simulated application of $RC_{A\text{-}L}$ (cf. Figure 4.5(a) to Figure 4.5(b); cf. Figure 4.5(c) to Figure 4.5(d)).

The same terrain features are seen in all plots in Figure 4.5, but become less prominent as S_ℓ and H'_F are reduced in the four simulation data sets. Table 4.5 shows the decrease in S_ℓ has a larger effect than the decrease in H'_F, with the $S_M$met2 maximum only ∼0.06 m less than $S_M$met1, but both $S_R$met1 and $S_R$met2 are ∼0.16 m less than $S_M$met1 and $S_M$met2 respectively.

Statistic	met1		met2	
	$S_{\ell M}$	$S_{\ell R}$	$S_{\ell M}$	$S_{\ell R}$
Min	−0.070	−0.039	−0.064	−0.029
Max	0.424	0.256	0.368	0.206
Mean	0.038	0.024	0.030	0.020
STD	±0.064	±0.038	±0.052	±0.031
RMS	±0.074	±0.045	±0.060	±0.037

Table 4.5: Statistics for fixANLN$_{RC}$−fixANLN (no RC) for each of the four different meteorological/S_ℓ data sets. Both ANLN LSAs fixed at 32 AHD tide-gauges to CARS2006 + MSL. Units are in metres.

Table 4.5 indicates that the magnitude of error in AHD heights due to neglecting URE may be 0.20−0.40 m. Any new levelling-based AVD would contain similar errors if RCs are not applied. However, it is impossible to estimate the error budget for the simulated $RC_{A\text{-}L}$ presented here, because the variability of the actual meteorological conditions from the assumed *average winter* conditions are not known. There is potential for the effect of URE on the ANLN to be much more rigorously assessed if metadata including the time and date of levelling observations in the ANLN were available.

For this simulation (where winter conditions are assumed), levelling conducted in seasons other than winter could have errors in H_F of up to 300 W/m^2 (Section 3.5.1), while using $t_s = 2$ (to compute H_F) can also cause errors of nearly 200 W/m^2 within one day (Figure 3.3). Errors of 0.2 in estimating C_f or W_f from average winter meteorological data can cause H_F errors of between 20 and 70 W/m^2 (Section 3.5.1). Although easier to make reasonably accurate assumptions for S_ℓ (these are dependent on terrain and sighting conditions, rather than time and date of observation), variations of 10−20 m in S_ℓ can impact on $Z_{i,\ell}$, particularly for third-order levelling (maximum S_ℓ of 90 m; see Figure 3.6). Any of the aforementioned variations from assumed input data could completely invalidate retrospective $RC_{A\text{-}L}$. However, these variations are likely to be

local, in the expectation that average conditions will prevail across the entire ANLN, so that the simulated results presented here are a best estimation of URE given the available information.

4.3 Summary

The objective of this Chapter has been to retrospectively simulate the possible errors in heights that could result in any new levelling-based AVD (or possible errors existing in the AHD) from not applying RC to the ANLN to remove/reduce URE. Because the ANLN does not contain metadata detailing time and date of levelling observations, and meteorological conditions at this time, it was necessary to use assumed data for the evaluation of H_F, T_a and P_a, while approximations such as assuming constant terrain gradient for sub-sections (typically 5 km) also have to be made. Sensitivity analysis showed that the estimation of H_F causes large uncertainty in the simulated results (potentially up to 300 W/m^2 in some cases), with the effect of changes in $Z_{i,\ell}$ (primarily caused by variations in S_ℓ) also contributing to the uncertainty of the results (maximum error potentially 50% of simulated $RC_{A\text{-}L}$ itself).

The magnitude of URE accumulating with height change is highly dependent on the maximum S_ℓ of each levelling type. Third-order levelling (comprising 71% of the ANLN; $S_{\ell M}$ = 90 m) appears particularly susceptible to URE, potentially reaching 6 mm per 10 m of height difference. Loop closures for the ANLN show no decrease after the application of simulated $RC_{A\text{-}L}$, but a combination of masking errors and the effect of the crude approximation of H_F at the local level make this test inconclusive. The use of H'_F in $RC_{A\text{-}L}$ as suggested by Angus-Leppan (1979) does not appear to introduce a significant north-south slope (shown here to reach only 20 mm) in MC ANLN (under the assumptions used in $S_M$met1) when compared to using H_F in $RC_{A\text{-}L}$.

The maximum difference between ANLN adjusted heights with and without simulated $RC_{A\text{-}L}$ was between 0.42 m and 0.21 m (depending on which of the four assumed data sets were used), and is highly correlated with high elevations and dry, sunny

conditions. The maximum differences can be compared with the estimated maximum error for the AHD of $\sim\pm0.35$ m between the centre of Australia and the coast (Roelse et al., 1971, 79). It is not possible to conduct further investigations into refraction until the appropriate metadata (if available) is added to the ANLN.

5. MEAN SEA LEVEL AND SEA SURFACE TOPOGRAPHY EFFECTS ON THE AHD

Physical heights have long been related to mean sea level (MSL) as a close (and observable) approximation of the geoid. However, improvements in geodetic measurement accuracy have shown that the use of MSL as the zero-reference surface for vertical datums is no longer satisfactory (e.g., Section 1.1.1; Vaníček, 1991; Zilkoski et al., 1992). It is shown here that the mean sea surface (MSS; basically, MSS = MSL; Tapley and Kim, 2001, 372) slopes upwards (with respect to the geoid) towards the equator in Australian regional seas (cf. Fischer, 1975; Sturges, 1967, 1974) and is the chief cause of the north-south slope in the AHD (Featherstone, 2004, 2006). Details of methods for computing sea surface topography (SSTop) at tide-gauges (SSTop_{TG}) from SSTop models (SSTMs) for application in a least-squares adjustment (LSA) of the Australian National Levelling Network (ANLN) to 'correct' for MSS slope are presented (cf. Merry and Vaníček, 1983). It is demonstrated that the effects of SSTop can be removed from any new levelling-based Australian vertical datum (AVD) by constraining any ANLN LSA to MSL + SSTM heights at AHD tide-gauges. In addition, the Tasmanian AHD offset to mainland AHD is estimated using SSTM and GNSS minus AGQG09 and EGM2008, providing updated results to Rizos et al. (1991), Rapp (1994) and Featherstone (2000, 2002a).

5.1 MSL as a zero-reference for vertical datums

National levelling-based vertical datums require a zero-reference, i.e., a point (or points) where the height is equal to zero. The zero-reference chosen depends on the height system employed; for orthometric heights (H^O) it is the geoid and for normal heights (H^N) it is the quasigeoid (see Chapter 7). However, these surfaces cannot be directly observed in practice (Vaníček, 1991). Hence, MSL is typically adopted as the zero-

reference, as it is a close approximation of these surfaces that can be observed by averaging tide-gauge records. Levelling networks are usually connected to MSL at tide-gauges, with the LSA of the network constrained to MSL at one, or multiple, tide-gauges (cf. Sections 1.1.1 and 5.1.2; Vaníček, 1991) so as to realise heights at BMs related to local MSL. Note that the geoid and quasigeoid are coincident over the ocean (Vaníček and Krakiwsky, 1982, 421), and very similar in low-lying coastal areas. Thus, in this Chapter the geoid height (N) and height anomaly (ζ; also quasigeoid height) are considered equivalent because here the study is restricted to the low-lying Australian coast and regional seas.

5.1.1 Definition of MSL

MSL is defined by time-averaged tide-gauge observations of sea level over a specific epoch (Vaníček, 1991). MSL at the coast (for a vertical datum zero-reference) is usually calculated from hourly tide-gauge observations of sea level (Pugh, 1987, 302). However, MSL can also be derived from satellite altimetry (e.g., Mather et al., 1979) and steric (or hydrostatic) levelling (e.g., Godfrey, 1973), although these methods are rather problematic at the coast (e.g., Section 5.2.1; Deng et al., 2002; Dunn and Ridgway, 2002).

Tide-gauge observations of instantaneous sea surface height at time t ($H_{ISS(t)}$) differs from MSL height $H_{MSL(t)}$ so that (cf. Pugh, 1987, 17)

$$H_{ISS(t)} = H_{MSL(t)} - T(t) - S(t) \tag{5.1}$$

where $T(t)$ is the tidal and $S(t)$ the meteorological surge components of $H_{ISS(t)}$ at t (cf. Tapley and Kim, 2001, 374).

$T(t)$ is due to the gravitational attraction of the Moon and, to a lesser extent, the Sun (Vaníček and Krakiwsky, 1982, 126), and is regular and well defined (Pugh, 1987, 59). The most dominant tidal pattern is the semi-diurnal tide (tidal cycle $\sim$12 hours), but longer period tides such as the annual and 18.61 year lunar nodal tide also contribute to $T(t)$ (Section 5.2.4). For further information, the reader is referred to Pugh (1987,

Chapters 3 and 4), Melchior (1978), or Mitchell (1973b, Chapter 4).

$S(t)$ consists of the non-tidal residual, after $T(t)$ is removed from Equation (5.1). Short period surges are primarily caused by winds, irregular extremes of atmospheric pressure and heavy rainfall causing floods and raised river levels that change the sea surface height (SSH) in coastal regions (see Pugh, 1987, Chapter 6). Note that $S(t)$ described here as a component of the difference between $H_{ISS(t)}$ and $H_{MSL(t)}$ should not be confused with the semi-permanent difference between MSL and the geoid (sea surface topography; SSTop; Section 5.2.1).

5.1.2 MSL as zero-reference for the AHD

AHD on the mainland (referred to here as AHD(mainland)) was realised by a LSA of the Australian Levelling Survey (ALS; now ANLN) in 1971 fixed to MSL (held at zero) at 30 mainland tide-gauges (Figure 5.1; Roelse et al., 1971). The Tasmanian (Tas) levelling network was re-adjusted in 1983 (initial adjustment 1979; NMC, 1979), held fixed to MSL (held at zero) at two Tas tide-gauges (Figure 5.1) to realise the AHD in Tas (referred to here as AHD(Tas)) (ICSM, 2006). MSL values adopted for AHD(mainland) zero-reference came from up to three years of tide-gauge observations (1966−1968) at 29 tide-gauges, with four years (1957−1960) at Karumba (Roelse et al., 1971). MSL observations for one year (1972) at the Hobart and Burnie tide-gauges were adopted as the zero-reference for AHD(Tas) (ICSM, 2006).

AHD(mainland) and AHD(Tas) are technically two separate vertical datums, as their zero-references are based on spatially and temporally different MSL observations. Attempts have been made to quantify the offset between AHD(mainland) and AHD(Tas) (e.g., Rizos et al., 1991; Rapp, 1994; Featherstone, 2000), but the magnitude of the offset is spatially variable due to AHD distortions (Featherstone, 2002a). For a re-examination of of the AHD(mainland)−AHD(Tas) offset, see Section 5.8.

Figure 5.2 shows local MSS/MSL and how they are related to the geoid, AHD, SSTop (cf. Section 5.2.1) and ellipsoid (cf. Section 5.4.4). By adopting MSL as the zero-

reference for AHD (AHD_0), a local offset is introduced between AHD_0 and the geoid at the tide-gauge (O_{TG}). O_{TG} is equivalent to SSTop (Section 5.7), but quantifying SSTop or defining the geoid is rather problematic at the coastally located tide-gauges (e.g., Hipkin, 2000).

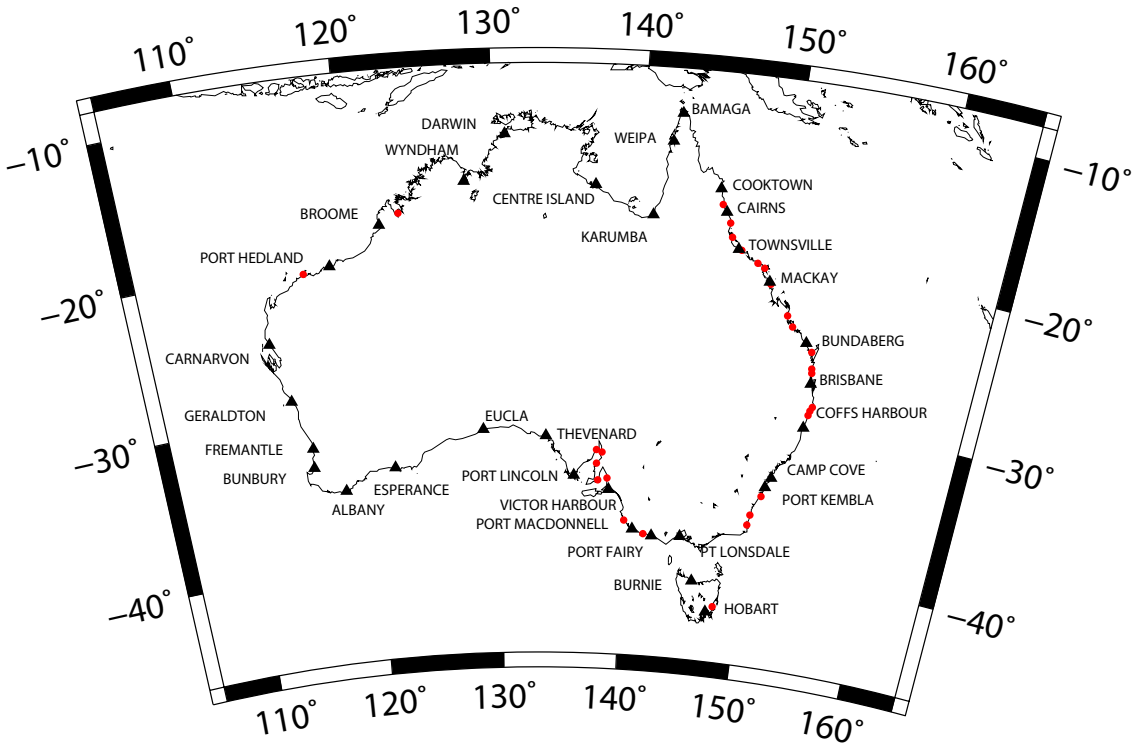

Figure 5.1: AHD tide-gauges represented by black triangles (labelled) and additional 27 tide-gauges connected (see Section 5.3.5) to ANLN represented by red circles (unlabelled). Lambert projection.

The effect of O_{TG} was to introduce a slope into the AHD through the adoption of MSL as AHD_0 (e.g., Hamon and Greig, 1972; Mitchell, 1973b; Leppert et al., 1975; Coleman et al., 1979). Featherstone (2004) identified a north-south discrepancy between the AHD and AUSGeoid98 (AG98; Featherstone et al., 2001), with considerable evidence indicating the error is in the AHD, rather than AG98 (Featherstone, 2006; Featherstone and Morgan, 2007). Evidence indicating that the north-south slope in the AHD is caused solely by adopting MSL as AHD_0 is presented in Section 5.7.

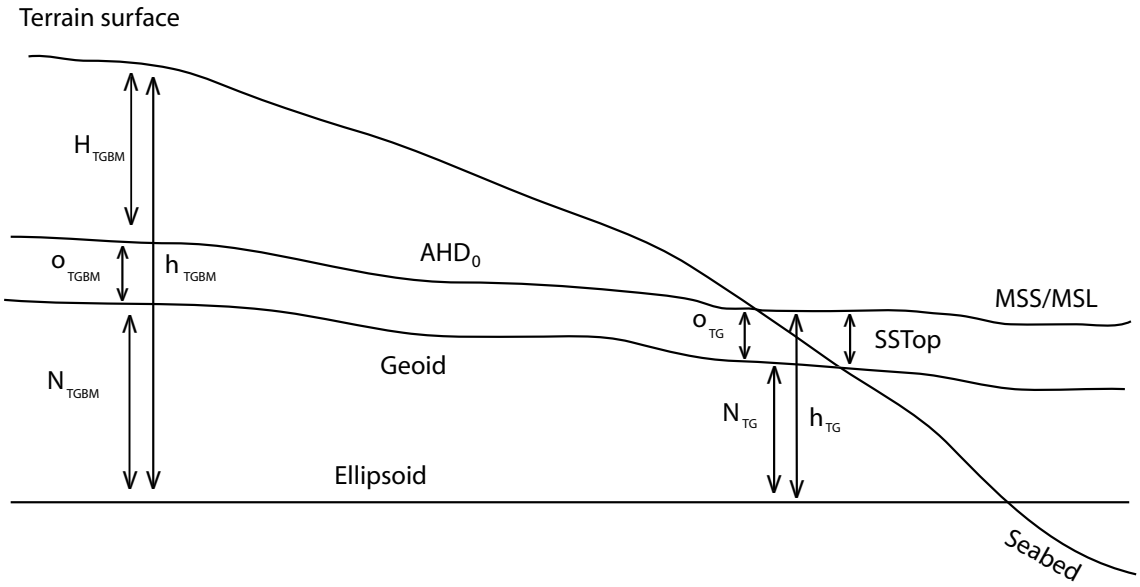

Figure 5.2: MSS/MSL, AHD, SSTop, quasigeoid/geoid and ellipsoid. The offset between the vertical datum (AHD) zero-reference (AHD_0) and the geoid at the coast (tide-gauge; O_{TG}) and inland at the tide-gauge benchmark (TGBM; O_{TGBM}) is assumed to be constant (within a few km) of the coast. The vertical datum/geoid offset is spatially variable and is equivalent to SSTop at the coast because the AHD is fixed at MSS/MSL = zero.

5.2 Problems associated with using MSL as AHD_0

5.2.1 Sea Surface Topography

SSTop is the systematic departure of MSL from the geoid (e.g., Merry and Vaníček, 1983). Tapley and Kim (2001, 374) divide SSTop into two parts; the inverse barometer (IB) effect caused by atmospheric pressure, and mean dynamic ocean topography (MDT) resulting from steady-state ocean circulation, although Seeber (2003) points out that these definitions are not consistent in the literature. Here, SSTop refers to mean SSTop, which is the difference between the time-averaged MSS without IB corrections, and the mean geoid which can reach ∼2 m (Rapp, 1994; Hipkin et al., 2004). MDT is the IB corrected MSS minus the geoid (cf. Andersen and Knudsen, 2009). However, (mean) SSTop is also dependent on the observation period and secular changes in MSS (e.g., Fenoglio-Marc and Tel, 2010).

The primary causes of SSTop are non-gravitational factors including ocean currents, water density variations, air pressure and wind stress (Merry and Vaníček, 1983; Pugh,

1987; Hipkin, 2000). However, river discharge (cf. Morgan, 1992) and seabed topography (cf. Dunn and Ridgway, 2002) also contribute to the variability of SSTop in coastal regions (Merry and Vaníček, 1983), with the dynamic balance between evaporation and precipitation over different ocean basins also contributing (Hipkin, 2000).

The spatial variability of SSTop in a relative sense (cf. Hipkin et al., 2004) at different tide-gauges is of most interest for the AHD, due to the strategy of fixing all 32 tide gauges to MSL. There are several methods for estimating SSTop (Vaníček, 1991): i) oceanic levelling (e.g., Godfrey, 1973), ii) satellite-derived MSS combined with a gravimetric geoid model (e.g., Mather et al., 1979; Andersen and Knudsen, 2009), or iii) the local zero-frequency response analysis of Merry and Vaníček (1983).

Oceanographic levelling methods comprise pipeline (hydrostatic), steric and geostrophic levelling (Coleman et al., 1979). Pipeline levelling requires the use of a long liquid-filled tube and is therefore of no practical use in determining SSTop over oceans, but steric and geostrophic methods are relevant to this study (also see Section 5.3).

Steric levelling is based on the assumption that there is a level of no (or little) motion below an ocean depth of ∼1,000 m (Godfrey, 1973; Pugh, 1987). Below this level, the isobaric reference surface is assumed to coincide with an equipotential surface of the Earth's gravity field. Integrating upwards over a column of seawater with variable density (due to varying temperature and salinity) above the isobaric reference surface realises the variable SSH (Hamon and Greig, 1972). Hence, steric levelling provides only *relative* heights i.e. height differences, rather than absolute heights, as the SSH realised here is relative to an arbitrary pressure depth.

Geostrophic levelling uses observed (e.g., from drifting buoys) ocean current velocities (Torge, 2001, 79), and assuming a state of equilibrium, provides a difference in levels where the sea surface slope is perpendicular to the direction of flow (Pugh, 1987, 325). Geostrophic levelling can be used in shallow waters (although not close to the shore), while steric levelling can only be conducted in deep (>1,000 m) water (Coleman et al., 1979).

The so-called 'direct' method (e.g., Vaníček, 1991) of determining SSTop (referred to here as geodetic SSTop) involves the subtraction of a geoid model from satellite altimetry-derived MSS (e.g., Mather, 1979; Andersen and Knudsen, 2009). Mather (1974, 1975) formulated methods of realising geodetic SSTop, later using altimetric data to model SSH of Australian regional seas (Mather, 1979). Geodetic SSTMs have generally been unreliable in the past due to limitations in the accuracy of available geoid models, despite accurate measurements of SSH (to a few cm) from satellite altimetry (Bingham and Haines, 2006). However, the introduction of improved geoid models, such as EGM2008 (Pavlis et al., 2008) has markedly improved geodetic SSTMs (e.g., Section 5.3.4; Andersen and Knudsen, 2009), particularly over the open oceans, although the accuracy of satellite altimetry (e.g., Deng et al., 2002; Volkov et al., 2007) and geoid determination (e.g., Hipkin, 2000) both remain problematic in the coastal zone (cf. Section 5.5.2).

Oceanographic SSTM (e.g., Section 5.3.1; Ridgway et al., 2002), geodetic methods (e.g., Section 5.3.4; Andersen and Knudsen, 2009), and a combination of these methods (e.g., Section 5.3.2; Rio and Hernandez, 2004) are compared in Section 5.5.

5.2.2 Tide-gauges

Modern tide-gauges can be situated on the coastline, or on the seafloor. The traditional method of sea level observation is a tide-gauge situated on the coast, which measures the instantaneous height difference between the sea surface and a fixed point on the coastline (e.g., Wöppelmann et al., 2006). Here, only coastal tide-gauges will be discussed.

Mechanical tide-gauges (stilling well and float) that could automatically record continuous changes in the instantaneous sea surface have been available since the mid-nineteenth century (Pugh, 1987, 27). Although some of these type of gauges are still operational, they have been largely replaced by three types of modern gauges (Wöppelmann et al., 2006): i) pressure systems that measure the sub-surface pressure, ii) acoustic systems, and iii) radar systems (IOC, 2006). For full details on tide-gauge

mechanisms, see Pugh (1987, Chapter 2), or IOC (2006, Chapter 3).

The selection of tide-gauge site can affect the quality of the sea level observations. Pugh (1987) describes the preferred location for a coastal tide gauge: relatively deep water, experiencing the full tidal range, but not directly exposed to waves or strong currents, while headlands and harbours with restricted entrances should be avoided because of their effect on local sea level (cf. Roelse et al., 1971, 23). Local coastal variations due to the shape of the seabed (Dunn and Ridgway, 2002) and ocean currents (cf. Merry and Vaníček, 1983), and the fact that many tide-gauges are placed in harbours that are located on or near rivers for maritime navigation (e.g., Mitchell, 1973b; Merry and Vaníček, 1983; Morgan, 1992) are particularly problematic.

Vertical instability of the tide-gauge can lead to biased realisations of MSL. Vertical movements of the tide-gauge can be caused by a range of factors, including instability of the structure on which the tide-gauge is mounted (cf. Mitchell, 1973b, 154), coastal land subsidence (e.g., Belperio, 1993), crustal movement and glacial isostatic adjustment (GIA) (e.g., Bouin and Wöppelmann, 2010). While damage to the tide-gauge or its supporting structure may cause apparently abrupt changes in MSL, changes due to the previous three causes will be gradual and often difficult to identify (e.g., Buble et al., 2010). Continuous and episodic GNSS monitoring and/or GIA models applied at tide-gauges can provide a method of identifying vertical movement at the tide-gauge and removing this effect from the MSL signal observed at the tide-gauge (e.g., Wöppelmann et al., 2006). However, GNSS has time-scale limitations because observations only span the last $10-20$ years.

All of the issues described in this section have impacted on the accuracy of MSL derived from AHD tide-gauge observations. Mitchell (1973b, Sect 7.4) provides a summary of possible errors in the stilling well and float AHD tide-gauges, based on the reports of Easton (1968) and Easton and Radok (1970). Coleman et al. (1979) suggest possible AHD tide-gauge errors due to all causes of $100-150$ mm. However, it is likely that this is a maximum error range, with a 'noise' level of $50-100$ mm considered more realistic (and adopted as best 'guestimate' MSL error for AHD tide-gauges in this

Chapter). The suggested error of 50−100 mm is based on comparisons between several AHD tide-gauges and similarly (spatially) sited newer (and more accurate) tide-gauges connected by levelling. This crude estimate (50−100 mm) compares well with the ±60 mm (cf. Section 8.5.3) adopted for MSL *a priori* STD (1σ) in the final combined LSA (see Chapter 8).

Due to the distortions in the ANLN (Chapter 2), it is preferable to use as many tide-gauges to constrain the ANLN as possible (cf. Vaníček, 1991). Assuming maximum tide-gauge-derived MSL errors of ∼100−150 mm (but more typically 50−100 mm), MSL error is less than the largest levelling errors in the ANLN (>0.5 m; Section 2.4.2). The 32 AHD tide-gauges, are probably the best data-set (at this stage) for constraining any new levelling-based AVD due to problems obtaining additional tide-gauge data (particularly levelling connections to tide-gauges; see Section 5.3.5).

5.2.3 Secular changes in MSL

MSL can also change over long periods (secular changes), which can occur on a global basis (eustatic changes; Pugh, 1987, 301), causing the vertical datum zero-reference to no longer be MSL. Estimates of global sea level rise indicate a 20th century increase of ∼1.7 mm year^{-1} (Church and White, 2006). The sea level change is thought to be the result of thermal expansion of the oceans, with some contribution from melting glaciers and ice caps (Church et al., 2008).

Because most comparisons in this Chapter use MSL + SSTop at tide-gauges that are relative to the Albany tide-gauge (Section 5.5.2), the effects of absolute MSL changes on the results are likely to be small, assuming MSL changes remains approximately constant at all tide-gauges. However, there is regional variability in sea level change and also variability between coastal sea-level change observed by tide-gauges and open-ocean sea level change observed by satellite altimetry (e.g., White et al., 2005; Holgate and Woodworth, 2004; Fenoglio-Marc and Tel, 2010). This may cause some temporal variations between datasets observed at different epochs which, although probably small, are difficult to separate from other errors (cf. Section 5.6.1).

5.2.4 Long-period tides

There are several long-period tides that can affect the determination of MSL. These include the solar semi-annual, solar annual, pole tide, lunar perigee and lunar nodal tides (Mitchell, 1973b). The semi-annual and annual tides have periods of 0.5 and 1 solar year, and are influenced by the gravitational attraction of the Sun (Vaníček, 1978). The pole tide is generated by the Chandler wobble of the axis of the rotation of the Earth. The period (Chandler period) of the pole tide is 433 days and has an amplitude of ∼10 mm (Currie, 1975), while the lunar perigee tide has a period of 8.85 years and maximum amplitude of ∼20 mm (Vaníček, 1978). As such, the complete signal of the semi-annual and annual tides are included in MSL estimates that include at least one year of tide-gauge observations (cf. Roelse et al., 1971, 36), with the magnitude of the pole and lunar perigee tide (10 mm and 20 mm respectively) considered insignificant (cf. ∼50−100 mm 'noise' in tide-gauge observations of MSL), so these four tides will not be discussed further.

The lunar nodal tide is the result of the inclination between the planes of the Moon's orbit and the ecliptic, and has a period of 18.61 years (e.g. Shaw and Tsimplis, 2010). To capture the full tidal signature (including nodal tide) in all tidal constituents, tide-gauge observations of sea level should extend to 18.61 years (e.g., Featherstone and Kuhn, 2006). However, AHD tide-gauges were observed for up to only three years or four years (only one year in Tas). The magnitude of the error in MSL resulting from a time-limited observation of the full tidal signature is unclear, with differences (details following) between modelled and observed (over 18.61 years) nodal tide identified (cf. Amin, 1993; Shaw and Tsimplis, 2010).

Vaníček (1978) modelled the nodal tide at several northern U.S. sites, finding maximum nodal tide of ∼20 mm (average 7 mm). However, Amin (1993) compared modelled and observed (18.61 years) nodal tide at Darwin, Wyndham, Geraldton and Fremantle tide-gauges (see Figure 5.1), where the maximum observed amplitude was at Darwin (47 mm compared to 10 mm for the modelled nodal tide). The amplitude for both observed and modelled nodal tide decreased for tide-gauges located further south (Darwin is the most

northerly of the four sites). By comparison, Shaw and Tsimplis (2010) found reasonable agreement between modelled and observed nodal tide at four eastern Atlantic Ocean and ten Mediterranean coastal tide-gauges. The maximum amplitude was ∼50 mm at an eastern Atlantic tide-gauge, but generally no more than 10 mm at the Mediterranean tide-gauges. Although the 18.61 year nodal tide may be significant in some instances (assuming maximum of ∼50 mm), the indications are that it is generally below the 'noise' level for MSL observed at AHD tide-gauges (∼50−100 mm; Section 5.2.2), and will therefore be considered insignificant for this study.

5.3 Data and models used

5.3.1 CSIRO Atlas of Regional Seas 2006

The Commonwealth Scientific and Industrial Research Organisation (CSIRO) Atlas of Regional Seas (CARS; Ridgway et al., 2002) is a high-resolution seasonal climatology. The version used for this study is CARS2006 (CSIRO Marine Laboratories, http://www.marine. csiro.au/ dunn/cars2006/), which now covers the Southern Hemisphere and equatorial regions (0°E to 360°E and 70°S to 26°N, but only to 10°N in the Atlantic) on a 0.5° x 0.5° grid. It is based on the BLUElink Ocean Archive (BOA; CSIRO Marine Laboratories), which is a collection of global high-quality buoy and shipboard deep water hydrographic cast data (i.e., hydrographic instruments lowered, or 'cast' from ships) (Dunn, 2008). Six water properties are mapped: temperature, salinity, oxygen, nitrate, silicate and phosphate.

The irregularly spaced data were interpolated onto a uniform grid, with Ridgway et al. (2002) using a space-time (four-dimensional) locally weighted least-squares method based on loess mapping (Cleveland and Devlin, 1988). Annual and semi-annual harmonic components were fitted at the same time as the data was smoothed and projected onto the spatial quadratic function. The spatial resolution of the mean fields is variable as the interpolation radius for each grid point is determined by data density rather than fixed distances. A lower limit of 200 km where the data are dense and upper limit of

1,500 km where the data are sparse is imposed, with the effective resolution a function of data density, local bathymetry and geometry (Ridgway et al., 2002).

All versions of CARS contain schemes to account for the effects of sea bottom topography (topographic adjusted relief; TAR), and land barriers (barrier adjusted relief; BAR) (Dunn and Ridgway, 2002). The incorporation of this spatial and temporal complexity is expected to improve the coastal representation of SSTop, although by how much is not stated in the literature, nor is an estimate of coastal SSTop given. A crude error estimate for CARS2006 at Australian tide-gauges may be $50-100$ mm given estimates made by Rio and Hernandez (2004) for CMDT Rio05 (details in Section 5.3.2), while ± 80 mm is adopted for CARS2006 *a priori* STD in the combined LSA described in Chapter 8. Steric height is realised by integration of the temperature and salinity fields in CARS based on a depth of 2,000 m (Ridgway and Dunn, 2003). Where the water depth is <2,000 m, interpolation (ocean ridges), vertical regression procedures (depths >400 m) and locally weighted extrapolation (continental slope and shelf areas) methods have been used (Ridgway and Dunn, 2003).

No mention is found in the published literature of tidal or barotropic corrections for CARS2006, so it is assumed that CARS2006 is in a mean-tide system and has not had IB corrections applied, although Dunn (2006) states that corrections for interannual signals have been applied in the Gulf of Carpentaria (cf. Tregoning et al., 2008). The observation epoch for all versions of CARS is not defined, as all oceanographic data available from the last 50 years has been included in the climatology (Dunn, 2006). For further details, see Dunn and Ridgway (2002), Ridgway et al. (2002), Ridgway and Dunn (2003) and Dunn (2006, http://www.marine.csiro.au/∼dunn/cars2006/).

5.3.2 Combined Mean Dynamic Topography Rio05

The Rio03 Combined Mean Dynamic Topography, (CMDT Rio03; Rio and Hernandez, 2004) combines four different data types (Lagrangian drifting buoys, hydrological profiles, altimetric data and the EIGEN-2 geoid model; Reigber et al., 2003) to estimate a global MDT on a $0.5^\circ \times 0.5^\circ$ grid. The version used here is Rio05, which

uses the same methods as those described in Rio and Hernandez (2004), but with the EIGEN-GRACE 03S geoid (Reigber et al., 2004) replacing the EIGEN-2 geoid.

Several steps were involved in the computation of Rio05. The first was the so-called direct method where the EIGEN-GRACE 03S geoid (to degree 30) is subtracted from the altimetric CLS01 MSS (Hernandez et al., 2001). Altimetric data from four satellite missions were used in the CLS01 MSS during the period 1993−1999: GEOSAT, ERS-1 and -2, and TOPEX/Poseidon (T/P). The MSS heights in the region 80°S to 82°N were computed on a 2 arc-minute grid with an estimated global error of 30 mm. The resulting geodetic MDT (also to degree 30) contained zonal and meridonial velocities deduced from geostrophy (Rio and Hernandez, 2004).

MSS heights referenced to 1,500 m depth (cf. 2,000 m for CARS2006; Ridgway and Dunn, 2003) from the Levitus 1998 climatology were then introduced to improve the CLS01-EIGEN-2 solution from the direct method stage. Where depths are less than 1,500 m (and the Levitus climatology is not defined), multivariate objective analysis (Rio and Hernandez, 2004, Appendix A) is used to combine geostrophic velocities with the Levitus climatology referenced at 1,500 m to produce an extended climatology that is defined at all depths. This is the MDT 'first guess' (Rio and Hernandez, 2004).

Altimetric and *in situ* data are then combined, referred to as the synthetic method (Rio and Hernandez, 2004). The altimetric data used for the synthetic method are SSHs (relative to the ellipsoid) from ERS-1 and -2 and T/P, from which sea level anomalies (SLA) are obtained between 1993 and 1999 using repeat-track analysis. Objective multivariate analysis was used to interpolate the altimetric SLA to the time and position of the *in situ* hydrological profile (Rio and Hernandez, 2004).

The data used for the *in situ* measurements of the total MDT was obtained from satellite-tracked drifting buoys. These measurements were taken between 1993 and 1999 by more than 3,500 buoys, although the spatial distribution of these buoys was not ideal. The synthetic method relies on the geostrophic assumption, which is not valid at and close to the equator or very close to shore; *in situ* measurements between 3°S and 3°N were therefore rejected from the computation (Rio and Hernandez, 2004).

The final step is the combination of synthetic and direct approaches using multivariate objective analysis. Where the synthetic height and velocity estimates are available, they are used to improve the locally estimated MDT, but the (direct) geodetic solution has a higher influence in regions where synthetic and velocity data are sparse (e.g., at high latitudes). Estimation of errors in the MDT field was made by recomputing two CMDTs from the 1993−1995 and 1996−1998 datasets using the same methods and data described above. RMS differences between the the two fields were 100−140 mm in areas of strong currents and 40−50 mm in low variability areas (Rio and Hernandez, 2004). These RMS are comparable to the error 'guesstimate' of 50−100 mm for CARS2006 (Section 5.3.1).

5.3.3 GRACE Gravity Model 02 MDT

The GRACE Gravity Model 02 (GGM02) (Tapley et al., 2005) is derived from 363 days of data from the Gravity Recovery And Climate Experiment (GRACE; Tapley et al., 2004b) between April 2002 and December 2003. Tapley et al. (2003) describe the computation of a MDT using GGM01 and a MSS model computed from a combination of altimetry, such as Geosat Geodetic and Exact Repeat Missions, ERS-1 and -2 and T/P. The methods used for GGM01 MDT are also used to produce GGM02 MDT, but with GGM02 replacing GGM01 as the geoid model used.

As the MSS model has a spatial resolution equivalent to 1/24° or degree 8640 and GGM02 to only degree 120 (Tapley et al., 2005), the MSS is described by spherical harmonics to degree 120. The MDT could then be be computed from the MSS and geoid height as both models were now computed on a 1° grid and were directly comparable. This was simply a subtraction of the values gridded at the same point (Tapley et al., 2003) (MDT = MSS−geoid), with land areas masked. A weighted average was used to smooth the resulting MDT to a radius of 500 km (Tapley et al., 2005).

A second model, DOT_DNSCMSS08-EGM08_gau_ave_111km_dpc.txt (http://grace.jpl.nasa.gov/data/dot/; herein referred to as JPL08) from GRACE/JPL (Jet Propulsion Laboratory) is available at ftp://podaac.jpl.nasa.gov/pub/tellus/dot/200808/. This

model uses the Danish National Space Centre 2008 mean sea surface (DNSC08 MSS; Andersen and Knudsen, 2009) and EGM2008 (Pavlis et al., 2008), so will be similar to the The Danish National Space Centre 2008 mean dynamic topography (DNSC08 MDT) (Section 5.3.4; Andersen and Knudsen, 2009), but with a 111 km Gaussian smoothing filter applied.

5.3.4 Danish National Space Centre 2008 Mean Dynamic Topography

The 1 arc-minute DNSC08 MDT (Andersen and Knudsen, 2009) is the difference between the DNSC08 MSS and EGM2008 (Pavlis et al., 2008). The DNSC08 MSS has no polar gaps and is derived from satellite altimetry over 12 years (1993−2004) from a combination of eight different satellites. Although provided on a 1 arc-minute grid, Andersen and Knudsen (2009) suggest that a realistic spatial resolution for the MSS is 15−20 km.

The IB-corrected DNSC08 MSS is used in the DNSC08 MDT, which Andersen and Knudsen (2009) indicate is not suitable for comparisons with SSH derived from tide-gauges or GNSS (cf. Section 5.6.1). Andersen and Knudsen (2009) suggest the difference between IB- and no IB-corrected (NIB) DNSC08 MSS can reach several decimetres in the Southern Ocean close to Antarctica (cf. Tapley and Kim, 2001). However, Mitchell (1973b, Table 6.7) indicates the relative difference between IB corrections at AHD tide-gauges is usually only ∼30 mm, although it can reach 90 mm between Victor Harbour in the south and Weipa in the north (cf. Figure 5.1), where the IB corrections are smaller. A least-squares collocation (LSC) correlation length of 75 km was used to smooth DNSC08 MDT when the data was interpolated onto the 1 arc-minute grid. An approximate error for DNSC08 MDT is estimated from DNSC08 MSS and EGM2008 to be ∼90−120 mm (Andersen and Knudsen, 2009).

Interannual SLAs for the 12 years satellite altimetry sum to zero, suggesting minimal temporal bias in DNSC08 MDT over the 1993−2004 period. DNSC08 MSS uses a mean-tide system. Comparison between the NIB DNSC08 MSS corrected to the tide-free system and 320 GNSS levelled tide-gauges (GNSS in tide-free system; tide-gauges

and GNSS NIB) around the UK found a mean height difference of 12 mm and STD of ±63 mm (Andersen and Knudsen, 2009). However, the largest differences reached 0.8 m (cf. Figure 5.5; Table 5.4), which Andersen and Knudsen (2009) attribute to DNSC08 MSS error. The likely causes are: the coastal degradation of the tidal model used in DNSC08 MSS and unmodelled shallow water constituents (cf. Dunn and Ridgway, 2002), which could reach several decimeters (Andersen, 1999), the poor quality of coastal altimetry (cf. Deng et al., 2002), and that altimetric data is not usually available within 5−10 km of the coast.

5.3.5 Tide-gauge data

Requirements for tide-gauge data depend on the data sets used to imply SSTop at tide-gauges. These are:

1. SSTM: needs only tide-gauge latitude (ϕ_{TG}) and longitude (λ_{TG}) (herein, tide-gauge positions (ϕ_{TG},λ_{TG}) are referred to as Ω_{TG}) to which SSTop can be extrapolated from a SSTM grid;
2. ANLN: levelling-implied SSTop (Section 5.3.6) requires a levelled height difference between an ANLN BM and MSL at the tide-gauge;
3. GNSS−quasigeoid ($h - \zeta$)-implied SSTop height needs observed h at the tide-gauge and Ω_{TG} to interpolate/compute ζ at the tide-gauge (ζ_{TG}).

A set of 110 tide-gauges (evenly distributed) around Australia were used for the SSTM comparisons, with Ω_{TG} obtained from the Permanent Service for Mean Sea Level (PSMSL; http://www.pol.ac.uk/psmsl) (Woodworth and Player, 2003; PSMSL, 2003). The large number of tide-gauges were used to increase spatial resolution for improved analysis (cf. Figure 5.5). Levelling connections between the ANLN and MSL at the 32 AHD tide-gauges were available in the ANLN data.

However, obtaining levelling connections for the 110 PSMSL-listed Australian tide-gauges proved problematic. Because the National Tide Centre (NTC) and Australian

Hydrographic Office (AHO) collect tide-gauge information and metadata primarily for oceanographic-related purposes, levelling connections are not considered important. Tide-gauge records were supplied by the AHO (Z. Jayaswal 2008, pers. comm.) and NTC (P. Davill 2008, pers. comm.), from which height differences could be derived between ANLN BMs and MSL at 27 tide-gauges (all from AHO data; additional to 32 AHD tide-gauges). These additional 27 tide-gauges (distributed irregularly around the coast; see Figure 5.1) were added to 30 mainland AHD tide-gauges (Tas tide-gauges could not be used as they were not connected to the mainland by levelling) providing 57 tide-gauges for ANLN-SSTM comparisons (Section 5.6.1).

GNSS-derived h were not available at all tide-gauges (Section 5.3.7), so h at the 30 mainland AHD tide-gauge benchmarks (TGBMs) were used instead. These were generally <2 km away from AHD tide-gauges (but two were up to 10 km away). GNSS ϕ and λ were used to compute ζ (see Section 5.3.8) at the TGBM.

5.3.6 Minimally constrained adjustments of the ANLN

Three different LSAs of the ANLN are used here. These are: i) a minimally constrained LSA (MCLSA) of the current ANLN (Section 2.3), using all levelling data (supplementary and basic), referred to herein as MC_{SB}; ii) a MCLSA of the current ANLN, using only basic levelling data, referred to hereafter as MC_{B}; and iii) the MCLSA of the 1971 then-called Australian Levelling Survey (ALS) of Roelse et al. (1971, data from Annex C), hereafter referred to as MC_{R}. All of these MCLSAs were fixed to zero at MSL at the Albany AHD tide-gauge (Figure 5.1) so as to estimate ANLN-implied SSTop at tide-gauges relative to the Albany tide-gauge.

MC_{SB} and MC_{B} used the *a priori* STD estimates of Steed (2006) (see Section 8.3.4). The ANLN contains numerous gross errors (Chapter 2), which will affect the levelling-implied SSTop_{TG}. However, until the errors are rectified, or a comprehensive statistical analysis of the ANLN is conducted (cf. Section 8.4), the MCLSA (ANLN) height estimates used here are the best currently available.

5.3.7 GNSS data

A set of 1,052 3D GNSS geodetic coordinates (Hu, 2009, supplied by Geoscience Australia (GA); N. Brown 2009, pers. comm.) processed in the International Terrestrial Reference Frame 2005 at epoch 2000 (ITRF2005; Altamimi et al., 2007) are available. Only observations at AHD TGBMs are used here. Ideally, h would be observed directly at the tide-gauge (rather than TGBM), but these are not currently available at AHD tide-gauges (Section 5.4.4).

5.3.8 Quasigeoid models used

Two gravimetric quasigeoid models are used to compute $h - \zeta$ implied SSTop_{TG} (referred to as GNSS−geoid SSTop_{TG}; SSTop^{G}_{TG}). These are the gravimetric version of AUSGeoid09 (AGQG09; Featherstone et al., 2011) and EGM2008 (Pavlis et al., 2008). AGQG09 is distinct from the official version of AUSGeoid09 released by GA, which has been fitted to the AHD to provide a product which allows the direct transformation of GNSS-derived h to AHD heights (Featherstone et al., 2011). The reference field used for AGQG09 is the zero-tide version of EGM2008 to degree 2190 (Featherstone et al., 2011). AGQG09 height anomalies (ζ_{AG09}) were bi-cubically interpolated from a $1' \times 1'$ grid using **geoid_abs_tester.f** (Featherstone, 2001).

The tide-free release of EGM2008 (Pavlis et al., 2008) is a new global gravity model and is superior in Australia to AGQG09's 10-year-old predecessor, AG98 (Claessens et al., 2009). Tide-free EGM2008 height anomalies (ζ_{EGM08}) were computed at the topographic surface (cf. Section 6.2) using h at the TGBMs (h_{TGBM}) using **harmonic_synth.f** (Holmes and Pavlis, 2008). The difference between zero-tide and tide-free ζ_{EGM08} over Australia is <30 mm (cf. Figure 5.8), which is not significant compared to errors in the different datasets.

5.4 Methods of computing SSTop heights at tide-gauges

5.4.1 SSTM-implied SSTop heights at tide-gauges

SSTop_{TG} from SSTMs (SSTop^M_{TG}) was computed at 110 PSMSL tide-gauges around Australia for all five SSTMs (Section 5.3). The Generic Mapping Tools (GMT; Wessel and Smith, 2007) routine **surface** (Smith and Wessel, 1990) was used to re-grid each model at 15 arc-minute resolution. The selection of 15 arc-minutes was arbitrary, but influenced by CARS2006 and JPL08 being received on 15 arc-minute grids, so this resolution was retained for all SSTM. A tension factor of T = 0.25 was used in **surface** as recommended for smooth surfaces (Smith and Wessel, 1990). T = 1 was tested, but the maximum CARS2006 SSTop^M_{TG} was only ∼20 mm different to when T = 0.25 was used (most were much less).

The 15 arc-minute GMT grids were extrapolated towards the Australian continent. Bi-cubic interpolation using **geoid_abs_tester.f** (Featherstone, 2001) was then used to determine SSTM^M_{TG} at 110 PSMSL Ω_{TG} from the extrapolated GMT grid. The same method was used to compute SSTM^M_{TG} for the 32 AHD tide-gauges. See Section 5.5 for comparisons among the different SSTMs at tide-gauges.

5.4.2 Effect of Ω_{TG} uncertainty on SSTop^M_{TG}

Ω_{TG} (ϕ,λ) for the 110 PSMSL tide-gauges were provided to the nearest arc-minute. It is unknown how these positions were determined but it is assumed that they are accurate to the nearest arc-minute (same accuracy as ANLN Ω_{BM}; cf. Section 4.1.3), although the datum is unknown. Ω_{TG} for the AHD tide-gauges were obtained from the ANLN data set, also provided to the nearest arc-minute and assumed to be in AGD66 (Section 2.3.2).

AHD tide-gauges were also available in the PSMSL data-set, so PSMSL and ANLN Ω_{TG} could be compared. There were often several tide-gauge records per site in the

PSMSL file, making it difficult to know which PSMSL tide-gauge matched each AHD tide-gauge. In some instances, there were differences between PSMSL and ANLN Ω_{TG} of 3-5 arc-minutes, with a maximum of 11 arc-minutes at Brisbane, although this is almost certainly a different tide-gauge. It is often uncertain whether there are multiple tide-gauges at one location in the PSMSL file, or the result of different authorities (eg., NTC, AHO or local port authority) providing different Ω_{TG}. Thus, gross errors (assumed to be typographic, or different tide-gauges) of up to 5 arc-minutes are suspected in the PSMSL database when compared with AHD and NTC records. Efforts have been made to adopt the most accurate Ω_{TG}, but it is often impossible to determine the correct Ω_{TG}. As such, the simulated SSTop^M_{TG} ($\delta\text{SSTop}^M_{TG}$) includes Ω_{TG} uncertainty of $\sim\pm1$ km, but also possible gross errors (typographical or comparison of different tide-gauges) of up to 10 arc-minutes.

A simulated estimate of possible SSTop^M_{TG} error ($\delta\text{SSTop}^M_{TG}$) resulting from an error in Ω_{TG} ($\delta\Omega_{TG}$) is made here in the northeast (NE), southeast (SE), southwest (SW) and northwest (NW) directions. For example, a +1 arc-minute error in ϕ_{TG} ($\delta\phi_{TG}$) and λ_{TG} ($\delta\lambda_{TG}$) results in an error in the NE direction, while $\delta\phi_{TG} = -1$ arc-minute and $\delta\lambda_{TG} = +1$ arc-minute results in an error in the SE direction. Errors in different direction were computed to guard against the errors becoming larger in a particular direction of the SSTM field. CARS2006 was used in the test.

$\delta\Omega_{TG}$	CARS2006 $\delta\text{SSTop}^M_{TG}$		
arc-minute	Max (mm)	Min (mm)	Max STD (mm)
1	7	−7	±1
2	14	−14	±2
10	70	−72	±13

Table 5.1: SSTop^M_{TG} errors (CARS2006 used for this test; maximum, minimum and maximum STD) for $\delta\phi_{TG}$ and $\delta\lambda_{TG} = \pm1$, ±2 and ±10 arc-minutes in NE, SE, SW and NW directions.

CARS2006 $\delta\text{SSTop}^M_{TG}$ were computed in NE, SE, SW and NW directions for $\delta\phi_{TG}$ and $\delta\lambda_{TG} = \pm1$, ±2 and ±10 arc-minutes. The results are shown in Table 5.1, where maximum CARS2006 $\delta\text{SSTop}^M_{TG}$ in all directions when $\delta\Omega_{TG} = \pm1$ arc-minute is 7 mm, minimum −7 mm and maximum STD is ±1 mm (1σ). When $\delta\Omega_{TG} = \pm2$ arc-minute, $\delta\text{SSTop}^M_{TG}$ is <14 mm, while when $\delta\Omega_{TG} = \pm10$ arc-minute, $\delta\text{SSTop}^M_{TG}$ reaches 70 mm,

although the maximum STD is only ±13 mm. This demonstrates that CARS2006 is a very smooth model, and that $\delta\text{SSTop}^{M}_{TG}$ resulting from $\delta\Omega_{TG}$ (generally <3 arc-minutes) are below the 'noise' level of 50−100 mm for CARS2006 at tide-gauges.

5.4.3 Levelling-implied SSTop heights at tide-gauges

SSTop_{TG} can be realised from the MCLSA (ANLN) height at a tide-gauge (H^{MC}_{TG}) and MSL height at the same tide-gauge (H_{MSL}) (cf. Balasz and Douglas, 1979). Assuming that MCLSA (ANLN) with the normal-orthometric correction applied is a close approximation of an equipotential surface at MSL (cf. Filmer et al., 2010), then levelling-implied SSTop at the tide-gauge (SSTop^{L}_{TG}) is

$$\text{SSTop}^{L}_{TG} = H^{MC}_{TG} - H_{MSL} \tag{5.2}$$

H_{MSL} = zero for the AHD, so $\text{SSTop}^{L}_{TG} = H^{MC}_{TG}$ (cf. Figure 5.2). However, it is acknowledged that the ANLN contains gross and systematic errors (Chapter 2), which will propagate to the edge of the network in a MCLSA, thus distorting H^{MC}_{TG}. See Section 5.6.1 for comparison of SSTM with MC_{SB}, MC_{B}, and MC_{R} (Section 5.3.6).

5.4.4 $h - \zeta$ implied SSTop heights at tide-gauges

MSL h at a tide-gauge (h_{TG}) and ζ_{TG} can be used to derive SSTop^{G}_{TG} as (cf. Figure 5.2)

$$\text{SSTop}^{G}_{TG} = h_{TG} - \zeta_{TG} \tag{5.3}$$

Figure 5.2 illustrates the relation among h_{TGBM}: the normal-orthometric AHD height at the TGBM (H_{TGBM}), ζ at the TGBM (ζ_{TGBM}; shown in Figure 5.2 as geoid height N_{TGBM}) and ζ_{TG} (shown in Figure 5.2 as geoid height N_{TG}). The offset at the TGBM (O_{TGBM}) and at the tide-gauge (O_{TG}) represent the offset between AHD_0 and the quasigeoid (coincident with the geoid at sea level) caused by the AHD being fixed to MSL (held at zero) at the tide-gauges (Section 5.1.2; Roelse et al., 1971).

If it is assumed that $O_{TGBM} = O_{TG}$ locally around the tide gauge (where $O_{TG} = \text{SSTop}^{G}_{TG}$; cf. Hipkin et al., 2004), then

$$\text{SSTop}^{G}_{TG} = (h_{TGBM} - \zeta_{TGBM}) - H_{TGBM}. \tag{5.4}$$

Here, it is acknowledged that any errors in MSL, or levelling between the tide-gauge and TGBM will be present in SSTop^{G}_{TG} computed using Equation (5.4).

5.5 Comparison of SSTop models

5.5.1 Open sea comparisons

Comparisons between CARS2006 and the four other SSTMs (Section 5.3) over Australian regional seas are presented here. CARS2006 (Section 5.3.1) will be used as reference for comparison with the four other SSTM because this climatology is designed for Australian regional seas, and models the influence of bathymetry and land barriers (Dunn and Ridgway, 2002). It is thus expected to deliver improved coastal SSTop heights. 'Absolute' SSTop^{M}_{TG} at Albany tide-gauge is shown in Table 5.2(a).

SSTM	(a)	(b)	(c)
CARS2006	2.049		
Rio05	1.731	−0.318	−0.262
GGM02 MDT	0.612	−1.437	−1.399
DNSC08 MDT	0.592	−1.457	−1.611
JPL08	0.300	−1.749	−1.751

Table 5.2: Differences between CARS2006 and four other SSTM_{TG}. Column (a) shows absolute SSTM_{TG} for each other SSTM at the Albany tide gauge (based on different zero-references); (b) show differences between absolute CARS2006 and other SSTM_{TG} at the Albany tide-gauge; and (c) shows the mean height differences between absolute CARS2006 and other SSTop^{M}_{TG} at 110 tide gauges around Australia. Units are in metres.

The 'absolute' heights at Albany tide-gauge shown here are based on different zero-references (e.g., the oceanographic SSTMs are referenced to arbitrary pressure depths). The difference between CARS2006 and the other four SSTMs in Table 5.2(b) are an estimate of the zero-reference offset, which are used to bring all SSTMs to the CARS2006

zero-reference so that relative comparisons can be made (Figure 5.3). Table 5.2(c) is the mean difference between CARS2006 and each SSTM at the 110 tide-gauges around Australia (Section 5.3.5). These results partially justify using only the Albany tide-gauge difference as the zero-reference offset, because there is good agreement for Rio05 (56 mm), GGM02 MDT (38 mm) and JPL08 (−2 mm) (indicating the Albany value for each SSTM is not an outlier), but a larger difference can be seen for DNSC08 MDT (−154 mm; see later for discussion).

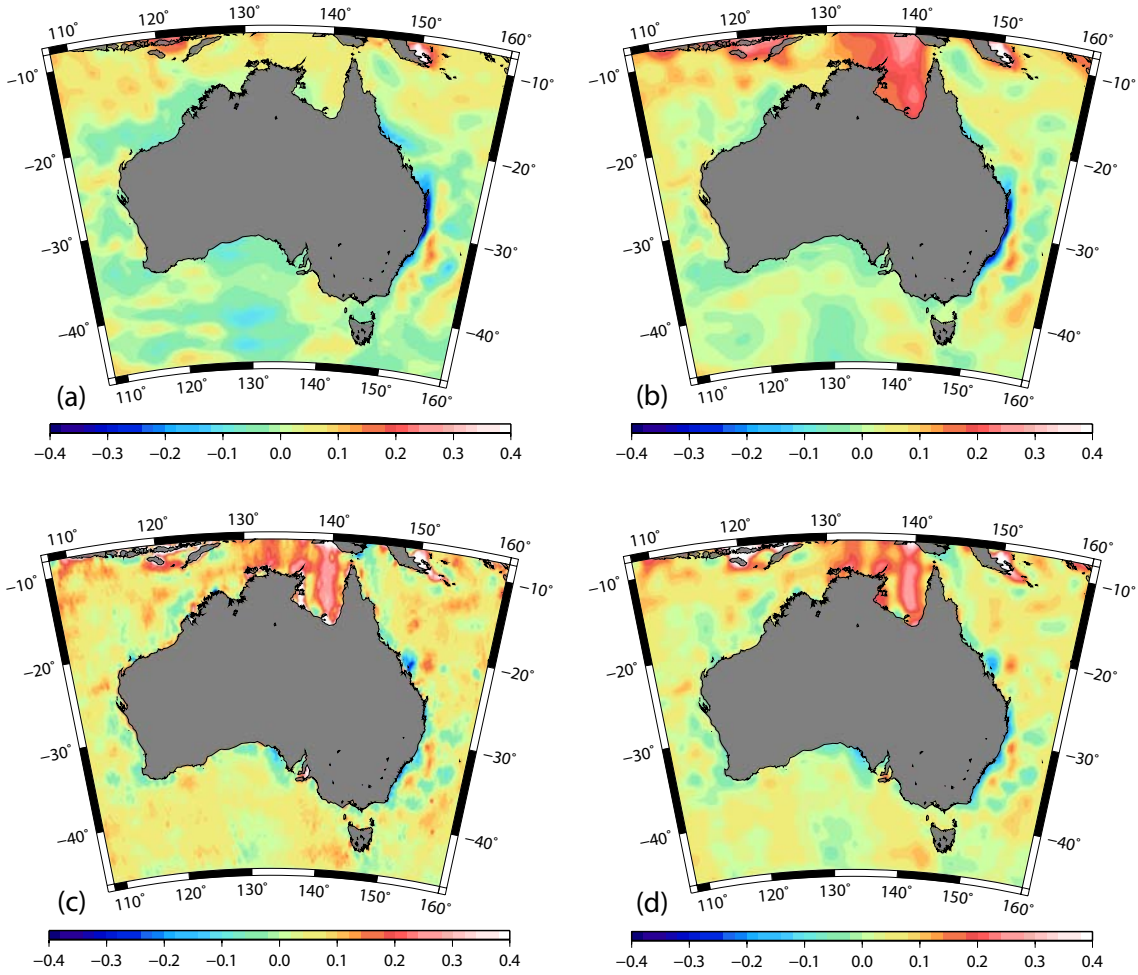

Figure 5.3: Relative height differences of CARS2006 to (a) Rio2005, (b) GGM02 MDT, (c) DNSC08 MDT and (d) JPL08. Lambert Projection, units are in metres. CARS2006 data from CSIRO Marine Laboratories.

The method used to compute the CARS2006−Rio05 differences was to compute a 4 arc-minute grid (increased from 15 arc-minutes to improve plot resolution) for CARS2006 and Rio05 using **surface** (Smith and Wessel, 1990), then subtract the Rio05 grid from the CARS2006 grid. The Rio05 offset to CARS2006 at the Albany tide gauge (Table 5.2(b)) is subtracted from the CARS2006−Rio05 height at each grid point

so that CARS2006 SSTop_{TG} = Rio05 SSTop_{TG} at Albany tide-gauge. This process was repeated one-by-one (using the relevant offset in Table 5.2) until the differences CARS2006−GGM02 MDT, CARS2006−JPL08, and CARS2006−DNSC08 MDT had been computed. The open sea comparisons are shown in Figure 5.3, with statistics in Table 5.3.

SSTM	CARS2006 minus SSTM				
	Max. (m)	Min. (m)	Mean (m)	STD (m)	RMS (m)
Rio05	0.528	−0.428	−0.016	±0.067	±0.068
GGM02 MDT	0.575	−0.406	0.015	±0.081	±0.083
DNSC08 MDT	3.285	−0.498	0.218	±0.275	±0.351
JPL08	1.025	−0.223	0.030	±0.078	±0.084

Table 5.3: Statistics for CARS2006 SSTM minus four other SSTMs in Australian regional seas (cf. Figure 5.3).

CARS2006−Rio05 differences (Figure 5.3(a); Table 5.3) vary mostly between ±100 mm, with an RMS of ±68 mm (cf. Vossepoel, 2007; Bingham and Haines, 2006). The most notable feature is along the east coast (∼24°S to 34°S; <−0.30 m; cf. Figure 5.5) that is probably attributable to the East Australian Current (EAC) (cf. Ridgway and Dunn, 2003) or the narrow shelf along the eastern coast (Figure 5.4). Coastal structures such as these are most likely to be best-identified by CARS2006 due to its improved mapping of bottom topography and land barriers (Dunn and Ridgway, 2002; Ridgway and Dunn, 2003).

CARS2006−GGM02 MDT (Figure 5.3(b); Table 5.3) also displays differences (∼−0.30 m) along the east coast of Australia (cf. Figure 5.3(a)). The medium wavelengths from the MSS and GGM02 (degree 120; Tapley et al., 2005) result in GGM02 MDT being a smooth model, without short-wavelength noise from the local MSS (cf. Figure 5.3(c)), achieving good agreement with an RMS of ±83 mm. However, a large difference of ∼0.30 m appears in the Gulf of Carpentaria extending to the southern coast of Irian Jaya. This region features shallow sea situated over a broad shelf (Figure 5.4). GGM02 MDT is a satellite altimetry MSS−(GRACE) geoid-derived SSTM (Tapley et al., 2003). The differences may be attributable to satellite altimetry errors at the coast (e.g., Deng et al., 2002; Deng and Featherstone, 2006), areas with shallow-sea tides (e.g., Andersen,

1999) or SSH anomalies (of ∼0.75 m) in the Gulf of Carpentaria (Forbes and Church, 1983), which affect the MSS model used in GGM02 (cf. Tregoning et al., 2008).

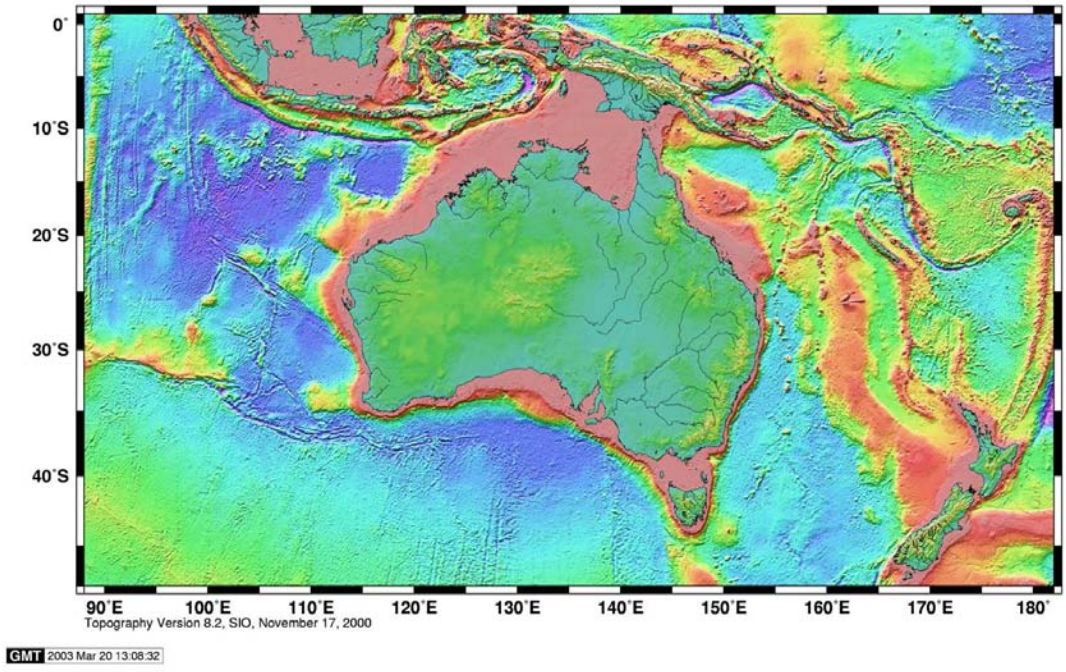

Figure 5.4: Bathymetry of the Australasian region. From Scripps Institute of Oceanography, http://topex.ucsd.edu/marine_topo/mar_topo.html, Accessed 29/10/08

CARS2006−DNSC08 MDT (Figure 5.3(c)) shows some large differences, with an RMS of ±0.351 (Table 5.3); noticeably larger than the other three comparisons. Short-wavelength features can be seen in CARS2006−DNSC08 MDT (Figure 5.3(c); cf. to Figure 5.3(a) and (b)), which is likely to be caused by satellite altimetry errors contaminating DNSC08 MSS. This short-wavelength noise is prominent in the coastal regions (cf. Deng et al., 2002; Deng and Featherstone, 2006; Madsen et al., 2007; Andersen, 1999; Andersen and Knudsen, 2009). The Gulf of Carpentaria feature seen in Figure 5.3(b) also appears here, and may be caused by the large SSH anomalies, affecting not only the satellite altimetry-derived DNSC08 MSS, but also the satellite altimetry-derived gravity anomalies used in EGM2008. However, insufficient data is currently available to isolate or quantify the effects, so these remain uncertain.

CARS2006−JPL08 (Figure 5.3(d)) long to medium-wavelength differences are similar to CARS2006−DNSC08 MDT, which is expected, as both JPL08 and DNSC08 MDT use DNSC08 MSS−EGM2008. However, there appears to be less short-wavelength

noise in JPL08 than DNSC08MDT, evidenced by the RMS of ±84 mm (cf. CARS2006−Rio05 and CARS2008−GGM02 MDT) and less extreme maximum and minimum values (Table 5.3). The improved statistics of JPL08 compared to DNSC08 MDT (cf. Table 5.3) indicate that the Gaussian average filter with 111 km half width (Chambers, 2008) employed by JPL08 has reduced the short-wavelength noise better than the Gaussian smoothing filter with half width of 75 km for DNSC08 MDT (Andersen and Knudsen, 2009).

5.5.2 Relative comparison of SSTMs at tide gauges

A relative comparison of SSTop heights at 110 PSMSL tide-gauges is made by subtracting the absolute SSTop height at Albany tide-gauge (Table 5.2) for each SSTM, respectively at each tide-gauge, so SSTop^{M}_{TG} for each SSTM is zero (MSL) at Albany tide-gauge. Figure 5.5 displays SSTop^{M}_{TG} at all 110 tide-gauges around Australia for the five SSTM relative to MSL (zero) at Albany tide-gauge.

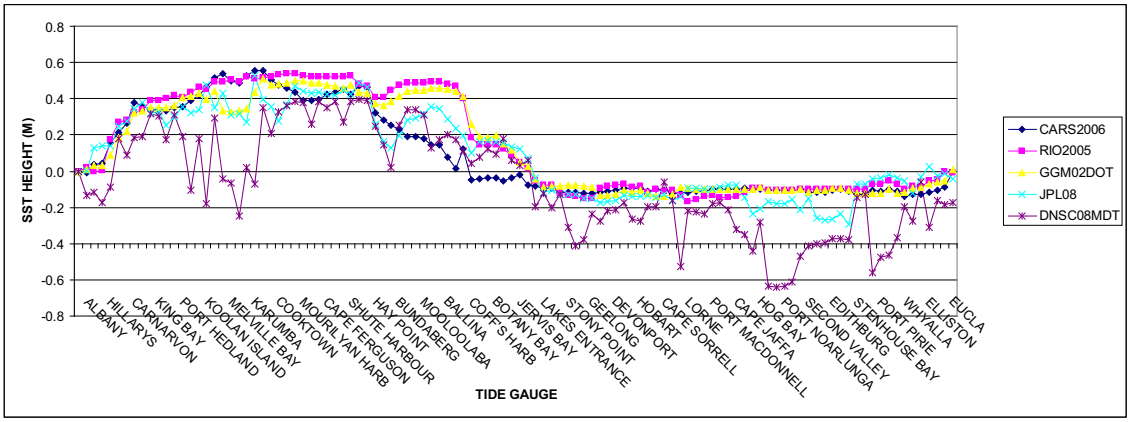

Figure 5.5: SSTop^{M}_{TG} of five SSTMs at 110 Australian tide-gauges. Offsets between the SSTMs have been removed by making SSTop^{M}_{TG} for all SSTMs equal to zero at the Albany tide gauge. The similarity of CARS2006 (blue), Rio05 (pink) and GGM02 MDT (yellow) can be seen at most tide-gauges. By comparison, short-wavelength coastal noise can be seen in DNSC08 MDT (purple), and to a lesser extent, JPL08 (cyan). CARS2006 data from CSIRO Marine Laboratories.

CARS2006, Rio05 and GGM02 MDT all show reasonable agreement at most tide gauges (Figure 5.5). These SSTMs are smoother and have less short-wavelength noise than the other two SSTMs (cf. Table 5.4). However, CARS2006, Rio05 and GGM02 MDT do show differences in several places (Figure 5.5), with GGM02 MDT differing by

up to 0.20 m in the Melville Bay - Karumba area (Gulf of Carpentaria; see Section 5.5.1 and Figure 5.3).

The most prominent feature for CARS2006−Rio05 and CARS2006−GGM02 MDT is a ∼0.4 m difference between Hay Point (central Queensland (Qld) coast) and Jervis Bay (central New South Wales (NSW) coast). The east coast differences are shown by Figure 5.3 to be confined to the coastal region, rather than extending over the sea (cf. Gulf of Carpentaria differences). It is assumed here that the complex bathymetry around the Great Barrier Reef (cf. Figure 5.4) and the effects of the EAC (e.g., Ridgway and Dunn, 2003) are better-modelled by the bottom topography (TAR) and land barrier (BAR) functions used in CARS2006 (e.g., Section 5.3.1; Dunn and Ridgway, 2002).

SSTM	CARS2006−SSTM				
	Max. (m)	Min. (m)	Mean (m)	STD (m)	RMS (m)
Rio05	0.058	−0.453	−0.056	±0.102	±0.116
GGM02DOT	0.205	−0.429	−0.038	±0.108	±0.114
DNSC08MDT	0.731	−0.235	0.154	±0.194	±0.248
JPL08	0.259	−0.220	0.002	±0.102	±0.102

Table 5.4: Statistics for CARS2006 SSTM minus four other SSTMs at 110 Australian tide-gauges (cf. Figure 5.5). SSTop^{M}_{TG} is zero at the Albany tide-gauge for all SSTMs.

DNSC08 MDT contains a large amount of short-wavelength noise at the 110 tide-gauges (Figure 5.5, also see Section 5.5.1). JPL08 also displays short-wavelength coastal noise in several regions (Figure 5.5), despite the statistics of differences to CARS2006 (Table 5.4) being comparable to those of Rio05 and GGM02 MDT. However, the different filtering methods used for JPL08 (111 km compared to 75 km Gaussian smoothing filter) appear to have reduced the short-wavelength noise seen in DNSC08 MDT (Figure 5.5), which is likely to be caused by satellite altimetry errors over coastal regions (cf. Section 5.5.1; Volkov et al., 2007) contaminating the DNSC08 MSS. The noisy nature of DNSC08 MDT and, to a lesser extent JPL08 in the coastal regions, indicate that they are of limited use for removing SSTop effects from MSL at tide-gauges.

5.6 SSTop height comparisons at tide-gauges

Independent estimates of SSTop_{TG} can be made through the use of MCLSA (ANLN) (Sections 5.3.6 and 5.4.3) and $h-\zeta$ (see Section 5.3.7). This section compares SSTop^{L}_{TG} with SSTop^{M}_{TG} at 57 mainland tide-gauges (30 AHD + 27 additional tide-gauges; Section 5.3.5) and SSTop^{G}_{TG} with SSTop^{M}_{TG} at 30 mainland AHD tide-gauges.

5.6.1 Comparison of SSTMs and levelling-implied SSTop heights at tide-gauges

Figure 5.6 shows the comparisons (at 57 tide-gauges; Section 5.3.5; also Figure 5.1) between the three 'best' SSTMs (CARS2006, Rio05 and GGM02 MDT; Section 5.5.2) and MC_{SB} (Section 5.3.6 for data used, and Section 5.4.3 for computation method) SSTop^{L}_{TG}. The differences between the three SSTMs have been discussed in Section 5.5.2. MC_{SB}-implied SSTop_{TG} (cf. Roelse et al., 1971) approximately follows the curve of the SSTop^{M}_{TG} (Figure 5.6), but displays large differences to SSTop^{M}_{TG} in different coastal regions.

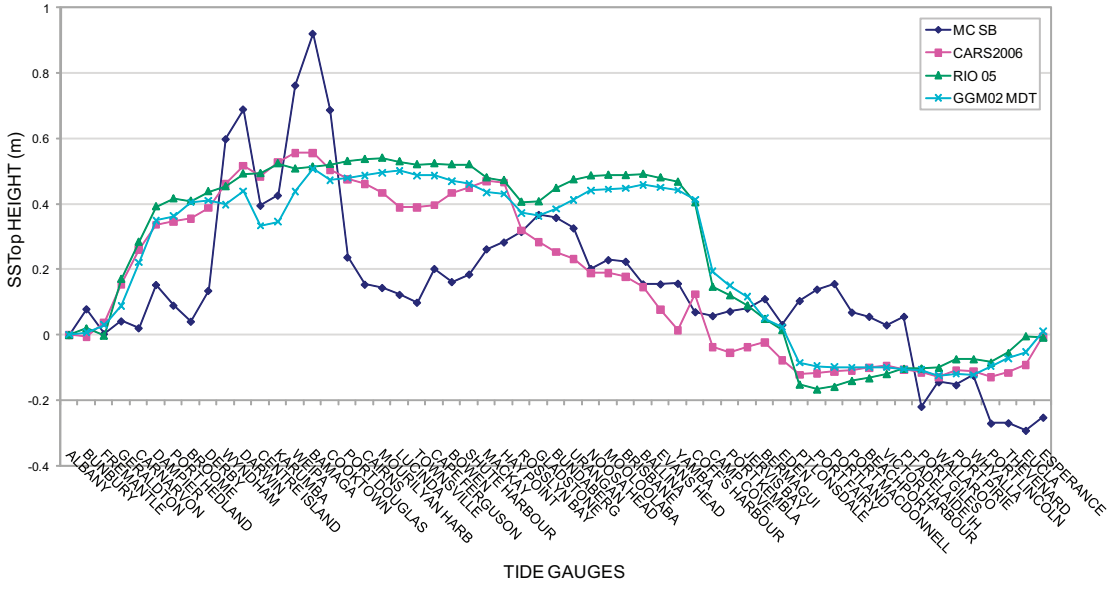

Figure 5.6: Comparison among MC_{SB} (blue), and CARS2006 (pink), Rio05 (green) and GGM02 MDT (cyan) at 57 tide-gauges, all fixed to zero at the Albany tide-gauge. CARS2006 data from CSIRO Marine Laboratories.

The cause of the large differences cannot be ascertained, but it is likely that the primary cause is gross levelling errors (blunders), and to a lesser extent, systematic levelling errors in the ANLN (Chapter 2). The largest differences are along the northern Western Australian (WA) coast, Cape York, the northern Qld coast and the Victorian (Vic) coast. Apparent levelling errors can be isolated by comparing height differences between specific tide-gauges; e.g., Fremantle-Carnarvon, Derby-Wyndham, Darwin-Centre Island, Karumba-Weipa-Bamaga-Cooktown-Port Douglas, Eden-Pt Lonsdale, Port Adelaide-Port Giles, and Whyalla-Port Lincoln. Whether these gross levelling errors are contained in coastal or interior levelling sections that propagate to the coast in the MCLSA cannot be determined with current data.

It must also be acknowledged that SSTop^{M}_{TG} and MSL errors at tide-gauges could both reach up to ∼100 mm at individual tide-gauges. Temporal effects (cf. Tapley et al., 2005; Rio and Hernandez, 2004) caused by comparing MSL (observed 1966−1968), ANLN levelling (∼1950−1970), CARS2006 (∼1950−2005), GGM02 MDT (2002−2003), and Rio05 (1993−1999) could also affect the comparison. In addition, different tidal systems (e.g. Rapp, 1989; Ekman, 1989) are used by different data sets, while IB corrections have not been applied to some models (Section 5.3). However, the (small) magnitude of differences between CARS2006, Rio05 and GGM02 MDT (STD of differences is 100−120 mm; Figure 5.6) suggest that these temporal effects are not significant when compared to the MC_{SB} SSTop^{L}_{TG}−SSTop^{M}_{TG} differences. Tidal and IB effects also appear to be reduced when the data sets are compared in a relative sense (offset removed at Albany tide-gauge).

SSTM	MC_{SB} SSTop^{L}_{TG} minus SSTop^{M}_{TG}				
	Mean (m)	Min (m)	Max (m)	STD (m)	RMS (m)
CARS2006	−0.024	−0.315	0.364	±0.180	±0.182
Rio05	−0.107	−0.421	0.407	±0.217	±0.242
GGM02 MDT	−0.082	−0.388	0.412	±0.205	±0.222

Table 5.5: Statistics for MC_{SB} SSTop^{L}_{TG} minus three other SSTop^{M}_{TG} at 57 Australian tide-gauges (cf. Figure 5.6)

By comparison, the apparently good agreement of the MC_{SB} SSTop^{L}_{TG} and CARS2006 SSTop^{M}_{TG} implied sea surface slope along the Qld−NSW coast between Gladstone and

Eden (cf. Rio05 and GGM02 MDT in this region; Figure 5.6) provides support to the assumption (Section 5.5.2) that CARS2006 is the 'better' SSTM in this region. Although the selection of the Albany tide-gauge as the zero-reference for these comparisons will affect the mean differences between MC_{SB} $SSTop^{L}_{TG}$ and $SSTop^{M}_{TG}$, Table 5.5 indicates that CARS2006 $SSTop^{M}_{TG}$ is in better agreement with MC_{SB} $SSTop^{L}_{TG}$ (maximum, minimum, STD and RMS) than other SSTMs. However, this apparent 'better' agreement between MC_{SB} $SSTop^{L}_{TG}$ and CARS2006 $SSTop^{M}_{TG}$ should be viewed cautiously, due to the large errors in MC_{SB}, and also because the use of the 57 (unevenly spatially distributed; Figure 5.1) tide-gauge set rather than 30 (evenly spatially distributed) AHD(mainland) tide-gauge set may affect the statistics (cf. Table 5.9).

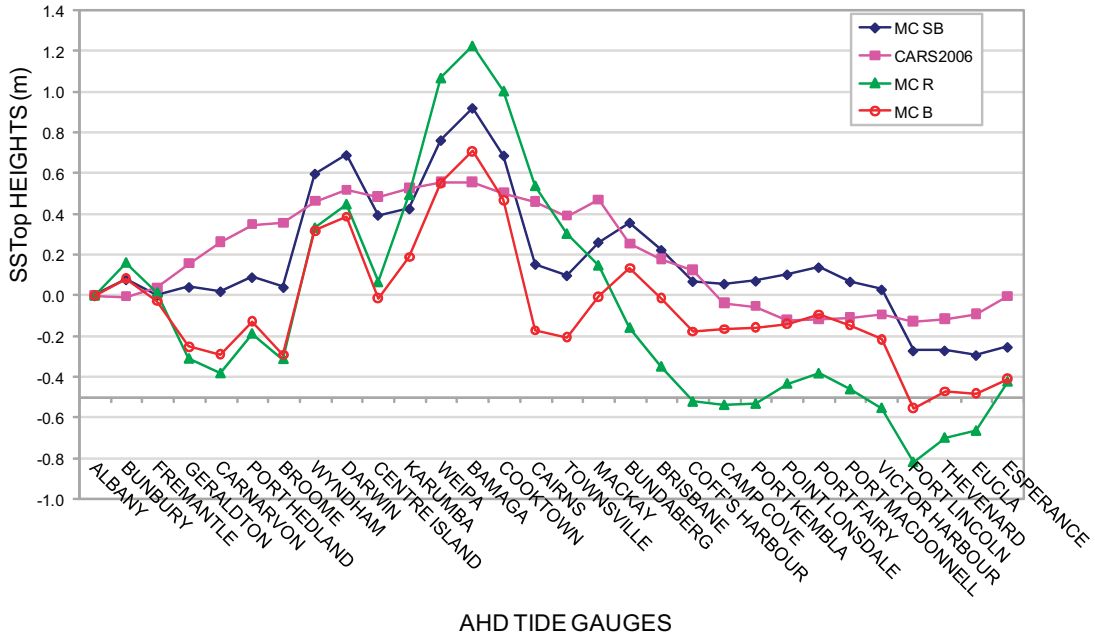

Figure 5.7: Relative comparison between MC_{SB} (blue), MC_{B} (red), MC_{R} (green), and CARS2006 (pink) at 30 AHD mainland tide-gauges. All MCLSA fixed to MSL (zero) at the Albany tide-gauge. CARS2006 data from CSIRO Marine Laboratories.

Comparisons of several different $SSTop^{L}_{TG}$ (Section 5.3.6) with CARS2006 $SSTop^{M}_{TG}$ are in Figure 5.7. MC_{R} $SSTop^{L}_{TG}$ implied sea surface slope on the east coast of Australia has been the subject of numerous investigations in the early to mid 1970s (e.g., Hamon and Greig, 1972; Mitchell, 1973b; Leppert et al., 1975), but was subsequently found (in 1975-76) to contain gross levelling errors on the Qld coast (Morgan, 1992). A comparison of the original MC_{R} (Roelse et al., 1971) and the current MC_{SB} and MC_{B} (for consistency, as Roelse et al. (1971) used only the basic network) in Figure 5.7

indicates that these errors have been removed from MC_{SB}.

MC_{SB} and MC_{B} SSTop_{TG} produce reasonably similar results (Figure 5.7), with an apparent levelling error in the basic levelling section between Fremantle and Geraldton. In addition to the errors on the Qld coast, levelling errors in MC_{R} appear between Centre Island-Karumba-Weipa when compared to MC_{SB}, MC_{B} and CARS2006 SSTop_{TG}. This indicates improvements in the ANLN data set since 1971, with support (based primarily on the Fremantle-Geraldton basic section) for the inclusion of the supplementary and basic network in a single LSA rather than than the basic network only (cf. Chapter 8.

5.6.2 Comparison of CARS2006 SSTop^{M}_{TG} and SSTop^{G}_{TG}

Differences among CARS2006, Rio05 SSTop^{M}_{TG}, AGQG09 and EGM2008 SSTop^{G}_{TG} (Section 5.4.4) are presented in Figure 5.8, with the statistics for these differences in Table 5.6. CARS2006 and Rio05 are used here, as they are considered the better two SSTMs in Australian coastal regions (Section 5.5.2).

H_{AG09} $(= h - \zeta_{AG09})$ and H_{EGM08} $(= h - \zeta_{EGM08})$ SSTop^{G}_{TG} display good agreement in Figure 5.8 with most differences at individual tide-gauges <50 mm, as also indicated by the similar differences between both SSTop^{G}_{TG} with CARS2006 and Rio05 SSTop^{M}_{TG} in the descriptive statistics in Table 5.6. However, site-dependent differences between both SSTop^{G}_{TG} and SSTop^{M}_{TG} reach $\sim$0.20 m at Port Hedland, and up to 0.15 m at Fremantle, Wyndham, Centre Island, Bamaga and Port Lincoln. The good agreement among CARS2006 and H_{AG09}- and H_{EGM08}-implied SSTop^{G}_{TG} along the Qld coast (Townsville to Camp Cove in Figure 5.8) indicates that CARS2006 is more accurate in this region than Rio05 (up to 0.30 m difference; Section 5.5.2).

These differences are caused by a combination of errors in SSTop^{M}_{TG} (previously estimated at $\sim$50$-$100 mm) and SSTop^{G}_{TG}. The abrupt SSTop^{G}_{TG} changes between some tide-gauges (compared to SSTop^{M}_{TG}; see Figure 5.8) suggest SSTop^{G}_{TG} errors, rather than SSTop^{M}_{TG} errors (particularly as AGQG09- and EGM2008-implied SSTop^{G}_{TG} are

similar). Causes for SSTop^G_{TG} error include: i) MSL error (maximum up to 150 mm) from tide-gauge observations propagating into AHD H_{TGBM} (cf. Equation (5.4)); ii) levelling error between the tide-gauge and TGBM, causing an error in AHD H_{TGBM} (cf. Equation (5.4)); iii) h error (mean STD ±26 mm (scaled by 10); N. Brown 2009, pers. comm.), or iv) ζ_{EGM08} or ζ_{AG09} error (∼130 mm; cf. Featherstone et al., 2011). However, whichever of these possible errors is responsible cannot be determined at this stage.

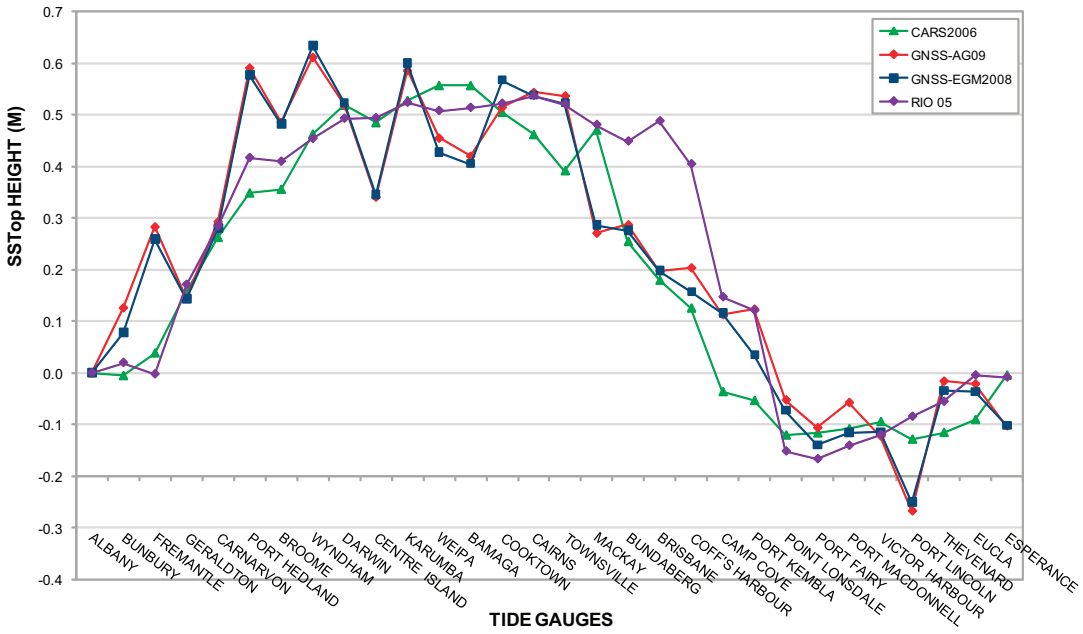

Figure 5.8: The differences among CARS2006 (green) and Rio05 (purple) SSTop^M_{TG}, $h - \zeta_{EGM08}$ (blue) and $h - \zeta_{AG09}$ (red) SSTop^G_{TG} at 30 AHD mainland tide-gauges. All SSTop_{TG} are relative to the Albany tide-gauge (held at zero). CARS2006 data from CSIRO Marine Laboratories.

Stat	CARS2006 minus		Rio05 minus	
	H_{AG09} (m)	H_{EGM08} (m)	H_{AG09} (m)	H_{EGM08} (m)
Mean	−0.038	−0.027	0.011	0.022
Min	−0.245	−0.228	−0.285	−0.260
Max	0.199	0.184	0.290	0.290
STD	±0.113	±0.106	±0.125	±0.123
RMS	±0.119	±0.110	±0.126	±0.125

Table 5.6: Statistics for CARS2006 and Rio05 minus H_{AG09} and H_{EGM08} at 30 mainland tide-gauges.

The differences in northern Australia (Port Hedland-Cooktown) could be influenced by large SSH anomalies (e.g., Tregoning et al., 2008), which may affect MSL observed from

tide-gauges (only up to three years for AHD), but also ζ_{EGM08} and ζ_{AG09}. In addition, errors in the satellite altimetry-derived gravity anomalies over the coast (e.g., Deng et al., 2002; Volkov et al., 2007) will also affect ζ_{EGM08} or ζ_{AG09}, but also the satellite altimetry and geoid contributions in Rio05. Both SSTop_{TG}^{G} suggest that CARS2006 is superior to Rio05 between Bundaberg and Port Kembla (Section 5.5.2; also see Figure 5.5) where differences up to ∼0.4 m exist between CARS2006 and Rio05 SSTop_{TG}^{M}.

5.7 Removing SSTop from AHD tide-gauges using SSTMs

The application of SSTMs and $h - \zeta$ SSTop_{TG} can be used to remove the effect of sea surface slope on MSL used to constrain vertical datums (cf. Vaníček, 1991). This section first quantifies the north-south trend implied by SSTop_{TG}^{L} and CARS2006 SSTop_{TG}^{M} (cf. Section 1.2), then it is demonstrated that subtracting CARS2006/Rio05, SSTop_{TG}^{M} or AGQG09/EGM2008 SSTop_{TG}^{G} from MC SSTop_{TG}^{L} at 30 AHD(mainland) tide-gauges effectively removes the influence of sea surface slope. This allows the LSA of any new levelling-based AVD to be constrained at multiple tide-gauges, but without a sea surface-induced north-south slope in the datum (cf. Chapter 8).

5.7.1 Sea surface slope implied by MSL at Australian tide-gauges

Linear regression of SSTop_{TG}^{L} and CARS2006 SSTop_{TG}^{M} as a function of latitude at 30 AHD(mainland) tide-gauges around Australia infers north-south sea surface slope in Australian coastal regions, increasing northwards (cf. Fischer, 1975). This north-south trend has propagated directly into the AHD (e.g., Featherstone, 2004, 2006) as a result of fixing the (then) ALS to all 30 AHD(mainland) tide-gauges to use MSL as AHD_0 (cf. Zilkoski et al., 1992).

The north-south slope can be be converted to mm (vertical) per 100 km (horizontal), to directly compare MC_{SB}- and CARS2006-implied SSTop_{TG} (Table 5.7). CARS2006 slope is 25.1 mm per 100 km (correlation 0.95), while MC_{SB} slope is 23.7 mm per 100

km (correlation 0.58). MC_R is included for comparison, and is shown to have a larger slope of 43.3 mm per 100 km (correlation 0.63) than MC_{SB}. A linear extrapolation over 3,000 km (approximate distance between northern tip of Cape York and the south coast of Vic) provides an approximation of the north-south AHD height error caused by fixing the AHD to MSL.

SSTop_{TG}	Slope/100 km (mm)	Total slope (m)	R^2
CARS2006	25.1	0.752	0.95
MC_{SB}	23.7	0.711	0.58
MC_R	43.3	1.299	0.63

Table 5.7: CARS2006, MC_{SB} and MC_R SSTop^L_{TG} slope per 100 km (in mm) as a function of latitude and correlation coefficient (R^2) at 30 mainland AHD tide-gauges. Total slope (over 3,000 km) is a linear extrapolation between Australia's northern- and southern-most points.

5.7.2 Removing the sea surface slope using SSTMs and quasigeoid models

Assuming the different realisations of SSTop at AHD tide-gauges are error-free, the expected residual at each tide-gauge is zero and can be expressed by the conditions

$$\mathrm{SSTop}^L_{TG} - \mathrm{SSTop}^M_{TG} = 0 \tag{5.5}$$

or

$$\mathrm{SSTop}^L_{TG} - \mathrm{SSTop}^G_{TG} = 0. \tag{5.6}$$

However, the residual at each tide-gauge is not zero, because modelled/derived SSTop_{TG} contain errors. It is assumed that the largest errors are contained in SSTop^L_{TG} (>0.5 m; Section 2.4.2), but SSTop^M_{TG} ($\sim$50$-$100 mm; Rio and Hernandez, 2004), tide-gauge observed MSL ($\sim$50$-$100 mm), h ($\sim$26 mm) and AGQG09/EGM2008 ζ ($\sim$130 mm) all have their own different error budgets (cf. Tables 5.5 and 5.6), that can only be crudely estimated for Australian coastal regions.

Although, each SSTop_{TG} residual will rarely be zero, due to errors in the data, it is the MSL slope that is important here. The slope is a function of the residuals for all SSTop_{TG}, and is computed from linear regression of the SSTop_{TG} residuals

(cf. Figure 5.7). The residuals for each tide-gauge are computed using Equations (5.5) and (5.6), but will generally be non-zero. Linear regression of SSTop_{TG} residuals result in a residual slope with respect to latitude (north-south slope; Figures 5.9 and 5.10), which can be calculated per 100 km (Table 5.8).

Figure 5.9(a) shows the residual slope when H_{EGM08}-implied SSTop^{G}_{TG} is subtracted from MC_{SB} SSTop^{L}_{TG}. Despite large residuals at some tide-gauges (up to $\pm$0.5 m; Table 5.9), the residual slope is virtually removed (0.98 slope ratio), shown in Table 5.8 to be 0.5 mm/100 km, or 16 mm over 3,000 km. A similar result is achieved for AGQG09 SSTop^{G}_{TG} (Figure 5.9(b)), demonstrating the similarity of EGM2008 and AGQG09 (cf. Section 5.8; Featherstone et al., 2011).

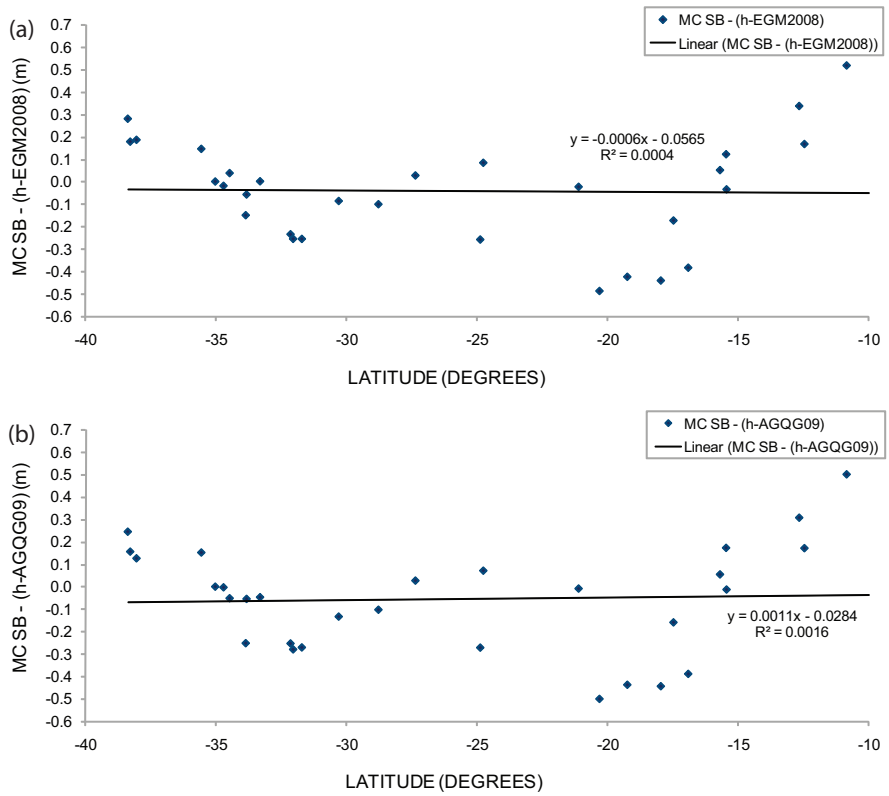

Figure 5.9: Linear regression for (a) $\text{MC}_{SB}-H_{EGM08}$ and; (b) $\text{MC}_{SB}-H_{AG09}$ as a function of latitude at 30 AHD(mainland) tide-gauges.

The residual slope from MC_{R} $\text{SSTop}^{L}_{TG}-\text{CARS2006}$ SSTop^{M}_{TG} is shown in Figure 5.10(a), and Table 5.8 to be much larger than that for MC_{SB}, with a slope of 18.3 mm per 100 km (549 mm per 3000 km; 0.58 slope ratio) remaining. Further evidence of the problems with the 1971 ALS (basic network only) is shown in Table 5.9, where the descriptive

statistics indicate the large size of the MC_R $SSTop^L_{TG}$−CARS2006 $SSTop^M_{TG}$ residuals. It appears that removing several gross levelling errors from the original MC_R (Roelse et al., 1971) and including all supplementary and basic levelling in a single MCLSA (MC_{SB}) has made a marked improvement in the amount of slope that can be removed using SSTM $SSTop_{TG}$. It is suggested that up to 40% of the original slope in the AHD identified by Roelse et al. (1971) is attributable to gross levelling errors in the original network, with adjustment techniques and extra redundancy from the supplementary network also contributing to the improvement.

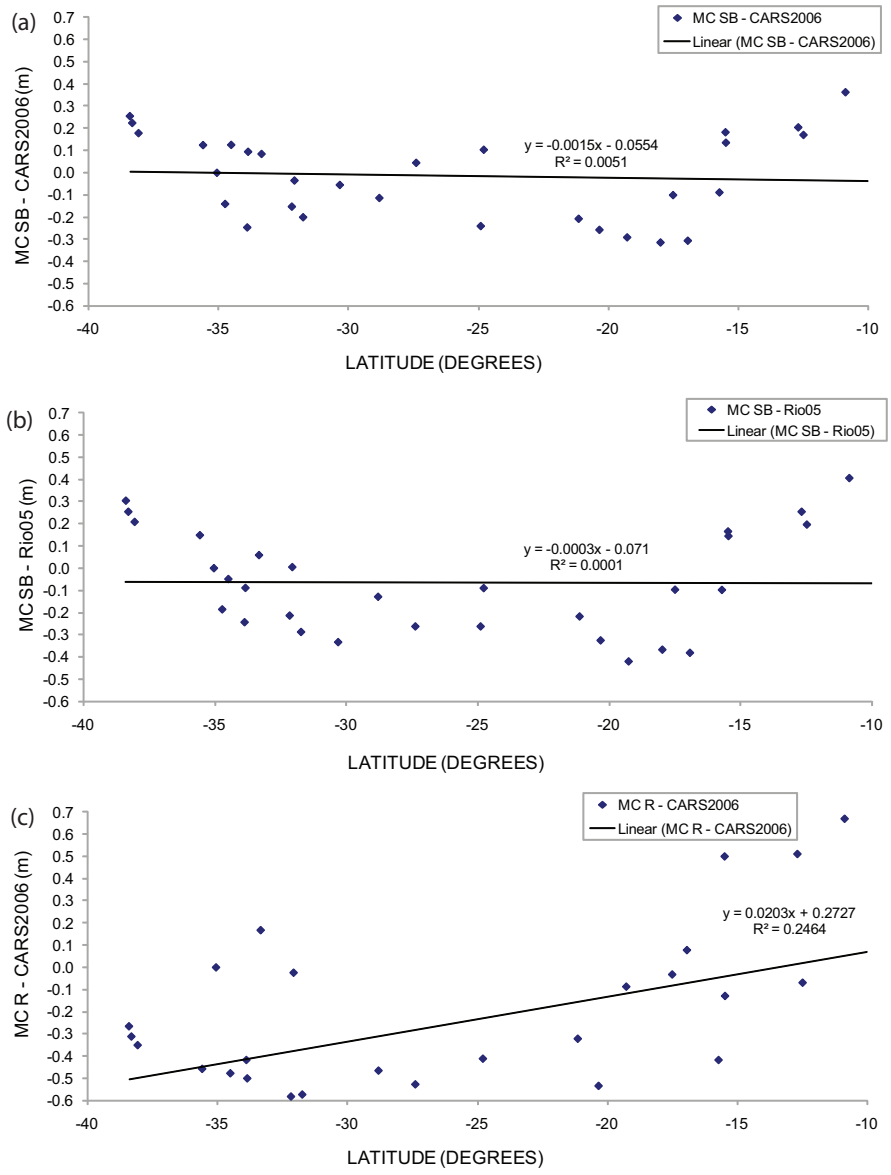

Figure 5.10: Linear regression (as a function of latitude) for (a) MC_{SB} minus CARS2006; (b) MC_{SB} minus Rio05; and (c) MC_R minus CARS2006. CARS2006 data from CSIRO Marine Laboratories.

The residual slope when CARS2006 and Rio05 SSTop^{M}_{TG} is subtracted from MC_{SB} SSTop^{L}_{TG} is shown in Figures 5.10(b) and 5.10(c). The results here are similar to those from MC_{SB} SSTop^{L}_{TG}−SSTop^{G}_{TG}, although SSTop^{M}_{TG} appear to slightly over-correct the slope (residual slope is negative; Table 5.8), which is indicated by a slope ratio >1. However, residual slopes of −42 mm (CARS2006) and −9 mm (Rio05) per 3,000 km are negligible (compared to expected data errors), demonstrating that oceanographic-only and geodetic-oceanographic (combined) SSTMs can effectively remove the effects of sea surface slope from any new LSA of the ANLN constrained at tide-gauges.

SSTop_{TG}	Slope per 100 km (mm)	Total slope (mm)	R^2	slope ratio
MC_{SB}−EGM08	0.5	15	0.00	0.98
MC_{SB}−AGQG09	0.9	27	0.00	0.96
MC_{SB}−CARS2006	−1.4	−42	0.01	1.06
MC_{SB}−Rio05	−0.3	−9	0.00	1.01
MC_{R}−CARS2006	18.3	549	0.25	0.58

Table 5.8: Residual sea surface slope per 100 km (in mm) as a function of latitude, correlation coefficient (R^2) and the ratio of the slope removed (where a ratio of one indicates that the SSTM implied slope is the same as the MC_{SB} or MC_{R} implied slope) at 30 mainland AHD tide-gauges by SSTop^{M}_{TG} and GNSS-ζ_{EGM08} SSTop_{TG} from MC ANLN SSTop_{TG}. Slope per 3,000 km is a linear extrapolation between Australia's northern- and southern-most points.

	MC_{SB} minus				MC_{R} minus
	CARS2006 (m)	Rio05 (m)	H_{AG09} (m)	H_{EGM08}	CARS2006
Mean	−0.015	−0.064	−0.056	−0.042	−0.256
Min	−0.315	−0.421	−0.500	−0.486	−0.690
Max	0.364	0.407	0.501	0.516	0.671
STD	±0.193	±0.232	±0.238	±0.237	±0.365
RMS	±0.194	±0.241	±0.245	±0.241	±0.447

Table 5.9: Statistics for MC_{SB} minus (a) CARS2006; (b) Rio 05; (c) H_{AG09}; and (d) H_{EGM08} and MC_{R}−CARS2006 at 30 Australian mainland tide-gauges.

Despite the CARS2006 results having the largest (although still insignificant) residual slope (−1.4 mm/100 km), Table 5.9 indicates that CARS2006 is the best fit to MC_{SB}, with the smallest maximum/minimum range, mean, STD and RMS. This further suggests that CARS2006 is the best-performing estimate of SSTop_{TG} and will be used to correct SSTop at tide-gauges for the final LSA of the ANLN to realise the Australian experimental vertical datum (AEVD; Chapter 8).

5.8 Offset between AHD(Tas) and AHD(mainland)

Several studies have attempted to establish the offset between AHD(mainland) and AHD(Tas) (hereafter referred to as O_{Tas}), using GNSS and geoid models of varying vintage and quality. Here, estimates of O_{Tas} are presented using five SSTMs, AGQG09- and EGM2008-implied SSTop_{TG}^{G}.

5.8.1 Definition of AHD(mainland)−AHD(Tas) offset

It is important to clarify how O_{Tas} is defined, because the offset is spatially variable (Featherstone, 2000, 2002a) due to the variable difference between AHD(mainland) and the geoid (primarily the north-south slope; see Sects 5.6 and 5.7). Therefore, O_{Tas} is dependent on which points are used on the AHD(mainland) and AHD(Tas). Rizos et al. (1991) used GNSS h and ζ computed from the OSU89A geopotential model (Rapp and Pavlis, 1990) to degree 360 (augmented by local terrestrial gravity for the high frequency component of ζ) at three tide-gauge locations along the Vic coast (Portland, Point Lonsdale and Lakes Entrance), and three along the northern Tas coast (Stanley, Burnie and Low Head) estimating O_{Tas} to be ∼0.10 m (AHD(mainland) above AHD(Tas)), but this was later revised up to 0.40 m (Featherstone, 2000, 2002a). By comparison, Rapp (1994) uses GNSS h and ζ computed from the geopotential models JGM-2 (Nerem et al., 1994) (degree 2 to 71) and OSU91A (Rapp et al., 1991) (degree 71 to 360) from locations distributed across Australia (85 mainland; 4 Tas), calculating O_{Tas} to be ∼0.30 m (AHD(mainland) above AHD(Tas)), as does Featherstone (2000, 2002a) (O_{Tas} 0.26±0.33 m; AHD(mainland) above AHD(Tas)), but using 1013 GNSS h and AUSGeoid98 ζ.

In an attempt to replicate the study of Rizos et al. (1991), Featherstone (2000, 2002a) used a subset of 13 GNSS points along the northern Tas coastline, and six along the Vic coastline, in addition to the study using 1013 points over all Australia. O_{Tas} calculated from this study was 0.12±0.12 m, with the AHD(mainland) again above AHD(Tas). Thus, two definitions of O_{Tas} are used: i) the mean offset for the entire

datum (Rapp, 1994; Featherstone, 2000, 2002a); and ii) the mean offset between the southern Vic coast and the northern Tas coast. Furthermore, as the AHD(Tas) is fixed at two tide-gauges (Burnie in the north; Hobart in the south), AHD(Tas) may also have a SSH-dependent slope (cf. Sects 5.6 and 5.7).

Strictly speaking, the O_{Tas} should only be estimated between AHD tide-gauges, but O_{Tas} will still be dependent on which AHD tide-gauges are selected. However, if it is assumed that the local variability in SSTop along the Vic and northern Tas coastlines is small (cf. Figure 5.3), then using a larger sample of tide-gauges will provide a more reliable estimate of O_{Tas}. For this study, O_{Tas} is defined as the mean difference between SSTop along the southern Vic and northern Tas coastline, defined at five Vic tide-gauges (Portland, Port Fairy, Lorne, Point Lonsdale, and Stony Point) and two Tas tide-gauges (Burnie and Devonport; see Figure 5.11) to semi-replicate (as close as possible given available GNSS observations at tide-gauges) the studies of Rizos et al. (1991) and Featherstone (2000, 2002a). Two additional tide-gauges in the south of Tas (Hobart and Spring Bay; see Figure 5.11) are then used to identify if there is a north-south slope in AHD(Tas).

5.8.2 Methods

The first method (see Section 5.4.1) used to determine O_{Tas} (negative O_{Tas} indicate AHD(mainland) to be above AHD(Tas)) requires SSTop^{M}_{TG} at the five Vic and two Tas tide-gauges (Burnie and Devonport; Figure 5.11). Differences were calculated between all SSTop^{M}_{TG} (total of 10 differences for each SSTM), from which statistics were calculated for each SSTM (Table 5.10). Note that this method only accounts for SSTop differences at tide-gauges; MSL errors are not included in the SSTM O_{Tas} (cf. Coleman et al., 1979; Kearsley et al., 1993a).

Equation (5.4) is used for EGM2008 and AGQG09 estimates of O_{Tas} based on methods described in Section 5.4.4, which are basically the same as those used by Rizos et al. (1991) and Featherstone (2000, 2002a). This method is dependent on the assumption that in the local area around the tide-gauge, O_{TG} remains constant ($O_{TGBM} = O_{TG}$;

see Figure 5.2; also cf. Hipkin et al., 2004). However, it should be acknowledged that O_{Tas} estimates using Equation (5.4) can be influenced by errors in MSL and levelling propagating into AHD H_{TGBM} in addition to h and ζ errors. The tide-gauges selected for this study all have recent Bernese-processed ITRF2005 (epoch 2000) GNSS h_{TGBM} (Hu, 2009) provided by GA (N. Brown 2009, pers. comm.).

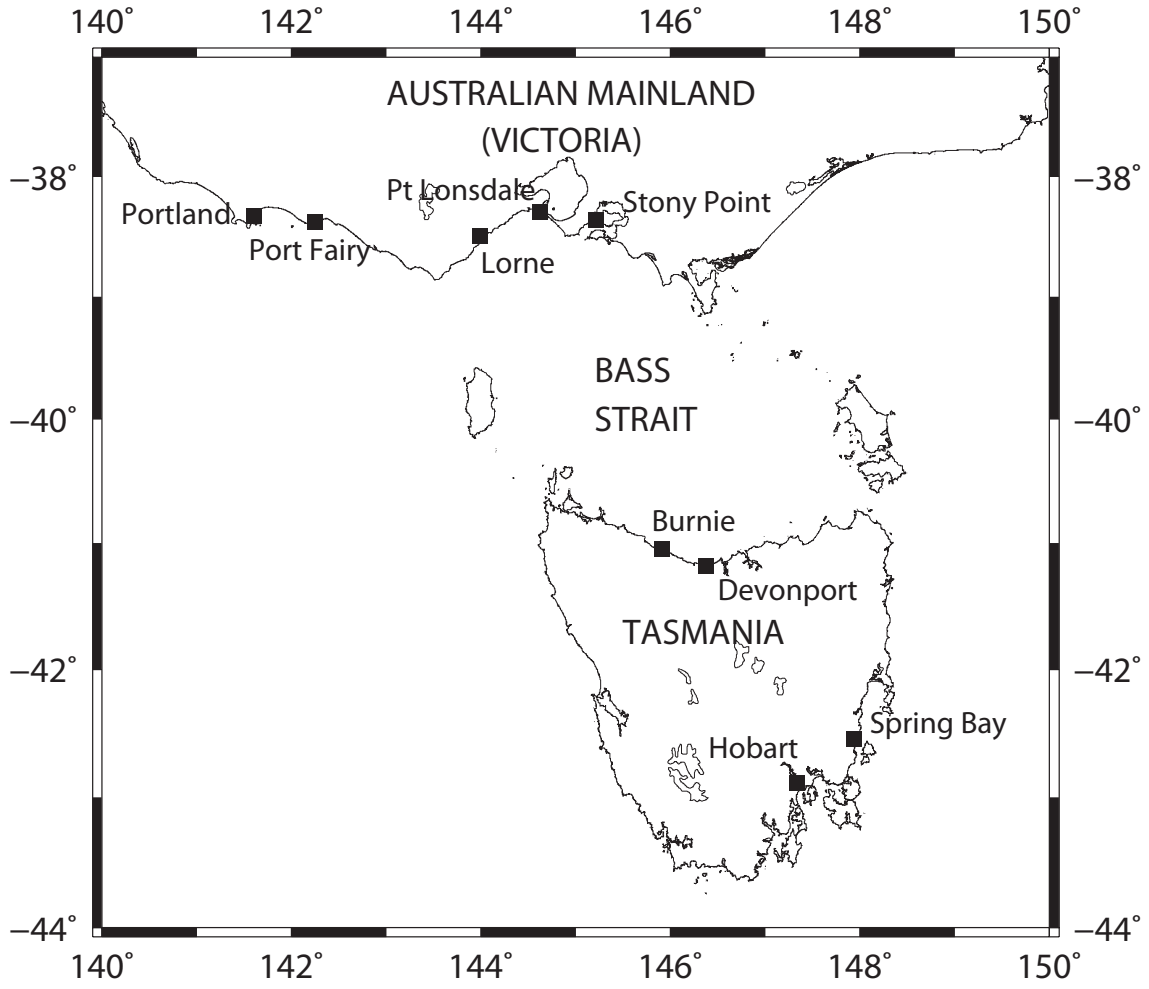

Figure 5.11: Tas and Vic tide-gauges (black squares) used to estimate O_{Tas}. Mercator projection.

5.8.3 Results

The mean of the 10 height differences (between the five Vic and two Tas tide-gauges; Burnie and Devonport) calculated for each SSTM and AGQG09- and EGM2008-implied SSTop^{G}_{TG} in Table 5.11 is the estimated O_{Tas}, with the STD of the mean differences adopted as the estimated error. All estimates range between 58±17 mm

(Rio05) and −48±24 mm (JPL08). The CARS2006 estimate of O_{Tas} (3±6 mm; Tas above mainland) suggests that the offset is negligible, but this does not include MSL errors (from tide-gauges). EGM2008 and AGQG09 similarly indicate that O_{Tas} is small (12±52 and 33±78 mm respectively). However, these estimates may be contaminated by h, quasigeoid, MSL, levelling and temporal (combination of these data sets/models) errors, which is reflected in the large maximum, minimum and STD (Table 5.10) compared to CARS2006, Rio05, GGM02 MDT and JPL08. It appears that AGQG09 is superior to EGM2008 in the Bass Strait region, with lower STD (±52 mm versus ±78 mm), and much lower maximum difference (90 mm versus 167 mm).

Stat	CARS2006 (mm)	Rio05 (mm)	GGM02 (mm)	JPL08 (mm)	DNSC08 (mm)	AGQG09 (mm)	EGM2008 (mm)
Mean	3	58	−42	−48	20	12	33
Max	12	81	−33	−18	306	90	167
Min	−7	31	−49	−77	−147	−67	−78
STD	±6	±17	±6	±24	±145	±52	±78
B−H	−22	−1	−15	−30	−8	53	42

Table 5.10: Statistics for O_{Tas} between five Vic and two Tas tide-gauges for five SSTM SSTop_{TG} and two SSTop^{G}_{TG}. The bottom row is the difference between Burnie and Hobart tide-gauges (Burnie minus Hobart). Negative O_{Tas} indicate AHD(Tas) to be lower than AHD(mainland).

Although the DNSC08 MDT O_{Tas} estimate is within the range of other estimates, the very large range and STD of the differences (maximum 306 mm; minimum −147 mm; STD ±145 mm) again indicate that DNSC08 MDT is not suitable for determining SSTop_{TG} (cf. Andersen and Knudsen, 2009). If only three AHD tide-gauges (Point Lonsdale, Port Fairy, and Burnie) are used for the same computations, O_{Tas} changes by <10 mm for all except DNSC08 MDT (−67 mm) and EGM2008 (−30 mm). Table 5.10 (bottom row) shows the SSTop_{TG} difference between Hobart and Burnie tide-gauges to be small. The magnitude of SSTM estimates are all less than 30 mm and indicate Hobart to be higher (Burnie minus Hobart). However, the two quasigeoid estimates indicate that Burnie is higher by ∼50 mm. These can be compared with the levelled height difference (from a MCLSA fixed at Hobart) of −32 mm, supporting the SSTM estimates.

Stat	CARS2006 (mm)	Rio05 (mm)	GGM02 (mm)	JPL08 (mm)	DNSC08 (mm)	AGQG09 (mm)	EGM2008 (mm)
Mean	12	61	−32	−32	33	−6	9
Max	26	92	−8	15	352	90	167
Min	−7	31	−49	−77	−147	−119	−120
STD	±11	±17	±12	±28	±145	±61	±77

Table 5.11: Statistics of O_{Tas} between five Vic and all four Tas tide-gauges (Figure 5.11) for four SSTM SSTop$_{TG}$ and two SSTop$^{G}_{TG}$. Negative O_{Tas} indicate AHD(Tas) to be lower than AHD(mainland).

On the basis that AHD(Tas) does not contain a significant north-south slope, O_{Tas} for the five Vic tide-gauges and all four Tas tide-gauges (Hobart and Spring Bay now included; Figure 5.11) was recomputed, to provide improved reliability from a larger sample (results in Table 5.11). There are only minor differences when compared with Table 5.10 (O_{Tas} and STD decreased in some cases when four Tas tide-gauges are used), further suggesting that O_{TG} is negligible (cf. Rizos et al., 1991; Rapp, 1994; Featherstone, 2000, 2002a). However, any small offset that may exist, can be removed in the re-adjustment of any new Australian vertical datum by applying CARS2006 SSTop$_{TG}$ (probably CARS2006) and constraining the ANLN to those tide-gauges (cf. Chapter 8).

5.9 Summary

A central feature of the AHD has been the adoption of MSL at 32 tide-gauges (30 mainland) as AHD$_0$. However, SSTop causes MSL to deviate from the geoid, introducing a long-studied north-south slope into the AHD. SSTop values can be estimated at tide-gauges to quantify the north-south sea surface slope and its effect on the AHD, but also to correct for the effects of SSTop at tide-gauges in the realisation of any new levelling-based AVD. SSTop at tide-gauges was obtained from SSTMs and also from GNSS h and quasigeoid models, which were compared to SSTop at tide-gauges implied by MCLSA of the ANLN. Five SSTMs were tested here (CARS2006, Rio05M, GGM02 MDT, JPL08 and DNSC08 MDT), along with EGM2008 and AGQG09 models.

CARS2006, Rio05, and GGM02 were compared to ANLN SSTop at tide-gauges, with general agreement, despite large residuals in some regions (∼0.40 m), which can be mostly attributed to errors in the ANLN. Comparisons between CARS2006 and Rio05 SSTop and EGM2008 and AGQG09 SSTop at 30 mainland tide-gauges demonstrated good agreement, but with apparently site-dependent noise in EGM2008 and AGQG09 SSTop at some tide-gauges. CARS2006 displayed a slightly better fit to both the ANLN and quasigeoid SSTop estimates than Rio05 SSTop at tide-gauges (∼110 mm versus ∼120 mm).

Subtracting SSTM or quasigeoid SSTop from MC_{SB} (current version of the complete ANLN) SSTop at 30 AHD(mainland) tide-gauges effectively removed the effect of sea surface slope, with MC_{SB} slope of 23.7 mm per 100 km reduced to <1.4 mm per 100 km for both SSTM and quasigeoid SSTop estimates. CARS2006 was considered the best-performing estimate of SSTop used, and will be used to correct AHD MSL at tide-gauges in the final LSA of the ANLN to realise a new experimental Australian vertical datum. In addition, it appears that the AHD(mainland)−AHD(Tas) offset is close to zero, which is less than indicated by previous studies.

6. COMPUTATION OF GRAVITY AT BENCHMARKS USING EGM2008 AND THE AUSTRALIAN NATIONAL GRAVITY DATABASE

Observed gravity is needed to realise physically meaningful heights that provide an indication of the direction of fluid flow. This Chapter describes a method to establish gravity at Australian National Levelling Network (ANLN) benchmarks (BMs) using the EGM2008 global gravity field model (Pavlis et al., 2008), and interpolation of terrestrial gravity from the 2007 release of the Australian National Gravity Database (ANGD2007; Murray, 1997; Tracey et al., 2007). BM gravity values (g_{BM}) are used in Chapter 7 to compute gravimetric height corrections (HCs), thus realising nation-wide physical heights across Australia.

The use of EGM2008- or ANGD2007-interpolated g_{BM} (herein referred to as EGM2008 g_{BM} and ANGD2007 g_{BM}) to compute HCs is necessary because only 9,527 (out of 87,591) ANLN BMs have directly observed gravity (see Section 6.4.1). However, these 9,527 BM-co-located gravity observations (g_{obs}) allow a partial validation of the EGM2008 g_{BM} and ANGD2007 g_{BM}. An investigation into the possible errors affecting g_{BM} is conducted following the validation.

6.1 Background on gravity and heights

6.1.1 Gravity and height systems

The gravity acceleration vector ($\mathbf{g}$) comprises the Earth's gravitation and the centrifugal acceleration of the Earth's rotation (Torge, 1989, 24). The Earth's gravity field consists of an infinite number of equipotential or level surfaces on which the gravity

potential (W) is constant. W and $\mathbf{g}$ are related by (Torge, 2001, 56)

$$\boldsymbol{g} = \nabla W. \tag{6.1}$$

The direction of $\mathbf{g}$ is tangential to the curved and torsioned plumbline, which is always orthogonal to the (non-parallel) equipotential surfaces (see Figure 7.1), while the magnitude of gravity (g) is the quantity measured by gravimeters g_{obs} (Torge, 2001, 56). Gravity units in the SI-system are ms^{-2}, but terms from the CGS-system (Gal = 10^{-2} ms^{-2}; mGal = 10^{-5} ms^{-2}; μGal = 10^{-8} ms^{-2}; Torge, 1989, 171) will be used here.

Physical heights are determined by the difference in gravity potential between the point P on the topographic surface (W_P) and the geoid (W_0), scaled to dimensions of length with a gravity value. Levelling networks provide the geometric height difference (Δn) relative to the local equipotential surface, but these need to be converted into potential differences that account for the non-parallelism of the equipotential surfaces and to ensure holonomity (e.g., Sansò and Vaníček, 2006). However, gravity potential cannot currently be measured directly, so g is combined with levelling to obtain (Heiskanen and Moritz, 1967, 162)

$$W_0 - W_P = C = \int_0^P g\, dn \tag{6.2}$$

where C is the geopotential number which is independent of the levelling route taken between the geoid and P. Orthometric heights (H^O), dynamic heights (H^D) and normal heights (H^N) are all based on C (see Chapter 7 for details) and thus require observed g in their realisation.

By comparison, normal-orthometric heights ($H^{N\text{-}O}$; e.g., Bomford, 1971, 230) use only normal (or theoretical) gravity (γ), while H^N also use γ and g (e.g., Heiskanen and Moritz, 1967, 170). The external gravity field of a level ellipsoid (e.g., GRS80; Moritz, 1980), is referred to as the normal gravity field, where the normal gravity vector $\boldsymbol{\gamma}$ and normal gravity potential U are related by (e.g., Torge, 2001, 105)

$$\boldsymbol{\gamma} = \nabla\, U. \tag{6.3}$$

6.1.2 Terrestrial gravity observation methods

Terrestrial g_{obs} can be obtained from absolute or relative gravimeters. Absolute g_{obs} are determined by the fundamental acceleration quantities of length and time (Torge, 2001, 171), while relative g_{obs} measures gravity difference between two points, using either time or length (Torge, 2001, 178). Terrestrial gravity networks usually comprise relative g_{obs} tied to a gravity datum realised by absolute g_{obs} (e.g., Tracey et al., 2007). The reader is referred to (Torge, 1989, Chapters 5 and 6) for a fuller treatment of absolute and relative gravity measurement.

6.1.3 Terrestrial gravity data used for this study

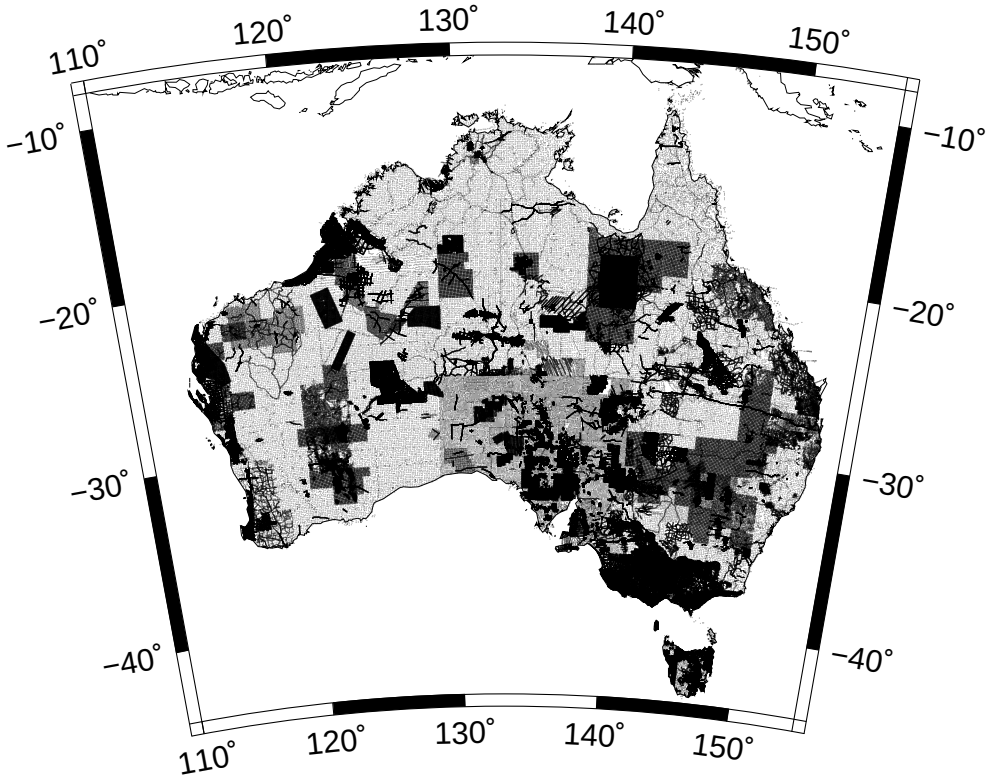

Figure 6.1: ANGD2007 Australian land gravity coverage (1,096,652 g_{obs}). Lambert projection.

ANGD2007 (**2007_V_GRAV_JETSTREAM.dat**; see Figure 6.1; Tracey et al., 2007) is the source of terrestrial gravity data used here, with the 2007 release used because it contains ANLN BM names that are not available in subsequent releases, but are necessary to identify g_{obs} co-located with ANLN BMs. ANGD2007 contains 1,246,613 land-based and marine g_{obs} (in μms^{-2}) (Wynne, 2007) which are tied to the Australian Absolute Gravity Datum 2007 (AAGD07; Tracey et al., 2007), which is 0.078 mGal less than IGSN71. ANGD2007 is used for two purposes here: i) as an alternative source (to EGM2008) of gravity data to compute g_{BM} (Section 6.3) (g_{BM} is required so that gravimetric HCs can be computed in Chapter 7), and ii) as a method of partial validation of EGM2008 g_{BM} and ANGD2007 g_{BM} by extracting co-located ANGD2007 g_{obs} for direct comparison at BMs (Section 6.4).

Australian terrestrial gravity data have been compiled over ∼60 years (e.g., Murray, 1997), leading to variable accuracy within ANGD2007 (Wynne, 2007). Error sources that degrade the quality of ANGD2007 include errors in g_{obs} height and horizontal position (ϕ, λ), and the gravity observations themselves (Barlow, 1977). Between 1959 and 1974, a reconnaissance gravity survey was conducted using helicopters as transport (surveying in a 'clover-leaf' pattern) to cover Australia at 11 km grid spacings (7 km in South Australia and Tasmania) (Fraser et al., 1976), with Bellamy and Lodwick (1968) describing the errors resulting from barometric heighting, and attempts to adjust these errors.

Fraser et al. (1976) estimated the errors within each helicopter reconnaissance gravity survey to be 0.3 mGal for g_{obs}, ±5 m for the barometric heights (which maps to ∼1 mGal in the simple Bouguer anomaly; cf. Equation (6.16)), and ±0.1 arc-minutes (∼±200 m) for (ϕ, λ). However, this could increase to 0.5 mGal for g_{obs} and ±10 m for barometric heights for ties between adjoining surveys (Fraser et al., 1976). Detailed surveys within the helicopter coverage were generally of higher quality, using surveyed heights instead of barometric heights (Barlow, 1977). The ANGD is also likely to contain systematic long-wavelength errors (Mather et al., 1976; Featherstone, 2005). The possible effects of ANGD2007 errors are discussed in Section 6.5.

Large amounts of gravity data have been added to the ANGD since the reconnaissance gravity surveys were completed in 1974 (e.g., the ANGD2007 contains ∼1.1 million observations compared to ∼700,000 in the 1996 release; Featherstone et al. (2001)), with new digital barometers and now GNSS observations improving gravity station height accuracy in recent years (Murray, 1997). Sproule et al. (2006) investigated ANGD2004, finding that it is generally free of localised gross errors, but the tidal system of the ANGD is unknown due to currently unavailable metadata (Featherstone et al., 2001). For further details on the ANGD, see Murray (1997), Fraser et al. (1976) Barlow (1977), Bellamy and Lodwick (1968) and Tracey et al. (2007).

6.2 Method of gravity re-construction at BMs using EGM2008

Gravimetric HCs (see Chapter 7) require g_{obs} on the surface of the Earth. Here, the EGM2008-implied gravity disturbance (to degree and order 2160) is used to 'reconstruct' g_{obs} on the Earth's surface at ANLN BM positions, using the method described in this section. Note that the actual point-wise g_{obs} can only be approximated by the limited spatial resolution of the modelled gravity field (the omission error).

6.2.1 EGM2008 gravity disturbance

The scalar gravity disturbance at a BM (δg_{BM}) is the difference between g_{BM} and normal gravity, continued upward to the BM (γ_{BM}) (cf. Heiskanen and Moritz, 1967, 84)

$$\delta g_{BM} = g_{BM} - \gamma_{BM} \tag{6.4}$$

which can be re-arranged to infer gravity at the BM as

$$g_{BM} = \gamma_{BM} + \delta g_{BM} \tag{6.5}$$

harmonic_synth.f (Holmes and Pavlis, 2008) was used to compute the spherical ap-

proximation of the EGM2008 δg_{BM}, where $\frac{\partial T}{\partial H}$ is replaced by $\frac{\partial T}{\partial r}$

$$\delta g_{BM} = \left.\frac{\partial T}{\partial r}\right|_{BM} \tag{6.6}$$

with T_{BM} the disturbing potential at the BM ($W_{BM} - U_{BM}$, where W_{BM} is gravity potential at the BM, and U_{BM} is normal potential at the BM), and r_{BM} the radial distance between the BM and the geocentre (increasing outwards). Note that **harmonic_synth.f** computes δg_{BM} (as shown in Equation (6.6)) with the sign opposite to convention (cf. Heiskanen and Moritz, 1967, 85).

6.2.2 Computation of r_{BM}

To compute r_{BM}, which is required to compute the EGM2008 height anomaly at the BM (ζ_{BM}) and δg_{BM}, **harmonic_synth.f** converts the geodetic latitude (ϕ_{BM}) (geodetic longitude is the same as geocentric longitude) to geocentric latitude (cf. Claessens, 2006, Section 2.1) at the ANLN BM ($\bar{\theta}_{BM}$) for spherical approximation of the required values. The formula for geodetic to geocentric conversion used by **harmonic_synth.f** is

$$\bar{\theta}_{BM} = \arctan\left[\frac{(\nu(1-e^2)+h_D)\sin\phi_{BM}}{(\nu+h_D)\cos\phi_{BM}}\right] \tag{6.7}$$

where ν is the prime vertical radius of curvature

$$\nu = \frac{a}{\sqrt{1-e^2\sin^2\phi_{BM}}} \tag{6.8}$$

e^2 is the square of the first numerical eccentricity of the GRS80 ellipsoid, and a is the length of the semi-major axis. Note that $\bar{\theta}_{BM}$ is the geocentric latitude in spherical polar coordinates, not the co-latitude θ_{BM}.

Derived ellipsoidal heights (with respect to an assumed geocentric reference frame that is consistent with GDA94) at the ANLN BM (h_D) can be computed as

$$h_D = H_{BM}^{N\text{-}O} + \zeta_{BM} \tag{6.9}$$

where $H_{BM}^{N\text{-}O}$ is the AHD normal-orthometric height at the ANLN BM and ζ_{BM} is the height anomaly at the BM. $H_{BM}^{N\text{-}O}$ is used as a first approximation of h_D to initially

obtain the unknown EGM2008-derived ζ_{BM} (ζ_{EGM08}; using **harmonic_synth.f**) for use in Equation (6.9). A second iteration is sufficient to realise h_D to the nearest mm (AHD−EGM2008 bias notwithstanding, which is variable: mean +0.063 m, maximum +0.648 m, minimum −0.535, computed by Claessens et al. (2009) at 254 co-located GNSS−AHD points), which is then used in Equation (6.7) by **harmonic_synth.f** to compute r_{BM}.

6.2.3 Computation of normal gravity on the GRS80 ellipsoid

To compute γ_{BM}, γ is first computed on the GRS80 ellipsoid using the closed formula of Somigliana (e.g., Moritz, 1980),

$$\gamma = \frac{a\gamma_e \cos^2 \phi_{BM} + b\gamma_p \sin^2 \phi_{BM}}{\sqrt{a^2 \cos^2 \phi_{BM} + b^2 \sin^2 \phi_{BM}}} \tag{6.10}$$

where b is the length of the semi-minor axis, γ_e is the value of normal gravity at the equator, and γ_p is the value of gravity at the pole. For numerical computations, Moritz (1980) recommends the form

$$\gamma = \gamma_e \frac{1 + k \sin^2 \phi_{BM}}{\sqrt{1 - e^2 \sin^2 \phi_{BM}}} \tag{6.11}$$

where k is (Moritz, 1980)

$$k = \frac{b\gamma_p}{a\gamma_e} - 1 \tag{6.12}$$

which is used to compute γ on the ellipsoid at the ANLN BM position (Ω_{BM}). See Table 7.3 or Moritz (1980) for GRS80 parameter values.

6.2.4 Second-order free-air correction

The second-order free-air correction (δg_{F2}) is used to compute γ_{BM}. The linear value of 0.3086 mGal m^{-1} is often used to approximate the change in gravity with height in 'free-air' on the assumption that the vertical gradient of gravity near the Earth's surface is linear and generated by a spherical Earth (Featherstone, 1995). However, δg_{F2} is advocated by Featherstone (1995) and Hackney and Featherstone (2003) as it accounts for Newton's inverse square law and the Earth's ellipticity.

The δg_{F2} is (Hackney and Featherstone, 2003)

$$\gamma_h - \gamma = \delta g_{F2} = \frac{2\gamma}{a}(1 + f + m - 2f \sin^2 \phi_{BM})h_D - \frac{3\gamma}{a^2}h_D^2 \tag{6.13}$$

where f is the geometrical flattening of the ellipsoid and m is the geodetic parameter (ratio of gravitational and centrifugal forces at the equator). h_D is used here rather than $H^{N\text{-}O}$ (cf. Featherstone, 1995) as γ is calculated upwards from the GRS80 ellipsoid (not the quasigeoid) to the ANLN BM on the surface. γ_{BM} is thus computed

$$\gamma_{BM} = \gamma - \delta g_{F2} \tag{6.14}$$

and re-constructed g_{BM} computed using Equation (6.5), or in full from the previous equation

$$g_{BM} = \gamma - \delta g_{F2} + \delta g_{BM}(\text{EGM2008}) \tag{6.15}$$

A validation process for EGM2008-derived g_{BM} is conducted in Section 6.4.

6.3 Method of g_{BM} computation using ANGD2007

Firstly, a grid of simple planar Bouguer gravity anomalies is computed from ANGD2007 (see Sections 6.3.1 and 6.3.2 for details) which are then interpolated to ANLN BMs, with a reverse Bouguer reduction realising modelled gravity at the BM (see Section 6.3.3).

6.3.1 The Bouguer gravity anomaly

The Bouguer anomaly (Δg_B) can be given in the form (cf. Torge, 2001, 266)

$$\Delta g_B = g_{obs} - \delta g_{TOP} + \delta g_{AC} + \delta g_{FC2} - \gamma \tag{6.16}$$

where δg_{TOP} is the attraction of the topographical masses, and δg_{AC} is the atmospheric correction.

Here, the simple planar Bouguer anomaly Δg_{SPB} is used, where δg_{TOP} is approximated by the Bouguer plate (BP; cf. Section 6.5.2; Vaníček et al., 2004; Goos et al., 2003;

Reilly, 1972). The gravitational attraction of the BP (δg_{BP}) is (cf. Torge, 2001, 266)

$$\delta g_{BP} = 2\pi G \rho H^{N\text{-}O} \tag{6.17}$$

where G is the universal gravitational constant, ρ is the mass-density of the BP (usually 2670 kg m^3, taken as a constant) and $H^{N\text{-}O}$ is the AHD $H^{N\text{-}O}$ of g_{obs}, used as an approximation of H^O.

The atmospheric correction is applied to remove the effect of the mass of the atmosphere (e.g., Featherstone and Dentith, 1997; Kuhn et al., 2009), which is included in the mass of the GRS80 reference ellipsoid (Moritz, 1980). However, this effect is small; Kuhn et al. (2009) quantify the range of the correction over Australia as between 0.871 mGal and 0.668 mGal.

δg_{F2} is used as an approximation of the actual free-air gravity gradient (Section 6.2.4; Equation (6.13); Featherstone, 1995). It is important to clarify that in geophysics, Δg_B is defined at the location of g_{obs} (usually on the Earth's surface), but in geodesy, Δg_B is defined on the geoid (see Kuhn et al., 2009; Hackney and Featherstone, 2003). Here, we use the geodetic interpretation, with Δg_B computed at the geoid (e.g., Heiskanen and Moritz, 1967, 131), so that AHD $H^{N\text{-}O}$ (as an approximation of H^O) is used in Equations (6.18) and (6.19), not h (cf. Hackney and Featherstone, 2003). γ is computed using Equation (6.11), with the combined equations for the free air anomaly (Δg_F) from Featherstone (1995)

$$\Delta g_F = g_{obs} - \gamma \left\{ 1 - 2(1 + f + m - 2f \sin^2 \phi_{BM}) \frac{H^{N\text{-}O}}{a} + 3 \left(\frac{H^{N\text{-}O}}{a} \right)^2 \right\} \text{for } H^{N\text{-}O} \geq 0 \tag{6.18}$$

and

$$\Delta g_F = g_{obs} - \gamma \left\{ 1 - 2(1 + f + m - 2f \sin^2 \phi_{BM}) \frac{H^{N\text{-}O}}{a} - 3 \left(\frac{H^{N\text{-}O}}{a} \right)^2 \right\} \text{for } H^{N\text{-}O} < 0 \tag{6.19}$$

with δg_{AC} added to Equations (6.18) and (6.19). The simple planar Bouguer anomaly is thus computed

$$\Delta g_{SPB} = \Delta g_F - 2\pi \rho G H^{N\text{-}O} \tag{6.20}$$

6.3.2 Gridding Δg_{SPB}

Δg_{SPB} are then interpolated onto a 2 arc-minute grid (Figure 6.2) using the tensioned spline algorithm (Smith and Wessel, 1990), with T = 0.25 (recommended by Wessel and Smith, 2007). The Δg_{SPB} is shown to be adequate in Australia by Goos et al. (2003). The grid resolution of 2 arc-minutes (∼4 km) was selected arbitrarily, but also considering that the distance between BMs is typically ∼5 km and the observational spacings of ANGD2007 g_{obs} is ∼11 km, with ∼7 km in South Australia (e.g., Figure 6.1; Fraser et al., 1976).

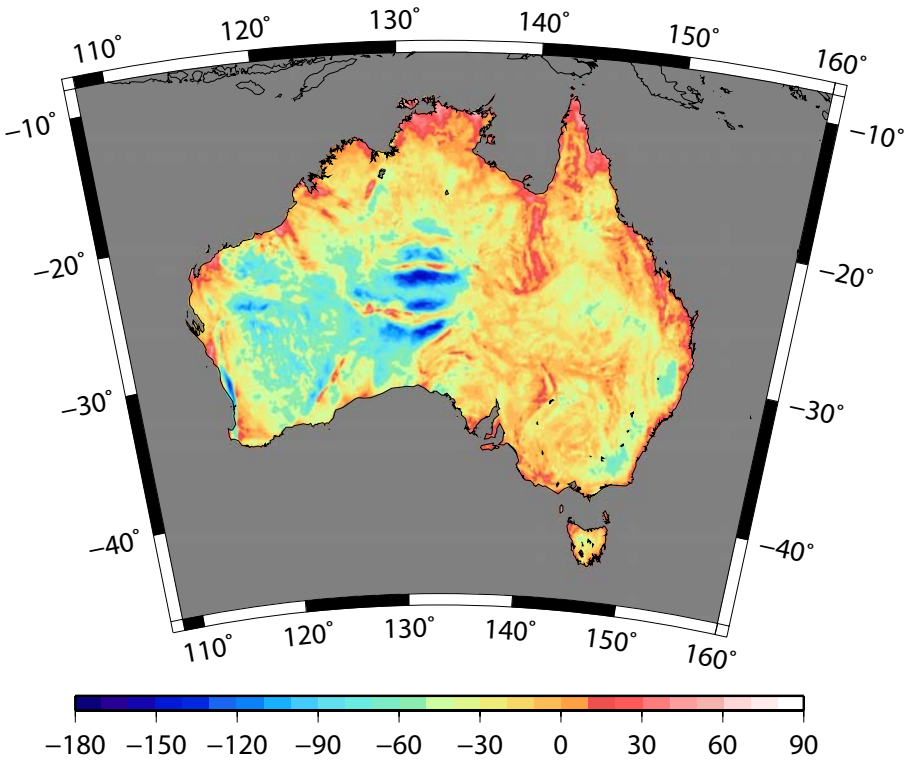

Figure 6.2: Gridded Δg_{SPB} from ∼1.1 million land ANGD2007 g_{obs}. Lambert projection, units are in mGal.

6.3.3 Computation of ANGD2007 g_{BM}

Δg_{SPB} were bi-cubically interpolated from the 2 arc-minute grid to ANLN BMs using **geoid_abs_tester.f** (Featherstone, 2001). The reverse Δg_{SPB} (cf. Equation (6.20))

$$g_{BM} = \Delta g_{SPB} + \gamma - \delta g_{F2} + \delta g_{BP} - \delta g_{AC} \tag{6.21}$$

was then used to realise ANGD2007 g_{BM}.

6.4 Validation of EGM2008 and ANGD2007 g_{BM}

An attempt was made to validate the 're-constructed' EGM2008 and interpolated ANGD2007 g_{BM} using ANGD2007 g_{obs} co-located with ANLN BM (cf. Sproule et al., 2006). Co-located ANGD2007 g_{obs} are defined as ANGD2007 g_{obs} that have been observed directly on the ANLN BMs, and can thus use the more precise levelled AHD height rather than rely on the less precise barometric height used for most ANGD2007 g_{obs}.

6.4.1 Identifying ANGD2007 g_{obs} co-located with ANLN BM

Co-located ANLN BM and ANGD2007 g_{obs} were identified using latitude and longitude ($\phi_{g_{obs}}$, $\lambda_{g_{obs}}$ for ANGD2007 g_{obs}; ϕ_{BM}, λ_{BM} for ANLN BMs) and AHD $H^{N\text{-}O}$ ($H^{N\text{-}O}_{g_{obs}}$ for ANGD2007 g_{obs}; $H^{N\text{-}O}_{BM}$ for ANLN BMs) conditions. This was necessary because BM identifiers in each database were often slightly different (e.g., ANLN BM 81/05 is ANGD2007 station 81−5; or 7917 is 79−17), making any attempts to match BMs in each file unreliable. Conditions to match ANLN BM and ANGD2007 g_{obs} were: $|\phi_{BM} - \phi_{g_{obs}}|$ and $|\lambda_{BM} - \lambda_{g_{obs}}|$ to both be <1 arc-minute and AHD $\left|H^{N\text{-}O}_{BM} - H^{N\text{-}O}_{g_{obs}}\right|$ <10 mm.

$(\phi_{BM}, \lambda_{BM})$ are accurate to ∼1 arc-minute (Roelse et al., 1971), with Murray (1997) suggesting $(\phi_{g_{obs}}, \lambda_{g_{obs}})$ are ∼0.1 arc-minute (166 m) or better (possibly too optimistic for pre-GNSS gravity surveys; cf. Wynne, 2007), justifying the relatively large horizontal search area. The small $H^{N\text{-}O}$ tolerance of 10 mm was adopted on the assumption that where ANGD2007 g_{obs} was observed on an ANLN BM, the AHD $H^{N\text{-}O}_{BM}$ was adopted.

Co-located BMs identified under these conditions numbered 9,527 (Figure 6.3), not including the numerous duplicate stations held in ANGD2007 (possibly up to 1,000). Visual checks on the co-located BM names indicate that the co-located BMs were correctly identified. However, it is possible that some co-located stations were not

identified for some reason, or some were erroneously included due to recording or typographical error in ANGD2007 (cf. Sproule et al., 2006). For instance, AHD $H_{BM}^{N\text{-}O}$ is assigned to the wrong g_{obs}. Within the 9,527 co-located points, maximum AHD $H_{BM}^{N\text{-}O}$ is 1,751.75 m, minimum 0.85 m, and mean 274.73 m, suggesting a good representation of Australian topography (cf. maximum 2,228.0 m, minimum −16.0, mean 272.5 m computed from GEODATA DEM-9S in Hirt et al., 2010b).

6.4.2 EGM2008- and ANGD2007-derived g_{BM} validation results

EGM2008 g_{BM} and co-located ANGD2007 g_{obs} will be compared, but because EGM2008 uses terrestrial gravity from ANGD (it is not known which release was used), EGM2008 g_{BM} and ANGD2007 g_{obs} are not totally independent. However, the use of GRACE gravity for the long-wavelength component of EGM2008, plus processing and reduction methods used in its development are likely to have partially reduced the correlation between EGM2008 g_{BM} and ANGD2007 g_{obs}. On the other hand, ANGD2007-derived g_{BM} are highly dependent on the 9,527 co-located g_{obs} used here in the validation. Therefore, ANGD2007 g_{BM} will be re-computed after the 9,527 co-located g_{obs} are temporarily removed from ANGD2007 (cf. Featherstone and Sproule, 2006), which will reduce the direct correlation between ANGD2007 g_{BM} and co-located ANGD g_{obs}.

	EGM2008 g_{BM} minus co-located ANGD2007 g_{obs}	ANGD2007 g_{BM} minus co-located ANGD2007 g_{obs}
Min	−41.33	−24.24
Max	56.75	14.07
Mean	1.87	0.01
STD	±4.96	±2.19
RMS	±5.30	±2.19

Table 6.1: Statistics for EGM2008 g_{BM} minus co-located ANGD2007 g_{obs}, and ANGD2007 g_{BM} minus co-located ANGD2007 g_{obs} at 9,527 BMs. Units are in mGal.

Table 6.1 presents the descriptive statistics of differences between EGM2008 g_{BM} and co-located ANGD2007 g_{obs}. The RMS of the differences indicate that the EGM2008-derived gravity is 'noisier' than ANGD2007-derived gravity, with the 'noise' in both caused by (i) errors in the original datasets (EGM2008 and ANGD2007) and (ii) the

methods used to realise g_{BM} (see Section 6.5). Figure 6.3(a) indicates that the largest EGM2008 g_{BM} minus co-located ANGD2007 g_{obs} differences are in the mountainous Australian Alpine region (∼37°S, 147°E; cf. Claessens et al., 2009). Differences >10 mGal in magnitude can also been seen in Tasmania (in mountains, ∼42°S, 147°E), along the Great Dividing Range, and along the coast in south western Western Australia (Darling Fault/Scarp, ∼33°S, 116°E). Differences of up to 10 mGal in magnitude are also noticeable in other areas of rugged topography such as the King Leopold Ranges (∼17°S, 128°E), Hammersley Range (∼22°S, 118°E), and the MacDonnell and Petermann Ranges (∼25°S, 131°E).

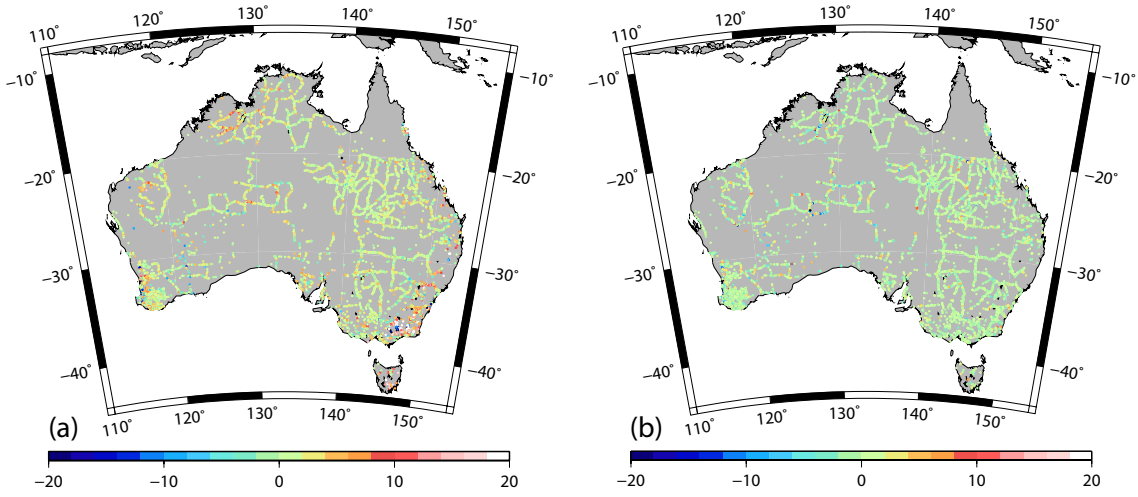

Figure 6.3: Differences between ANGD2007 g_{obs} and (a) EGM2008 g_{BM}; and (b) ANGD2007 g_{BM} at 9,527 co-located ANLN BMs. Lambert projection, units in mGal.

The mean difference of 1.87 mGal between EGM2008 g_{BM} minus co-located ANGD2007 g_{obs} indicates a bias (but statistically insignificant, 1.87±4.96 mGal), which could be caused by a combination of factors. These include long-wavelength errors (>1113 km) >10 mGal in the terrestrial gravity (Featherstone, 2003), different tidal systems, where EGM2008 is tide-free but the tidal system of ANGD2007 is unknown (if ANGD2007 is assumed mean tide, maximum error is 0.04 mGal at $\phi = 12°$S, using Ekman, 1989), differences between the ANGD2007 gravity datum (AAGD07) and the gravity datum used in EGM2008 (IGSN71; AAGD07 is 0.078 mGal less than IGSN71; Tracey et al., 2007), or the exclusion of the zero-degree term in EGM2008 (∼0.15 mGal; Lemoine et al., 1998). However, because it is the relative gravity differences between BMs that will determine the accumulated height corrections to be applied to the ANLN, these errors are unlikely to be significant here. Indeed, computing Helmert H^O from

EGM2008 g_{BM} (Chapter 7) with and without the 1.87 mGal bias showed Helmert H^O differences of $\leqslant$0.1 mm.

By comparison, the ANGD2007 g_{BM} minus co-located ANGD2007 g_{obs} is 0.01 mGal $\pm$2.19 mGal (Table 6.1(b)), which is somewhat smaller than the EGM2008 g_{BM} minus co-located ANGD2007 g_{obs} statistics. This is expected, because although the co-located g_{obs} were removed from ANGD2007 before computation of ANGD2007 g_{BM} for this validation, they are from the same data set and related to the same datum. Figure 6.3(b) indicates that large differences (>10 mGal in magnitude) are randomly scattered over the continent, rather than clustered in particular regions as for EGM2008 g_{BM} minus co-located ANGD2007 g_{obs}. Generally, the ANGD2007 g_{BM} are in good agreement to co-located ANGD2007 g_{obs}.

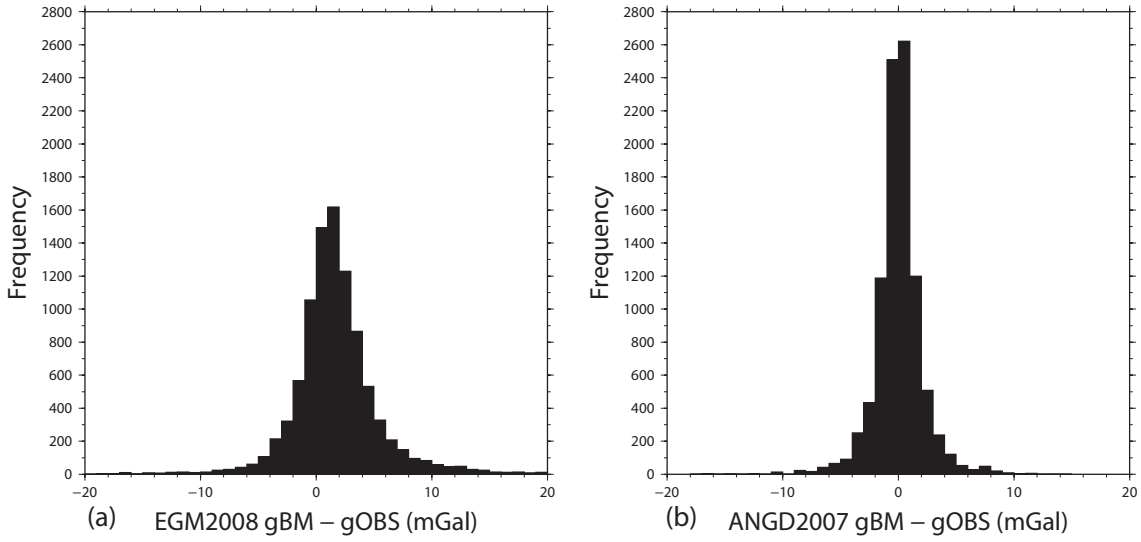

Figure 6.4: Histogram of differences at 9,527 co-located ANGD2007 g_{obs}: (a) EGM2008 g_{BM} minus ANGD2007 g_{obs}; and (b) ANGD2007 g_{BM} minus ANGD2007 g_{obs}. Kurtosis for (a) is 18.92; (b) is 11.27. Units are in mGal.

EGM2008 g_{BM} minus co-located ANGD2007 g_{obs} differences (Figure 6.4(a)) and ANGD 2007 g_{BM} minus co-located ANGD2007 g_{obs} (Figure 6.4(b)) are normally distributed, but with high kurtosis. There appear to be only a handful of outliers for EGM2008 g_{BM} minus co-located ANGD2007 g_{obs} that are >12.79 mGal (99% confidence; STD scaled by 2.58; Table. 6.1(a)) although maybe more for ANGD2007 g_{BM} minus co-located ANGD2007 g_{obs} >5.65 mGal (99% confidence; Table. 6.1(b)). Although ANGD2007 g_{BM} are a better fit with co-located ANGD2007 g_{obs} (as expected), it is difficult to

determine which g_{BM} is the best representation of the Australian gravity field (cf. Featherstone and Kirby, 2000; Featherstone, 2005; Claessens et al., 2009). Possible causes for errors in the ANGD2007 and EGM2008 g_{BM} are investigated in Section 6.5.

6.5 Error sources in EGM2008- and ANGD2007-derived g_{BM}

Section 6.4 presents differences between ANGD2007 g_{obs} taken directly on ANLN BMs (co-located), and (i) EGM2008-derived g_{BM} and (ii) ANGD2007-derived g_{BM}. Because co-located ANGD2007 g_{obs} are observed directly at the ANLN BM, and can use the more precise levelled AHD height rather than the less precise barometric height, it is assumed that the only error in co-located ANGD2007 g_{obs} relates to the precision of the gravity measurement itself (maximum of 0.5 mGal for ties between helicopter surveys (Fraser et al., 1976); less for more recent surveys (Murray, 1997)), so that co-located ANGD2007 g_{obs} is considered here (for validation purposes) to be an 'errorless' set of control data. Thus differences in EGM2008 g_{BM} or ANGD2007 g_{BM} to these control data are interpreted as errors.

g_{BM} errors can result from the original data, or the methods used to compute g_{BM} from these original data sets. ANGD2007 error sources are discussed in Section 6.1.3, but possible errors in EGM2008 are more difficult to determine because they comprise the errors in the original gravity data plus the processing methods used, which is made more difficult by the relative lack of published literature from the EGM2008 developers.

Evaluations and comparisons for EGM2008 over Australia by Claessens et al. (2009) and Featherstone et al. (2011) provide a guide for possible EGM2008 uncertainties in this region. Thus, this Section deals primarily with g_{BM} errors resulting from the interpolation/computation methods used to derive g_{BM} from EGM2008 and ANGD2007 (Sections 6.2 and 6.3), and whether these errors have a significant impact on the gravimetric HCs computed in Chapter 7 from g_{BM} (see Section 7.5 and Section 7.7). No geoid computations have been performed during the research for this thesis.

6.5.1 Effect of inconsistent geodetic datums on EGM2008 g_{BM}

ANLN Ω_{BM} are assumed to be on the non-geocentric Australian Geodetic Datum 1966 (AGD66; G. Holloway 2009, pers. comm.), but Australia's current geodetic datum is the Geocentric Datum of Australia 1994 (GDA94) (Section 2.3.2). However, EGM2008 is geocentric, causing a difference between EGM2008 positions and ANLN (ϕ_{BM}, λ_{BM}) of ∼190 m in a north-easterly direction (e.g., Featherstone, 1995). Here, possible errors in EGM2008 δg and ζ resulting from using ANLN AGD66 Ω_{BM}, rather than GDA94 Ω_{BM} will be quantified.

Grid transformation software GDAit (Dept of Geomatics, University of Melbourne; http://www.geom.unimelb.edu.au/gda94/) was used to transform all 87,591 ANLN Ω_{BM} from AGD66 Ω_{BM} to GDA94 Ω_{BM}. EGM2008 δg and ζ were computed at AGD66 Ω_{BM} and compared to GDA94 Ω_{BM} EGM2008 δg and ζ computed for the same BM (cf. Featherstone, 1995). The maximum difference between AGD66 Ω_{BM} and GDA94 Ω_{BM} δg ($\Delta\delta g$) was +2.07 mGal, minimum −2.33 mGal, mean −0.00(2) mGal, with STD and RMS both ±0.24 mGal (Figure 6.5(a)).

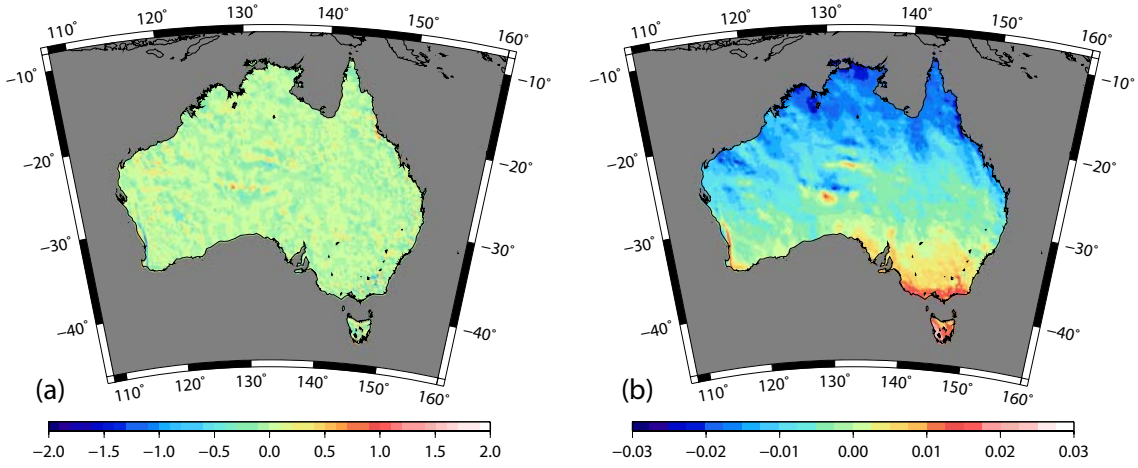

Figure 6.5: Differences between AGD66 and GDA94 Ω_{BM} computed (a) EGM2008 δg (mGal) and; (b) EGM2008 ζ (m).

Differences for EGM2008 ζ computed at AGD66 Ω_{BM} and GDA94 Ω_{BM} were <30 mm in magnitude (Figure 6.5(b)), which will propagate directly into h_D and therefore EGM2008-derived g_{BM}. However, considering that h_D contains errors of up to ∼±0.5 m due to the north-south slope and other distortions in the AHD (see Section 1.2), the

likely errors caused by the ANLN (ϕ_{BM}, λ_{BM}) and EGM2008 (ϕ, λ) being on different geodetic datums are insignificant.

6.5.2 Effect of using 2D rather than 3D Bouguer field for ANGD2007 g_{BM}

There are certain assumptions made in Δg_{SPB} that could cause errors in ANGD2007-derived g_{BM}. The use of δg_{BP} (in Δg_{SPB}) in place of δg_{TOP} (in Δg_B; Equation (6.16)) simplifies computation, but is a crude approximation of the actual gravitational attraction of the topographic masses. The planar terrain correction (δ_{PTC}) approximates the terrain residual to the BP (infinite plate of constant thickness determined by the H^O of g_{BM}) and can be added to the Δg_{SPB} to form the complete planar Bouguer anomaly (Δg_{CPB}) (Kuhn et al., 2009).

By comparison, the spherical Bouguer shell (SB; with gravitational attraction δg_{SB}) is also of constant thickness, but with the gravitational attraction much larger than the δg_{BP} and is given as (cf. Kuhn et al., 2009)

$$\delta g_{SB} = 4\pi G\rho H^{N\text{-}O} \tag{6.22}$$

The spherical terrain correction (δg_{STC}) is applied to δg_{SB} to account for terrain residual to the spherical shell, which to balance the much larger δg_{SB} is much larger than the δ_{PTC}. The application of the δg_{STC} to δg_{SB} results in the complete spherical Bouguer anomaly (Δg_{CSB}).

The Δg_{SPB} is considered a 2D or 'surface' anomaly rather than a 3D or 'solid' anomaly (Vaníček et al., 2004). 2D Δg_{SPB} provide a smooth surface for gridding (e.g., Hackney and Featherstone, 2003), which is an advantage here, given the 1 arc-minute uncertainty in Ω_{BM}, but omission of the high frequency signal from terrain residual to the BP (i.e. not applying the δ_{PTC}) can result in spatial aliasing where g_{obs} sampling is inadequate. However, Goos et al. (2003) found the effect of not applying the δ_{PTC} to Δg_{SPB} to be insignificant in Australia (cf. Zhang and Featherstone, 2004). In addition, Kuhn et al. (2009) shows maximum δ_{PTC} (for 1,095,065 Australian land g_{obs} of ANGD2007) computed at $\phi_{g_{obs}}$ and $\lambda_{g_{obs}}$ ($\Omega_{g_{obs}}$) to be 30 mGal (cf. Kirby and Featherstone, 1999;

Featherstone and Kirby, 2002), but with a mean of only 0.2 mGal (92% of δ_{PTC} are <0.5 mGal). Thus δ_{PTC} across most of Australia are generally assumed to be insignificant (<ANGD2007 g_{BM} minus co-located ANGD2007 g_{obs} RMS of ±2.19 mGal; see Table 6.1) for g_{BM} used for gravimetric HC (cf. Sections 7.5 and 7.7).

It is acknowledged that, despite the additional complexity involved in the computation (cf. Forsberg and Tscherning, 1981), Δg_{CSB} should be used for computing ANGD2007 g_{BM} as a reasonable approximation of a 3D, or 'solid' Δg_B (cf. Vaníček et al., 2004; Reilly, 1972). However, given the uncertainty of Ω_{BM} and $\Omega_{g_{obs}}$ (up to ∼1.8 km), and the small magnitude of δ_{PTC} in Australia (Kuhn et al., 2009) it is questionable whether the use of complete Δg_{BS} would be of benefit. For instance, in mountainous regions such as the Australian Alps, computing δ_{PTC} at $\Omega_{g_{BM}}$ which may be 1 km distant from the true location of g_{BM} could introduce additional errors. In addition, under the method used here, the δ_{PTC} would be subtracted from the Δg_{SPB} as g_{obs} is reduced to the geoid (at $\Omega_{g_{obs}}$), then added to Δg_{SPB} as it is restored to the terrain surface (after interpolation to Ω_{BM}) to realise g_{BM}. Thus, the error from not applying δ_{PTC} is the difference between the δ_{PTC} at $\Omega_{g_{obs}}$ and Ω_{BM} and will generally be less than the maximum δ_{PTC} in Australia of 30 mGal.

6.5.3 Effect of errors in observed gravity station heights

Errors in barometrically observed heights (H_b) at gravity stations are estimated to be within ±5 m within each helicopter survey, but this can increase to ±10 m for ties between each survey (Fraser et al., 1976; Barlow, 1977), although Bellamy and Lodwick (1968) suggest that this may be occasionally exceeded in mountainous terrain. Height errors of ±5 m and ±10 m can result in Δg_{SPB} errors of ∼±1 mGal and ∼±2 mGal respectively (Fraser et al., 1976).

The effect of H_b errors on ANGD2007 g_{BM} are determined by their effect on the Δg_{SPB} used to grid the gravity data (Section 6.3). Barlow (1977) suggests that Δg_{SPB} errors resulting from H_b errors are likely to be between 1.5 and 2.5 mGal, including interpolation errors, although this is dependent on grid spacings and terrain (cf. Bellamy and

Lodwick, 1968). However, Figure 6.3(b) does not indicate larger ANGD2007 g_{BM} differences to be clustered in the mountainous south east like for EGM2008 g_{BM} in Figure 6.3(a). In addition, ANGD2007 has been significantly densified in the last couple of decades with gravity surveys using digital barometers and GNSS positioning (Murray, 1997), which both reduce error in gravity station height. Although these denser grids (appearing in Figure 6.1 as darker areas) only cover specified regions, it is likely that they have diluted the effect of H_b errors in Δg_{SPB}, but this is not possible to quantify.

The RMS of ANGD2007 g_{BM} minus co-located ANGD2007 g_{obs} is $\pm$2.19 mGal, which is a similar magnitude to Δg_{SPB} errors caused by H_b. This suggests that H_b are not the cause of the larger ANGD2007 g_{BM} minus co-located ANGD2007 g_{obs}, where the largest difference of -24.24 mGal would require a $\sim$123 m height error (using 0.1967 m^{-1}; Heiskanen and Moritz, 1967, 131), which is far larger than any error attributable to H_b. Thus, although H_b errors certainly contribute to the noisy nature of the differences, they are unlikely to be the cause of errors >3 mGal, a number of which can be seen in Figure 6.3(b) (but not clustered in mountainous regions). A g_{BM} error of 3 mGal will result in a maximum error of $\sim$10 mm in the orthometric or normal correction in rugged terrain at high elevations (Figures 7.4 and 7.5), but will be much less for most of Australia, and is thus considered insignificant in terms of the resultant H^O or H^N (see Chapter 7). It is more likely that some of these larger ANGD2007 g_{BM} minus co-located ANGD2007 g_{obs} differences are blunders, or interpolation errors in rugged terrain caused by (i) ANLN Ω_{BM} positional error (cf. Section 6.5.6), or (ii) the removal of the 9,527 co-located g_{obs} from ANGD2007 during the validation process.

The effect of H_b errors on EGM2008 g_{BM} is less direct, but more problematic. Because there is relatively limited information about the methods used in EGM2008 over Australia, it is difficult to postulate as to how H_b errors could have propagated into the EGM2008 coefficients. There are many sources of error that may cause errors in the EGM2008 coefficients that will then propagate into EGM2008 δg, and thus into EGM2008-derived g_{BM} (Section 6.2). Kearsley (1986) suggests that a $\pm$3 mGal error in the mean global Δg_F for a 11 km by 11 km grid (Pavlis et al., 2008, suggest an error of 1-2 mGal in Δg_F over Australia) causes a $\pm$50 mm geoid error on level terrain. A 50

mm error in geoid height is equivalent to 0.015 mGal in free-air, which suggests that H_b errors are insignificant for EGM2008 g_{BM} (RMS ±5.30 mGal; Table 6.1). Although this error may increase in mountainous areas, it is unlikely to become significant when propagated into gravimetric HC, and does not appear to be likely to be the sole cause of the >10 mGal differences between EGM2008 g_{BM} and co-located ANGD2007 g_{obs} (Figure 6.3(a)).

6.5.4 Correlation among EGM2008 g_{BM}, co-located ANGD2007 g_{obs}, height and BM positional error

The influence of height on differences between 9,527 EGM2008 g_{BM} minus co-located ANGD2007 g_{obs} can be seen in Figure 6.6(a) where differences between EGM2008 g_{BM} and co-located ANGD2007 g_{obs} (mGal) are shown as a function of height (m). Up to about 900 m in elevation there does not appear to be a noticeable trend, although there is a cluster of positive differences (EGM2008 g_{BM} larger than co-located ANGD2007 g_{obs}) in the 150−600 m height range. The cause of this effect is not clear, although uncertainty in BM position in regions of rugged topography (Section 6.5.6) and omission error in the EGM2008 g_{BM} (Section 6.5.5) are both likely to contribute significantly to these differences.

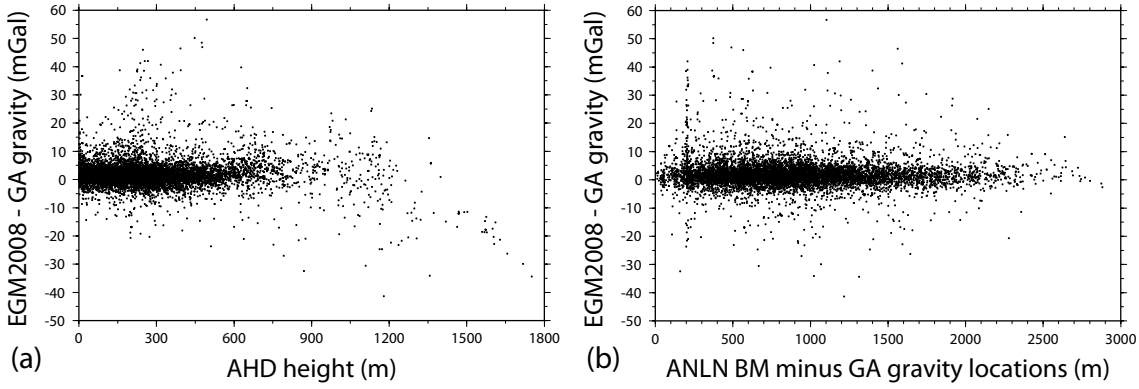

Figure 6.6: Differences between EGM2008 g_{BM} and co-located ANGD2007 g_{obs} as a function of (a) height; and (b) calculated distance between Ω_{BM} and $\Omega_{g_{obs}}$.

Figure 6.6(b) shows differences between EGM2008 g_{BM} and co-located ANGD2007 g_{obs} as a function of calculated distance between Ω_{BM} and $\Omega_{g_{obs}}$. Correlation of large EGM2008 g_{BM} minus co-located ANGD2007 g_{obs} differences with large $\Omega_{BM}-\Omega_{g_{obs}}$

distance would indicate that Ω_{BM} (and $\Omega_{g_{obs}}$) uncertainty makes a large contribution to the differences. However, Figure 6.6(b) does not indicate any such association; EGM2008 g_{BM} minus co-located ANGD2007 g_{obs} differences do not appear to increase as the distance between $\Omega_{BM}-\Omega_{g_{obs}}$ increases.

A possible explanation may be that Ω_{BM} and $\Omega_{g_{obs}}$ are equally poor. For example, the calculated distance between Ω_{BM} and $\Omega_{g_{obs}}$ may be relatively small (e.g., 200 m), but both Ω_{BM} and $\Omega_{g_{obs}}$ could actually be 1−2 km from their true position. If this is the case, the quoted $\Omega_{g_{obs}}$ error in ANGD2007 (rarely >500 m; cf. Murray, 1997) may be overly optimistic. Alternatively, the EGM2008 omission error signal may contribute more to the Ω_{BM} and $\Omega_{g_{obs}}$ differences than the effects of Ω_{BM} positional error.

6.5.5 Effects of omission error on EGM2008-derived g_{BM}

Signal omission error (e.g., Torge, 2001, 273) may contribute to the difference between EGM2008 g_{BM} and co-located terrestrial ANGD2007 g_{obs}. Terrestrial g_{obs} contain all gravity field information (including the high frequency signal), but the spatial resolution of EGM2008 is 5 arc-minutes (∼9 km), resulting in the omission of high frequency gravity signals <5 arc-minutes (e.g., Hirt et al., 2010c). Rugged terrain like the Australian Alps (elevations up to 2,228 m), are particularly susceptible to omission error (cf. Figures 6.3 and 6.7; Claessens et al., 2009).

An estimate of omission error can be computed using the residual terrain model (RTM) technique (Forsberg and Tscherning, 1981; Forsberg, 1984, 1985). A subset of 239 ANLN BMs co-located with ANGD2007 g_{obs} in the Australian Alps (cf. Figures 6.8 and 6.7) was used to test the effect of omission error on EGM2008 g_{BM} by comparison to co-located terrestrial ANGD2007 g_{obs} in this region. Note that the RTM technique does not provide the complete omission error, due to the assumption of a linear relationship between topography and gravitational potential (e.g., Hirt et al., 2010a), uncertainty in the digital elevation model (DEM), and the neglect of local topographic mass-density variation (constant density of 2670 kg m^{-3} used; e.g., Hirt et al., 2010c). Omission error estimates at BMs in the Australian Alps subset shown here were computed from

the RTM by Hirt (2009, pers. comm.), using the data and methods described in Hirt (2010), Hirt et al. (2010c) and Hirt et al. (2010a).

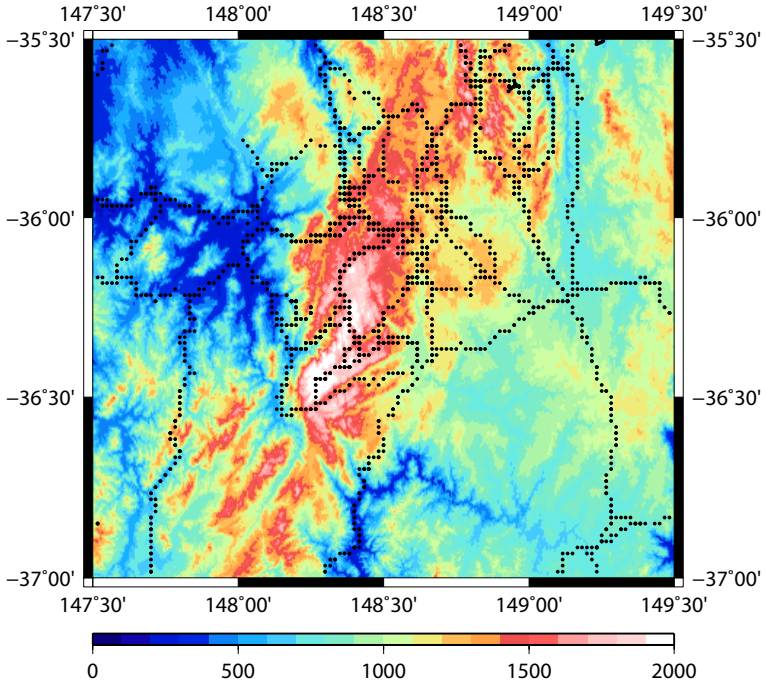

Figure 6.7: SRTM heights (m) in the Australian Alpine subset, and ANLN BMs (black dots), demonstrating the rugged terrain and the levelling section routes.

The magnitude of the RTM-estimated omission error was subtracted from EGM2008 δg_{BM} (thus becoming an approximate 'correction'; referred to as EGM2008+RTM δg_{BM}). EGM2008+RTM δg_{BM}, was then used to re-compute EGM2008 g_{BM} (referred to as EGM2008+RTM g_{BM}), as per Section 6.2. Differences between EGM2008+RTM g_{BM} minus co-located ANGD2007 g_{obs} differences and EGM2008 g_{BM} minus co-located ANGD2007 g_{obs} differences are shown in Table 6.2.

Stat	EGM2008 g_{BM}	EGM2008+RTM g_{BM}
Min	−16.73	−23.78
Max	46.00	28.13
Mean	5.67	2.27
STD	±9.66	±5.20
RMS	±11.20	±5.67

Table 6.2: Descriptive statistics for EGM2008 g_{BM} (no RTM) minus co-located ANGD2007 g_{obs}, and EGM2008+RTM g_{BM} minus co-located ANGD2007 g_{obs}. Differences are at 239 BMs in the Australian Alps. Units in mGal.

Decreases in the mean, STD and RMS for EGM2008+RTM g_{BM} minus co-located ANGD2007 g_{obs} by a factor of ∼2 (compared to EGM2008 g_{BM} (no RTM) minus co-located ANGD2007 g_{obs}) indicates a significant improvement (cf. Hirt et al., 2010a). The maximum difference also decreases by ∼18 mGal, but the minimum is worse by ∼7 mGal, although the maximum and minimum are now more symmetrical about the mean. This test indicates that as much as 50% the large EGM2008 g_{BM} minus co-located ANGD2007 g_{obs} differences identified in the Australian Alps (Figure 6.3; cf. Claessens et al., 2009) may be caused by omission error in EGM2008.

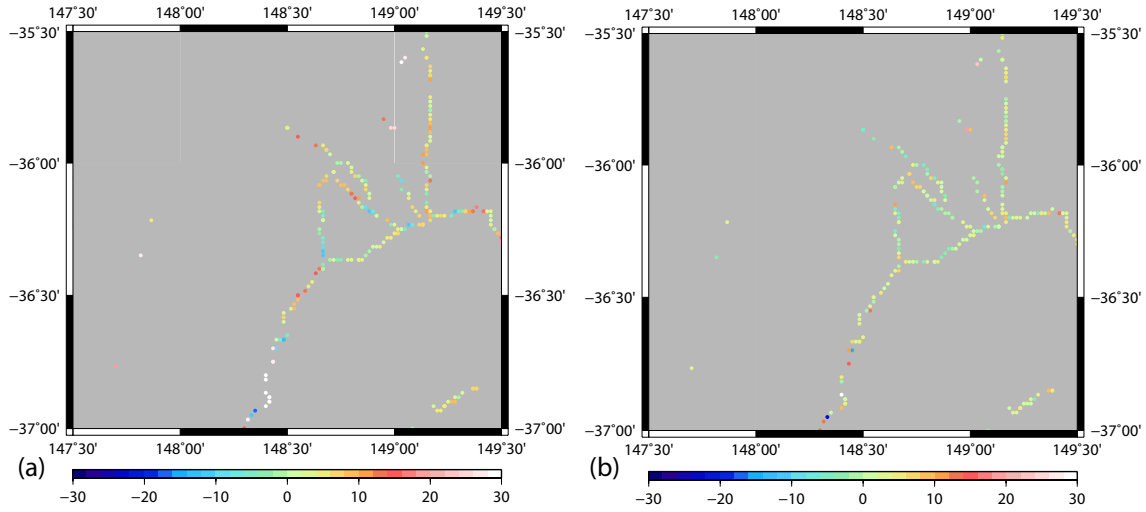

Figure 6.8: Differences for (a) EGM2008 g_{BM} (no RTM) minus co-located ANGD2007 g_{obs}, and (b) EGM2008+RTM g_{BM} minus co-located ANGD2007 g_{obs}. Differences are at 239 BMs in the Australian Alps (minimum $H_{BM}^{N\text{-}O}$ 218.66 m, maximum $H_{BM}^{N\text{-}O}$ 1,399.08 m, and average $H_{BM}^{N\text{-}O}$ 907.74 m. Mercator projection, units in mGal.

6.5.6 Effects of Ω_{BM} positional uncertainty on EGM2008 g_{BM} in the Australian Alps

Uncertainty in Ω_{BM} of 1 arc-minute (∼1.8 km) can result in EGM2008 g_{BM} being computed at a different location to g_{obs} (also subject to $\Omega_{g_{obs}}$ uncertainty). A simulation of the effects of ±1 arc-minute errors in ANLN ϕ_{BM} ($\delta\phi_{BM}$) and λ_{BM} ($\delta\lambda_{BM}$) on EGM2008 δg_{BM} is conducted here to quantify the possible errors. A subset of 2,453 ANLN BMs in the Australian Alps was used as a test area (Figure 6.7) where maximum errors are likely to occur in the rugged terrain. The method used in Section 5.4.2 to simulate the effects of positional errors is used here, where EGM2008 δg (using **harmonic_synth.f**) is computed 1 arc-minute from Ω_{BM} in NE, SE, SW, and NW

directions from each ANLN BM in the test area. The difference between δg_{BM} (at ANLN Ω_{BM}) and EGM2008 δg 1 arc-minute away ($\Delta\delta g$; Table 6.3) is the possible error.

The distribution of $\Delta\delta g$ for each direction is not well represented by a normal curve, so STD is not shown in Table 6.3. Instead, the mode is shown to represent the most probable value in an asymmetrical distribution. The largest mean $\Delta\delta g$ (of the four directions) is 1.33 mGal, and the minimum −1.22 mGal, with the largest mode 5.24 mGal and minimum −6.67 mGal. However, Figure 6.9 shows the distribution of all 9,812 $\Delta\delta g$ ($\Delta\delta g$ for each direction combined into one histogram) to reasonably represent a normal curve, although slightly peaked (kurtosis 1.41). The mean for all 9,812 $\Delta\delta g$ is 0.15 mGal, STD and RMS both ±6.65 mGal, maximum +31.76 mGal, and the minimum −27.09 mGal.

Stat	NE	SE	SW	NW
Mean	0.52	1.33	−0.05	−1.22
Mode	−4.93	−1.37	5.24	−6.67
Max	28.89	31.76	15.36	17.62
Min	−14.62	−18.40	−27.09	−24.04

Table 6.3: Statistics for simulated errors in EGM2008 δg ($\Delta\delta g$; in NE, SE, SW and NW directions) resulting from ANLN ϕ_{BM} and λ_{BM} positional uncertainty (±1 arc-minute) in the Australian Alps. Mode is shown here rather than STD because the distribution for each direction is not Gaussian. Units are in mGal.

Maximum differences are compared to provide an estimate of the percentage of maximum/minimum differences between EGM2008 g_{BM} and co-located ANGD2007 g_{obs} can be attributed to ANLN Ω_{BM} uncertainty. A comparison of Table 6.1 with Table 6.3 shows that the maximum $\Delta\delta g$ is ∼56% of the largest difference between EGM2008 g_{BM} and co-located ANGD2007 g_{obs} (+56.75 mGal; Table 6.1), while the minimum $\Delta\delta g$ is ∼66% of the difference between EGM2008 g_{BM} and co-located ANGD2007 g_{obs} (−41.33 mGal; Table 6.1). This suggests that ∼50% of the EGM2008 g_{BM} minus co-located ANGD2007 g_{obs} differences identified in Section 6.4.2 (particularly in mountainous regions; see Figure 6.3) could be attributable to uncertainty in ANLN Ω_{BM} (and possibly $\Omega_{g_{obs}}$; cf. Figure 6.6).

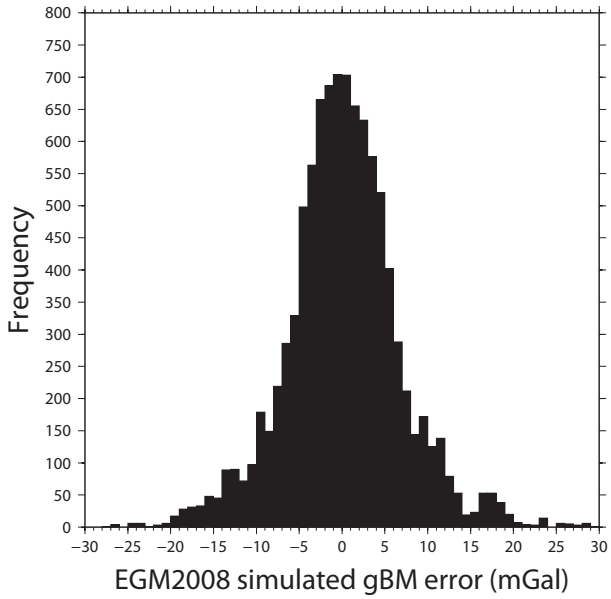

Figure 6.9: Histogram of $\Delta\delta g$ using 9,812 combined differences (NE, SE, SW, NW) in the Australian Alps. Units are in mGals.

6.5.7 Effects of Ω_{BM} positional uncertainty on γ

The effect of $\delta\phi_{BM}$ (± 1 arc-minute) on γ computed on the GRS80 ellipsoid is investigated, as an error in γ will propagate into EGM2008 g_{BM} through γ_{BM} (Equation (6.5)). Heck (1990) and Featherstone (1995) both investigated the effect of a datum transformation ($\sim$190 m northeast; or $\sim$135 m in latitude) between AGD66 and WGS84 on γ, which propagated into Δg_F (cf. Section 6.5.1). Heck (1990) estimated a constant error in Δg_F (caused by AGD66$-$WGS84 difference on γ) of -0.01 mGal across Australia, while Featherstone (1995) computed the difference across the continent, finding Δg_F errors between -0.05 and -0.14 mGal, mostly in the north-south direction, but also containing a long-wavelength longitudinal component.

Although it is expected that the effect of the γ error on EGM2008 g_{BM} will be small compared to those quantified in Section 6.5.5 and Section 6.5.6 in the Australian Alps, an estimate of this error is warranted for completeness. A crude estimate of γ error due to a 1 arc-minute error in $\delta\phi_{BM}$ of -1.29 mGal can be made by simply extrapolating the -0.01 mGal error of Heck (1990), estimated for a 135 m horizontal datum shift (north-south component), over 1,800 m ($\sim$1 arc-minute of latitude). Applying the same criteria to the estimates of Featherstone (1995), a maximum of -0.65 mGal and

minimum of −1.83 mGal can be obtained (cf. Mitchell, 1973a). For comparison, γ is re-computed using simulated ±1 arc-minute errors in ϕ_{BM} for the 87,951 ANLN BMs.

The possible error in GRS80 γ was found in the simulation to be 0.55−1.51 mGal where $\delta\phi_{BM} = +1$ arc-minute (increasing southward). Mean GRS80 γ error is 1.25 mGal (using $\delta\phi_{BM} = -1$ arc-minute gave the same magnitude, but decreasing southward). The mean GRS80 γ error for +1 arc-minute error in $\delta\phi_{BM}$ from this simulation is of comparable magnitude to the crude estimate calculated from Heck (1990) (−1.29 mGal). The minimum and maximum from the simulation (0.55−1.51 mGal) can be compared to 0.65−1.83 mGal calculated by Featherstone (1995). These results indicate that the effect of ±1 arc-minute uncertainty in ϕ_{BM} on GRS80 γ will be <2 mGal which is insignificant for EGM2008 g_{BM} (RMS ±5.30 mGal; see Table 6.1).

6.5.8 Discussion

It is not clear at this time whether EGM2008- or ANGD2007-implied g_{BM} is superior. A combination of error sources could affect the differences between ANGD2007 g_{BM} (e.g., poor g_{obs} sampling in rugged terrain; long-wavelength errors; ANGD2007 $\Omega_{g_{obs}}$ and ANLN Ω_{BM} uncertainties; ANLN $H^{N\text{-}O}$ at g_{BM} and H_b errors at g_{obs}) and EGM2008 g_{BM} (e.g., commission and omission errors; ANLN Ω_{BM} errors, plus a range of data, reduction and processing approximations in EGM2008). Other factors such as inconsistent tidal systems, gravity and geodetic datums and the variable bias in the AHD could also contribute. However, most of these errors appear to be insignificant over most of Australia, because Figures 7.5 and 7.7 indicate that a 5 mGal error at g_{BM} (EGM2008 g_{BM} minus co-located ANGD2007 g_{obs} RMS is ∼±5 mGal) will propagate into H^O and H^N at about 15 mm in rugged terrain at elevations of 2000 m. For most of Australia at lower elevations and in benign terrain, the H^O and H^N error will be much less than 15 mm from a 5 mGal Δg error.

However, the cluster of EGM2008 g_{BM} errors in the Australian Alps (Figure 6.3(a); cf. Claessens et al., 2009) is of some concern. These differences are likely to be caused primarily by EGM2008 omission error (Section 6.5.5) and ANLN Ω_{BM} uncertainties in-

troducing errors into δg_{BM} (Section 6.5.7), although unknown reduction and processing approximations in EGM2008 are also likely to contribute. This cluster of differences in the Australian Alps is not apparent for ANGD2007 g_{BM} (Figure 6.3(b)), suggesting that the quality of the terrestrial data used in EGM2008 does not cause the large errors (10−56 mGal) in EGM2008 g_{BM}, although the terrestrial data used by EGM2008 is likely to contribute to the 'noise' level at the 1-2 mGal level, with H_b uncertainties at g_{obs} assumed to be the main contributor.

Improvement in the accuracy of ANLN Ω_{BM} (by GNSS field observation accurate to ∼1 m in ϕ, λ and H; the latter requiring gravimetric ζ) is required to improve the accuracy and rigour of both methods of computing g_{BM}. Correctly listed uncertainties for g_{obs} (e.g., the effect of H_b) in the ANGD (cf. Claessens et al., 2009) could allow weighting of the data to reduce the effect of H_b errors in earlier surveys. In addition, denser gravity surveys (cf. Angus-Leppan, 1982) in Australian regions with high elevations and rugged terrain are required, preferably observed directly at ANLN BMs. High density terrestrial gravity surveys will provide the best g_{BM} if normal or orthometric corrections are to be used for any new levelling-based AVD.

6.6 Summary

It has been demonstrated that gravity values can be 're-constructed' from EGM2008 δg. Validation with 9,527 co-located ANGD2007 g_{obs} indicates that differences of between 56.75 mGal and −41.33 mGal exist at some co-located ANGD2007 g_{obs}, with the mean difference 1.87±4.96 mGal (although using RTM reduces the RMS by ∼50% in the Australian Alps). The larger differences appear in rugged mountainous terrain and are caused by a combination of EGM2008 omission error and ANLN Ω_{BM} positional uncertainty (appear to account for all of the error, ∼50% each) propagating into EGM2008 δg, GRS80 γ, and subsequently into EGM2008 g_{BM}. However, gross errors in ANGD2007 ($H^{N\text{-}O}$ or g_{obs}) are possible.

ANGD2007-derived g_{BM} are computed by reducing g_{obs} to a grid of Δg_{SPB}, then interpolating to ANLN Ω_{BM}. ANGD2007 g_{BM} show better agreement with co-located ANGD2007 g_{obs} (0.01±2.19 mGal) than EGM2008 g_{BM}, but this is expected as they are from the same data set (co-located ANGD2007 g_{obs} removed from ANGD2007 g_{BM} computation for validation). Numerous errors sources are likely to affect both EGM2008 g_{BM} and ANGD2007 g_{BM}, although they generally appear to be at, or below the 'noise' level for each, which is interpreted as being approximately the RMS of differences between co-located ANGD2007 g_{obs} and each of EGM2008- and ANGD2007-derived g_{BM}. EGM2008 g_{BM} and ANGD2007 g_{BM} will be used in gravimetric HCs in Chapter 7, which may provide an indication as to the 'superior' gravity source.

7. HEIGHT SYSTEMS AND THEIR EFFECTS ON THE ANLN

A height system is defined by its zero-reference and the measurement path between the zero-reference and the point P, on the topographic surface (Figure 7.1). This Chapter describes the different height systems available, assesses their susceptibility to input data errors, and then applies height corrections (HCs) to the Australian National Levelling Network (ANLN) for three commonly used height systems (Helmert orthometric, normal and normal-orthometric) to evaluate how they will affect any new levelling-based Australian vertical datum (AVD).

7.1 Background

7.1.1 Ellipsoidal heights

GNSS has made heights above the ellipsoid surface (Q_0 in Figure 7.1) readily obtainable. Ellipsoidal heights (h) are conceptually simple to deal with as they are the linear distance between Q_0 on the well defined surface of a particular ellipsoid and P (see Figure 7.1). This straight line $Q_0{-}P$ is always normal to the ellipsoid surface and thus referred to as the ellipsoidal normal. Although reference ellipsoids can generate their own gravity field if given GM (e.g., GRS80; Moritz, 1980) (also see Table 7.3), h are not dependent on gravity (Featherstone and Kuhn, 2006). However, they can be transformed to orthometric or normal heights via geoid or quasigeoid models, respectively (see Figure 7.1). h is dependent on the reference ellipsoid being used. Many different reference ellipsoids have their own defined location, orientation, size and shape and can be classified as local or global depending on the position of their origin (e.g., Featherstone and Kuhn, 2006). GNSS provides derived ellipsoidal heights on a global geocentric ellipsoid.

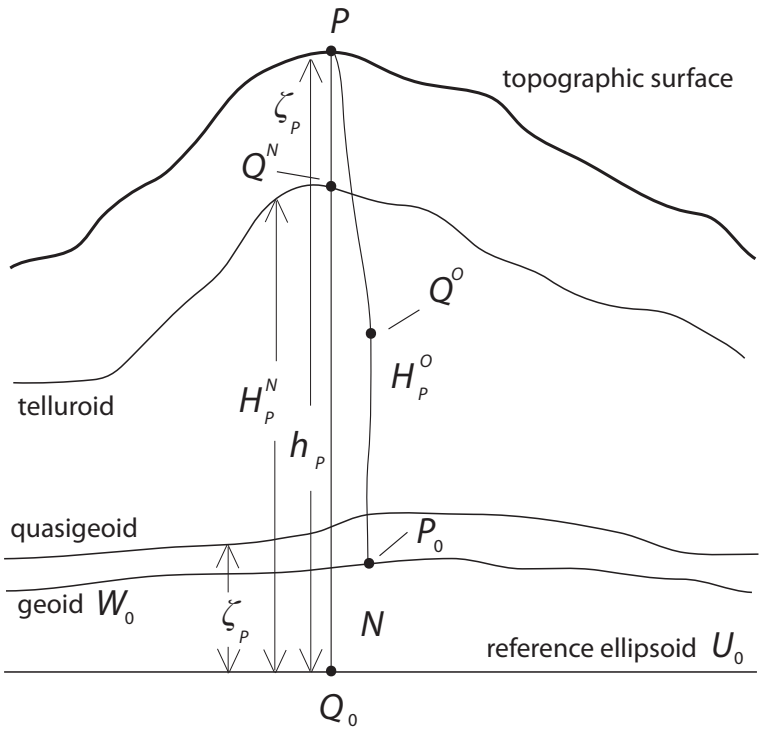

Figure 7.1: The orthometric height of P (H_P^O) is the distance along the (curved and torsioned) plumbline P–P_0. The normal height of P (H_P^N) is the distance along the curved (not straight as drawn for convenience) normal plumbline Q^N–Q_0. The ellipsoidal height of P (h_P) is the length of the straight ellipsoid normal between P and the reference ellipsoid Q_0. The geoid-ellipsoid separation N allows H_P^O and h_P to be related, while the height anomaly ζ_P relates H_P^N and h_P. The point Q^N is on the telluroid ($W_P = U_{Q^N}$) and Q^O is the approximate midpoint along the plumbline P-P_0.

7.1.2 Physical heights

Physical height systems are based on geopotential numbers (C; defined in Section 6.1.1), which correctly define unrestricted fluid flow. However, C has units of $\mathrm{m^2 s^{-2}}$, which diminishes their practical use. A gravity-related height (in metres) can be realised by dividing C by some gravity value, which has units of $\mathrm{ms^{-2}}$. The only height system that guarantees the flow of fluid from a greater to a lower height and has units of length are dynamic heights (Heiskanen and Moritz, 1967, 163)

$$H^D = \frac{C}{\gamma_0} \tag{7.1}$$

where γ_0 is an arbitrary scaling factor, usually normal gravity at 45° latitude (e.g., Heiskanen and Moritz, 1967; Jekeli, 2000), but this is examined in Section 7.9.1. Despite having units of metres, H^D have no geometric meaning and is merely the potential relative to the geoid in distance units (Jekeli, 2000). For this reason H^D is of limited

practical use, although they have relevance for scientific purposes such as monitoring lake levels or other physical phenomenon (e.g., International Great Lakes Datum 1985; Zilkoski et al., 1992).

H^D can be realised by applying dynamic corrections (DCs) to levelled height differences along the levelling line (Heiskanen and Moritz, 1967, 163)

$$DC_{1\text{-}2} = \sum_{1}^{2} \frac{\bar{g}_s - \gamma_0}{\gamma_0} \Delta n \tag{7.2}$$

where $\bar{g}_s$ is mean gravity on the topographic surface (usually the mean value of gravity between BM1 (g_1) and BM2 (g_2)), and Δn is the levelled (geometric) height difference between BM1 and BM2. Due to the limited practical use of H^D, they will not be considered further.

Two other commonly used physical heights exist: orthometric heights (H^O) and normal heights (H^N). H^O (Section 7.4) are often considered natural heights above the geoid (Heiskanen and Moritz, 1967). However, H^O requires surface gravity in their realisation (Equations (7.25) and (7.26)), and could therefore not be implemented for the AHD, as there was insufficient gravity data available at that time (cf. Section 7.1.3; Mitchell, 1973a). In addition, a 'true' H^O cannot be practically realised (cf. Dennis and Featherstone, 2003), without knowledge of the variable behaviour of gravity along the plumbline within the topography (cf. Figure 7.1; Strange, 1982). For this reason, numerous versions of H^O have been developed, each with different methods of approximating the integral mean of gravity along the plumbline ($\bar{g}$) (Section 7.4).

To avoid the assumptions made in H^O, Molodensky (Molodensky et al. 1962, loc. cit.) introduced the concept of H^N (Heiskanen and Moritz, 1967, 291; also see Section 7.6). H^N use the integral mean of normal gravity along the normal plumbline ($\bar{\gamma}$) instead of an approximated $\bar{g}$ (Heiskanen and Moritz, 1967, 171). However, surface gravity is still required for H^N (in addition to $\bar{\gamma}$; Equations (7.38) and (7.39)), so could not be used in the AHD due to the lack of gravity data in 1971. H^N refers to the quasigeoid (Figure 7.1), which is not an equipotential surface so has lesser physical meaning than H^O.

7.1.3 The AHD and normal-orthometric heights

Height systems using only normal gravity are referred to as normal-orthometric heights ($H^{N\text{-}O}$; Bomford, 1971, 230). $H^{N\text{-}O}$ are generally employed only where there are no (or insufficient) surface gravity observations (g_{obs}) to compute H^O or H^N. This was the situation in Australia in 1971, where a truncated version of the Rapp (1961) normal-orthometric correction (NOC_R; Equation (7.5)) was used (Roelse et al., 1971). Many national vertical datums using $H^{N\text{-}O}$ are often incorrectly termed orthometric heights (including Australia), despite not using gravity in their realisation (e.g., Holloway, 1988; Ziebart et al., 2008; Abeyratne et al., 2010).

However, sufficient gravity data now exists in Australia (although acknowledging the problems identified in Chapter 6) to retrospectively investigate the effects of gravimetric HCs to the ANLN (cf. Mitchell, 1973a). Gravity values can be computed at ANLN BM (g_{BM}) using EGM2008 (Pavlis et al., 2008) or the Australian National Gravity Database (ANGD), as shown in Chapter 6. This allows H^O and H^N to be computed nationally through corrections to the ANLN (Section 7.9; Filmer et al., 2010), with possible effects of the gravity errors identified in Chapter 6 on Helmert orthometric corrections (HOC) and normal corrections (NC) also investigated (see Sections 7.5 and 7.7).

7.2 Normal-orthometric heights

The general concept of $H^{N\text{-}O}$ is that the normal gravity field completely replaces the actual gravity field, with C replaced by normal potential numbers (C^N), which are (cf. Jekeli, 2000, 10)

$$C^N = U_P - U_{N\text{-}O} \tag{7.3}$$

where U_P is normal potential on the topographic surface and $U_{N\text{-}O}$ is normal potential on the zero-reference for $H^{N\text{-}O}$ (discussed in Section 7.8.2). In analogy to H^N and H^O, $H^{N\text{-}O}$ are

$$H^{N\text{-}O} = \frac{C^N}{\bar{\gamma}} \tag{7.4}$$

Note that normal-orthometric-corrected loop closures are dependent on the levelling route taken (Heck, 1995, 311) and are therefore non-holonomic (cf. Sansò and Vaníček, 2006), i.e., the loop will not necessarily close, even if error-free.

There are numerous versions of the normal-orthometric correction (NOC): Rapp (1961, NOC_R), Bomford (1971, NOC_B), New Zealand (e.g., Amos and Featherstone, 2009, NOC_{NZ}), and Heck (1995, NOC_H). All of these NOC will be defined and briefly discussed here, but the focus of this investigation will be on the NOC_R as it is the height system used in the AHD (Roelse et al., 1971).

7.2.1 Rapp's normal-orthometric correction

The NOC_R reads (Rapp, 1961, 16)

$$NOC_R = (A\bar{H} + B\bar{H}^2 + C\bar{H}^3)\phi_{1\text{-}2} \tag{7.5}$$

where $\bar{H}$ is the average $H^{N\text{-}O}$ between BM1 and BM2, with $\phi_{1\text{-}2}$ the latitude difference (arc-minutes) between BM1 and BM2. The coefficients A, B and C are computed using (Rapp, 1961, 17)

$$A = 2\sin 2\bar{\phi}\,\alpha'\left(1 + \cos 2\bar{\phi}\left(\alpha' - \frac{2\kappa}{\alpha'}\right) - 3\kappa\cos^2 2\bar{\phi}\right)Q \tag{7.6}$$

$$B = 2\sin 2\bar{\phi}\,\alpha' t_2\left(t_3 + \frac{t_4}{2\alpha'} + \cos 2\bar{\phi}\left(\frac{3}{2}t_4 + 2\alpha' t_3 - \frac{2\kappa t_3}{\alpha'}\right)\right)Q \tag{7.7}$$

$$C = 2\sin 2\bar{\phi}\alpha' t_2^2\, t_3\left(t_3 + \frac{t_4}{2\alpha'} + \cos 2\bar{\phi}\left(2t_4 - \frac{2\kappa t_3}{\alpha'}\right)\right)Q \tag{7.8}$$

where Q is 1 arc-minute in radians and $\bar{\phi}$ is the mid-latitude between BM1 and BM2. The constants α', κ, t_2, t_3 and t_4 are computed using (Rapp, 1961, 11,14)

$$\alpha' = \frac{\beta}{2 + \beta + 2\epsilon} \tag{7.9}$$

$$\kappa = \frac{-2\epsilon}{2 + \beta + 2\epsilon} \tag{7.10}$$

$$t_2 = \frac{2(1 + f + c')}{a\left(1 + \frac{\beta}{2} + \epsilon\right)} \tag{7.11}$$

$$t_3 = \frac{1 - d_3}{2} = 1 - t_4 \tag{7.12}$$

$$t_4 = 1 - t_3 \tag{7.13}$$

with a the semi-major axis of the reference ellipsoid, β the gravity flattening of the reference ellipsoid, f the geometric flattening of the reference ellipsoid, and ϵ described by (Rapp, 1961, 7) as a constant in the normal gravity formula, and described by Moritz (1980) as f_4 in the Chebyshev series approximation of the gravity formula. Rapp (1961, 13) defines d_3 as

$$d_3 = \frac{(3f - 2.5\,c')}{2} \tag{7.14}$$

and c' as (Rapp, 1961, 12)

$$c' = \frac{\omega^2 a^3}{GM} \tag{7.15}$$

with ω the angular velocity of the Earth's rotation and GM the product of the Earth's mass and universal gravitational constant.

7.2.2 Bomford's normal-orthometric correction

NOC_B is (cf. Bomford, 1971, 230)

$$NOC_B = -\bar{H}(\phi_{1\text{-}2})(0.0053 \sin 2\bar{\phi}) \sin 1'' \tag{7.16}$$

where $\phi_{1\text{-}2}$ is in arc-seconds, and 0.0053 is a coefficient that has a value similar to β in Section 7.2.1 (see Table 7.3). The reference ellipsoid used for NOC_B is not stated. For full details of the NOC_B, see Bomford (1971, 228-230).

7.2.3 New Zealand normal-orthometric correction

The NOC_{NZ} applied to the New Zealand levelling network is (Amos, 2007, 30)

$$NOC_{NZ} = -\left[2A_{NZ} \sin 2\bar{\phi} \left[1 + \left(A_{NZ} - \frac{2B_{NZ}}{A_{NZ}}\right) \cos 2\bar{\phi}\right] Q\right] \bar{H}\delta\phi_{1\text{-}2} \tag{7.17}$$

where the coefficients A_{NZ} and B_{NZ} are 0.002 506 and 0.000 007 respectively. The second $\bar{\phi}$ in Equation (7.17) is shown in Amos (2007, 30) as ϕ, and is not defined; it is assumed here that this variable is intended to be $\bar{\phi}$. In addition, $\bar{H}$ is defined as the average height at each instrument setup along the levelling line (Amos, 2007,

30), but here is interpreted as the average height of BM1 and BM2, as the instrument heights are rarely available. NOC_{NZ} is based on GRS67 (International Association of Geodesy, 1971) parameters and is a truncated form of NOC_R (Amos and Featherstone, 2009).

7.2.4 Heck's normal-orthometric correction

NOC_H (Heck, 1995, 311) is

$$NOC_H = -\frac{f}{R}\sum_{1}^{2}(H_1 \sin 2\phi_1 \cos \alpha_{1\text{-}2} d_{1\text{-}2}) \tag{7.18}$$

where R is the radius of the Earth, H_1 is $H^{N\text{-}O}$ of BM1 (start point of sub-section), ϕ_1 the latitude of BM1, $\alpha_{1\text{-}2}$ the azimuth, and $d_{1\text{-}2}$ the horizontal distance, both from BM1 to BM2. For computation of NOC_H (Section 7.2.5), GRS80 f (Table 7.3) and R = 6371 km (Moritz, 1980) are used, with $d_{1\text{-}2}$ = 1.85 km (∼1 arc-minute of latitude) and $\alpha_{1\text{-}2} = 0°$ indicating a north-south levelling line.

7.2.5 Comparison of four versions of NOC

Site	JP	BM	ϕ (S)	λ (E)	Height (m)
T1	1126	16/30	36° 27′	148° 00′	2120.018
T2	not JP	7559 SPM	41° 44′	146° 00′	1180.820
T3	not JP	not BM	43° 38′	146° 50′	2228.000

Table 7.1: Test sites for NOC. TS1 is in the Australian Alps, TS2 is located in the mountainous region of central Tasmania, and TS3 is a fictitious location near the southern tip of Tasmania.

Differences between the four NOCs (Sections 7.2.1 to 7.2.4) were estimated at three test sites (TS; Table 7.1): TS1 is in the Australian Alps , TS2 is in central Tasmania, and TS3 is fictitious, near Australia's most southern point (ϕ is ∼43° 38′S) with a height equivalent to Australia's highest point (Mt Kosciuszko; AHD $H^{N\text{-}O}$ is ∼2,228 m). These three TSs were selected because the NOC tends to be larger at high

elevations, and where ϕ is closest to 45° (Rapp, 1961). The NOC estimated for the four versions at the three TSs can be considered maximum values for Australia.

Estimates ($\phi_{1\text{-}2}$ = 1 arc-minute) for the four different NOC versions at the three TSs are in Table 7.2 (cf. Amos, 2007, 30). The differences are small, with NOC_R and NOC_H $\leqslant$0.002 mm different at any site, NOC_B $\leqslant$0.006 mm different to NOC_R, with NOC_{NZ} $\leqslant$0.183 mm different to NOC_R. Amos (2007) suggests that NOC_{NZ} is less rigorous than NOC_R and NOC_H. However, if 0.183 mm (per 1 arc-minute) is linearly extrapolated over 100 km (letting 1 arc-minute = 1.8 km), the difference between NOC_R and NOC_{NZ} is $\sim$10 mm, which is insignificant for all but the most precise levelling (cf. ICSM, 2007). However, the $NOC_R - NOC_{NZ}$ difference will be larger at elevations above 2,228 m, suggesting that this difference may become significant for levelling networks such as New Zealand (e.g. Amos and Featherstone, 2009), and even more so in the Himalayas (cf. Rapp, 1997). From this test, it appears that there is little practical difference in Australia among these four NOCs (particularly among NOC_R, NOC_H, and NOC_B).

Site	NOC_R	NOC_B	NOC_H	NOC_{NZ}
TS1	3.118	3.124	3.120	2.951
TS2	1.804	1.807	1.805	1.708
TS3	3.426	3.431	3.426	3.243

Table 7.2: Values (in mm) for four different NOCs at TS1, TS2 and TS3.

7.2.6 Errors resulting from truncation of NOC_R

Only the first two terms in Equation (7.5) (containing A and B coefficients) were computed and applied to the AHD, as the third term in Equation (7.5) (containing the C coefficient) was considered negligible (Roelse et al., 1971, 65). To test this, NOC_R was re-computed, firstly using all terms in Equation (7.5) and then only the first two terms. This test confirmed that the truncation error is negligible (<0.001 mm per 1 arc-minute of latitude at $H^{N\text{-}O}$ = 2,228 m). Despite this, the complete Equation (7.5) has been used for this study, as the additional computation is minimal with modern

computing power.

7.2.7 Comparison of NOC_R computed from different reference ellipsoids

Rapp (1961) used the 1924 International Ellipsoid (IE1924; Hayford, 1909) and 1930 International Gravity Formula (IGF1930; Cassinis, 1930) in the development and testing of NOC_R. However, the AHD uses the Geodetic Reference System 1967 (GRS67; International Association of Geodesy, 1971) parameters (Roelse et al., 1971), which has now been superseded by GRS80 (Moritz, 1980). The NOC-relevant parameters for these three reference ellipsoids are in Table 7.3.

Parameter	Units	Hayford/IE1924	GRS67	GRS80
a	metres	6 378 388	6 378 160	6 378 137
f	unitless	1/297.0	1/298.25	1/298.257 222 101
GM	m^3 s^-2	398 632$\times 10^9$	398 603 $\times 10^9$	398 600.5 $\times 10^9$
ω	rad s^{-1}	7.292 115 $\times 10^{-5}$	7.292 115 $\times 10^{-5}$	7.292 115 $\times 10^{-5}$
β	unitless	0.005 288 4	0.005 302 4	0.005 302 4
ϵ	unitless	0.000 005 9	0.000 005 9	0.000 005 9

Table 7.3: Parameters used in the NOC from the 1924 International (Hayford) Ellipsoid and 1930 International Gravity Formula, GRS67 and GRS80.

The effect of these different reference ellipsoids on the NOC_R was tested by evaluating the NOC_R (using Equations (7.5) to (7.15); $\phi_{1\text{-}2} = 1$ arc-minute) for IE1924/IGF1930, GRS67 and GRS80 at TS1, TS2, and TS3 (Table 7.1). Table 7.4 shows the NOC_R changes by <0.001 mm when using GRS67 compared to GRS80. Using IE1924/IGF1930 parameters, the IE1924/IGF1930 NOC_R−GRS80 NOC_R difference reaches a maximum of 0.009 mm at TS3. If this difference is linearly extrapolated over 100 km (letting 1 arc-minute = 1.8 km), the difference accumulates to 0.5 mm for heights <2,000 m, which is negligible for all ANLN orders (Roelse et al., 1971, Annex H) or ICSM (2007) classes of levelling.

Site	Hayford (mm)	GRS67 (mm)	GRS80 (mm)
T1	3.110	3.118	3.118
T2	1.799	1.804	1.804
T3	3.417	3.426	3.426

Table 7.4: Values of NOC_R computed at T1, T2, T3 ($\phi_{1\text{-}2}$ =1 arc-minute) for IE1924/IGF1930, GRS67 and GRS80 parameters.

7.3 NOC_R sensitivity to input data errors

The sensitivity of the NOC_R to errors in the input data are examined here. Using the general law of error propagation (e.g., Section 3.5.3; Lyons, 1991), the NOC_R (Equation (7.5)) is partially differentiated with respect to each variable

$$\frac{\partial NOC_R}{\partial A} = \bar{H}\phi_{1\text{-}2} \tag{7.19}$$

$$\frac{\partial NOC_R}{\partial B} = \bar{H}^2\phi_{1\text{-}2} \tag{7.20}$$

$$\frac{\partial NOC_R}{\partial C} = \bar{H}^3\phi_{1\text{-}2} \tag{7.21}$$

$$\frac{\partial NOC_R}{\partial \bar{H}} = (A + 2B\bar{H} + 3C\bar{H}^2)\phi_{1\text{-}2} \tag{7.22}$$

$$\frac{\partial NOC_R}{\partial \phi_{1\text{-}2}} = A\bar{H} + B\bar{H} + C\bar{H}^2 \tag{7.23}$$

The total differential for the error in NOC_R (δNOC_R) is thus

$$\delta NOC_R = \frac{\partial NOC_R}{\partial A}\delta A + \frac{\partial NOC_R}{\partial B}\delta B + \frac{\partial NOC_R}{\partial C}\delta C + \frac{\partial NOC_R}{\partial \bar{H}}\delta\bar{H} + \frac{\partial NOC_R}{\partial \phi_{1-2}}\delta\phi_{1\text{-}2} \tag{7.24}$$

7.3.1 NOC_R sensitivity to errors in $\bar{\phi}$

GRS80 parameters (Table 7.3) and assumed $\bar{\phi} = 35°$S were used to compute numerical values for coefficient A with $\bar{\phi}$ errors ($\delta\bar{\phi}$) of 1, 5 and 10 arc-minutes to simulate errors in coefficient A (δA; Table 7.5). Numerical values were then computed for $\frac{\partial NOC_R}{\partial A}\delta A$ (first term in Equation (7.24)) using assumed values $\bar{H}$ = 1,000 m, $\phi_{1\text{-}2} = 3$ arc-minutes (∼5 km; a typical ANLN sub-section length). Note that for all sensitivity analyses in

this Chapter, the resultant errors are characterised by their magnitudes because the actual error can be positive or negative.

$\delta\bar{\phi}$ (arc-mins)	δA	δNOC_R (mm)
1	0.30×10^{-9}	0.001
5	0.15×10^{-8}	0.005
10	0.30×10^{-8}	0.009

Table 7.5: δNOC_R resulting from errors in coefficient A (δA; unitless).

δNOC_R resulting from δA where $\delta\bar{\phi}$ is 1, 5 or 10 arc-minutes is shown in Table 7.5. When $\delta\bar{\phi}$ is 1 arc-minute, δNOC_R is 0.001 mm ($\phi_{1\text{-}2}$ = 3 arc-minutes; δNOC_R = 0.0003 mm when $\phi_{1\text{-}2}$ = 1 arc-minute), increasing to 0.009 mm when $\delta\bar{\phi}$ is 10 arc-minutes (δNOC_R = 0.001 mm per arc-minute of levelling). δNOC_R for δB and δC were <0.001 mm. Given that BM ϕ uncertainty for the ANLN is ~1 arc-minute, δNOC_R resulting from δA is not a significant source of NOC_R error when $\bar{H}$ = 1,000 m.

7.3.2 NOC_R sensitivity to errors in $\bar{H}$

The sensitivity of NOC_R to errors in $\bar{H}$ ($\delta\bar{H}$) is calculated by evaluating Equation (7.22) and then the fourth term in Equation (7.24). GRS80 parameters and assumed values of $\bar{H}$ = 1,000 m, $\phi_{1\text{-}2}$ = 3 arc-minutes, and $\bar{\phi} = 35°$ were used. Increments of 1 m were used for $\delta\bar{H}$.

The increase in δNOC_R can be seen in Figure 7.2, where δNOC_R increases linearly as $\delta\bar{H}$ increases. The NOC_R appears to be rather insensitive to errors in $\bar{H}$; $\delta\bar{H}$ needs to be ~23 m to cause δNOC_R to be 0.1 mm. Indeed, even when $\delta\bar{H}$ is 200 m, δNOC_R is <1 mm ($\phi_{1\text{-}2}$ = 3 arc-minutes), leading to the conclusion that even large $\delta\bar{H}$ have little effect on the NOC_R.

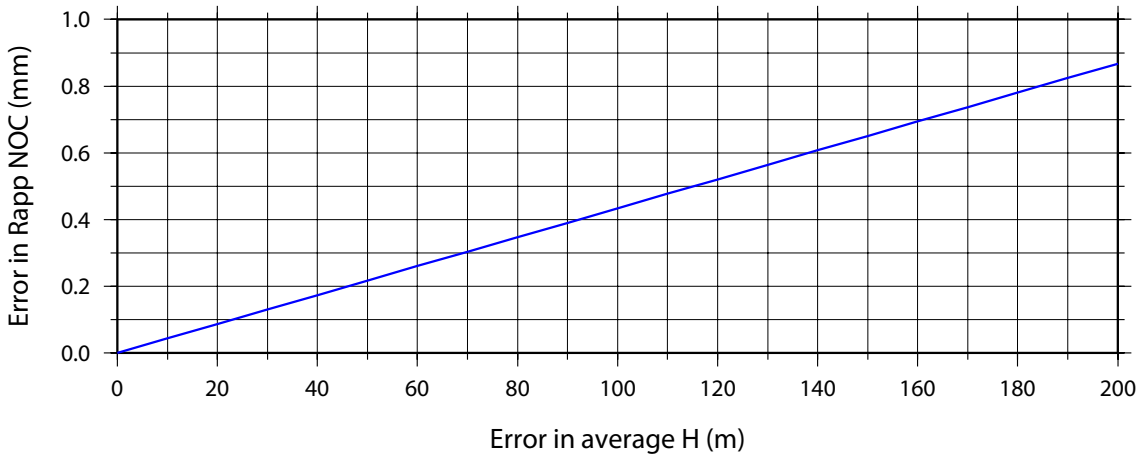

Figure 7.2: δNOC_R resulting from $\delta \bar{H}$.

7.3.3 NOC_R sensitivity to errors in $\phi_{1\text{-}2}$

The effect of $\phi_{1\text{-}2}$ errors ($\delta\phi_{1\text{-}2}$) can be seen in Figure 7.3. Here, Equation (7.23) and then the fifth term in Equation (7.24) are evaluated with assumed values of $\bar{H} = 1{,}000$ m, and $\bar{\phi} = 35°\text{S}$. Increments of 1 arc-minute were used for $\delta\phi_{1\text{-}2}$.

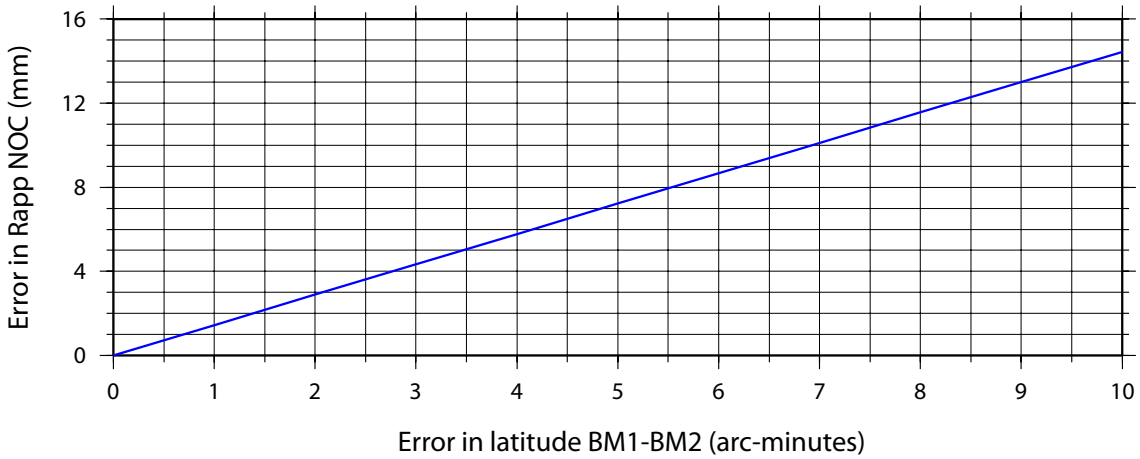

Figure 7.3: δNOC_R caused by $\delta\phi_{1\text{-}2}$.

δNOC_R increases linearly to ~14.5 mm when $\delta\phi_{1\text{-}2} = 10$ arc minutes (Figure 7.3), or ~1.5 mm per 1 arc-minute of $\delta\phi_{1\text{-}2}$. ANLN ϕ_{BM} absolute positional uncertainty is ~±1 arc-minute, so $\delta\phi_{1\text{-}2}$ will tend to cancel out over multiple levelling sub-sections, rather than accumulate. Therefore, δNOC_R of 1−2 mm may propagate into $H^{N\text{-}O}$ at some BMs, but should not exceed this. Despite NOC_R appearing to be more sensitive to $\delta\phi_{1\text{-}2}$ than errors in the coefficients (A, B, C) or $\bar{H}$, the resulting 1−2 mm (maximum) errors at AHD $H^{N\text{-}O}$ is insignificant for a third-order network such as the ANLN, where

BMs are typically 5 km apart (third-order levelling standard deviation (STD; 1σ) over 5 km is $\pm$9.4 mm using $4.2\sqrt{d}$; see Table 2.4).

7.4 Orthometric heights

H^O is defined by (Heiskanen and Moritz, 1967, 166)

$$H^O = \frac{C}{\bar{g}} \tag{7.25}$$

where C is the geopotential number and $\bar{g}$ is the integral mean of gravity along the plumbline between the Earth's surface and the geoid. H^O is thus defined as the distance along the curved and torsioned plumbline between the surface point P and the point P_0 on the geoid (Figure 7.1). However, a 'true' H^O is difficult to compute exactly (e.g., Jekeli, 2000), because $\bar{g}$ is inside the topography and cannot be easily measured (cf. Strange, 1982; Tenzer et al., 2005). There are a number of different methods of approximating $\bar{g}$ (Sections 7.4.2−7.4.5), resulting in several variants of orthometric heights (e.g., Helmert, 1890; Niethammer, 1932; Mader, 1954; Strang van Hees, 1992; Kao et al., 2000; Hwang and Hsiao, 2003; Tenzer et al., 2005).

H^O can be realised by two methods. The first method (C-based method) is to compute C and $\bar{g}$ at each BM, then use Equation (7.25) to compute H^O discretely at each BM (e.g., Marti and Schlatter, 2002). Alternatively, orthometric corrections (OC) can be computed and directly applied to Δn (HC method; e.g., Filmer et al., 2010; Allister and Featherstone, 2001; Hwang and Hsiao, 2003; Strang van Hees, 1992; Kao et al., 2000). The OC is (Heiskanen and Moritz, 1967, 168)

$$OC_{1\text{-}2} = \sum_{1}^{2} \frac{\bar{g}_s - \gamma_0}{\gamma_0} \Delta n + \frac{\bar{g}_1 - \gamma_0}{\gamma_0} H_1^O - \frac{\bar{g}_2 - \gamma_0}{\gamma_0} H_2^O \tag{7.26}$$

with the method of computing $\bar{g}$ at BM1 ($\bar{g}_1$) and BM2 ($\bar{g}_2$) determining the version of H^O used. H_1^O is H^O at BM1, likewise for H_2^O. γ_0 is the value of normal gravity at 45° latitude. The HC method (Equation (7.26)), is used to compute H^O in this study, rather than the C-based approach. This is for consistency, as the NOC_R is applied as a correction to Δn.

7.4.1 Helmert orthometric heights

Helmert (1890) H^O are conceptually simple and easy to compute, with the simplified gravity reduction of Poincaré-Prey (hereafter referred to as SPP; Heiskanen and Moritz, 1967, 164) used to approximate $\bar{g}$. The SPP at the midpoint between the topographic surface and the geoid (Q^O; see Figure 7.1) defines Helmert $\bar{g}$ ($\bar{g}^H$), and is (cf. Heiskanen and Moritz, 1967, 167)

$$\bar{g}^H = g_{BM} - \left(\frac{1}{2}\frac{\partial\gamma}{\partial h} + 2\pi G\rho\right) H^O_{BM} \tag{7.27}$$

where $\partial\gamma/\partial h$ is the linear vertical gradient of normal gravity (cf. Equation (6.13); used as an approximation of the actual gravity gradient), G is the universal gravitational constant, and ρ is the Earth's topographic density. The right hand term (inside the parenthesis) is the gravitational value of the Bouguer plate (BP; Equation (6.22); Section 6.5.2).

Using $\partial\gamma/\partial h = -0.3086$ mGal m^{-1}, $\rho = 2670$ kg m^3 and $G = 6.6742\times10^{-11}$ m^{3}kg^{-1}s^{-2} (CODATA-02; Mohr and Taylor, 2005, 43), Equation (7.27) simplifies to (Heiskanen and Moritz, 1967, 167)

$$\bar{g}^H = g_{BM} + 0.0424 H^O_{BM} \tag{7.28}$$

where $\bar{g}^H$ and g_{BM} are in Gals and H^O_{BM} is in km. The SPP reduction makes a number of approximations, including using the BP (thus neglecting terrain effects residual to the BP) and constant ρ (neglecting variations in topographic density (cf. Niethammer, 1932; Mader, 1954; Hwang and Hsiao, 2003; Tenzer et al., 2005; Allister and Featherstone, 2001).

7.4.2 Niethammer orthometric heights

A better estimate of a 'true' H^O than Helmert H^O (using SPP; Equation (7.28)) requires the inclusion of terrain corrections (TC) in the evaluation of $\bar{g}$. The Niethammer (1932) method (from Dennis and Featherstone, 2003) is

$$\bar{g}^N = g_{BM} - \left(\frac{1}{2}\frac{\partial\gamma}{\partial h} + 2\pi G\rho\right) H^O_{BM} + \delta g^T + \bar{\delta} g^T \tag{7.29}$$

where δg^T is the TCs applied at the BM, with $\bar{\delta} g^T$ the integral mean TC between the BM and geoid. Niethammer (1932) produced tables to allow the computation of $\bar{\delta} g^T$, with Rapp (1961, 63) providing a modified version of Equation (7.29), with a computer program to evaluate $\bar{\delta} g^T$ (Strange, 1982). However, computation of $\bar{g}^N$ to realise Niethammer (1932) H^O are more computationally demanding and complex than Helmert H^O.

7.4.3 Mader orthometric heights

A similar (although slightly less complex) estimate of $\bar{g}$ to that of Niethammer (1932) is made by Mader (1954)

$$\bar{g}^M = g_{BM} - \left(\frac{1}{2} \frac{\partial \gamma}{\partial h} + 2\pi G\rho \right) H^O_{BM} + \frac{1}{2}(\delta g^T - \delta g^T_0) \tag{7.30}$$

where δg^T_0 are TCs computed at the geoid. Here, the assumption is made that the TC value changes linearly through the topography, so that the arithmetic rather than the integral mean TC is computed. A modified version of Mader (1954) H^O is developed by Hwang and Hsiao (2003).

7.4.4 Rigorous orthometric heights

More accurate determination of $\bar{g}$ have been made by Tenzer et al. (2005), referred to as rigorous H^O, where $\bar{g}$ within the topography along the plumbline comprises two parts: i) mean normal gravity, which is independent of the actual gravity field, and ii), the mean value of the actual gravity disturbance ($\bar{\delta} g$), consisting primarily of geoid-generated, terrain roughness, and topographical mass-density effects, with a smaller contribution from the atmospheric masses. Rigorous H^O can be applied as corrections to Helmert H^O (Santos et al., 2006; Kingdon et al., 2005), although they are more complex than Niethammer H^O to compute.

7.4.5 Discussion of the different versions of H^O

The major advantage of Helmert H^O compared to Niethammer, Mader or rigorous H^O is the ease of computation. However, Helmert H^O are the poorest approximation of a 'true' H^O, compared to the other H^O versions (Dennis and Featherstone, 2003). This is because the SPP does not account for the terrain effect (terrain roughness), the geoid-generated gravity disturbance, or topographic mass density variations ($\delta\rho$; Tenzer et al., 2005; Kingdon et al., 2005; Santos et al., 2006). Niethammer, Mader and rigorous H^O account for terrain roughness through the TC, but only rigorous H^O accounts for the effect of the geoid's mass on $\bar{g}$ and lateral (not radial) $\delta\rho$ (cf. Strange, 1982; Allister and Featherstone, 2001; Hwang and Hsiao, 2003).

The assumption of constant density is made because numerical values for variable ρ are usually not available (cf. Strange, 1982). However, ρ can vary by $\sim$600 kg m^{-3} (Heiskanen and Moritz, 1967, 169), possibly up to $\sim$1,000 kg m^{-3} in extreme cases like the Darling Fault in Western Australia (Allister and Featherstone, 2001). H^O errors (δH^O) due to $\delta\rho$ range from a theoretical estimate of 25 mm when H^O = 1,000 m and $\delta\rho$ = 600 kg m^{-3} (Heiskanen and Moritz, 1967, 169), to 96 mm from field tests where H = 2,000 m and $\delta\rho \sim$ 570 kg m^{-3} (Strange, 1982). However, Strange (1982) indicates that δH^O rarely exceeds 30 mm for elevations up to 2,000 m. Field results in Taiwan (Hwang and Hsiao, 2003) also indicate that for heights up to 3,500 m, the maximum δH^O is only a few mm where $\delta\rho$ is 300$-$400 kg m^{-3}. By comparison, Kingdon et al. (2005) found δH^O between $-$45 mm and +65 mm in a test area in Canada where H^O varied between 0 m and 3227 m and $\delta\rho$ between $-$180 kg m^{-3} and +310 kg m^{-3}.

The differences among Helmert, Niethammer and Mader H^O are caused by the different treatment or omission of TCs. Heiskanen and Moritz (1967, 169) describe how Mader (1954) found 60 mm difference between Neithammaer and Helmert H^O, but only 30 mm between Niethammer and Mader H^O at H^O = 2,504 m. Santos et al. (2006) also found little difference between Niethammer and Mader H^O. Maximum Niethammer$-$Helmert H^O differences of 60 mm described in Heiskanen and Moritz (1967, 169) can be compared to 30 mm (Santos et al., 2006, maximum H^O $\sim$2,800

m), and 310 mm (Kingdon et al., 2005, maximum H^O 3,227 m), using only the terrain roughness component from the rigorous H^O.

Maximum differences between rigorous and Helmert H^O are 130 mm at ∼2,800 m (Santos et al., 2006), 170 mm at 3,227 m (Kingdon et al., 2005), while Marti and Schlatter (2002) found maximum differences of 40−50 mm (at ∼2,500 m) to Helmert H^O using an (undefined) orthometric H^O where $\bar{g}$ is computed rigorously from mass models. However, Dennis and Featherstone (2003) used a simulated gravity field from a well-defined mountain mass, computed 'true' orthometric H^O and Niethammer H^O, finding a near-perfect agreement between them. Mader H^O were also computed and found to agree in most situations, but the differences increased in mountainous terrain (of unspecified height).

While rigorous-type H^O provide more accurate orthometric heights than Helmert H^O, the differences appear to be <40 mm for heights <2,000 m. For heights above this, the extra computational work required for rigorous, Niethammer and Mader H^O are probably justified. It is acknowledged that for a high accuracy geoid-based height system, rigorous H^O are required. However, given Australia's generally low terrain (Section 1.1.2), and the poor quality of Australian gravity data and BM positional information (Section 6.5; possibly causing H^O errors larger than the difference between rigorous and Helmert H^O; cf. Section 7.5), only Helmert H^O will be tested in Australia.

7.5 *OC* sensitivity to input data errors

In this section, the effect of input data errors on the *OC* is investigated (cf. Section 7.3). Note that errors due to input data errors are distinct from errors due to approximations made for the different versions of H^O, as discussed in Section 7.4.5. Table 7.6 shows the input data that will be used in the *OC* sensitivity analysis. These five test sections (TSs) are existing ANLN sub-sections, with EGM2008-derived gravity at BMs (g_{BM}; see Section 6.2).

The partial derivative of the OC (Equation (7.26)) with respect to each variable is (cf. Equations (7.19)− (7.23))

$$\frac{\partial OC}{\partial \bar{g}_s} = \frac{\Delta n}{\gamma_0} \tag{7.31}$$

$$\frac{\partial OC}{\partial \Delta n} = \frac{\bar{g}_s - \gamma_0}{\gamma_0} \tag{7.32}$$

$$\frac{\partial OC}{\partial \bar{g}_1} = \frac{H_1^O}{\gamma_0} \tag{7.33}$$

$$\frac{\partial OC}{\partial \bar{g}_2} = -\frac{H_2^O}{\gamma_0} \tag{7.34}$$

$$\frac{\partial OC}{\partial H_1^O} = \frac{\bar{g}_1 - \gamma_0}{\gamma_0} \tag{7.35}$$

$$\frac{\partial OC}{\partial H_2^O} = -\frac{\bar{g}_2 - \gamma_0}{\gamma_0} \tag{7.36}$$

with the total differential (cf. Equation (7.24))

$$\delta OC = \frac{\partial OC}{\partial \bar{g}_s}\delta \bar{g}_s + \frac{\partial OC}{\partial \delta n}\delta n + \frac{\partial OC}{\partial \bar{g}_1}\delta \bar{g}_1 + \frac{\partial OC}{\partial \bar{g}_2}\delta \bar{g}_2 + \frac{\partial OC}{\partial H_1^O}\delta H_1^O + \frac{\partial OC}{\partial H_2^O}\delta H_2^O \tag{7.37}$$

γ_0 is constant, so is not tested here. Note that although H^O should be used in the OC, AHD $H^{N\text{-}O}$ is used in these tests as it is the only height available. The difference between H^O and AHD $H^{N\text{-}O}$ over Australia is generally <0.1 m, reaching a maximum of 0.44 m (Section 7.9.5), which has a negligible effect (∼1 mm; Figure 7.6) on δOC.

Test Section	Δn (m)	ϕ_{BM1} (S)	AHD $H_1^{N\text{-}O}$ (m)	AHD $H_2^{N\text{-}O}$ (m)	EGM2008 g_1 (Gals)	EGM2008 g_2 (Gals)
TS4	14.836	26° 04′	505.686	520.523	978.860390	978.849108
TS5	15.082	35° 38′	1032.153	1047.230	979.553221	979.554246
TS6	60.197	35° 41′	1458.857	1519.056	979.437617	979.418736
TS7	174.637	36° 31′	1848.747	2023.388	979.433646	979.381902
TS8	0.124	36° 27′	2227.960	2228.084	979.303916	979.303875

Table 7.6: Test sections (TSs; selected from ANLN) used to test OC and NC sensitivity to input data errors.

The TSs in Table 7.6 (summary of data used) have been selected from the ANLN and are designed to test the sensitivity of the OC in a range of terrain conditions (e.g., small and large Δn and elevation). The TS elevations are all >500 m, and because OCs increase with height, these TS will provide a more challenging test than at elevations <500 m. TS4 is located in central Australia (Figure 1.1), with TS5−TS8 in the Australian Alps (Figure 7.8), which features the highest terrain in Australia.

7.5.1 *OC* sensitivity to Δn errors

δOC due to error in Δn ($\delta\Delta n$) was found to be <2 mm when δn was 1 m for TS4−TS8. An error in Δn of 1 m is generally caused by an undetected gross levelling error (maximum ANLN loop misclosure is 0.93 m; Filmer et al., 2009). Equation (7.32) shows that δOC resulting from $\delta\Delta n$ is dependent on $\bar{g}_s$, which depends mostly on H^O and ϕ_{BM}. Because γ_0 is computed at 45°, ϕ_{BM} in northern Australia should cause largest δOC resulting from $\delta\Delta n$. As the most northerly TS in Table 7.6 is at ϕ_{BM} = 26° 04′S, an additional TS near Bamaga at the northern tip of Cape York (ϕ_{BM} = 11° 28′S, AHD $H^{N\text{-}O}$ = 88.927 m) was used. This demonstrated that δOC resulting from $\delta\Delta n$ was <3 mm when δn was 1 m, which is not considered significant.

7.5.2 *OC* sensitivity to $\bar{g}_s$ errors

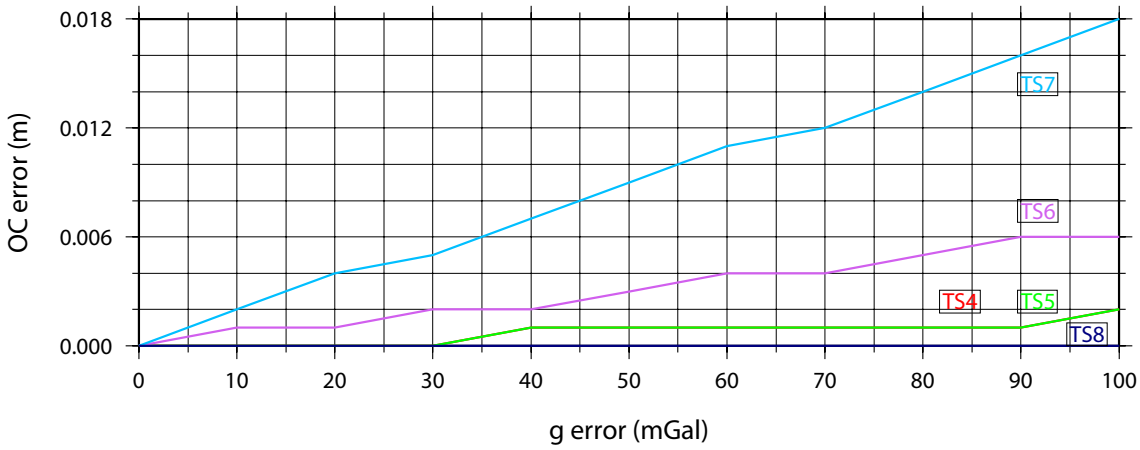

Figure 7.4: δOC resulting from $\delta\bar{g}_s$ which is the error in mean observed surface gravity ($\bar{g}_s$) between BM1 and BM2. Note that δOC at TS4 and TS5 are the same; TS5 is plotted over TS4. δOC at TS8 is zero. The non-linear effect is due to rounding in the computation.

The effect on δOC of errors in $\bar{g}_s$ ($\delta\bar{g}_s$) is computed through Equation (7.31) and the first term in Equation (7.37), using TS in Table 7.6 and γ_0 = 45°S. The results are in Figure 7.4, showing that when $\delta\bar{g}_s$ is ∼50 mGals (e.g., Section 6.4.2), δOC is 9 mm for TS7 (Δn = 174.637 m). Equation (7.31) shows that δOC resulting from $\delta\bar{g}_s$ is directly proportional to Δn (δOC ∼5 mm per 100 m Δn where $\delta\bar{g}_s$ is 50 mGal). The sensitivity of δOC to $\delta\bar{g}_s$ is therefore greater in steep, mountainous terrain, where Δn will be larger. However, Figure 7.4 indicates that even when $\delta\bar{g}_s$ and Δn are very

large (e.g., TS7, ∼100 mGal and 175 m) respectively, δOC is <20 mm, although it is acknowledged that for short sub-sections (say <2 km) and high precision levelling, this may be significant.

7.5.3 OC sensitivity to $\bar{g}$ errors

The magnitude of δOC due to errors in $\bar{g}_1$ ($\delta\bar{g}_1$) and $\bar{g}_2$ ($\delta\bar{g}_2$) computed here are the result of errors in the value of g_{BM} (cf. Section 6.4.2), not due to variations between different versions of OC (see Section 7.4.5 for this discussion). As Equation (7.33) and Equation (7.34) provide the same result, but with opposite sign (ignoring differences between H_1^O and H_2^O), only Equation (7.33) will be evaluated to investigate $\delta\bar{g}_1$.

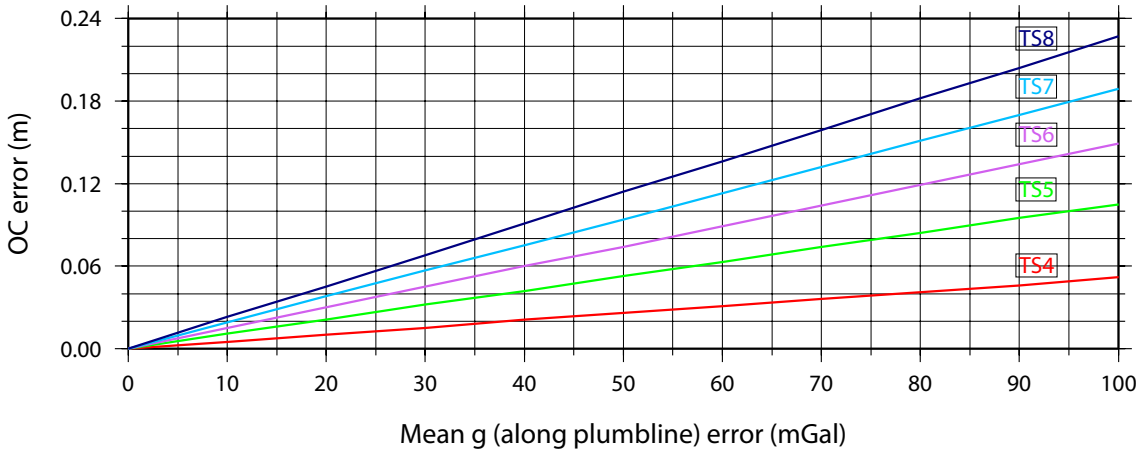

Figure 7.5: δOC resulting from $\delta\bar{g}$ which is the error in the integral mean of gravity ($\bar{g}$) along the plumbline between the topographic surface and the geoid.

Equation (7.33) is evaluated using all TS in Table 7.6, and the third term in Equation (7.37). Equation (7.33) indicates δOC to be proportional to H_1^O, with the magnitude of δOC approaching 0.12 m when $\delta\bar{g}$ ∼50 mGal (Figure 7.5; TS8, $H_1^{N\text{-}O}$ = 2,227.960 m). When $\delta\bar{g}$ ∼100 mGal, δOC exceeds 0.20 m at TS8 (cf. Heiskanen and Moritz, 1967, 169; δOC is 0.10 m for $\delta\bar{g}$ = 100 mGal and H_1 = 1,000 m). However, this error does not accumulate, as an error in $\bar{g}_1$ only affects H^O at BM1. Thus δOC is rather sensitive to $\delta\bar{g}$, indicating that OC require reasonably accurate g_{BM}; say, ±10 mGal, where δOC ∼25 mm when $H^{N\text{-}O}$ is 2,228 m.

7.5.4 OC sensitivity to H^O errors

Equation (7.35) and the fifth term of Equation (7.37) are used to evaluate the sensitivity of δOC to H^O errors (δH^O; Equation (7.35) is considered representative of δH^O; cf. Section 7.5.3). Figure 7.6 shows that when δH^O is 10 m (TS4), δOC is -18 mm. Equation (7.35) indicates that δOC will be negative when $\bar{g} < \gamma_0$ (when $\delta\bar{g}$ is positive; cf. Section 7.9.1), demonstrating dependency on ϕ_{BM} and H^O, both of which affect the magnitude of g_{BM} from which $\bar{g}$ is calculated. δOC appears to be reasonably insensitive to δH^O (if maximum AHD $\delta H^{N\text{-}O}$ is $\sim$2 m, δOC is only $\sim$4 mm at TS4), although in situations where δH^O may be $>$2 m, the magnitude could reach the cm level, which is significant for precise levelling.

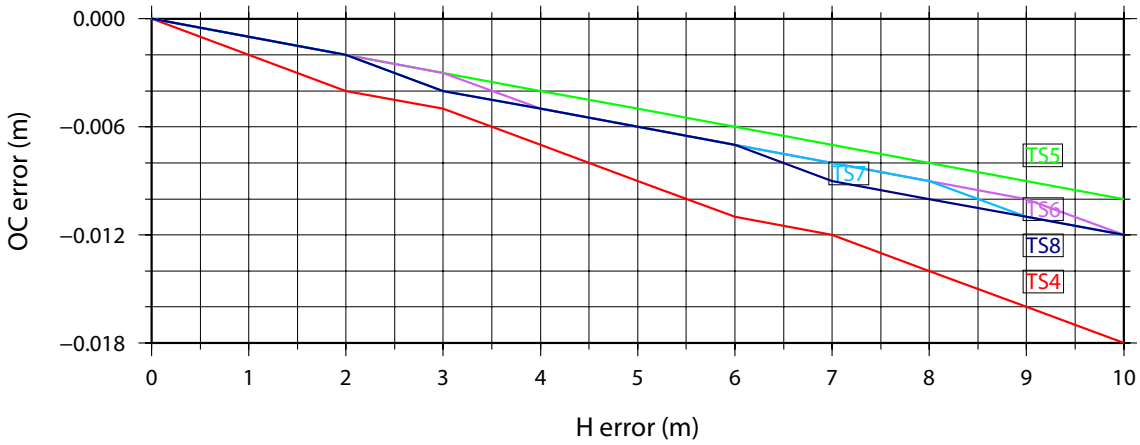

Figure 7.6: δOC resulting from δH^O_1.

7.6 Normal heights

In 1945, Molodensky (Molodensky et al., 1962, loc. cit.) introduced the concept of the normal height system H^N (Heiskanen and Moritz, 1967, 291). This avoids the problems involved with H^O, which require approximations of gravity inside the Earth's topography (cf. Strange, 1982).

7.6.1 Molodensky's theory

Molodensky replaced $\bar{g}$ with the integral mean of normal gravity ($\bar{\gamma}$) along the normal plumbline between the ellipsoid and telluroid (Heiskanen and Moritz, 1967, 171)

$$H^N = \frac{C}{\bar{\gamma}} \tag{7.38}$$

The telluroid is points-wise defined by the points on the normal plumbline (Q^N) where normal potential (U_Q) is equal to potential at P (W_P; see Figure 7.1). The normal height at P, (H_P^N) is defined as the distance along the slightly curved normal plumbline between Q^N on the telluroid and Q_0 on the ellipsoid. Although the height anomaly (ζ_P) is defined between the telluroid and topographic surface, ζ_P can be plotted above the reference ellipsoid to map the quasigeoid (Figure 7.1). The quasigeoid is not an equipotential surface (nor is the telluroid) in either the normal or actual gravity field (Jekeli, 2000), so has lesser physical meaning. Thus, for practical purposes, H_P^N is the normal height of P above the quasigeoid in analogy to H_P^O (Section 7.4.1).

The formula to compute $\bar{\gamma}$ is derived from the second-order free-air gravity correction (Heiskanen and Moritz, 1967, 170; also see Section 6.2.4)

$$\bar{\gamma} = \gamma \left[1 - (1 + f + m - 2f \sin^2 \phi_{BM}) \frac{H^N}{a} + \left(\frac{H^N}{a} \right)^2 \right] \tag{7.39}$$

where γ is normal gravity on the ellipsoid at the point of computation (Equation (6.11)) and m is the geodetic parameter (ratio of gravitational and centrifugal forces at the equator). Equation (7.39) can be used to compute $\bar{\gamma}$ in the same way that the SPP reduction is used to compute $\bar{g}$. The critical difference is that $\bar{\gamma}$ can be computed analytically and without assumptions and approximations, whereas $\bar{g}$ requires assumptions to be made regarding the topographic masses (cf. Section 7.4.1).

7.6.2 Practical computation of normal heights

Like H^O, H^N can be realised through discreet computation at BMs using C, or by applying normal corrections (NC) to Δn in analogy to OC (Equation (7.26)), with $\bar{\gamma}$

replacing $\bar{g}$

$$NC_{1\text{-}2} = \sum_{1}^{2} \frac{\bar{g}_s - \gamma_0}{\gamma_0}\delta n + \frac{\bar{\gamma}_1 - \gamma_0}{\gamma_0}H_1^N - \frac{\bar{\gamma}_2 - \gamma_0}{\gamma_0}H_2^N \tag{7.40}$$

Equation (7.40) is used to compute H^N in this study. As with the OC, γ_0 is the value of normal gravity at 45° latitude.

7.7 NC sensitivity to input data errors

Here, NC errors (δNC) resulting from input data errors are given similar treatment to OC errors in Section 7.5. In analogy with Equations (7.31) to (7.46), the partial derivatives of the NC are

$$\frac{\partial NC}{\partial \bar{g}_s} = \frac{\Delta n}{\gamma_0} \tag{7.41}$$

$$\frac{\partial NC}{\partial \Delta n} = \frac{\bar{g}_s - \gamma_0}{\gamma_0} \tag{7.42}$$

$$\frac{\partial NC}{\partial \bar{\gamma}_1} = \frac{H_1^N}{\gamma_0} \tag{7.43}$$

$$\frac{\partial NC}{\partial \bar{\gamma}_2} = -\frac{H_2^N}{\gamma_0} \tag{7.44}$$

$$\frac{\partial NC}{\partial H_1^N} = \frac{\bar{\gamma}_1 - \gamma_0}{\gamma_0} \tag{7.45}$$

$$\frac{\partial NC}{\partial H_2^N} = -\frac{\bar{\gamma}_2 - \gamma_0}{\gamma_0} \tag{7.46}$$

The total differential of NC is (cf. Equation (7.37))

$$\delta NC = \frac{\partial NC}{\partial \bar{g}_s}\delta \bar{g}_s + \frac{\partial NC}{\partial \Delta n}\Delta n + \frac{\partial NC}{\partial \bar{\gamma}_1}\delta \bar{\gamma}_1 + \frac{\partial NC}{\partial \bar{\gamma}_2}\delta \bar{\gamma}_2 + \frac{\partial NC}{\partial H_1^N}\delta H_1^N + \frac{\partial NC}{\partial H_2^N}\delta H_2^N \tag{7.47}$$

Equations (7.41) and (7.42) are identical to Equations (7.31) and (7.32) for the OC. Therefore, like δOC, δNC is <20 mm when $\bar{g}_s$ error is <100 mGal (Figure 7.4; see Section 7.5.2 for discussion), and will be <3 mm where $\delta\Delta n$ <1 m. δNC resulting from δH^N and $\delta\bar{\gamma}$ in Equation (7.40) are of similar magnitude to the effects of δH and $\delta\bar{g}$ on δOC. While $\delta\bar{g}$ can be large, $\delta\bar{\gamma}$ is generally assumed to be errorless. However, $\delta\bar{\gamma}$ is affected by δH^N and errors in ϕ_{BM} ($\delta\phi_{BM}$) in Equation (7.39).

7.7.1 $\bar{\gamma}$ sensitivity to ϕ_{BM} and H^N errors

Here, the effects of δH^N and $\delta\phi_{BM}$ on $\bar{\gamma}$ are investigated (GRS80 ellipsoid parameters used in Equation (7.39) are considered errorless). The partial derivative of $\bar{\gamma}$ with respect to H^N is

$$\frac{\partial\bar{\gamma}}{\partial H^N} = -\frac{\gamma}{a}\left[1 + f + m - 2f\sin^2\phi_{BM} - \frac{2H^N}{a}\right] \tag{7.48}$$

$\delta\bar{\gamma}$ caused by δH^N is then

$$\delta\bar{\gamma} = \frac{\partial\bar{\gamma}}{\partial H^N}\delta H^N \tag{7.49}$$

with $\delta\bar{\gamma}$ computed for all TS (Table 7.6). $\delta\bar{\gamma}$ increases linearly as δH^N increases, at 0.1542−0.1543 mGal m^{-1}, with the slightly lesser rate at higher elevations (TS6, TS7, TS8). This is approximately half the linear vertical gradient of normal gravity (0.3086 mGal m^{-1}).

$\delta\bar{\gamma}$ caused by $\delta\phi_{BM}$ is more complex than the effects of δH^N, because $\bar{\gamma}$ is dependent on γ (Equation (7.39)), which itself is dependent on ϕ_{BM} (cf. Section 6.5.7; Featherstone, 1995; Heck, 1990). Instead of using the general law of error propagation to assess the sensitivity of $\bar{\gamma}$ to $\delta\phi_{BM}$, a simulation is used to evaluate $\delta\bar{\gamma}$ when $\delta\phi_{BM}$ is 1 and 2 arc-minutes. Both γ (Equation (6.11)) and $\bar{\gamma}$ (Equation (7.39)) are computed using ϕ_{BM} for all TS (Table 7.6), then re-computed at ϕ_{BM} +1 arc-minute, then +2 arc-minutes (cf. Section 6.5.6). Although somewhat crude, this method provides an estimate of the full effect of $\delta\phi_{BM}$ on $\delta\bar{\gamma}$.

The magnitude of $\delta\bar{\gamma}$ when $\delta\phi_{BM}$ is 1 arc-minute range between 1.19 mGal at TS4 up to 1.44 mGal at TS8. Most of this error is attributable to $\delta\gamma$ due to the influence of $\delta\phi_{BM}$ in Equation (6.11). The 1.19 mGal ($\phi = 26°\ 04'$S) to 1.44 mGal ($\phi = 36°\ 31'$S) range is within the 0.55−1.51 mGal ($\delta\phi_{BM}$ = 1 arc-minute; ϕ between 10° 44′S and 43° 17′S) range for $\delta\gamma$ identified in Section 6.5.7. The indication is that ϕ_{BM} has less influence on Equation (7.39) than Equation (6.11).

As maximum ANLN δH^N is unlikely to exceed 2 m (more likely <1 m), maximum $\delta\bar{\gamma}$ due to δH^N should be <0.3 mGal. It is also unlikely for ANLN $\delta\phi_{BM}$ to exceed 2

arc-minutes (more likely <1 arc-minute), resulting in maximum $\delta\bar{\gamma}$ due to $\delta\phi_{BM}$ being <3 mGal. From this analysis, maximum $\delta\bar{\gamma}$ caused by δH^N and $\delta\phi_{BM}$ (for the ANLN) is ∼4 mGal.

7.7.2 *NC* sensitivity to $\bar{\gamma}$ errors

δNC caused by $\delta\bar{\gamma}$ (Equation (7.43) and third term of Equation (7.47)) is proportional to H^N and equivalent to δOC caused by $\delta\bar{g}$ (Equation (7.33)). The difference in magnitude between δNC resulting from $\delta\bar{\gamma}$ and δOC caused by $\bar{g}$ (see Section 7.5.3) is that $\delta\bar{g}$ can be as large as 50−60 mGal (due to g_{BM} errors; Section 6.4.2), but $\delta\bar{\gamma}$ is unlikely to exceed 4 mGal (see Section 7.7.1). Figure 7.5 indicates that when $\delta\bar{\gamma}$ is 4 mGal (substitute $\delta\bar{\gamma}$ for $\delta\bar{g}$), δNC is ∼10 mm at TS8. By comparison, if δg is 50 mGal, δOC is almost 0.12 m at TS8.

7.7.3 *NC* sensitivity to H^N errors

The effect of δH^N on δNC (Equation (7.45) and fifth term of Equation (7.47)) is also equivalent to δOC caused by δH^O (Equation (7.35) and fifth term of Equation (7.37)). Some small variation may occur due to $\bar{\gamma}$ replacing $\bar{g}$ (cf. Equations (7.45) and (7.33)), but it is likely that δNC is generally <20 mm (when δH^N is 10 m; TS4), as shown in Figure 7.6. As maximum AHD $H^{N\text{-}O}$ is ∼2 m, δNC is more likely to be <4 mm.

It has been shown here that *NC* is sensitive to the same variables as *OC*, with the major difference that maximum $\delta\bar{\gamma}$ in the *NC* is much smaller than maximum $\delta\bar{g}$ for *OC*, thus reducing the size of δNC compared to δOC. However, it is also demonstrated that $\bar{\gamma}$ is not errorless, as errors in the input values for ϕ_{BM} and H^N will propagate into $\bar{\gamma}$ and subsequently the H^N. Of the three height corrections tested, the NOC_R is least sensitive to input errors (Section 7.3), followed by the *NC* (Section 7.7), with the *HOC* most susceptible to input data errors (Section 7.5).

7.8 Discussion on theoretical differences among $H^{N\text{-}O}$, H^O and H^N

Differences between $H^{N\text{-}O}$, H^O and H^N can be identified through the separation of their respective zero-references. This section discusses the theoretical treatment of these differences.

7.8.1 Geoid-quasigeoid separation

h_P is related to H_P^O via the geoid height (N_P; Figure 7.1) and to H_P^N by the height anomaly (ζ_P; Figure 7.1). The difference $N-\zeta$ therefore defines the difference between H^O and H^N. Heiskanen and Moritz (1967, 327) develop an approximate relation

$$N = \zeta + \frac{\bar{g}-\bar{\gamma}}{\bar{\gamma}} H^O \tag{7.50}$$

where

$$\bar{g}-\bar{\gamma} \simeq \Delta g_{SPB} \tag{7.51}$$

where Δg_{SPB} is the simple planar Bouguer anomaly (cf. Section 6.3.1). $N-\zeta$ (C_2) then becomes (Rapp, 1997)

$$C_2 \simeq \frac{\Delta g_{SPB}}{\bar{\gamma}} H^O = H^N - H^O \tag{7.52}$$

Equation (7.52) is used by **harmonic_synth.f** to compute N (Holmes and Pavlis, 2008). EGM2008-computed $N-\zeta$ is shown in Figures 7.10(c) and 7.11(c).

This approximate relation (Equation (7.52)) was used by Rapp (1997) to make a global estimation of C_2 finding a maximum of C_2 of about 3 m in the Himalaya mountains, while an Australian study by Featherstone and Kirby (1998) estimated maximum C_2 to be ∼0.15 m in central Australia (cf. Section 7.9.4; Filmer et al., 2010). However, this did not include the highest mountains in the Australian Alps due to spatial aliasing of g_{obs} in the ANGD. By comparison, Sünkel (1983) computed the geoid and quasigeoid in Austria, finding $N-\zeta$ to be +0.35 m at a height of ∼3,000 m.

Attempts to derive a more rigorous relation for $N-\zeta$ include Sjöberg (1995, 2006, 2010) and Tenzer et al. (2006). Sjöberg (2006) suggests the effect of lateral topographic

density variation and the joint topographic roughness term may be up to a metre (or more) in the highest mountains, while Tenzer et al. (2006) find that the application of their more rigorous formula (Section 7.4.4) can result in errors of some decimetres in terrain up to 3,227 m (Kingdon et al., 2005). Flury and Rummel (2009) found maximum $N - \zeta$ of 0.48 m in two Alpine test areas; Germany (maximum height of 2,962 m) and Austria (maximum height 3,798 m) using a rigorous treatment of the effect of the topographic masses on $\bar{g}$. This result was found to be ∼50 % of the Δg_{SPB}-dependent approximation (Equation (7.52)).

7.8.2 Compatibility of $H^{N\text{-}O}$ and gravimetric quasigeoid models

In terms of compatibility with quasigeoid models, AHD $H^{N\text{-}O}$ has been considered similar to H^N for practical purposes, such as using AUSGeoid98 to transform GNSS derived ellipsoidal heights to the AHD (e.g., Featherstone, 2008). However, despite the closeness of the quasigeoid and the $H^{N\text{-}O}$ zero-reference, they are inconsistent, as follows.

Gravity values are required for the HOC (Equation (7.26)) and NC (Equation (7.40)) and C in H^O (Equation (7.25)) and H^N (Equation (7.38)). In contrast, no relation to actual gravity or geopotential appear in the NOC_R (Equations (7.5) to (7.15)). Therefore, the difference between H^N and $H^{N\text{-}O}$ is of interest since it leads to a theoretical incompatibility between $H^{N\text{-}O}$ and gravimetric quasigeoid models. However, different versions of the $H^{N\text{-}O}$ will refer to slightly different zero-references (e.g., Rapp, 1961; Heck, 1995; Bomford, 1971).

The difference between H^N and $H^{N\text{-}O}$ can be derived through Equations (7.38) and (7.4). Thus,

$$H^N - H^{N\text{-}O} = \frac{C}{\bar{\gamma}} - \frac{C^N}{\bar{\gamma}} = \frac{W_P - W_0}{\bar{\gamma}} - \frac{U_P - U_{N\text{-}O}}{\bar{\gamma}} \tag{7.53}$$

which becomes

$$H^N - H^{N\text{-}O} = \frac{(W_P - U_P) - (W_0 - U_{N\text{-}O})}{\bar{\gamma}}. \tag{7.54}$$

If we let the value of normal potential at the $H^{N\text{-}O}$ zero-reference ($U_{N\text{-}O}$) be equal to

$U_R + \delta U$ (where U_R is normal potential at the intersection of the normal plumbline $P{-}Q_0$ and quasigeoid in Figure 7.1 and δU is the unknown normal potential difference between U_R and $U_{N\text{-}O}$) and knowing the disturbing potential at point P ($T_P = W_P - U_P$), we get

$$H^N - H^{N\text{-}O} = \frac{T_P - (W_0 - (U_R + \delta U))}{\bar{\gamma}} \tag{7.55}$$

which becomes

$$H^N - H^{N\text{-}O} = \frac{T_P - (W_0 - U_R)}{\bar{\gamma}} + \frac{\delta U}{\bar{\gamma}} \tag{7.56}$$

By definition in Molodensky et al. (1962), W_P is equal to U_{Q^N} (the value of normal potential at the telluroid for point P; see Figure 7.1), so

$$T_P = U_{Q^N} - U_P \tag{7.57}$$

As ζ computed at the Earth's surface is mapped from the ellipsoid (U_0) to realise the quasigeoid, and assuming changes in the gradient of normal potential ($\partial U/\partial h$) between the telluroid and ellipsoid are negligible (the gradient changes linearly by $\sim$0.003 m^2 s^{-2}, or 0.3 mm per 1,000 m height), it can be said that

$$(U_0 - U_R) = (U_{Q^N} - U_P) \tag{7.58}$$

As the potential values (considered on a global basis) $W_0 = U_0$ (whereby, gravity effectively drops out), it is now found from Equations (7.55) to (7.58)

$$\frac{T_P - (W_0 - U_R)}{\bar{\gamma}} = 0 \tag{7.59}$$

thus, Equation (7.59) reduces to

$$H^N - H^{N\text{-}O} = \frac{\delta U}{\bar{\gamma}} \tag{7.60}$$

This shows that H^N and $H^{N\text{-}O}$ are not coincident, but depend on δU, which varies point-wise from place to place. If the value of δU were known, the difference between H^N and $H^{N\text{-}O}$ could be computed using Equation (7.60). However, this value is not known; it can only be estimated from the $H^{N\text{-}O}{-}H^N$ differences using the ANLN (see Section 7.9.5).

Regardless, it is shown that $H^{N\text{-}O}$ does not refer to the quasigeoid, but to another, poorly defined, zero-reference. This distinction is important for those attempting to use GNSS-derived ellipsoid heights and gravimetric quasigeoid models to realise accurate (cm-level) $H^{N\text{-}O}$, particularly in mountainous regions.

7.9 Comparison of different height systems over Australia

HOC, NC and NOC_R are computed for the ANLN, with EGM2008- and ANGD2007-derived g_{BM} (Chapter 6) both used for the HOC and NC, and GRS80 parameters for NOC_R. Tests to determine which latitude is most suitable for the computation of γ_0 are conducted in Section 7.9.1. Loop closures are then used (Section 7.9.2) to test the different HCs and gravity data sources (cf. Ramsayer, 1959; Kao et al., 2000; Hwang and Hsiao, 2003; Angus-Leppan, 1982).

Lastly, to enable comparisons among Helmert H^O, H^N, and $H^{N\text{-}O}$ (Sections 7.9.4 and 7.9.5), four identical minimally constrained least-squares adjustments (MCLSA) of the ANLN were run, the only variation being the different HC applied: no correction, HOC (MC_{HOC}; EGM2008 and ANGD2007), NC (MC_{NC}; EGM2008 and ANGD2007) and NOC_R (MC_{NOC_R}; GRS80). The Survey Network Adjustment Program (SNAP) developed at Land Information New Zealand (LINZ; http://www.linz.govt.nz/geodetic /software-downloads) was used for the MCLSA, with Steed (2006) *a priori* error estimates adopted (cf. Section 2.3.8). All adjustments were fixed to MSL (held to zero) at the Albany tide-gauge (Western Australia; 35° 02′S, 117° 53′E). Thus, as the (non-gravity) levelling errors (common to each adjustment) propagate similarly in each adjustment (thus cancelling each other), any variations in adjusted height is solely the result of the different HC applied.

7.9.1 Selection of constant latitude for γ_0

Although the convention is for γ_0 to be the value of normal gravity at 45°, Heiskanen and Moritz (1967, 169) consider γ_0 to be an arbitrary constant and only suggest that 45° be used. Allister and Featherstone (2001) and Kao et al. (2000) query whether a central latitude with respect to the region of the levelling network may be more appropriate. Here, the effect of using normal gravity at $\phi = 25°$ (γ_{25}; approximate central latitude for Australia) as γ_0 instead of normal gravity at $\phi = 45°$ (γ_{45}) in the HOC (Equation (7.26)) and NC (Equation (7.40)) is tested; firstly using loop closures

(cf. Section 7.9.2), then by comparison of adjusted heights. EGM2008 g_{BM} is used for this test.

Order	# loops	HOC_{25}	HOC_{45}	NC_{25}	NC_{45}
All	1366	5.219	5.210	5.217	5.209
First	56	2.414	2.408	2.407	2.404
Second	20	2.800	2.792	2.801	2.795
Third	975	4.225	4.218	4.225	4.218
Fourth	37	6.333	6.320	6.320	6.309
Third OW	256	9.204	9.187	9.200	9.185

Table 7.7: Comparisons between c_L (mm) for 1,366 supplementary and basic loops of the ANLN (cf. Table 2.4) with HOC_{25}, HOC_{45}, NC_{25} or NC_{45} (using EGM2008 gravity) applied using γ_{45} or γ_{25}.

Table 7.7 shows computed c (c_L; Equation (2.3); cf. ICSM, 2007) for ANLN loop closures (cf. Filmer and Featherstone, 2009) with HOC applied using γ_{45} (HOC_{45}) and γ_{25} (HOC_{25}) and with NC applied using γ_{45} (NC_{45}) and γ_{25} (NC_{25}). Although the differences are very small (generally <0.02 mm), c_L for HOC_{45} is always less than c_L for HOC_{25}, with c_L for NC_{45} similarly always less than that for NC_{25}.

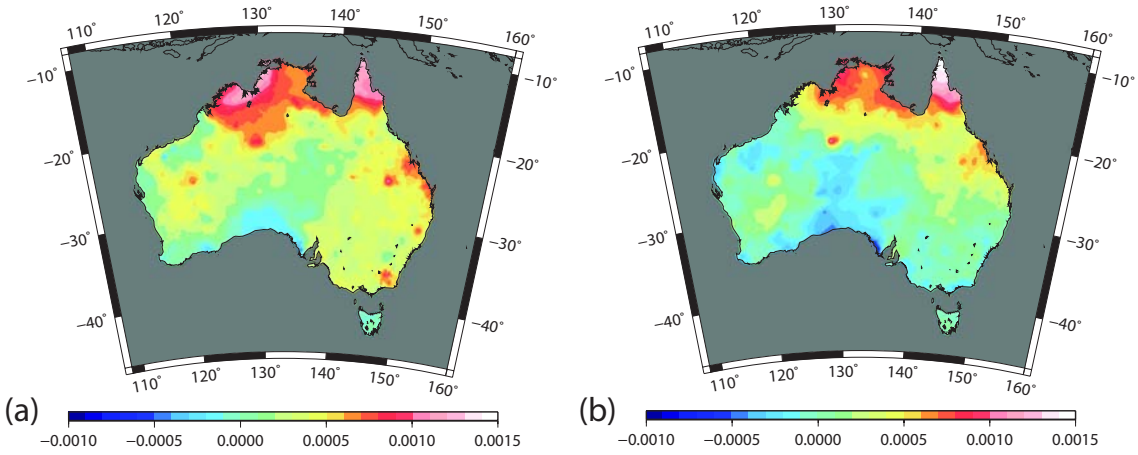

Figure 7.7: Difference between (a) Helmert $H^O_{25} - H^O_{45}$, and (b) $H^N_{25} - H^N_{45}$. Lambert projection, units in metres.

The differences between H^O and H^N (from MC_{HOC} and MC_{NC}; EGM2008 g_{BM}) using γ_{45} (H^O_{45}; H^N_{45}) and γ_{25} (H^O_{25}; H^N_{25}) are shown in Figure 7.7. Helmert $H^O_{25} - H^O_{45}$ (Figure 7.7(a)), are between 0.5 mm and 1.3 mm, with $H^N_{25} - H^N_{45}$ (Figure 7.7(b)), between 0.7 mm and 1.6 mm. Thus, the choice of γ_{45} or γ_{25} appears to have negligible effect on H^O and H^N. Due to the slightly smaller ANLN loop closures when using γ_{45}, and

that it is the convention (e.g., Heiskanen and Moritz, 1967, 169), γ_{45} will be used for the remainder of this study for HOC and NC.

7.9.2 Loop closure analysis

The effectiveness of the HCs may be seen in comparisons of levelling loop closures, as gravimetric HCs should theoretically reduce loop misclosures (cf. Sansò and Vaníček, 2006). However, the presence of other systematic levelling errors in the ANLN (Section 2.1.4), such as refraction (e.g., Chapters 3 and 4; Angus-Leppan, 1984), staff mis-calibration (e.g., Craymer and Vaníček, 1986) or expansion (e.g., Rüeger, 1997) and staff settlement (e.g., Entin, 1959) may tend to mask the benefits of applying HCs. As such, the higher precision levelling is relied upon.

c_L (Equation (2.3)) is used here as a measure of loop misclosure (cf. Section (2.4)). A comparison of loop closures for the entire ANLN is conducted first, followed by a comparison for 18 first-order loops in the Australian Alps (cf. Filmer et al., 2010). Heights in this region are often >1,000 m, rising to 2,228 m at Australia's highest point, Mt Kosciuszko (∼36° 30′S, ∼147° 15′E). Kao et al. (2000) make the point that improved loop closures do not necessarily result in more accurate heights on BMs in the loop. However, as there are no 'known' heights to check against, loop closures are a useful first test for the different HCs.

Order	# loops	No HC	HOC EGM	HOC ANGD	NC EGM	NC ANGD	NOC_R GRS80
All	1366	5.210	0.000	0.001	−0.001	0.001	0.005
First	56	2.517	−0.106	−0.025	−0.110	−0.027	−0.052
Second	20	2.879	−0.088	−0.076	−0.085	−0.085	−0.040
Third	975	4.213	0.004	0.004	0.004	0.003	0.004
Fourth	37	6.275	0.042	0.039	0.031	0.036	0.031
Third OW	256	9.185	0.002	−0.005	0.000	−0.004	0.000

Table 7.8: c_L (mm) differences are shown for 1,366 ANLN loop closures with HC applied compared to no HC. Positive values for HOC, NC (both using EGM2008 and ANGD2007 g_{BM}), and NOC_R (using GRS80 parameters) closures indicate higher c_L compared to no HC; negative indicate lower c_L (i.e., HC decreases loop misclosure).

Table 7.8 shows differences between c_L when no HC is applied and when the HOC (EGM2008; HOC_{EGM08} and ANGD2007; HOC_{ANGD}), NC (EGM2008; NC_{EGM08} and ANGD2007; NC_{ANGD}) and NOC_R are applied. The c_L for all 1,366 ANLN loops display no significant decrease for the HOC and NC (whether using EGM2008 or ANGD2007 g_{BM}) compared to no HC, while the NOC_R makes the closures slightly larger, suggesting that other errors are masking the benefits of the HC. However, the first-order levelling was ∼0.1 mm less (cf. Allister and Featherstone, 2001) and the second-order levelling almost 0.09 mm less for both HOC_{EGM08} (cf. Ramsayer, 1959; Hwang and Hsiao, 2003) and NC_{EGM08}. The NOC_R reduces loop misclosure in the first- and second-order levelling, but only by ∼50% of the HC using EGM2008 g_{BM} (cf. Rapp, 1961; Kao et al., 2000). The decrease in c_L for HOC_{ANGD} and NC_{ANGD} (compared to no HC) in the first-order levelling is only 1%, whereas the HOC_{EGM08} and NC_{EGM08} decreases by 4%. Indeed, even NOC_R c_L is less than HOC_{ANGD} and NC_{ANGD} for first-order loops, although it is acknowledged that there appears to be negligible difference between c_L using EGM2008 and c_L using ANGD2007 g_{BM} for lower precision levelling.

One explanation for the smaller first-order loop closures using EGM2008 g_{BM} is that most first-order levelling is located along the Great Dividing Range, where elevations are often >1,000 m. Poor sampling of ANGD2007 g_{obs} can occur in steep mountainous areas (Figure 7.8), where g_{obs} are taken predominately in accessible areas, often along roads that run through valleys (ANGD2007 maximum g_{obs} height is 1,975 m; Australia's maximum BM height is 2,228 m). This may lead to spatial aliasing in the ANGD2007 g_{BM} (cf. Featherstone and Kirby, 2000), resulting in HOC_{ANGD} and NC_{ANGD} being systematically too small. It is assumed (cf. Abeyratne and Featherstone, 2008) that some type of gravity 'reconstruction' procedure (e.g., Lemoine et al., 1998; Featherstone and Kirby, 2000) was used for EGM2008 to reduce the effect of spatial aliasing of ANGD2007 g_{obs} in the Australian Alps.

This would offer an explanation for the apparent superiority of EGM2008-derived g_{BM} over ANGD2007-derived g_{BM} for the loop closure comparison. It is also possible that the effect of barometric height (H_b) errors at gravity stations (Section 6.5.3), which

Bellamy and Lodwick (1968) suggest is exacerbated in mountainous terrain, could contribute to the systematic degradation of gravimetric HCs using ANGD2007-derived g_{BM} (Tables 7.8 and 7.9). However, this is likely to comprise only a small component of the differences in loop closures for HCs using EGM2008- or ANGD2007-derived g_{BM}, because the 2-3 mGal errors caused by H_b errors at ANGD2007 gravity stations are relatively small when compared to the possible error from spatial aliasing of ANGD2007 g_{obs}. For example, the 253 m difference between ANGD2007 maximum g_{obs} height (1,975 m) and maximum ANLN BM height (2,228 m) could result in a Δg_{SPB} error of $\sim$50 mGal using 0.1967 m $^{-1}$ (Heiskanen and Moritz, 1967, 131).

The third-order (and third-order one-way; OW) loop misclosures were virtually unchanged compared to no HC, with fourth-order indicating that HCs have made the loop closures larger. However, these are much lower quality levelling observations, so do not provide a sound test of small HCs. ICSM (2007) does not recommend applying HCs to levelling with precision lower than class LC (equivalent to third-order shown here) as the random levelling noise is larger than the magnitude of the corrections. As such, the results from the fourth-order will not be considered further. Note that two-way and third-order one-way/fourth-order loops are not included here due to the small sample (8 and 14 loops respectively) and their low precision (cf. Chapter 2).

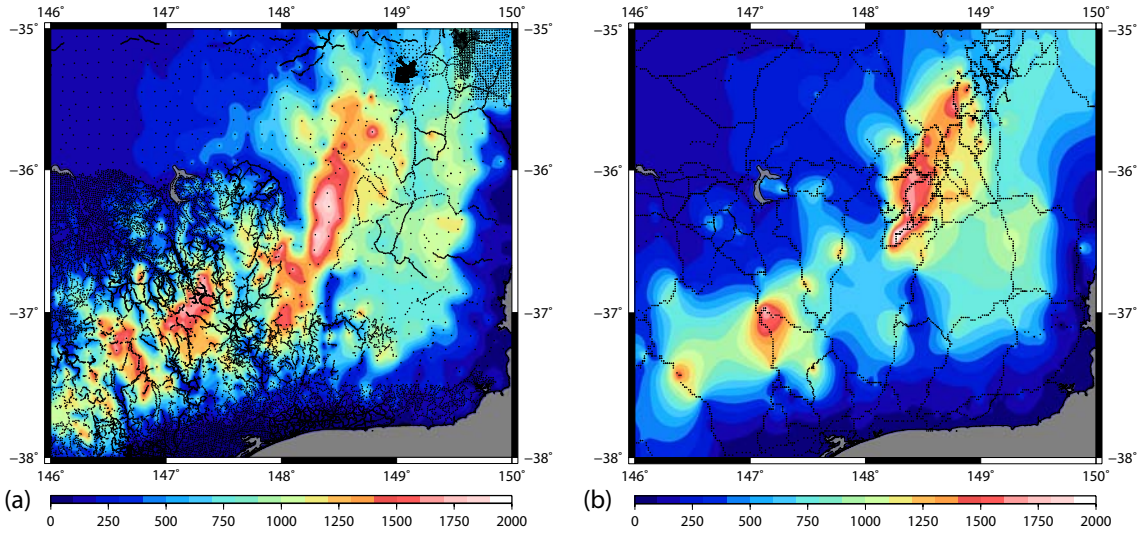

Figure 7.8: AHD $H^{N\text{-}O}$ in the Australian Alps at (a) ANGD2007 g_{obs} (black dots, maximum $H^{N\text{-}O}$ is 1,975 m), and (b) ANLN BMs (black dots, maximum $H^{N\text{-}O}$ is 2,228 m). Mercator projections, units in metres.

A comparison of maximum, minimum and mean c_L for the 18 first-order loops in the Australian Alps is shown in Table 7.9. The use of STD is not appropriate here as c_L does not have a normal distribution (Section 2.4.2; Morgan, 1992; Filmer and Featherstone, 2009). Table 7.9 indicates a decrease (compared to no HC c_L) in mean c_L of 0.47 mm (13%) for both HOC_{EGM08} and NC_{EGM08}, but HOC_{ANGD} and NC_{ANGD} show decreases of only 0.30 mm (8.5%). Mean c_L in the 18 Australian Alps loops for the NOC_R decreased by 0.22 mm (6%). The decrease in c_L is also reflected in the minimum and maximum for each different HC.

	No HC	*HOC* EGM	*HOC* ANGD	*NC* EGM	*NC* ANGD	NOC_R GRS80
Min	0.367	0.193	0.393	0.180	0.413	0.146
Max	14.464	11.630	13.518	11.629	13.544	13.865
Mean	3.540	3.068	3.237	3.072	3.241	3.319

Table 7.9: c_L (mm) for 18 first-order ANLN loops in the Australian Alps.

While acknowledging that the decrease in loop misclosure for the first-order levelling is small for both Tables 7.8 and 7.9, Table 7.8 suggests a general decrease in c_L as the quality of levelling improves. Thus, as other levelling errors (mentioned earlier) decrease in the better quality levelling, the HCs appear to become more relevant. The effect of not applying HCs at high elevations is indicated by the larger decrease in loop misclosures for the first-order levelling (using HOC_{EGM08} and NC_{EGM08}) in the Australian Alps (13%; Table 7.9), compared to first-order levelling for all ANLN loops (4%; Table 7.8). HOC_{ANGD} and NC_{ANGD} (Table 7.9) appear to be affected by the spatial aliasing of ANGD2007 g_{BM} in the Alps (discussed earlier), as they do not reduce c_L by as much as HOC_{EGM08} and NC_{EGM08} indicating that *HOC* and *NC* (neither appears superior to the other) using EGM2008 g_{BM} provides better results.

7.9.3 Effect of not applying HCs

Figure 7.9 demonstrates the effect of a MCLSA of the ANLN (no HC) compared to MC_{NOC_R} (a north-south trending difference of about 0.5 m over the continent). The convergence of the normal equipotential surfaces towards the pole dominates the

differences (cf. Rapp, 1961). Despite the lack of clear improvement from applying the NOC_R, NC or HOC to the entire ANLN in the loop closures (Table 7.8), the requirement for HCs in the north-south direction remains, because it is a systematic error that accumulates.

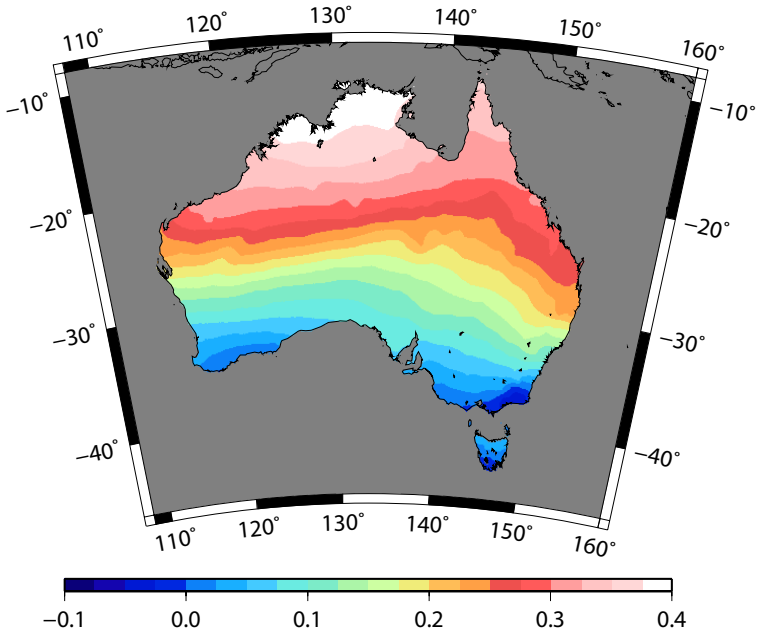

Figure 7.9: MC_{NOC_R} minus MCLSA of the ANLN with no HC applied. Comparisons are made at 4,247 ANLN supplementary and basic JPs. Lambert projection, units are in metres.

7.9.4 Differences between Helmert H^O and H^N

Figure 7.10 presents differences among Helmert H^O and H^N using EGM2008-derived g_{BM} (Figure 7.10(a)), Helmert H^O and H^N using ANGD-derived g_{BM} (Figure 7.10(b)), and geoid height N_{EGM} and height anomaly ζ_{EGM} (Figure 7.10(c)) computed from EGM2008 in **harmonic_synth.f** (see Section 7.8.1). $N_{EGM}-\zeta_{EGM}$ (Figure 7.10(c)) is computed at all ANLN BMs (94,186) compared to 4,247 JPs (from MCLSA).

Similar structures are seen in Figures 7.10(a), (b), and (c), with the increased differences correlated with height. The most notable features are the differences in central Australia around the MacDonnell and Petermann Ranges (∼25°S, 131°E; maximum difference ∼100 mm), where heights reach ∼1,000 m and contain large changes in gravity, and along the Great Dividing Range, where elevations reach 2,228 m at Mt Kosciuszko.

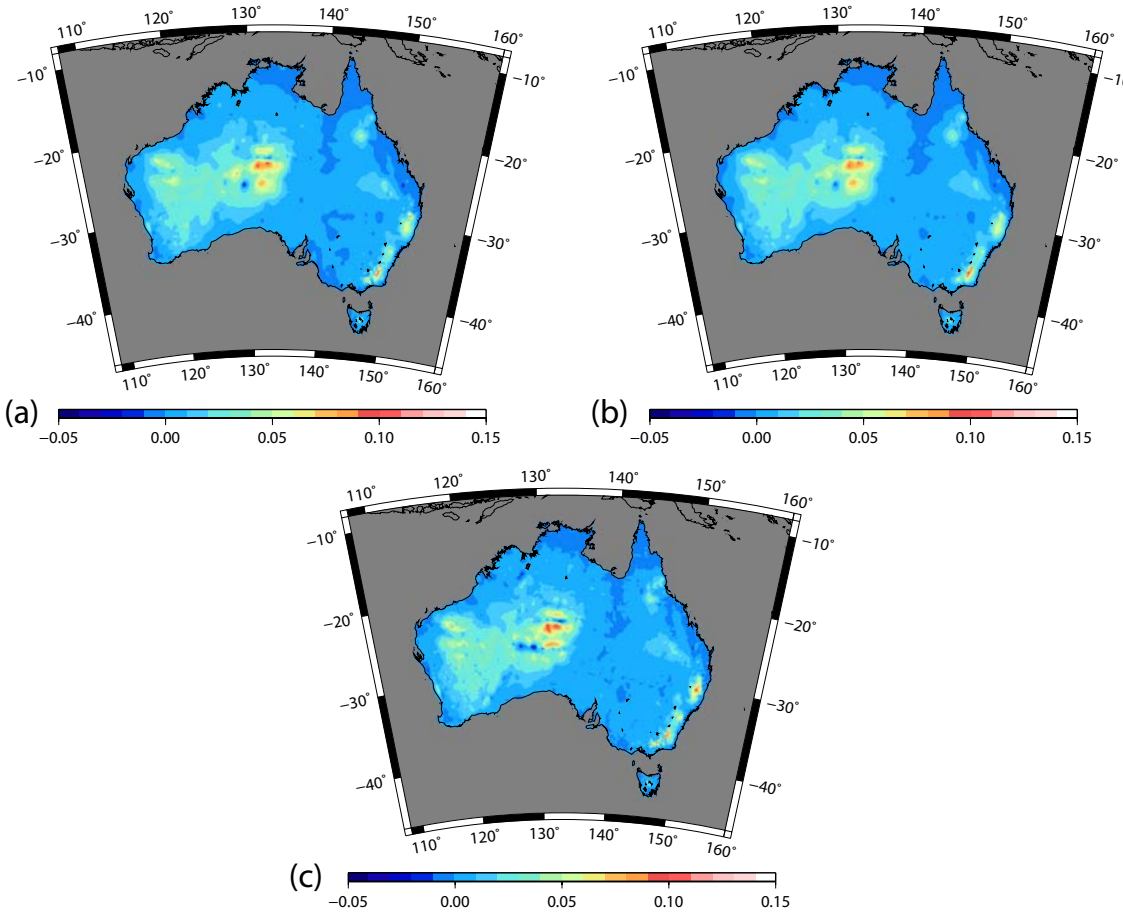

Figure 7.10: Difference over Australia among (a) Helmert $H^O - H^N$ (EGM2008 g_{BM}); (b) Helmert $H^O - H^N$ (ANGD2007 g_{BM}) and; (c) EGM2008 $N - \zeta$. Comparisons are at 4,247 ANLN JPs in (a) and (b) and at 94,186 ANLN BMs in (c). Lambert projection, units are in metres.

Table 7.10 contains the statistics of the differences between Helmert H^O and H^N over Australia (Figure 7.10) and the Australian Alps (Figure 7.11). The maximum differences in the east are ∼100 mm in places along the Great Dividing Range (Figure 7.10), with a sharp spike in the Australian Alps (Figure 7.11) of 0.26 m using EGM2008 g_{BM}. EGM2008 $N - \zeta$ computed in **harmonic_synth.f** provides similar results to Helmert $H^O - H^N$ using EGM2008 g_{BM}. However, maximum Helmert $H^O - H^N$ using ANGD2007 g_{BM} is 0.15 m in the Australian Alps.

The maximum EGM2008-derived difference of 0.26 m in the Australian Alps (Table 7.10) can be compared to the ∼0.15 m difference that Featherstone and Kirby (1998) found in the MacDonnell Ranges, but the ANGD heights used by Featherstone and Kirby (1998) did not contain the highest elevations in the Australian Alps. Some

	Australia			Alpine Region		
Stat.	(a)	(b)	(c)	(a)	(b)	(c)
Min	-23	-19	-40	-9	-10	-20
Max	263	148	264	263	148	264
Mean	7	8	9	34	35	31
STD	±17	±16	±16	±43	±34	±35
RMS	±18	±17	±18	±55	±49	±47

Table 7.10: Statistics showing differences among; (a) Helmert $H^O - H^N$ (EGM2008 g_{BM}); (b) Helmert $H^O - H^N$ (ANGD2007 g_{BM}); and (c) EGM2008 $N - \zeta$. Comparisons are at 4,247 (Australia) and 241 (Alps) ANLN JPs in (a) and (b) and at 94,186 (Australia) and 6,856 (Alps) ANLN BM in (c). Units in mm.

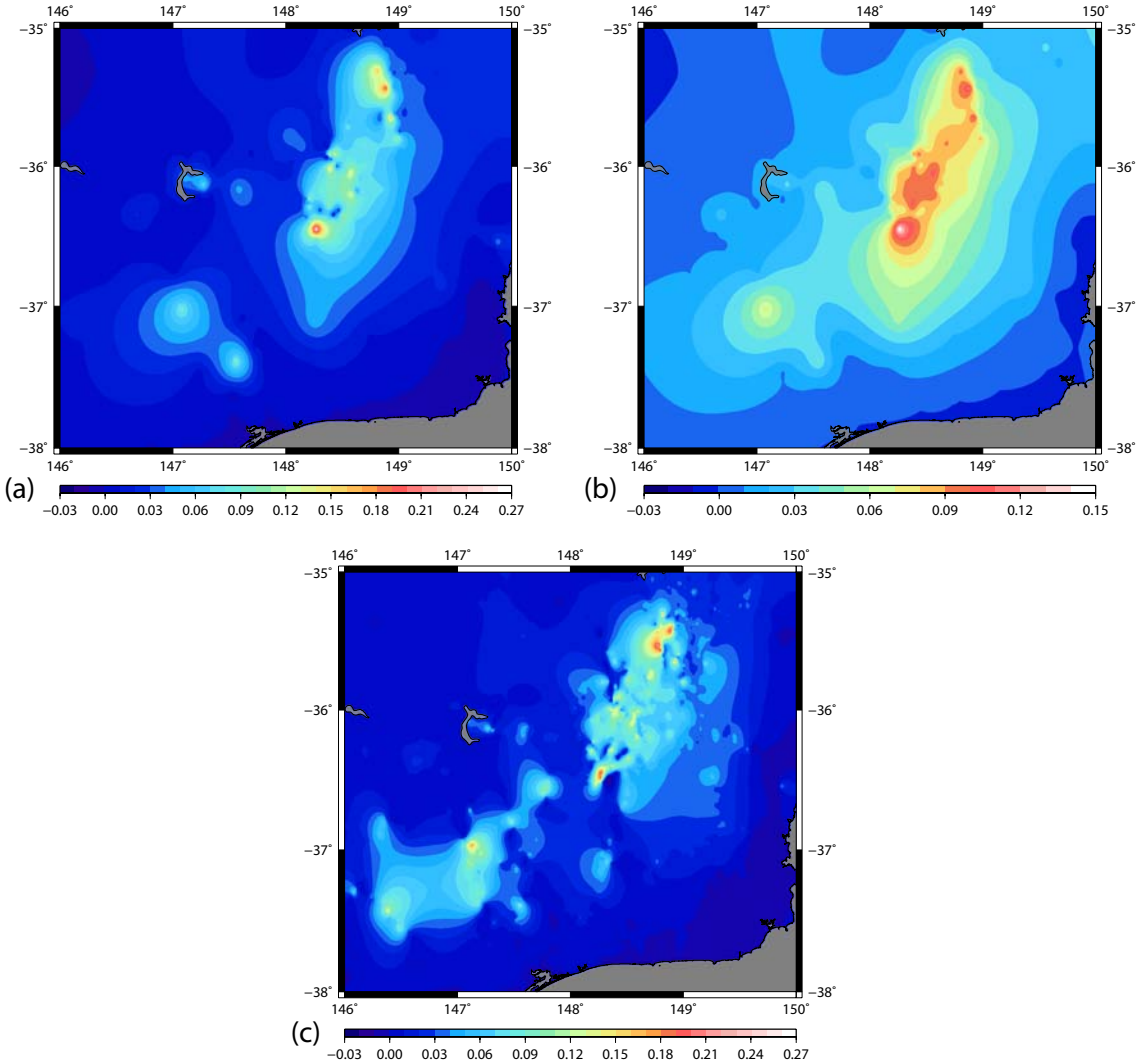

Figure 7.11: Differences in the Australian Alps among (a) Helmert $H^O - H^N$ (EGM2008 g_{BM}); (b) Helmert $H^O - H^N$ (ANGD2007 g_{BM}) and; (c) EGM2008 $N - \zeta$. Note different scale for (b) due to smaller differences. Comparisons are at 241 ANLN JPs. Mercator projection, units in metres.

international comparisons include Marti and Schlatter (2002), who computed $H^O - H^N$ differences of ∼0.48 m at elevations of ∼2,500 m in Switzerland, while Flury and Rummel (2009) found differences of ∼0.24 m and ∼0.48 m at the Zugspitze (Germany's highest mountain; 2,941 m) and Grossglockner (Austria's highest mountain; 3,798 m) European Alpine regions, respectively.

7.9.5 $H^{N\text{-}O}$ differences to Helmert H^O and H^N

Differences between Helmert $H^O - H^{N\text{-}O}$ and $H^N - H^{N\text{-}O}$ for Australia and the Australian Alps subset are presented in Table 7.11. Maximum Helmert H^O (EGM2008 g_{BM}) − $H^{N\text{-}O}$ for Australia is 0.44 m; in the Australian Alps subset, the maximum is the same, but with the RMS much higher at ±0.088 m. When Helmert H^O uses ANGD2007 g_{BM}, the maximum difference to $H^{N\text{-}O}$ is 0.31 m, with the RMS in the Australian Alps also less than when Helmert H^O uses EGM2008 g_{BM}. This indicates (not unexpectedly) much larger differences between the Helmert H^O and $H^{N\text{-}O}$ in mountainous regions (cf. Rapp, 1961; Kao et al., 2000). For H^N (EGM2008 g_{BM}) − $H^{N\text{-}O}$, the maximum is 0.18 m, but when H^N uses ANGD2007 g_{BM}, the difference is ∼0.16 m, providing further evidence that H^N is less sensitive to g_{BM} variations than Helmert H^O (cf. Sections 7.7 and 7.5).

	Australia				Australian Alps			
Stat.	(a)	(b)	(c)	(d)	(a)	(b)	(c)	(d)
Min	−27	−27	−24	−29	−25	−30	−24	−29
Max	440	311	177	163	440	311	177	163
Mean	4	2	−4	−6	53	48	19	13
STD	±26	±24	±12	±11	±70	±56	±29	±25
RMS	±27	±24	±13	±12	±88	±74	±35	±28

Table 7.11: Statistics for differences among (a) Helmert H^O (EGM2008 g_{BM})$-H^{N\text{-}O}$; (b) Helmert H^O (ANGD2007 g_{BM}) − $H^{N\text{-}O}$; (c) H^N (EGM2008 g_{BM}) − $H^{N\text{-}O}$; (d) H^N (ANGD2007 g_{BM}) − $H^{N\text{-}O}$. Comparisons are at 4,247 (Australia) and 241 (Alpine region) ANLN JPs. Units in mm.

Given that H^N and $H^{N\text{-}O}$ have previously been considered the same for practical purposes (see Section 7.8.2), a smaller difference than between Helmert H^O and $H^{N\text{-}O}$ is not unexpected. However, it confirms that H^N and $H^{N\text{-}O}$ are not consistent (cf. Equa-

tion (7.60)) and in mountainous regions >1,000 m can differ by ∼50 mm. This empirical evidence supports the derivation and discussion in Section 7.8.2.

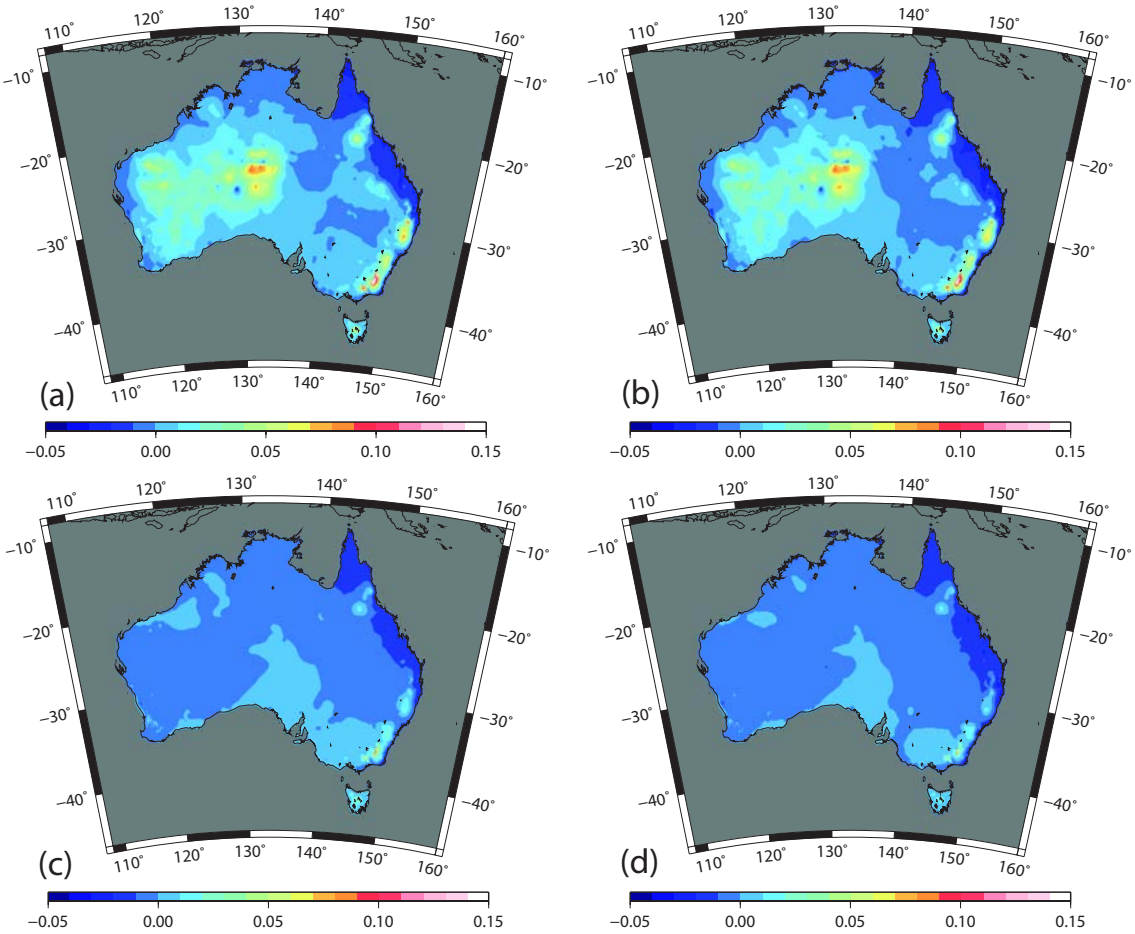

Figure 7.12: Difference over Australia among (a) Helmert H^O (EGM2008 g_{BM}) − $H^{N\text{-}O}$; (b) Helmert H^O (ANGD2007 g_{BM}) − $H^{N\text{-}O}$; (c) H^N (EGM2008 g_{BM}) − $H^{N\text{-}O}$; (d) H^N (ANGD2007 g_{BM}) − $H^{N\text{-}O}$. Comparisons are at 4,247 ANLN JPs. Lambert projection, units in metres.

Figures 7.12(a) and 7.12(b) show Helmert $H^O - H^{N\text{-}O}$ differences over Australia, with Figures 7.13(a) and 7.13(b) showing the Helmert $H^O - H^{N\text{-}O}$ differences in the Australian Alpine region. The differences approach 0.10 m in Central Australia, with the maximum of 0.44 m in the Australian Alps. The differences between using EGM2008 g_{BM} and ANGD2007 g_{BM} are not obvious in Figures 7.12(a) and 7.12(b), but were identified in Table 7.11.

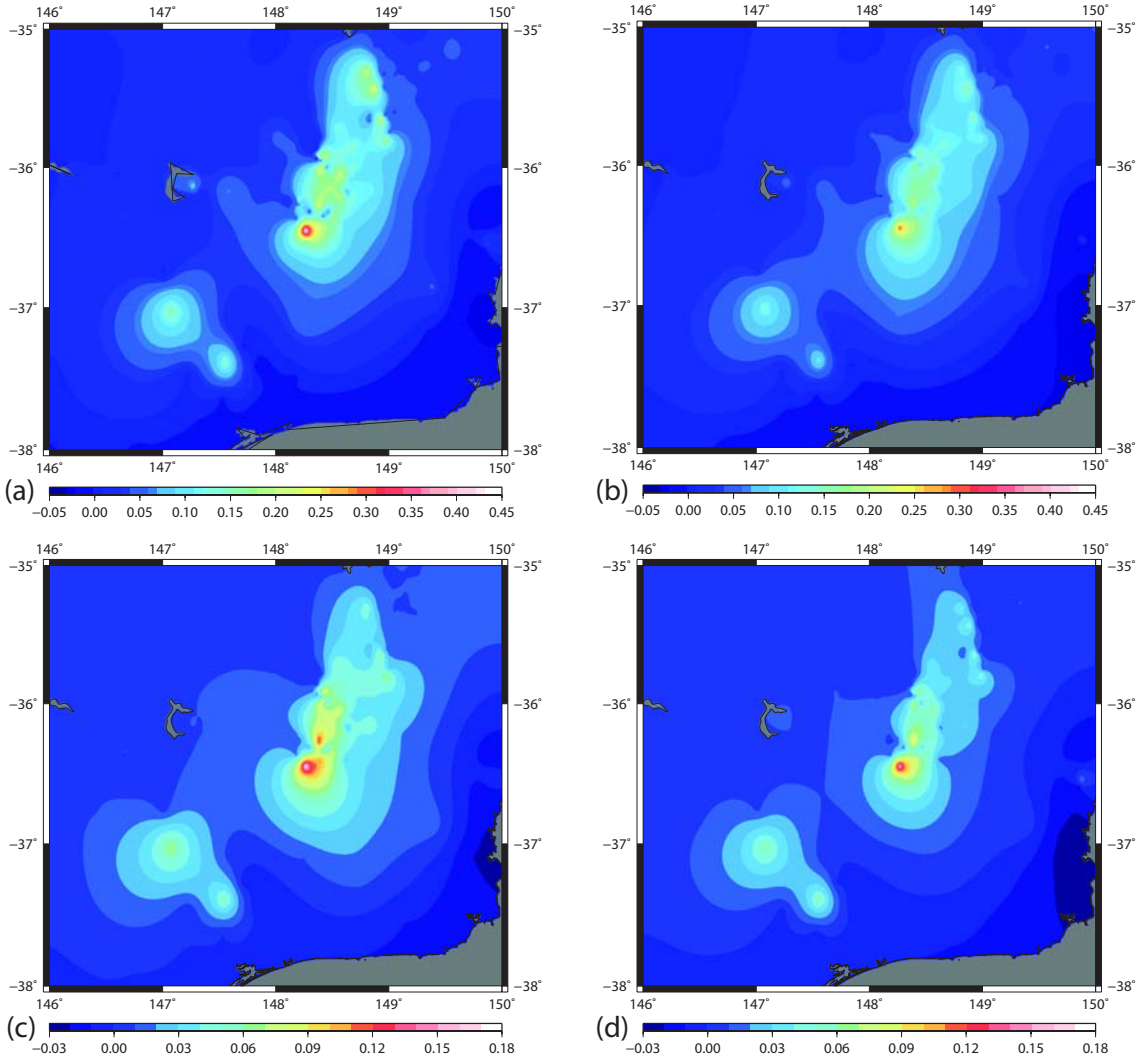

Figure 7.13: Differences in the Australian Alps among (a) Helmert H^O (EGM2008 g_{BM}) − $H^{N\text{-}O}$; (b) Helmert H^O (ANGD2007 g_{BM}) − $H^{N\text{-}O}$; (c) H^N (EGM2008 g_{BM}) − $H^{N\text{-}O}$; (d) H^N (ANGD2007 g_{BM}) − $H^{N\text{-}O}$. Comparisons at 241 ANLN JPs. Mercator projection, units are metres.

$H^N - H^{N\text{-}O}$ differences are much less over most of Australia (Figures 7.12(c) and 7.12(d)) and are generally no more than 20−30 mm in most places, but increase to ∼50 mm or more in higher-elevated regions (>1,000 m) in Tasmania and the Great Dividing Range (Figures 7.13(c) and 7.13(d)). Maximum differences between $H^N - H^{N\text{-}O}$ using EGM2008 g_{BM} and ANGD2007 g_{BM} are <20 mm (Table 7.11). The maximum differences in the Australian Alps spike in the Mt Kosciuszko area. The surrounding mountainous areas show differences <0.25 m for Helmert H^O (EGM2008 g_{BM}) − $H^{N\text{-}O}$ (Figure 7.13(a)) and <0.10 m for H^N (EGM2008 g_{BM}) − $H^{N\text{-}O}$ (Figure 7.13(b)).

7.9.6 Discussion on differences among H^O, H^N and $H^{N\text{-}O}$

Although ANGD2007 g_{BM} shows better agreement with co-located ANGD2007 g_{obs} (Section 6.4.2), the results in Section 7.9.2 suggest that EGM2008 g_{BM} is better for estimating HCs, particularly in mountainous regions. This is despite the large ($\sim\pm$ 50 mGal) EGM2008 g_{BM} minus co-located ANGD2007 g_{obs} differences in these mountainous regions (Figure 6.3). The first-order loop closures for HOC and NC are consistently smaller using EGM2008 g_{BM} than for ANGD2007 g_{BM} (Table 7.8), especially in mountainous regions (Table 7.9) suggesting that EGM2008 g_{BM} better represents Australian gravity than ANGD2007 g_{BM} (Section 7.9.2). It is assumed that this is mostly the result of the EGM2008 pre-processing methodology which has reduced the effects of spatial aliasing of ANGD2007 g_{obs} (e.g., Featherstone and Kirby, 2000), but with a possible (but probably small) contribution from systematic effects of H_b errors at ANGD2007 g_{obs} (e.g., Bellamy and Lodwick, 1968) (also see Section 6.5.3).

It follows that the differences among the different height systems in Section 7.9.4 and Section 7.9.5 using EGM2008 g_{BM} are accepted in preference to the differences using ANGD2007 g_{BM}. It is assumed that the apparent inadequacy of ANGD2007 g_{BM} is caused by the large spacings of ANGD2007 g_{obs} ($\sim$11 km for most of Australia; cf. Torge, 2001, 250), which are inadequate in mountainous areas (cf. Hirt and Flury, 2008; Flury and Rummel, 2009; Papp et al., 2009; Angus-Leppan, 1982). Combined with poor spatial sampling in these rugged areas, this leads to spatial aliasing (e.g., Featherstone and Kirby, 1998). Aliasing of ANGD2007 g_{BM} will not be identified by the validation with co-located ANGD2007 g_{obs}.

The choice of preferred height system from those tested is rather problematic. Helmert H^O provides the best physical representation of heights, but is more sensitive to large errors in g_{BM} than H^N or $H^{N\text{-}O}$. There appears to be little difference between H^N and $H^{N\text{-}O}$ <1,000 m, although above this height, H^N better represents the physical terrain. It has the advantage that errors in $\bar{\gamma}$ are unlikely to exceed $\sim$4 mGal, compared to errors in $\bar{g}$ reaching 50$-$60 mGal, which can introduce Helmert H^O errors >0.10 m (Figure 7.5). Given the problems providing accurate g_{BM} values in Australia at this

time, H^N is considered the preferred height system at this stage. H^N is superior to $H^{N\text{-}O}$ as it provides a better physical representation at high elevations, is a well defined system, and is compatible with gravimetric quasigeoid models (Section 7.8.2).

However, for the longer term, H^O with a gravimetric geoid is the preferred option as it relies wholly on actual gravity, thus providing the best physical height system. For this to happen, g_{obs} accuracy needs improving (cf. Section 6.4.2), the sampling needs to be denser, and g_{obs} 3D location needs to be accurately known (cf. Sections 6.5.6 and 6.5.7). It is also recommended that future research involve testing rigorous (Tenzer et al., 2005), Niethammer and Mader H^O in Australia (cf. Section 7.4.5) with a view to implementation in a geoid-based height system when improved data sets are available, as Helmert H^O are likely to be inadequate for a high accuracy vertical datum (cf. Kingdon et al., 2005).

7.10 Summary

$H^{N\text{-}O}$, H^O and H^N systems are introduced and assessed in this Chapter. $H^{N\text{-}O}$ do not require gravity observations, because normal gravity is used here to approximate the Earth's gravity field. The Rapp (1961) NOC was used for the AHD, but comparison with the New Zealand, Bomford (1971) and Heck (1995) NOCs revealed any difference in the magnitude of the correction to be negligible. A sensitivity test of the Rapp (1961) NOC indicated that errors in input data have minimal effect on the computed corrections.

H^O are based on C and better reflect the Earth's gravity field than $H^{N\text{-}O}$ or H^N. However, a 'true' orthometric height is difficult to compute because the integral mean of gravity along the plumbline is inside the topography and is usually approximated, giving rise to different variants: Mader, Niethammer, rigorous and Helmert H^O. Helmert H^O are the least rigorous, but easiest to compute, and is the H^O version used here. The OC is susceptible to input data errors, particularly g_{BM}, with an error in g_{BM} of 50 mGal propagating into $\bar{g}$ and causing an error in the computed OC of $\sim$0.12 m at

elevations of ∼2,000 m . H^N are also based on C, but use the integral mean of normal gravity along the normal plumbline, rather than actual gravity as in H^O. Although normal corrections are susceptible to the same errors as orthometric corrections, errors in mean normal gravity are <4 mGal, leading to an error in the normal correction of ∼10 mm at elevations of ∼2,000 m.

Comparisons using the ANLN with the three HCs gave differences between Helmert H^O and H^N of up to 0.26 m (EGM2008 g_{BM}) and 0.15 m (ANGD2007 g_{BM}) in the Australian Alps. Loop closure analysis suggests that EGM2008 g_{BM} is superior to ANGD2007 g_{BM} for computing HCs. Helmert H^O (EGM2008) are up to 0.44 m higher than $H^{N\text{-}O}$ at heights of ∼2,000 m in the Australian Alps, while differences >0.10 m appear in several locations (of high elevation) around Australia. H^N and $H^{N\text{-}O}$ are only ∼20 mm different over most of Australia, but reach 0.17 m in the Australian Alps, and can be up to 50 mm in other areas >1,000 m elevation. A theoretical derivation indicates that AHD $H^{N\text{-}O}$ is not consistent with ζ from global and regional gravimetric quasigeoid models, which is supported by the numerical study.

H^N is the most suitable height system for Australia at this time because it is clearly defined, compatible with gravimetric quasigeoids and less susceptible to gravity errors than H^O. By comparison, to realise accurate H^O (compatible with the gravimetric geoid), terrestrial g_{obs} on all ANLN BMs (particularly in mountainous areas) are required, or if this is not possible, then denser gravity surveys (possibly airborne gravity) are needed, with accurate ANLN BM positions observed for interpolation. The results of this Chapter have been published in the Journal of Geodesy (Filmer et al., 2010).

8. CONSTRAINED READJUSTMENT OF THE ANLN

The least-squares adjustment (LSA) of the Australian Levelling Survey (ALS; see Section 2.2) in 1971 to realise the AHD was staged due to the lack of computing power available at that time (Roelse et al., 1971). However, the entire Australian National Levelling Network (ANLN; Section 2.3) can now be simultaneously LS-adjusted using the CSIRO Atlas of Regional Seas 2006 (CARS2006; Ridgway et al., 2002) at tide-gauges (cf. Chapter 5) and Global Navigation Satellite System (GNSS) ellipsoidal heights (h) with the gravimetric component of AUSGeoid09 (AGQG09; Featherstone et al., 2011) to apply weighted constraints to control long-wavelength levelling errors in the ANLN (cf. Ahmad et al., 1993; Kearsley et al., 1993a; Hwang, 1997; Zilkoski et al., 1992). The vertical datum produced from this (so-called) combined LSA (CLSA; cf. Balasubramania, 1994, 16) is an interim, experimental version (referred to as the Australian Experimental Vertical Datum; AEVD), that can be considered a 'first iteration' towards developing a new vertical datum for Australia (AVD).

This Chapter will first describe the process used to detect outliers in the ANLN levelling observations (e.g., Baarda, 1968; Schwarz and Kok, 1993; Teunissen, 2006a,c,b) and re-weight those levelling observations identified as gross errors (cf. Chapter 2). Levelling sections identified as outliers are re-weighted rather than rejected because of the large number of outliers. If all were removed, redundancy in some parts of the network would be seriously reduced, particularly in the interior of Australia, where many of the outliers are found (Section 8.1.4) and would also mean that heights would be unavailable in these areas. The following sections will cover the determination of the zero-reference for AEVD and methods used to produce the CLSA. The software program used for all adjustments is Survey Network Adjustment Program (SNAP; http://www.linz.govt.nz/geodetic /software-downloads) developed by Chris Crook at Land Information New Zealand (LINZ). SNAP allows weighted constraints to be used through the 'float' command for constraints listed in the SNAP command file. Normal

height corrections (Section 7.6) were computed using Equation (7.40) with EGM2008-derived gravity (Section 6.2) which were applied to the ANLN for all LSA, producing an AEVD based on normal heights (H^N).

8.1 Outlier detection methods

The ANLN contains gross and systematic errors (Chapter 2), but because re-levelling is not currently possible, a method to identify and treat these errors is required (cf. Sections 2.4.1 and 2.5). Here, the method based on Baarda (1968) is used, as this is compatible with SNAP output (see Section 8.4). LS estimation is used in the Baarda (1968) method, but it is acknowledged that robust estimation can also be used for outlier detection (e.g., Gao et al., 1992), where the sum of the absolute residuals is minimised (Fuchs, 1982), rather than the sum of the squares of the residuals in LS estimation (e.g., Teunissen, 2006a, 6).

The LS functional model for observation equations is (Teunissen, 2006b, 45)

$$E\{\underline{\mathbf{y}}\} = \mathbf{A}\mathbf{x} \tag{8.1}$$

where $E\{\underline{\mathbf{y}}\}$ is the expectation or mean of the (m x 1) vector of observables $\underline{y}$ (the underscore indicates that y is a random variable), $\mathbf{A}$ is the (m x n) design matrix and $\mathbf{x}$ is the (n x 1) unknown parameter vector. The stochastic model is (Teunissen, 2006b, 45)

$$D\{\underline{\mathbf{y}}\} = \mathbf{Q}_{\mathbf{y}} \tag{8.2}$$

where $D\{\underline{\mathbf{y}}\}$ is the dispersion or variance of the observables and $\mathbf{Q}_{\mathbf{y}}$ is the variance matrix of the observables.

8.1.1 Hypothesis testing

When the functional and stochastic models are correct, the LS estimate $\underline{\hat{\mathbf{x}}}$ will be unbiased and have minimal variance. However, there may be errors in either the

functional model or stochastic model, resulting in a poor estimation of $\underline{\hat{\mathbf{x}}}$. By testing the correctness of the model (Equations (8.1) and (8.2); null hypothesis H_0) against a different model

$$E\{\underline{\mathbf{y}}\} = \mathbf{A}\mathbf{x} + \mathbf{C}\nabla \tag{8.3}$$

(alternative hypothesis H_A), with the vector $\mathbf{C}\nabla$ being the model error, the validity of $\underline{\hat{\mathbf{x}}}$ can be checked. There may be numerous H_A, requiring a testing procedure. Teunissen (2006c, 132-136) describes such a procedure that includes three steps: detection, identification and adaption (Sections 8.1.2, 8.1.3 and 8.1.4). However, statistical tests are estimates and depend largely on the strength of the model, which can be determined using the concept of reliability (Teunissen, 2006b, 45; also see Section 8.1.5).

Errors made in hypothesis testing are either type I or II errors. Type I errors are made when H_0 is rejected incorrectly, while type II errors are when H_0 is accepted, but is false (Teunissen, 2006b, 51). The level of significance (α) determines the probability of a type I error occurring, while the probability of a type II error occurring is given as β_t. However, the power of the test (γ_P; $\gamma_P = 1 - \beta_t$), is often used to describe the probability of type II errors occurring (Teunissen, 2006b, 65). The critical value (CV) at which H_0 is rejected depends on the selection of α. For example, selecting $\alpha = 0.001$ (0.1%) indicates that a type I error will occur in 1 out of 1000 tests (Teunissen, 2006b, 54).

8.1.2 Detection

The detection step checks the overall validity of H_0 using the variance factor ratio (VFR; cf. Harvey, 2006, 145) test. The VFR test is also referred to as the global or overall model test (e.g., Knight et al., 2010; Teunissen, 2006c), and is (e.g., Teunissen, 2006c, 133)

$$\text{VFR} = \frac{\hat{\sigma}^2}{\sigma^2} > \frac{\chi^2_\alpha(D_F, 0)}{D_F} \tag{8.4}$$

where $\hat{\sigma}^2$ is the *a posteriori* variance factor, σ^2 the *a priori* variance factor of unit weight, χ^2_α the chi-squared distribution with α the chosen significance level and D_F the degrees of freedom or redundancy ($m - n$). If the VFR is $>\chi^2_\alpha(D_F, 0)$ (taken from

χ^2 tables for the respective α and D_F), then the VFR test fails (cf. Section 8.4.1). The VFR test may fail if there are gross or (unmodelled) systematic errors in the observations, or the *a priori* standard deviations (STDs) are over- or under-optimistic (cf. Knight et al., 2010). However, while the VFR test (when used as an overall model test) can indicate the presence of errors, it does not identify the type and location of errors (Teunissen, 2006c, 62).

8.1.3 Identification

The identification step attempts to identify the type of error that has caused the rejection of H_0 (VFR test fails) using outlier detection (OD) methods (Teunissen, 2006c, 62). The OD method used here (see Section 8.4.1) is based on the data snooping technique of Baarda (1968), where each individual observation is tested for a gross error (e.g., Schwarz and Kok, 1993). The test used here is the w-test because it is used in SNAP. When the variance matrix Q_y is diagonal, it becomes (Teunissen, 2006c, 134)

$$w_i = \frac{\hat{e}_i}{\sigma_{\hat{e}_i}} \tag{8.5}$$

where w_i is the w-test of the i^{th} observation, $\hat{e}_i$ the LS residual for this observation and $\sigma_{\hat{e}_i}$ the STD of the residual. w_i is also known as the standardised residual (SR; e.g., Koch, 1988, 339), which is output by SNAP. An alternative method of outlier detection to the Baarda (1968) method is the τ test (Pope, 1976). However, Schwarz and Kok (1993) find that both methods provide similar results, with neither demonstrating a clear advantage. As such, the w-test is used here.

8.1.4 Adaption

The adaption step requires some form of corrective measures when errors have been identified (Teunissen, 2006c, 63). This can involve either re-measurement of the erroneous observations, adding additional parameters that model the identified errors, or re-weight or remove observations. When gross errors are identified, re-measurement is the desired option. However, re-measuring sections of the ANLN is a large task (cf.

Morgan, 1992) and not possible for this project. Therefore, re-weighting or removing identified errors are the only remaining options (see Section 8.4.2). Re-weighting is preferred, because removing large numbers of outliers in the ANLN would lead to an unsatisfactory loss of redundancy and benchmark (BM) coverage. This is particularly so in regions with multiple outliers (usually in remote areas where the ANLN is already sparse; see Figure 2.2), because removing all outliers may result in removing much of the network.

Iterative outlier detection and re-weighting (ODRW) is used in Section 8.4, where, following a minimally constrained LSA (MCLSA) of the ANLN, the observation with the highest |SR| is re-weighted. The MCLSA is then repeated, with the observation with the highest |SR| again re-weighted (e.g., Schwarz and Kok, 1993). This process is continued one observation at a time (cf. Ding and Coleman, 1996), until no observation shows |SR| > |CV|.

8.1.5 Internal reliability

Reliability refers to the strength of the model (Equations (8.1) and (8.2)), with internal reliability described by the minimal detectable bias (MDB; Teunissen, 2006b, 66), which is referred to as the marginal detectable error (MDE) in SNAP (cf. Harvey, 2006). The MDB is the size of model error that can just be detected with a probability γ_P (Section 8.1.1) using the w-test and is (Teunissen, 2006b, 66)

$$|\nabla_i| = \sigma_{y_i} \sqrt{\frac{\lambda_p(\alpha, 1, \gamma_P)}{r_i}} \tag{8.6}$$

where λ_p is the non-centrality parameter, σ_{y_i} is the *a priori* STD of the i^{th} observation, and r_i is the i^{th} local redundancy number which is a dimensionless number that always lies in the closed interval $0 \leq r_i \leq 1$ (Harvey, 2006, 203).

r_i is given as (Teunissen, 2006c, 104)

$$r_i = 1 - \frac{\sigma^2_{\hat{y}_i}}{\sigma^2_{y_i}} \tag{8.7}$$

where $\sigma^2_{y_i}$ the *a priori* and $\sigma^2_{\hat{y}_i}$ the *a posteriori* variance of the same observation. Commonly used values for geodetic networks are $\alpha = 0.001$ and $\gamma_P = 0.80$ (Teunissen, 2006b, 67). When $|\nabla_i|$ is large, the size of the error must also be large for the w-test to correctly detect it. The influence of r_i on $|\nabla_i|$ can be seen in Equation (8.6), where a large r_i (close to 1), will result in a small MDB, allowing smaller errors to be found.

8.2 Data used

The data used in the CLSA are: a recently available set of 1,052 3D GNSS coordinates (Hu, 2009, supplied by GA; N. Brown 2009, pers. comm.) processed in the International Terrestrial Reference Frame 2005 (ITRF2005; Altamimi et al., 2007), the ANLN (Section 2.3), CARS2006 (Section 5.3.1) and AGQG09 (Section 5.3.8). Additional information such as ANLN loop closures (Section 2.4) are used to assist ODRW decisions (e.g., estimating magnitude of error in a suspect section) where misclosures for adjacent loops both containing the suspect section are of similar magnitude, but opposite signs.

Preliminary comparisons of MCLSA of the ANLN (MC ANLN; H^N_{MC}) and the 1,052 GNSS (h)−AGQG09 (ζ_{AG09}) heights (referred to herein as H_{AG09}) found nine H_{AG09} with differences of 1−1.5 m to surrounding $H_{AG09}-H^N_{MC}$ differences. These nine H_{AG09} (located in Queensland; Qld) were considered outliers, so were removed from the dataset (cf. Featherstone et al., 2011) as they were suspected to have blunders in the processed ITRF h. G. Johnston (2010, pers. comm.) later confirmed that some GNSS observations in Qld were processed without antenna heights. One additional GNSS point (33EC) was not properly connected to the ANLN, so was also removed. This left 1,042 GNSS points available, with the appropriate number constrained and the remainder used to test the CLSA (Sections 8.5.4 and 8.5.5).

8.3 Stochastic model for LSA of the ANLN

8.3.1 Difficulties estimating *a priori* STD for LSA

The choice of stochastic model (or more specifically assigning *a priori* STD to the observations) for the LSA of the ANLN poses a number of difficulties. Although predominately a third-order network (Morgan, 1992), the ANLN contains numerous different types of levelling (of varying precision; heteroscedastic; e.g., Hekimoğlu and Berber, 2003), many of rather poor quality (Chapter 2). In addition, the different ANLN levelling types (see Sections 2.3.3−2.3.7) are affected differently by gross (Section 2.1.5) and systematic (Section 2.1.4) levelling errors.

Rigorous methods such as variance component estimation (VCE; e.g., Rao, 1971) can be used to obtain precision estimates for the stochastic model (e.g., Kotsakis and Sideris, 1999). However, the presence of systematic errors will reduce the effectiveness of this method (Fotopolous, 2005) and the gross errors will also bias the variance estimates. Correlations also exist among the observations (e.g., the interdependence of refraction and magnitude of height difference; Chapter 3), but here will be assumed not to exist, so the variance-covariance (VCV) matrix is diagonal (cf. Lucht, 1971).

Here (Section 8.3.4), *a priori* STD for the different levelling types will be estimated from empirical loop closure information (Section 2.4) and ICSM (2007) c-value (cf. Section 2.3.8; Kearsley et al., 1993a; Steed, 2006), which determines the maximum allowable misclosure between forward and backward levelling runs, and loop misclosures. *a priori* STD estimates from a combination of these two sources are the only available. Note that Steed (2006) *a priori* STD estimates have previously been considered adequate for comparison purposes requiring LSA of the ANLN in this thesis (e.g., Sections 2.3.8, 4.2.4, and 7.9).

8.3.2 Estimating *a priori* STD from ICSM (2007) *c*-value

A defined maximum allowable misclose between forward and backward levelling runs is the established method of identifying and rejecting blunders or systematic errors in levelling (Schomaker and Berry, 1981, 3-6). ICSM (2007) uses Equation (2.2) ($r_m = c\sqrt{d}$), where r_m is the maximum allowable misclose (mm), c determines r_m for the different class/order of levelling (ICSM, 2007, A-13; also see Table 2.3 in Section 2.3) and d is the distance between BMs in km. ICSM (2007) suggests that c is derived from empirical observations, but does not indicate the basis for adopting these particular values, although it is stated that c is at 1 STD (1σ). However, it is unlikely that c is 1σ given that observations are not usually rejected at the 68% confidence level (see Section 2.3.8). Schomaker and Berry (1981, 3-6) indicate that values equivalent to c are at the 95% confidence level in the US.

Attempting to derive *a priori* STD (equivalent to σ_1; unit STD over 1 km; see Equation (2.1) and Section 2.1.3) for levelling observations from c is rather problematic (cf. Section 2.3.8). Steed (2006) estimates *a priori* STD for the different ANLN levelling types, based on the assumption that ICSM (2007) c is 2σ (cf. Schomaker and Berry, 1981) and can thus be divided by two to provide an estimate of *a priori* STD (σ_1). By comparison, Kearsley et al. (1993a) suggests that c is usually based on 3σ, and that dividing c by three for each levelling class/order will yield *a priori* STD. However, it is not clear that simply scaling c by two (for 2σ) or three (for 3σ) to obtain *a priori* STD is appropriate. Here, it is suggested that c is based on the STD of the differences of the forward and backward levelling runs and not the observations themselves, as suggested by Kearsley et al. (1993a) and Steed (2006), although it is not clear whether Schomaker and Berry (1981) expect the observations or the misclosures to exceed the (95%) tolerance 5% of the time.

Letting Δn_F be the height difference of the forward run, and Δn_B the backward run, the misclose (ε_L) is

$$\varepsilon_L = \Delta n_F - \Delta n_B \tag{8.8}$$

where ε_L must be less than $c\sqrt{d}$. Assuming that Δn_F and Δn_B have the same STD

(σ_{obs}; $\sim\sigma_1$) which are normally distributed with zero mean $N(0, \sigma)$ and using the linear propagation of errors, it is postulated that the STD of ε_L (σ_L) is (assuming ε_L is also $N(0, \sigma)$)

$$\sigma_L = \sqrt{\sigma_{obs}^2 + \sigma_{obs}^2} = \sqrt{2\sigma_{obs}^2}. \tag{8.9}$$

Now, assuming that c is intended to reject observations at the 95% confidence level (scaled by 1.96 for 1D; e.g., ICSM, 2007, A-19), then

$$c = 1.96\sqrt{2\sigma_{obs}^2} \tag{8.10}$$

so that, rearranging,

$$\sigma_{obs} = \frac{c}{2.771858} \tag{8.11}$$

which indicates that c should be divided by 2.771858 for c-derived (at 1σ) *a priori* STD (σ_c; note that $\sigma_c = \sigma_{obs}$ in Equation (8.11)) (cf. Steed, 2006; Kearsley et al., 1993a). This can be compared with Bomford (1971, 239) suggesting that the criterion for rejecting levelling runs should be when the misclosure of Δn_F and Δn_B is $\sim$2.5 times the expected STD of the observations. σ_c are shown in Table 8.1 (column a). To calculate σ_c, ICSM (2007) c is adopted for first- to fourth-order, with the Steed (2006) interpretation of c (see Table 2.3) adopted for third-order one-way (OW) and two-way (undefined order; UO; Steed, 2006) sections (see Section 8.3.4).

8.3.3 Estimating *a priori* STD from levelling loop closures

Estimates of *a priori* STD can also be made using empirical data, such as average computed c (c_L; Equation (2.3); also see Section 2.4.1) from 1,366 ANLN levelling loops (Table 2.4). c_L is the unit loop misclosure for one km of levelling (mm), which propagates according to $\sqrt{d}$ (cf. Section 2.1.3). However, while adopting average c_L as *a priori* unit STD (Table 8.1) is a more accurate representation of *a priori* STD for the ANLN, these estimates are also not without problems.

It is likely that c_L are over-optimistic (see Section 2.4.3) because compensating errors (opposite sign, but similar magnitude; Holloway, 1988) in different sections comprising

the loop allow c_L to be below ICSM (2007) c, despite containing potentially large errors. The bias in c_L resulting from undetected compensating errors is likely to be exacerbated in the OW levelling and larger loops where multiple compensating errors may be present, resulting in c_L not properly reflecting the quality of the levelling.

8.3.4 *a priori* STD selected for LSA

Estimates of *a priori* STD for LSA of the MC ANLN (σ_c, c_L) are shown in Table 8.1, including those finally adopted for the CLSA (σ_A). Also shown are empirically determined *a priori* STD for US levelling data (σ_{US}; first-order, class II; second-order, class II; third-order), as shown in Zilkoski et al. (1992). A comparison with ANLN second- and third-order *a priori* STD (Table 8.1) indicate good agreement among σ_c, c_L and σ_{US}. However, while first-order σ_{US} and σ_c are in good agreement, c_L is larger by 1 mm, providing evidence that ANLN so-called first-order levelling is not of first-order quality (cf. Section 2.4.3; Morgan, 1992).

Roelse et al. (1971)	STD (1σ; mm)				
Order	σ_c	c_L	σ_{ST}	σ_{US}	σ_A
First	1.4	2.4	2.0	1.4	3.0
Second	2.9	2.8	4.0	2.8	3.0
Third	4.3	4.2	6.0	4.2	4.5
Fourth	6.5	6.3	9.0	NA	6.5
Third OW	13.0	9.2	18.0	NA	13.0
Two-way	13.0	10.6	18.0	NA	13.0

Table 8.1: *a priori* STD estimates (1σ) comparing: c-derived STD (σ_c), ANLN empirically-derived STD (c_L; Table 2.4), Steed (2006) c-derived σ_{ST}, US empirically-derived STD (for one km of single-run levelling) (σ_{US}; Zilkoski et al., 1992) and ANLN STD estimates adopted for CLSA (σ_A).

In addition, a study comparing the 1975-76 first-order levelling along the NSW-Qld coast to sea surface topography models (SSTMs; cf. Section 5.3) suggested large errors in this survey. This was particularly so between Bundaberg and Cairns (apparent systematic differences; cf. Morgan, 1992), where a new OW rapid first-order technique was employed. The general conclusion is that although ANLN first-order c_L suggests that ANLN first-order is more precise than second-order levelling (by 0.4 mm), it

is appropriate that both are assigned the same *a priori* STD. First- to fourth-order levelling were assigned *a priori* STD (Table 8.1) based on a pragmatic combination of σ_c and c_L, generally increased slightly to allow for the possibility of hidden gross or systematic errors (e.g., Morgan, 1992; Holloway, 1988) in c_L, and the generally noisier nature of the ANLN (cf. Kearsley et al., 1993a).

A comparison of σ_c, c_L and σ_{US} with Steed (2006) *a priori* STD (σ_{ST}) suggests that the Steed (2006) strategy of dividing c by two provides *a priori* STD that are too large. Although the VFR for MC ANLN using σ_{ST} (VFR = 1.077) passes the VFR test (<1.100; χ^2_α VFR CV for $\alpha = 0.001$) suggesting σ_{ST} is appropriate, the ANLN is known to contain many errors. It is postulated that the higher σ_{ST} is hiding the errors, indicating that the 'true' *a priori* STD is similar to that suggested by σ_A (Section 8.4.1).

Third-order OW and two-way UO σ_c is dependent on adopting $c = 36$ (as per Steed, 2006). σ_{ST} for third-order OW and two-way UO (Table 8.1) appear too high, but on the other hand, it is likely that compensating errors in these third-order OW and two-way UO sections cause c_L to be over-optimistic. Determining realistic *a priori* STD estimates for third-order OW and two-way UO sections is therefore rather problematic. In this case, σ_c appears the most realistic number (13 mm), and is adopted here for third-order OW and two-way UO *a priori* STD (Table 8.1). It is acknowledged that all of the *a priori* STD estimates in Table 8.1 are something of a best 'guesstimate' based on the available information.

8.4 Outlier detection in the ANLN

This section describes the ODRW process and results. The confidence level used here is 99.9% based on $\alpha = 0.001$ (Teunissen, 2006b, 67), providing a CV of ±3.29.

8.4.1 Outlier detection and identification method for the ANLN

The detection (cf. Section 8.1.2) and identification (cf. Section 8.1.2) of levelling errors in the ANLN is described here. The *a priori* STD estimates used are σ_A in Table 8.1. SNAP outputs a standardised residual (SR; absolute SR output by SNAP; |SR|) that is equivalent to w_i (Equation (8.5); see Section 8.1.3).

The iterative process began with a MC ANLN fixed at MSL (held to zero) at the Albany tide-gauge (35°02′S, 117°53′E; for AHD(mainland)) and the Hobart tide-gauge (42°52′S, 147°20′E; for AHD(Tas)). The initial MC ANLN statistics can be seen in Table 8.2. The number of observations with |SR| >3.29 was 148 out of 7,305 observations (2,018 degrees of freedom), which is ∼2.0% of observations. If the 1,042 GNSS points are removed (these were all connected by a single observation, but none are constrained in this ODRW process), this becomes 6,263 observations and ∼2.4%. However, as one large error may cause several observations to have |SR| > |CV|, the true number of outliers is likely to be less than 148 (cf Ding and Coleman, 1996).

	pre-ODRW	post-ODRW
VFR	1.583	1.145
# outliers (|SR| >3.29)	148	0
maximum |SR|	6.743	3.214
SSR	3195.3	2310.9

Table 8.2: MC ANLN statistics before and after the ODRW process. SSR is the sum of squared residuals; D_F = 2,018.

The VFR from the initial MC ANLN is 1.583 (Table 8.2). CV for VFR for $\chi^2_\alpha(D_F, 0)$ (D_F = 2018) is 1.100 (calculated at http://www.stat.tamu.edu/w̃est/applets/chisq demo.html), indicating the VFR test has detected discrepancies between the observations and the functional and/or stochastic models (cf. Knight et al., 2010). Here, it is assumed that the stochastic model is satisfactory as no better information is available, but also because it is known that there are gross errors and systematic errors in the ANLN (Chapter 2) that are assumed to be primarily responsible for the failure of the VFR test.

For the identification phase (cf. Section 8.1.3) the SR of the observations are examined (SNAP lists observations from the highest |SR|), with all observations with |SR| >3.29 considered outliers. The observation with the highest |SR| was then re-weighted (cf. Section 8.4.2) with a MC ANLN re-adjusted with the re-weighted observation. The ODRW process is continued until |SR| < |CV| for all observations.

8.4.2 Re-weighting strategy

ANLN loop misclosures (Chapter 2) and MDB values (Equation (8.6)) output for each observation were used as a guide to re-weight the observation with the highest |SR| for each iteration of MC ANLN (see Section 8.1.4 for why re-weighting is used in preference to removing outliers). Adjacent loop misclosures (Figure 8.1) for a levelling section with the highest |SR| provide a first estimate of the magnitude of the error (for adjacent loop closures with similar magnitude, but opposite signs; all levelling loops summed clockwise), which can be used as an estimate for the re-weighted *a priori* STD (σ_{RW}; cf. Harvey, 2006, 198). The MDB also provides a guide for σ_{RW}, as it indicates the minimum error that can be detected in the observations given the network redundancy and *a priori* STD.

After re-weighting, the LSA of the MC ANLN is re-run (iterative ODRW; e.g., Schwarz and Kok, 1993). If the observation has been correctly re-weighted, the |SR| for that observation in the new MC ANLN should be close to one, indicating that the LS residual for the observation is similar to its STD. If |SR| <1, the new residual for the observation can provide an estimate of the error and can be used as a second iteration for σ_{RW} (e.g., Harvey, 2006, 198).

However, difficulties were encountered in some regions with multiple errors (see the example below), where the MDB could be larger than the adjacent loop misclosures, which could also be of different magnitudes and/or have the same sign. This situation made estimating σ_{RW} difficult for some observations, with the risk that a good observation could be re-weighted (type I error; see Section 8.1.1), or one (or more) observations may contain errors, but be accepted as correct (type II error). Using a

significance level of $\alpha = 0.001$ is intended to reduce the possibility of type I errors, but at the expense of increasing the likelihood of type II errors.

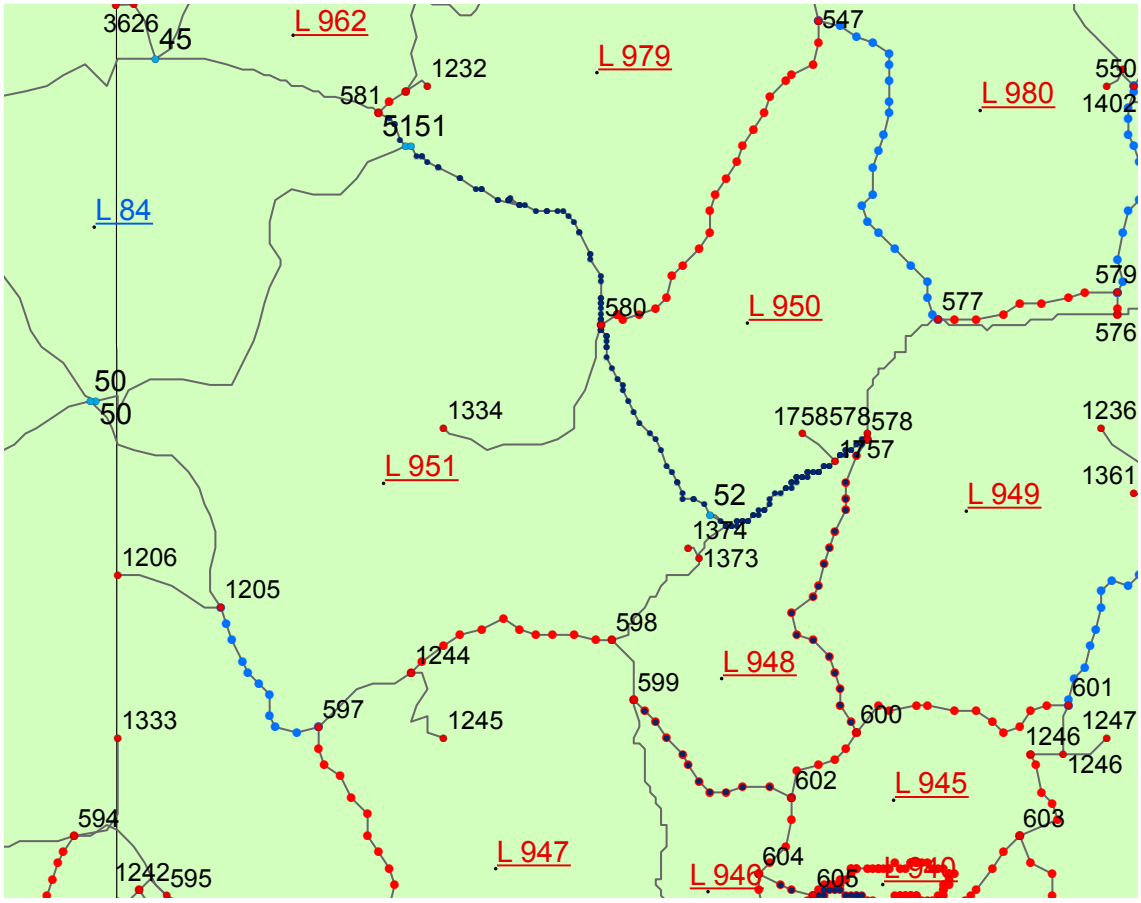

Figure 8.1: Loops 950 (L 950 in red) and 951 (L 951 in red) in western Qld near the Northern Territory border (straight vertical line). BMs highlighted as dark blue are in sections with initial |SR| < |CV|, red are third-order OW sections, light blue are two-way, and thin grey lines represent third-order sections (cf. Figure 2.2).

Some observations were difficult to assess, but many were quite straightforward. For example third-order section 52−580 (Qld; Figure 8.1) had an |SR| of 5.30 and MDB of 0.398 m. This section is common to loops 950 and 951, which have loop misclosures of +0.451 m (c_L of 20.5 mm) and −0.462 m (c_L of 17.3 mm) respectively. The *a priori* STD of 0.0398 m was re-weighted to 0.450 m on the basis that the MDB indicates the error is at least 0.398 m and considered the lower bound for the magnitude of error, with 0.462 m (adjacent loop misclosure) the upper bound. The re-weighted *a priori* STD (0.450 m) for the section 52−580 observation resulted in an |SR| of 1.11 for this observation after re-adjustment, with the number of observations above the |CV| falling from 118 to 109, indicating that this error was causing other observations

to have |SR| > |CV|.

Although re-weighting section 52−580 (σ_{RW} = 0.450 m) appears to be the appropriate decision, it is confused by the fact that neighbouring loops 948 and 949 have misclosures of −0.633 m (c_L = 32.0 mm) and +0.557 m (c_L = 25.2 mm). No section that comprises loop 949 appeared as the highest |SR| in the ANLN-only ODRW process, although section 578−600 was identified and re-weighted in the CLSA stage (Section 8.5.5). This suggests that a type II error resides in loop 949, possibly because the re-weighting of levelling section 52−580 has allowed the error in this observation to be absorbed into the surrounding region sufficiently for the observation's |SR| to be below the |CV| (cf. Prószyñski, 2000). This is the masking effect where the influence of one gross error is masked by the presence of a second (or more) adjacent gross error (Hekimoğlu, 1997).

The ODRW process was continued until |SR| <3.29 for all observations (Table 8.2). At this stage, the VFR was 1.145, which still fails the VFR test for χ^2_α (VFR CV = 1.100; see Section 8.4.1). The options to achieve VFR <1.100 were to increase α from 0.001 (lowering the |CV|, and thus increasing outliers), and repeat the ODRW process, or to scale the *a priori* STD so that VFR is one. Due to the suspected multiple outliers in some regions of the ANLN, difficulties estimating σ_{RW}, and the possible loss of strength in the network if too many sections (particularly in regions of low redundancy) were re-weighted, the 'pragmatic' solution of scaling the *a priori* STD was adopted.

8.4.3 Results of MC ANLN ODRW process

Figure 8.2 shows differences between post-ODRW and pre-ODRW H^N_{MC}. The overall effect of the ODRW process is to increase H^N_{MC}, with post-ODRW H^N_{MC}−pre-ODRW H^N_{MC} having a mean of +0.105 m, STD ±0.091 m and RMS of ±0.139 m (see Table 8.3(a)), although the differences are not a good approximation of a normal distribution (Figure 8.3). There are about six locations scattered through central and central-eastern Australia (Figure 8.2) where post-ODRW H^N_{MC}−pre-ODRW H^N_{MC} are less than −0.10 m, but the most prominent features are in central, north-western and north-eastern (Cape York) Australia where post-ODRW H^N_{MC}−pre-ODRW H^N_{MC} is

>0.30 m. Other regions in south eastern (Victoria), central and northern Australian indicate post-ODRW H^N_{MC} to be ∼0.15 m higher than pre-ODRW H^N_{MC}.

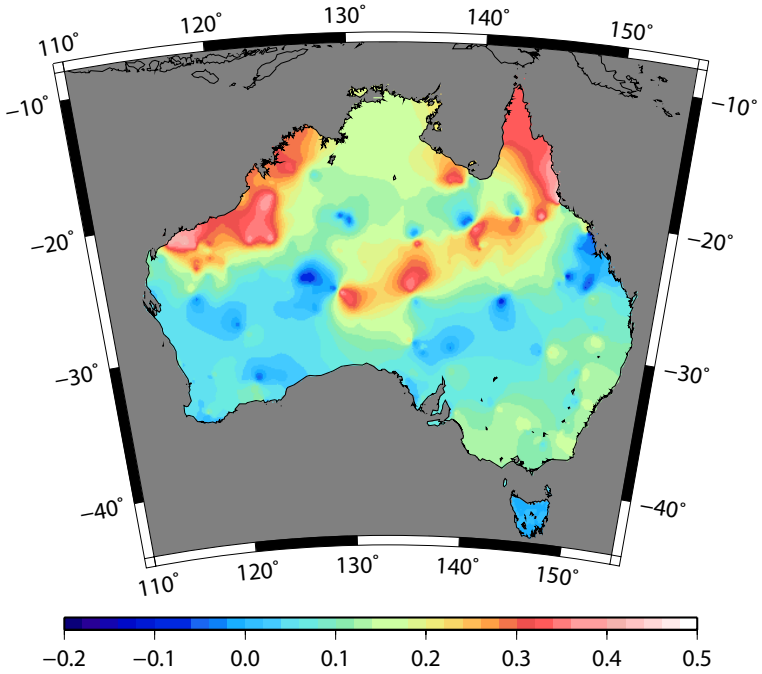

Figure 8.2: Differences between MC ANLN H^N_{MC} before and after the ODRW process. Differences at 4,247 ANLN JPs. Lambert projection, units in metres

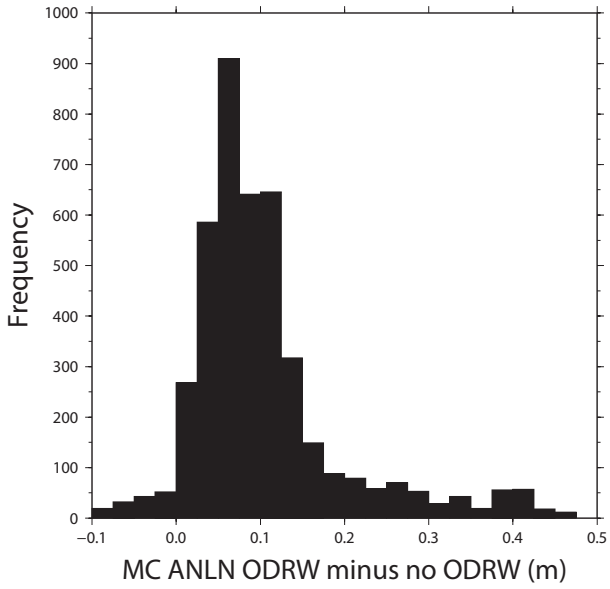

Figure 8.3: Histogram of differences between MC ANLN H^N_{MC} before and after the ODRW process. Differences at 4,247 ANLN JPs.

Table 8.3 (columns b and c), compare post-ODRW H^N_{MC} and pre-ODRW H^N_{MC} to 1042 H_{AG09} (Section 8.2). H_{AG09}−post-ODRW H^N_{MC}, minimum, maximum and mean are all less than (H_{AG09}−pre-ODRW H^N_{MC}), (−0.331 m difference in minimum; −0.073 m

difference in the maximum; −0.106 m difference in the mean) indicating the increase in post-ODRW H^N_{MC} compared to pre-ODRW H^N_{MC}. However, because there exists a currently unknown (Section 8.5.2) bias between MSL and H_{AG09} at the Albany tide-gauge, differences in maximum, minimum and mean do not indicate improvement from the ODRW process (or otherwise).

	(a)	(b)	(c)
Min	−0.115	−1.127	−1.458
Max	0.470	0.305	0.232
Mean	0.105	−0.165	−0.271
STD	±0.091	±0.180	±0.200
RMS	±0.139	±0.244	±0.336

Table 8.3: Statistics of differences among (a) H^N_{MC} before and after ODRW process; (b) H_{AG09} − pre-ODRW H^N_{MC} at 1,042 GNSS points; and (c) H_{AG09} − post-ODRW H^N_{MC} at 1,042 GNSS points. Units are in metres.

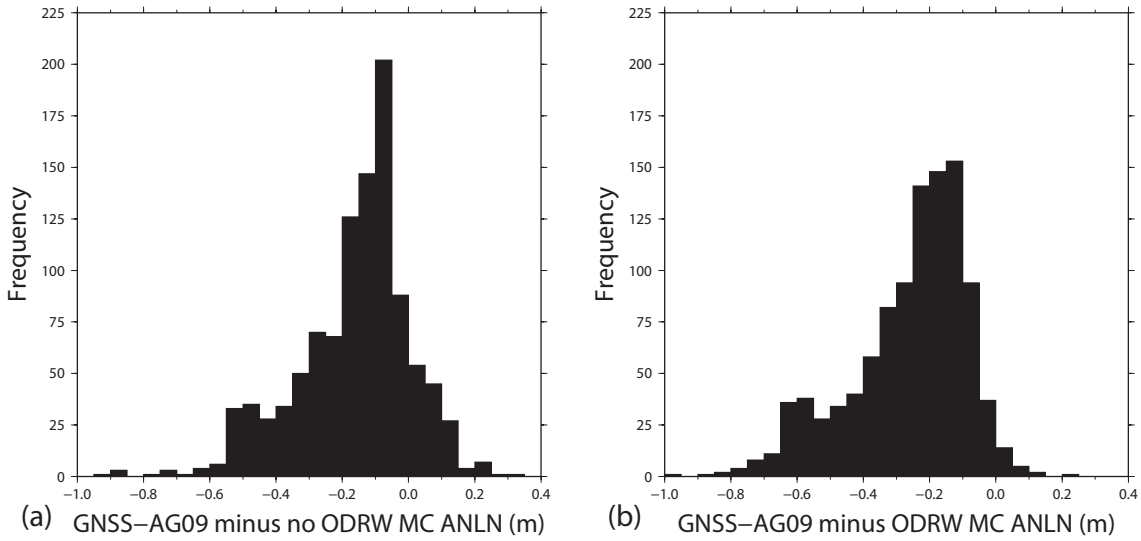

Figure 8.4: Histogram of differences between H_{AG09} and H^N_{MC} (a) before and (b) after the ODRW process. Differences at 1,042 GNSS points.

RMS of the $H_{AG09}-H^N_{MC}$ pre- and post-ORDW differences (±0.244 to ±0.336 m; although neither appear normally distributed; Figure 8.4) suggest that the ODRW process has not improved H^N_{MC} with respect to H_{AG09}. However, the 92 mm difference in RMS between the pre- and post-ODRW H^N_{MC} differences (at 1,042 points) compared to H_{AG09} is inconclusive, because H_{AG09} (particularly the ζ_{AG09} component) cannot be used as 'true' values because they contain errors that, although not well known, may be ∼±0.13 m (cf. Featherstone et al., 2011). The RMS values are also affected by the

bias between MSL and H_{AG09} at the Albany tide-gauge.

In addition, $H_{AG09} - H^N_{MC}$ (pre- and post-ORDW) differences do not closely approximate a normal distribution (Figure 8.4), so the STD and RMS from each set of differences should be used cautiously. Thus, it is assumed that the ODRW process has improved the ANLN in some regions (particularly in areas of high redundancy, e.g., south west Western Australia; WA), but this cannot be demonstrated by statistical improvements for the entire ANLN. However, where there is insufficient redundancy in the network (e.g., central Australia) and/or multiple errors close together (e.g., Qld), it is possible that large errors may remain undetected in the ANLN, causing the post-ODRW H^N_{MC} to be further from the 'true' height than pre-ODRW H^N_{MC}.

8.5 H_{AG09} and CARS2006 as weighted constraints for CLSA of the ANLN

8.5.1 Determination of zero-reference for the AEVD

Various proposals have been made to relate national vertical datums to a global vertical zero-reference (e.g., Rapp and Balasubramania, 1992; Balasubramania, 1994; Burša et al., 1999a,b, 2001, 2002; Ihde and Sánchez, 2005), but it has not yet been done. However, for the CLSA computed here, a relation to a global geopotential is not necessary, particularly as the AEVD is experimental. Therefore, the AEVD computed here will not be related to the World Height System (WHS) or global geopotential (cf. Ihde and Sánchez, 2005). For discussion and recommendations for further work relating to the placement of any new Australian vertical datum in a WHS, see Section 9.3.1. However, local datum unification between AHD(mainland) and AHD(Tas) will be achieved through CARS2006 at 30 AHD tide-gauges on the mainland and two in Tasmania (cf. Amos and Featherstone, 2009; Rummel and Teunissen, 1988; Zhang et al., 2009; Poutanen, 1999), by removing the existing SSTop offset (Section 5.8).

The (unknown) bias H_B between CARS2006 and H_{AG09} zero-reference needs to first be estimated, then removed. CARS2006 is based on the isobaric surface of equal pressure

at depth 2,000 m (Section 5.3.1; Dunn and Ridgway, 2002), which for MC ANLN has been translated vertically so that the CARS2006 SSTop height (H_{CARS}) is fixed to MSL (equal to zero) at the Albany tide-gauge (Section 5.3.6). This is an arbitrary solution, sufficient for the comparison of different MC ANLN. However, AGQG09 is based on the long-wavelength component of EGM2008, while the 1,042 GNSS h available are in ITRF2005 (Section 8.2). For the AEVD, all H_{CARS} at tide-gauges will be shifted vertically by H_B (0.132 m; Table 8.4) to align with H_{AG09} zero-reference), but retaining H_{CARS} relative height differences between AHD tide-gauges.

8.5.2 Method for removing bias between CARS2006 and AGQG09

H_B is estimated between H_{CARS} and H_{AG09} at 1,042 GNSS points (Figure 8.5). First, a LSA of the ANLN (4,247 junction points [JPs] after the ODRW process was applied to the ANLN) fixed at all 32 AHD tide-gauges with H_{CARS} applied at each tide-gauge as a SSTop correction (herein referred to as fixedANLN CARS; cf. Chapter 5), is computed. Fixing the ANLN to H_{CARS} at multiple tide-gauges is preferable to using MC ANLN fixed at one tide-gauge (cf. Vaníček, 1991), because the fixed LSA will partially suppress the coastal distortions at the tide-gauges, which are likely to be larger than the uncertainty in H_{CARS} (see Section 8.5.3). The ANLN JP heights from fixedANLN CARS (H_{CARS} at Albany tide-gauge = zero) are referred to as $\hat{H}_{CARS}$.

	(a)	(b)
Min	−0.624	−0.492
Max	0.347	0.478
Mean	−0.132	0.000
STD	±0.120	±0.120
RMS	±0.178	±0.120

Table 8.4: Statistics for $H_{AG09} - \hat{H}_{CARS}$ at 1,042 points (a) before H_B is removed from H_{CARS} and (b) after H_B is removed. Units in metres.

H_B is the average of the differences between H_{AG09} and $\hat{H}_{CARS}$ at 1,042 GNSS stations (Figure 8.5). The statistics of these differences ($H_{AG09} - \hat{H}_{CARS}$; before and after H_B is removed) are in Table 8.4, showing the mean difference to be −0.132 m, which is

adopted as the value for H_B. As this mean value is $H_{AG09} - \hat{H}_{CARS}$, the negative sign indicates that $\hat{H}_{CARS}$ are above H_{AG09}, so the 0.132 m bias is subtracted directly from H_{CARS} so as to align them with H_{AG09}.

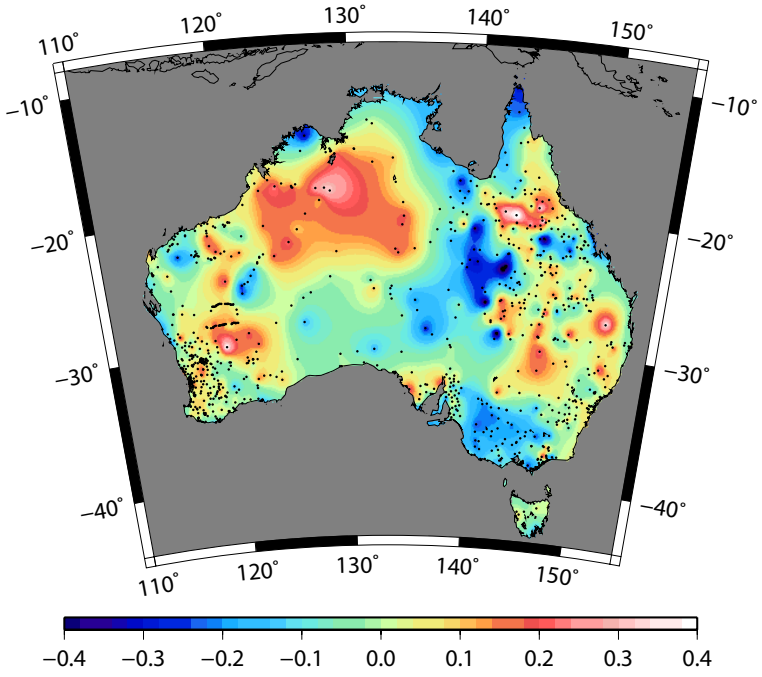

Figure 8.5: $H_{AG09} - \hat{H}_{CARS}$ at 1,042 GNSS points. Lambert projection, units in metres

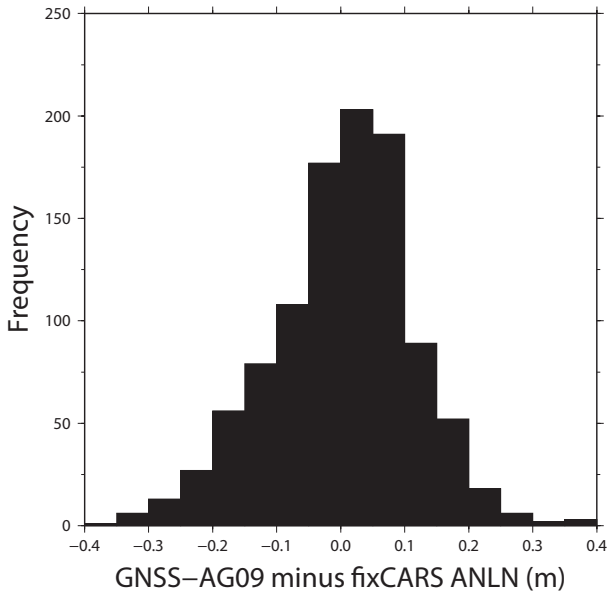

Figure 8.6: Histogram of $H_{AG09} - \hat{H}_{CARS}$ at 1,042 GNSS points. Units in metres

8.5.3 STD estimates for MSL + CARS2006 and H_{AG09} weighted constraints

Estimating MSL, H_{CARS} and H_{AG09} errors is rather problematic (cf. Ahmad et al., 1993; Kearsley et al., 1993a; Jiang and Duquenne, 1996; Kotsakis and Sideris, 1999; Fotopolous, 2005). Coleman et al. (1979) suggest maximum MSL error at AHD tide-gauges to be ∼0.15 m, but it is assumed for most tide-gauges to be less (only relative errors between tide-gauges are important here). Therefore, *a priori* STD estimates of MSL at AHD tide-gauges (σ_{TG}) are considered to be between ±0.05 m and ±0.10 m (cf. Section 5.2.2). *a priori* STD estimates for H_{CARS} at tide-gauges (σ_{CARS}) are not available, but are also likely to be between ±0.05 m and ±0.10 m. A combined *a priori* STD estimate of ±0.10 m is adopted for σ_{TG} and σ_{CARS}, but is based primarily on knowledge of residuals among the different data sets in Chapter 5 and can only be considered a best 'guesstimate'.

GNSS-derived h *a priori* STD estimates (σ_h) can be estimated from the internal precision of the processing. The average STD for the entire set is ±26 mm (internal precision scaled by 10; N. Brown 2009, pers. comm.), but reaches ±0.23 m. Here, σ_h of ±30 mm is adopted for all GNSS points, and although acknowledging that this may be a little small for some h, it is expected that larger individual σ_h will be absorbed into the combined H_{AG09} *a priori* STD. ζ_{AG09} is the weakest component of H_{AG09}, with *a priori* STD estimates (σ_{AG09}) difficult to determine. An estimate of ±0.13 m is made for σ_{AG09}, based on the fit of H_{AG09} to a fixed (at 32 AHD tide-gauges to MSL + CARS2006) LSA in Featherstone et al. (2011) (cf. ±0.12 m in Table 8.4). As such, ±0.15 m is adopted as the *a priori* STD estimate for H_{AG09} from a combination of estimated h and AGQG09 errors (cf. Ahmad et al., 1993; Kearsley et al., 1993a).

H_{AG09} and MSL + H_{CARS} constraints are treated as observations in the weighted LSA. This causes some problems where the absolute *a priori* STD for the tide-gauges and GNSS points are often higher than those of the individual levelling observations (cf. Zilkoski et al., 1992), particularly where the loops are small (the levelling STD is a function of the square-root of its length). Thus, the CLSA height (H^N_{CLSA}) will be more heavily influenced by the levelling. Similarly, H^N_{CLSA} at tide-gauges will be

heavily influenced by the levelling in coastal areas where there are inland distortions in the ANLN that propagate to the coast.

Initial tests indicated that *a priori* STD of ±0.10 m (MSL + H_{CARS}) and ±0.15 m (H_{AG09}) were too high to effectively influence local H^N_{CLSA}. Regions of large difference between the levelling and the constraints (e.g. North Qld) found H^N_{CLSA} to have large residuals to H_{AG09}. Whether these large residuals are caused by levelling errors, GNSS blunders (Section 8.2), AGQG09 errors or temporal changes in the Earth's surface or gravity field cannot currently be determined. However, as several of the residuals were >0.5 m (larger than expected maximum error in tide-gauge, H_{CARS} or H_{AG09}), it was likely that the errors are in the ANLN, so MSL + H_{CARS} and H_{AG09} *a priori* STD were tightened to reduce the residuals.

MSL + H_{CARS} *a priori* STD were reduced to ±0.05 m, and H_{AG09} to ±0.10 m. These new constraint *a priori* STD were tested in a second iteration CLSA, reducing the largest residuals at the MSL + H_{CARS} and H_{AG09} constraints. The constrained LSA and SR (both output from SNAP) provided information to assess the appropriateness of the updated constraint *a priori* STD. A visual assessment of the residuals indicated that most of the tide-gauge/H_{CARS} residuals were within ±0.10 m and most H_{AG09} residuals within ±0.15 m, so these *a priori* STD (tide-gauge/H_{CARS} *a priori* STD of ±0.05 m; H_{AG09} *a priori* STD of ±0.10 m) for the constraints were adopted (see Table 8.5 for details of CLSA constraint residuals after ODRW process). It is acknowledged that these STD estimates may be unrealistically small, but they are required to have an appropriate influence in the weighted LSA compared to the levelling.

8.5.4 Selection of GNSS points for constraints

Figure 8.5 shows the spatial distribution of the 1,042 GNSS points across Australia. Constraining all GNSS points is not warranted, as many are spatially very close together. In addition, the non-constrained points can be used to validate AEVD. A (seemingly) logical approach was taken, with two criteria; more GNSS points are selected in areas where gross levelling errors were known to exist (e.g., Qld), and gen-

erally, points are selected to achieve an even distribution of points over the continent. 268 GNSS points were selected manually to be used as constraints, with 774 points not constrained, which would be used to (semi-)independently validate AEVD (see Figure 8.8).

8.5.5 ODRW process in the CLSA

The CLSA was initially constrained at 268 H_{AG09} and 32 tide-gauges with H_{CARS}, with VFR = 1.2098 and 31 observations with |SR|>3.29. To pass the VFR test, the VFR needs to be <1.094 (χ^2_α CV for probability of 0.001, D_f = 2,316). A second ODRW process (CLSA ODRW; cf. Section 8.4) was undertaken for CLSA, to remove all significant outliers at $\alpha = 0.001$ and for the VFR to be $<\chi^2_\alpha$ CV. The ODRW method used is the same as that used in Sections 8.4.1 and 8.4.2.

Most outliers identified and re-weighted (as per Sections 8.4.1 and 8.4.2; also with reference to most recent MC ANLN) were ANLN sections. However, two H_{AG09} constraints with high |SRs| (44EB, NSW, |SR| = 4.09, residual = 0.377 m; 36QB, Qld, |SR| = 3.62; residual = −0.346 m) were removed from the CLSA (although retained in the 765 H_{AG09} validation points), as inspection of the levelling observations in the CLSA (and MC ANLN) did not indicate levelling errors. It is assumed for these cases that there are errors in the ζ_{AG09} (44EB $\sigma_h = \pm 0.021$ m; 36QB $\sigma_h = \pm 0.044$ m), the H_{AG09} connection to the ANLN, or there has been uplift or subsidence in these regions between the time of levelling and GNSS observations. Eleven additional GNSS points were constrained during the ODRW process to robustify areas where there were multiple levelling errors, so that a total of 277 H_{AG09} constraints were used for the CLSA. On several occasions where there was ambiguity over which observation (or observations) contained the levelling error (cf. Prószyñski, 2000), several sections in the local area were all re-weighted. It is possible that all contained errors, but the magnitude could not be determined.

On completion of the CLSA ODRW process (all observations with |SR|>3.29 re-weighted), VFR was 1.1011. This marginally fails the VFR test (>1.0929; χ^2_α CV

for $\alpha = 0.001$, $D_f = 2{,}325$). As with post-ODRW MC ANLN (Section 8.4.2), *a priori* STD is scaled (by 1.1012) so that VFR = 1. This course is taken as the pragmatic one, because there is some uncertainty over the *a priori* STD, plus the likelihood of systematic and gross errors remaining in the observations and constraints that cannot be confidently identified. This CLSA is adopted as the AEVD.

8.5.6 AEVD precision estimates

The internal precision of the AEVD heights ($\hat{H}^N$) is provided by the CLSA *a posteriori* STD (1σ; $\sigma_{\hat{H}^N}$), which is output by SNAP for each $\hat{H}^N$. Mean $\sigma_{\hat{H}^N}$ (for 4,247 ANLN JPs) is ±40 mm (adopted as the formal internal precision of the AEVD), reaching a maximum of ±379 mm at 24°S, 127°E and minimum of ±21 mm at 31° 53′S, 116° 46′E (see Figure 8.7). For the south west and south east corners of the AEVD, $\sigma_{\hat{H}^N}$ is generally <40 mm, but $\sigma_{\hat{H}^N}$ is >40 mm for parts of the north east (Qld), central, and northern central regions. $\sigma_{\hat{H}^N}$ is computed from ANLN *a priori* STD, so the 'spikes' in Figure 8.7 are intermediate JPs that are only connected to two sections (and often one spur line; e.g., Figure 2.6(a)) where both of these sections have been re-weighted because the erroneous section cannot be isolated. See Section 8.6 for an estimate of external error from the AEVD validation.

	MSL + H_{CARS}	H_{AG09}
Points	32	277
Min	−0.099	−0.222
Max	0.118	0.264
Mean	−0.005	0.001
STD	±0.047	±0.080

Table 8.5: CLSA residuals for MSL + H_{CARS} and H_{AG09} constraints. The residuals for both sets of constraints approximate a normal distribution.

Adjustment residuals from CLSA for 32 MSL + H_{CARS} (at tide-gauges) and 277 H_{AG09} constraints can be seen in Table 8.5. Maximum and minimum MSL + H_{CARS} residuals indicate that these constraints did not adjust by more than ±0.10 m (assigned *a priori* STD), with mean STD of the 32 tide-gauge/CARS2006 residuals ±0.047 m (residuals are close to a normal distribution). On the other hand, maximum and minimum for

277 H_{AG09} constraint residuals were +0.264 m and −0.222 m respectively, indicating some H_{AG09} residuals are larger than the H_{AG09} *a priori* STD, although mean STD of the 277 H_{AG09} residuals is ±0.080 m (*a priori* STD of ±0.15 m). These results suggest that the *a priori* STD assigned to the CLSA constraints were reasonable.

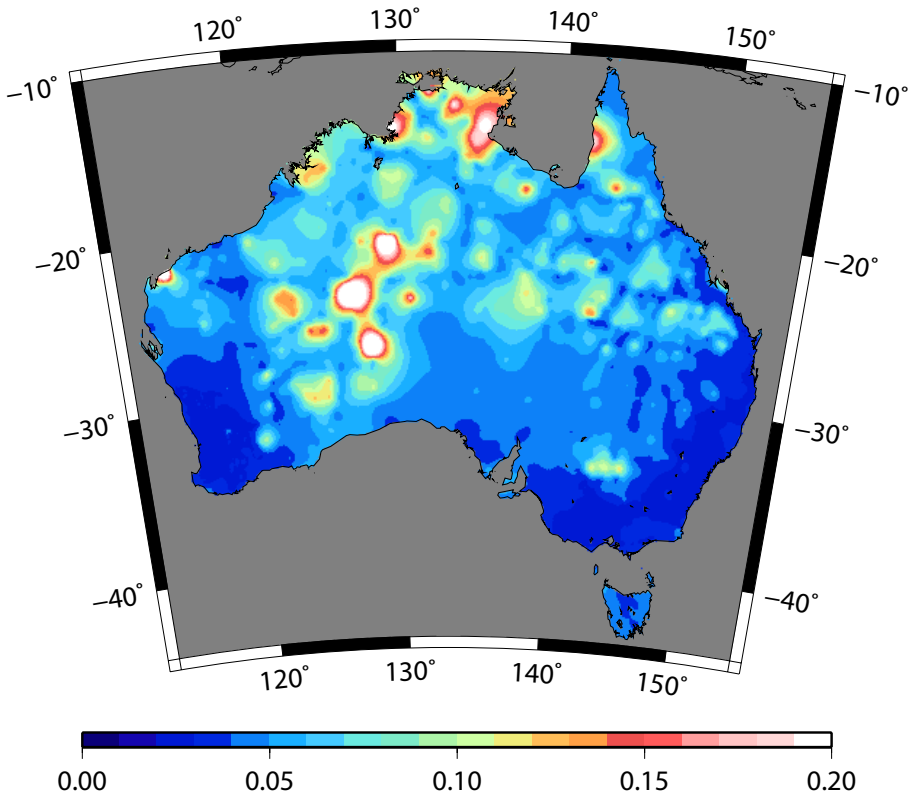

Figure 8.7: AEVD internal precision calculated in the CLSA. Mean internal precision is ±40 mm, with maximum ±0.379 m and minimum ±21 mm. Lambert projection, units in metres

8.6 Results and discussion for the AEVD

Although difficult to validate the AEVD, comparisons can be made to existing heights. Because compatibility of H_{AG09} and the AHD is a pressing issue, a closer fit of AGQG09 to $\hat{H}^N$, than to AHD is important. Figure 8.8(a) presents a (semi-independent) comparison of $\hat{H}^N$ to H_{AG09} at 765 points that were not used as constraints in the CLSA.

Figure 8.8(a) shows that the north-south slope has been removed (cf. Section 5.7), but numerous differences of ∼0.40 m still exist (Table 8.6). $H_{AG09}-\hat{H}^N$ differences are close to a normal distribution, with the RMS of these differences ±0.098 m, which

can be adopted as a best estimate of external precision. By comparison, Figure 8.8(b) ($H_{AG09}-$AHD $H^{N\text{-}O}$) shows the AHD north-south slope, but also similar regional distortions to $H_{AG09}-\hat{H}^N$.

The maximum magnitude of $H_{AG09}-$AHD $H^{N\text{-}O}$ differences is +0.74 m (~20°S, 145°E), which appears to be a regional distortion (also seen in Figure 8.8(a)) that is exacerbated by the AHD's north-south slope. The mean differences of both AHD $H^{N\text{-}O}$ and $\hat{H}^N$ to H_{AG09} (<0.020 m) indicate that any bias among AHD $H^{N\text{-}O}$, $\hat{H}^N$ and H_{AG09} is negligible. However, the RMS of the $H_{AG09}-$AHD $H^{N\text{-}O}$ differences is ±0.207 m, compared to ±0.098 m for the RMS of $H_{AG09}-\hat{H}^N$ differences, indicating that AEVD $\hat{H}^N$ is a significant improvement on the AHD $H^{N\text{-}O}$ (assuming that AGQG09 is a reasonably close representation of the quasigeoid).

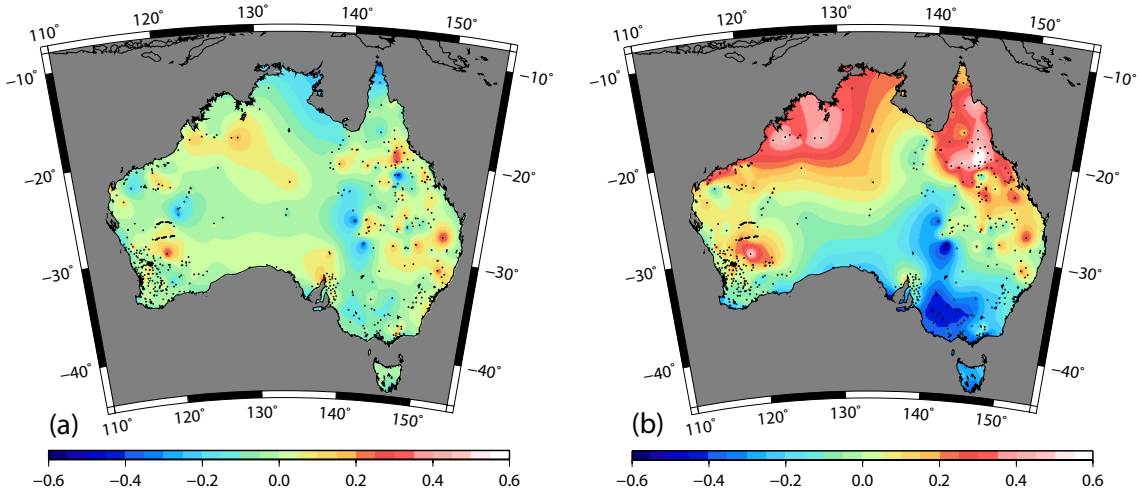

Figure 8.8: Differences between (a) $H_{AG09}-\hat{H}^N_{CLSA}$ from AEVD; and (b) $H_{AG09}-$AHD $H^{N\text{-}O}$ at 765 GNSS points that were not used as constraints in the CLSA. Lambert projection, units in metres

	$H_{AG09}-\hat{H}^N$	$H_{AG09}-$AHD	AHD$-\hat{H}^N$
Min	−0.459	−0.631	−0.537
Max	0.400	0.742	0.460
Mean	−0.010	0.012	−0.024
STD	±0.098	±0.207	±0.186
RMS	±0.098	±0.207	±0.187

Table 8.6: Statistics for $H_{AG09}-\hat{H}^N$ from AEVD (at 765 GNSS points not used in the CLSA); $H_{AG09}-$AHD (at 765 GNSS points not used in the CLSA); and AHD$-\hat{H}^N$ (at 4,247 ANLN JPs). Note that $H_{AG09}-\hat{H}^N$ and $H_{AG09}-$AHD can be compared, but AHD$-\hat{H}^N$ cannot be compared to the other two differences. Units in metres.

There are a number of reasons for $H_{AG09} - \hat{H}^N$ displaying differences with magnitude of up to 0.45 m. Although the average GNSS-derived h STD is $\pm$0.026 m (N. Brown 2009, pers. comm.; cf. Section 2.5.2), $\sim$20 GNSS h have STD lying outside $\pm$0.08 m (maximum of $\pm$0.23 m), so some of the differences may be attributable to 'noisy' GNSS-derived h. Furthermore, although eight Qld GNSS points were removed as apparent blunders ($H_{AG09} - H^N_{MC}$ differences of 1$-$1.5 m) it is possible that undetected blunders of up to 0.30 m (e.g., typographic error in h or assigned AHD $H^{N\text{-}O}$) remain in the GNSS data set. The accuracy of ζ_{AG09} cannot be reliably determined, but is estimated at $\sim\pm$0.13 m (Featherstone et al., 2011). However, errors of several decimetres in some regions are possible (Featherstone et al., 2011), indicating that in extreme cases, differences of up to say, 0.40 m could be caused by H_{AG09} through a combination of h (largest STD of $\pm$0.23 m) and ζ_{AG09} (possible maximum error of $\sim$0.25 m) errors.

In addition, the connections between GNSS points and ANLN JPs are derived from assigned AHD $H^{N\text{-}O}$, which have been shown in the the past to contain errors (cf. Section 2.7.2). Because many GNSS points (particularly in WA) are located on ANLN BMs mid-way between JPs, the existing levelling line becomes the GNSS-ANLN connection to the JP (BMs between JPs not adjusted). Therefore, an error can be identified in the ANLN section and subsequently re-weighted, but the GNSS-ANLN connection along this section will still contain the error (probable cause of the large CLSA residual at 44EB). Blunders in GNSS h or their ANLN connection are characterised by a large difference specific to a particular GNSS point, and not evident in surrounding GNSS points (see Figure 8.8).

It is possible that vertical displacement and uplift in ANLN BMs has also occurred in some regions (cf. Buckley et al., 2003; Chi and Reilinger, 1984) in the time since the levelling was completed (mostly pre-1971) and the GNSS observations were made (post-1990, but most since 2000). This displacement may be incorrectly interpreted as gross or systematic error in the levelling, or in the H_{AG09} constraints (cf. Kerr, 1981). However, because of the deficiencies in the ANLN file and lack of additional levelling data (see Section 2.3.2), these issues cannot be resolved at this time. However, it is likely that errors remaining in the ANLN make a large contribution to the differences

in Figure 8.8. Given what is now known about the ANLN (e.g., Chapter 2; Filmer and Featherstone, 2009), most levelling errors can be expected in Qld, the central and northern parts of WA and NT. Indeed, Qld and WA appear to contain most of the large differences in Figure 8.8, but this is also dependent on the density of GNSS points. NT does not contain any large differences, but contains only several GNSS points that were not needed in the CLSA.

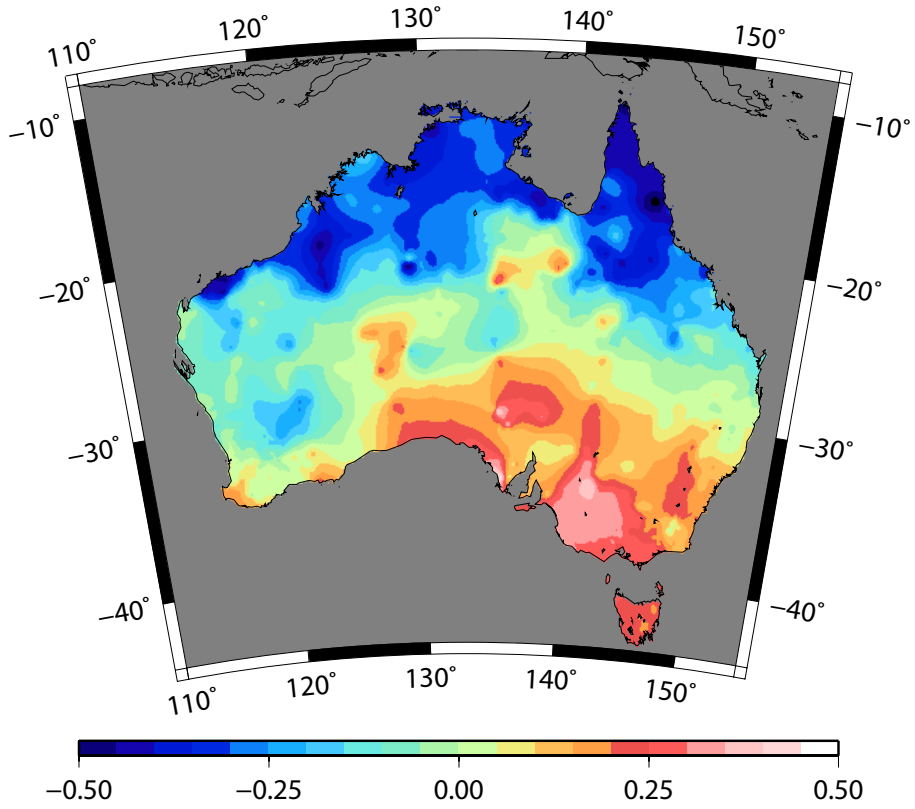

Figure 8.9: AHD $H^{N\text{-}O} - \hat{H}^N$. Differences calculated at 4,247 ANLN JPs. Lambert projection, units in metres

Finally a comparison between $\hat{H}^N$ from AEVD and the existing official AHD $H^{N\text{-}O}$ is in Figure 8.9 (cf. Figure 2.3). The north-south slope is the most prominent feature (cf. Chapter 5; Featherstone, 2004, 2006), but a number of other local features can also be seen through central Australia, which are probably differences caused by the ODRW process in the ANLN and the effects of constraining to H_{AG09} constraints.

8.7 Summary

To deal with errors in the ANLN before its use in the AEVD, an outlier detection and re-weighting process based on detection, identification and adaption was used. The VFR test is used to detect the presence of errors, the w-test combined with iterative data snooping identifies the erroneous observation, while the adaption phase involves re-weighting the section containing the error to reduce its influence on the LS-estimated heights. Data used for the AEVD are 1,052 3D GNSS h, the ANLN, AGQG09, and CARS2006.

Selecting *a priori* STD for the third-order OW and two-way UO is problematic, but c_L (computed from ANLN loop closures) and c-derived values show reasonable agreement for second- third- and fourth-order levelling. First-order levelling in the ANLN appears to be no better than ANLN second-order. Final *a priori* STD estimates were based on a combination of c_L and c-derived values. The ODRW process conducted for the ANLN did not show any statistical improvement compared to H_{AG09}, but is assumed to have reduced errors (by re-weighting the observation) in areas of high network redundancy. However, the effectiveness of this method in parts of the ANLN where there are multiple and/or compensating errors is difficult to assess.

H_{AG09} is adopted as the AEVD's zero-reference, with the difference between CARS2006 and H_{AG09} removed by translating CARS2006 vertically by 0.132 m. The bias was calculated as the average of 1,042 H_{AG09} differences to a LSA of the ANLN fixed at 32 tide-gauges with CARS2006 correcting MSL for SSTop. Accurate *a priori* STD estimates are not known for AGQG09, CARS2006 SSTop and MSL at tide-gauges, requiring a best 'guesstimate' at this stage.

A second ODRW process was conducted before the CLSA with the H_{AG09} and CARS2006 constraints identifying additional ANLN errors, but also some H_{AG09} outliers. The final CLSA was constrained at 32 AHD tide-gauges to MSL + CARS2006 and 277 H_{AG09} points to realise the AEVD. The AEVD was (partially) validated by comparisons between the fit of the AEVD and the AHD to 765 H_{AG09} points not used to constrain

the AEVD. This comparison demonstrates an improved fit of the AEVD to H_{AG09} points ($\pm$0.098 m RMS of 765 differences) compared to the AHD ($\pm$0.207 m RMS of 765 differences). The mean internal precision of the AEVD $\hat{H}^N$ is $\pm$0.04 m from the CLSA, while the best estimate of AEVD $\hat{H}^N$ accuracy is $\pm$0.10 m, based on AEVD validation at 765 H_{AG09} points.

9. CONCLUSIONS AND RECOMMENDATIONS

The focus of this research was an investigation into the problems with the current Australian Height Datum (AHD), to test new data sets to evaluate their suitability in any new Australian vertical datum (AVD), and finally, to compute an experimental version of a new AVD (referred to as the AEVD) that could perhaps be developed into a replacement for the AHD. Note that the Inter-governmental Committee for Surveying and Mapping (ICSM) has decided that the AHD will remain the official legal height datum for Australia for the foreseeable future, so this work does not foreshadow a new AVD.

9.1 Summary of research

The Australian National Levelling Network (ANLN) is the primary data set, but has been shown to contain numerous errors. In Chapter 2, loop-based investigations into gross levelling errors indicate that these are the primary cause of distortions in the AHD of ∼0.50 m, evident in re-adjustments of the ANLN (Chapter 8). Results from Chapter 2 were published in the Australian Journal of Earth Sciences (Filmer and Featherstone, 2009). Deficiencies in the ANLN data set prevented meaningful investigations into systematic levelling errors, although a simulation of the effect of atmospheric refraction errors on the ANLN/AHD was conducted (Chapter 4). Investigations into the north-south slope (Chapter 5) in the AHD using sea surface topography (SSTop) models (SSTMs), indicate the slope to be almost exclusively caused by fixing the then-ALS to MSL at 30 mainland tide-gauges to form the AHD.

Methods of computing gravity at ANLN benchmarks (BMs) using observed terrestrial gravity from the Australian National Gravity Database (ANGD) and the Earth Gravity Model 2008 (EGM2008) were described in Chapter 6. EGM2008-derived gravity

at BMs appears to be adequate for this purpose, although differences in the Australian Alps (reaching 50 mGal in magnitude) with observed terrestrial gravity remain unresolved. Chapter 7 investigated the effect of using Helmert orthometric, normal and normal-orthometric height corrections (HOC, NC and NOC respectively) on the ANLN, the results of which were published in the Journal of Geodesy (Filmer et al., 2010).

A statistical outlier detection process was conducted in Chapter 8 to identify and re-weight erroneous levelling sections, followed by a 'combined' least-squares adjustment (CLSA) of the ANLN using the CSIRO Atlas of Regional Seas 2006 (CARS2006) plus observed mean sea level (MSL) at AHD tide-gauges and Global Navigation Satellite System (GNSS) ellipsoid heights (h) minus AGQG09 height anomalies (ζ_{AG09}) as weighted constraints. The AEVD was shown to be $\sim$50% superior to the AHD when compared to 765 $h - \zeta_{AG09}$ heights (H_{AG09}) not used as constraints ($\pm$0.098 m for the AEVD compared to $\pm$0.207 m for the AHD). The mean STD from the CLSA (as a proxy for internal precision) of AEVD heights is $\pm$0.04 m, with estimated external accuracy of $\pm$0.10 m adopted from the fit of the AEVD to 765 H_{AG09} points.

9.2 Conclusions

This section is divided among different research areas, with conclusions for each presented.

9.2.1 Levelling errors in the ANLN

Loop-based investigations into the ANLN (Chapter 2) revealed the presence of gross errors approaching 1 m in some loops (mostly in remote regions), with the likelihood of numerous compensating errors remaining hidden. It is unknown whether the 117 loops with above-allowable misclose (71 of these comprise one-way levelling) can be attributed to observation error, recording/reduction error, or office transcription error.

Additional height information from GNSS and AUSGeoid98 was used to identify large errors in the ANLN. However, despite containing numerous errors, a large part of the ANLN (particularly southwest and southeast of Australia) is satisfactory to third-order standard. The unavailability of relevant information in the ANLN (see Section 9.3.3) prevented a proper investigation into systematic levelling errors.

9.2.2 Atmospheric refraction effects on the ANLN

A sensitivity analysis of the Angus-Leppan (1979) refraction correction (for it to be applied retrospectively) using assumed data indicated that changes in heat flux, instrument height, terrain slope and sight length could all have a large effect on the magnitude of the correction. The effects of high heat flux and long steady terrain gradients (e.g., 1 m height increase per 100 m distance) on unequal refraction error (URE) can cause a levelling section to exceed ICSM (2007) maximum allowable tolerance. This is particularly so for class LC and LD levelling because of the long maximum sight length allowed for these classes of levelling. Tabulated refraction corrections from Angus-Leppan (1979, Table V), should be used with caution, given the diurnal, seasonal and spatial variability of heat flux.

A simulation to estimate the effect of URE on AHD/ANLN heights using assumed data suggested that accumulated errors in height could reach $\sim$0.40 m. In addition, the simulation provided no indication that unequal heating by the Sun of north- and south-facing slopes contributes to a significant north-south slope in the ANLN as postulated by Angus-Leppan (1979). However, there is no metadata currently available to properly apply retrospective refraction corrections to the ANLN.

9.2.3 Sea surface slope and the AHD

Five SSTMs were tested using ANLN- and H_{AG09}-derived SSTop at tide-gauges, with the results suggesting that CARS2006 is the superior model in Australian coastal regions. However, all SSTM and H_{AG09}-derived SSTop demonstrated similar trends as a

function of latitude, indicating that fixing the then-ALS to MSL at 30 mainland tide-gauges is the sole cause of the north-south slope in the AHD. Large regional differences between ANLN-derived SSTop and SSTM- and H_{AG09}-derived SSTop (up to $\pm$0.42 m for SSTM; up to $\pm$0.52 m for H_{AG09}) are assumed to be levelling error-induced distortions in the minimally constrained adjustment of the ANLN. This indicates that it is preferable to constrain the ANLN to SSTop + MSL at multiple tide-gauges to realise a new AVD (option 4 in Section 1.1.1) because maximum error for SSTop + MSL at tide-gauges is likely to be <0.15 m. In addition, a re-assessment of the offset between mainland AHD and Tasmanian AHD indicates it is between 58$\pm$17 mm and $-$48$\pm$24 mm (positive indicating Tasmania above the mainland), which is different to previous estimates (by Rizos et al., 1991; Rapp, 1994; Featherstone, 2000, 2002a) of between $-$0.10 m and $-$0.30 m (mainland above Tasmania).

9.2.4 Computation of gravity at benchmarks

A method of computing EGM2008-derived gravity at ANLN BMs was introduced as an alternative to interpolating terrestrial gravity observations. Comparisons with observed terrestrial gravity indicated good agreement on flat terrain, but differences of up to $\sim$50 mGal appear in rugged terrain, particularly the Australian Alps. It is shown that EGM2008 omission error and uncertainty in the ANLN BM position (ϕ, λ) can cause errors in EGM2008-derived gravity that can account for most of these differences (maybe $\sim$50% each), although these require further investigation. However, BM gravity interpolated from terrestrial gravity also appears deficient in the Australian Alps, where gravity observations are taken along roads in valleys and do not contain gravity observations at higher elevations.

Errors in heights observed by barometers at gravity stations also contribute to errors similar to (or just below) the RMS of BM gravity interpolated from terrestrial gravity, although the effect is more difficult to determine in EGM2008-derived BM gravity. The effect of the barometer height errors at gravity stations may be able to be reduced by weighting the gravity observations with respect to height errors, so that gravity station

heights observed by GNSS or other precise survey methods are given more importance in BM gravity computations. This will only be possible where there are suitably dense GNSS controlled gravity surveys over Australia, particularly at high elevations.

9.2.5 Height systems and the ANLN

There are only minor differences (sub-mm per 1 arc-minute of latitude change) among *NOC*s computed using four different versions (Rapp (1961), Heck (1995), Bomford (1971) and New Zealand). The Rapp (1961) *NOC* is largely insensitive to input data errors. However, the orthometric correction is sensitive to some input data errors, particularly BM gravity. The *NC* is subject to the same data input errors as the orthometric correction, but is less susceptible to gravity-related errors because normal gravity computed at the BM is much less affected by data errors (<4 mGal; ∼10 mm height error at 2,000 m), than actual gravity (potentially up to 50 mGal in the Australian Alps if using EGM2008-modelled gravity; which generates a ∼0.12 mm height error at 2,000 m) computed at the BM.

Loop closure analysis indicates small decreases in loop misclosure when height corrections (HCs) are applied to first-and second-order loops (HCs using EGM2008 appear to perform better than when using terrestrial gravity). *HOC* and *NC* show the largest decrease in loop closures, although the *NOC* does show some decrease in closures. Levelling of third-order and lower quality do not show any decrease in loop closures after HCs are applied, suggesting that there are other gross and systematic errors in this levelling that are masking the benefits of applying HCs. However, it is shown that it is necessary to apply HCs for Australia to remove the latitude dependent convergence of the equipotential surfaces towards the south pole, which has a magnitude of ∼0.40 m in the north-south direction across Australia.

Differences between Helmert orthometric heights (H^O) and normal heights (H^N) are 0.26 m (Helmert H^O larger; both using EGM2008-derived gravity) and 0.15 m (both using terrestrial-derived gravity). Maximum differences between Helmert H^O and normal-orthometric heights ($H^{N\text{-}O}$) were 0.44 m (Helmert H^O larger), and were 0.17

m between H^N and $H^{N\text{-}O}$ (H^N larger). All maximum differences were in the Australian Alps, where elevations reach 2,228 m. H^N and $H^{N\text{-}O}$ are within 30 mm at heights <1,000 m, but above this height, the difference increases rapidly, indicating gravimetric quasigeoid models and $H^{N\text{-}O}$ are not compatible, particularly at elevations >1,000 m. H^N are more appropriate for any new levelling-based AVD at this stage, as they are less susceptible to existing errors in the gravity and ANLN data than Helmert H^O (and compatible with the current Australian gravimetric quasigeoid, AGQG09), although this may change if data sets can be upgraded in the future.

9.2.6 Adjustment strategies for the combined vertical datum

Reasonable estimates of *a priori* standard deviations (STDs) for first-, second-, third-, and fourth-order levelling of the ANLN can be made from average loop closures made in Chapter 2. It was also shown that ICSM (2007) c should be divided by ∼2.8 to provide STD estimates, rather than two as advocated by Steed (2006), or three suggested by Kearsley et al. (1993a). Statistical outlier detection methods appear to be effective in areas of the ANLN with high redundancy and few gross errors (e.g., south west Western Australia; WA), but is problematic in areas of low redundancy (e.g., central Australia), or areas with multiple large gross errors (Queensland). It is difficult to evaluate the benefits or otherwise of the outlier detection process and the subsequent re-weighting of sections found to be in error.

A combined least-squares adjustment (CLSA) of the ANLN constrained at H_{AG09}, and CARS2006 + MSL at tide-gauges provides a combined vertical datum using a normal height system. Although the AEVD is difficult to validate, a comparison with 765 H_{AG09} points not used to constrain the AEVD indicates that it is an improvement on the AHD (±0.098 m RMS compared to ±0.207 m RMS of 765 differences), both from the view of scientific rigour, but also for compatibility with gravimetric quasigeoid models. The formal AEVD error is ±0.04 m (internal precision from the CLSA), or ±0.10 m (accuracy adopted from the fit to 765 unconstrained H_{AG09}). However, it is possible that this could be reduced if information was available to retrospectively apply

refraction corrections to the ANLN.

9.3 Future directions and recommendations

The AEVD realised in Chapter 8 is a step towards a new vertical datum for Australia. However, further research is required in some areas, extending to how a new AVD will be related to a global vertical datum (GVD), and the complex issue of developing a time-dependent (dynamic) vertical datum. In addition, significant improvements in the available data sets are required, including additional levelling, gravity and GNSS observations (see Section 9.3.3). Significant improvements with respect to unification of national vertical datums, and formation of a global vertical datum, plus GNSS-geoid levelling are expected (1 cm geoid accuracy at spatial resolution of 100 km) when final data becomes available from the European Space Agency's (ESA's) Gravity field and steady-state Ocean Circulation Explorer (GOCE) satellite mission (e.g., Johannessen et al., 2003; Drinkwater et al., 2003). Indeed, Arabelos and Tscherning (2001) suggest that the accuracy of vertical datum transfer between Amsterdam and New York tide-gauges may improve by about one order of magnitude (0.57 m for EGM96; 0.06 m for the GOCE error model).

9.3.1 Global vertical datum

The concept of connecting the ∼100 local vertical datums (LVDs) (Ihde and Sánchez, 2005) around the world to form what has variously been referred to as a world vertical network (Colombo, 1980), global vertical datum (GVD; Balasubramania, 1994) or world height system (WHS; Ihde and Sánchez, 2005; Rapp and Balasubramania, 1992; Ihde et al., 2002) has been developed over several decades (cf. Rummel and Teunissen, 1988; Xu and Rummel, 1991; Xu, 1992), but has not yet been realised. While there have been notable improvements in global geopotential models in recent years (e.g., EGM2008), the low quality of some of the existing LVDs around the world continues to impede the realisation of a GVD. The AHD in its current form is not compatible

with any GVD. The north-south slope and regional distortions mean that any vertical offset to the GVD will be a function of its horizontal position, rather than a constant offset (cf. Featherstone, 2000). Therefore the development of a new AVD is necessary for Australia to benefit from any future GVD.

Future research and development to improve the AEVD should involve connection to a GVD, when realised. This can be implemented on a global scale using a global geoid model and GNSS heights, which has been done at a regional level (e.g., Amos and Featherstone, 2009; Rizos et al., 1991; Featherstone, 2000, 2002a; Poutanen, 1999), or computing geopotential differences between a global geopotential value and the LVD (e.g., Ardalan et al., 2010; Ardalan and Safari, 2005; Burša et al., 1999a,b, 2001, 2002, 2004; Zhang et al., 2009). However, using MSL and modern SSTMs to connect LVDs should not be discounted (perhaps combined with gravimetric methods), given the improvement in SSTMs and the apparent success of the connection of Tasmania to the mainland in AEVD (see Section 5.8).

However, the use of H_{AG09} as a zero-reference for AEVD (Section 8.5.1) means that AEVD is probably already similarly aligned with the zero-reference of an eventual GVD, (although the zero reference for a GVD is not yet decided; Ihde and Sánchez, 2005), but this will require further investigation. Distortions remaining in the AEVD suggest that offsets should be computed at multiple points evenly spatially distributed across Australia (or in areas where the ANLN is reliable), which would provide a mean offset to the GVD.

9.3.2 Dynamic vertical datums

Time-dependent variations in the surface of the Earth (here, only non-periodic variations are considered) cause inconsistencies within vertical datums (e.g., Carrera, 1984). There are numerous causes for the Earth's crust to uplift or subside (see Vaníček and Krakiwsky, 1982, Chapter 8.4), which may be continuous or discontinuous (episodic; Vaníček and Krakiwsky, 1982, 607). Natural changes include tectonic deformation, glacial isostatic adjustment (GIA; e.g., Hill et al., 2010), while human-induced vertical

movements include subsidence due to the removal of oil and gas (e.g., Fielding et al., 1998), underground water (e.g., Buckley et al., 2003), or uplift caused by sequestration of carbon dioxide below ground (e.g., Comerlati et al., 2006). However, it is often difficult to separate the causes of vertical deformation (e.g., Mellors and Boisvert, 2003). Australia has been relatively fortunate in regard to tectonic deformation (cf. Dentith and Featherstone, 2003), as it does not contain major active fault lines where significant vertical crustal motion occurs (cf. Amos and Featherstone, 2009; Vaníček et al., 1985). However, subsidence due to human activities do exist (e.g., Belperio, 1993).

Although there has been international research into the issue of time-dependent vertical datums (e.g., Carrera, 1984; Vaníček et al., 1985; Rangelova et al., 2009), there appears to be limited research in Australia with respect to vertical deformation and the AHD (cf. Wellman and Tracey, 1987). Repeat measurements are required for these studies, which is costly to provide through levelling (cf. Castle et al., 1976; Vaníček et al., 1980). GNSS has provided the means for multiple repeat observations, although these are spatially sparse and the height component of GNSS is weak compared to horizontal (e.g., Featherstone, 2008). Other space-based observations, such as interferometric synthetic aperture radar (InSAR; e.g., Rott, 2009) provides high resolution repeat observations of local areas, which has been used to identify vertical deformation, sometimes in combination with GNSS and tide-gauge measurements (Brooks et al., 2007). Time-variable gravity from the Gravity Recovery and Climate Experiment (GRACE; e.g., Tapley et al., 2004a,b) satellite mission can also be used to estimate vertical deformation (e.g., Panet et al., 2007).

The question of how to provide vertical velocities for a vertical datum is rather problematic. A national velocity model, appears the most practical way, but how that can be applied to the ANLN/AHD which has used levelling observed at multiple epochs ($\sim$1945-present day, although mostly 1960-1970; Roelse et al., 1971) is not clear. An alternative to levelling-only dynamic vertical datums is through time-dependent gravity (cf. Biró, 1983), which can produce a dynamic geoid-only vertical datum (e.g., NGS, 2007; Rangelova et al., 2009; Smith and Edwards, 2010).

Time-dependent gravity causes only small variations in the geoid model (Véronneau et al., 2006), so appear to have an advantage compared to vertical datums incorporating levelling, which are susceptible to large changes in the topographic surface. The absence of BMs in geoid-only vertical datums removes the necessity of constantly updating official heights, with the user observing the topographical surface in point-positioning mode (e.g., Featherstone and Dent, 2002). A physical height is thus realised through GNSS h and the geoid model (see Section 1.3.3 for discussion on this type of vertical datum), rather than adopting the BM height in classical levelling datums.

It is recommended that future research is directed into the problem of time-dependent heights in Australia. A vertical velocity model derived from space-derived repeat measurements, supported by local levelling campaigns, and tide-gauge observations appears the best option. However, implementation of vertical velocities into future versions of AEVD is rather problematic, and would require updates of the ANLN database to contain dates of levelling observations (see below), with possible re-observation in problem areas (cf. NGS, 2007; Rangelova et al., 2009; Smith and Edwards, 2010). Alternatively, downweighting levelling observations in problem areas and densifying GNSS observations may allow the velocity model to be delivered through the GNSS-geoid constraints. The question of whether a fully dynamic, or semi-dynamic vertical datum is appropriate also needs to be examined. This is an area that requires more work in the future.

9.3.3 Recommendations

Although a combined vertical datum is recommended as the preferred datum type for the development of an 'official' new AVD, it is suggested that a levelling-only datum (constrained using option 3 in Section 1.1.1) is retained for scientific type studies including independent development and validation of other Australian and international height 'products'.

Numerous recommendations are made from this thesis, but the major impediment in developing a new AVD (of any type) is the low-quality and incomplete data sets

available. Although it has been shown that significant improvements can be made to the AHD using the currently available data, to deliver a new national vertical datum that will fully service Australia's height requirements over coming decades (as the AHD has since 1971), the following data and research objectives need to be fully addressed. Data requirements are as follows:

1. **The ANLN:** The ANLN should be updated with existing State and Territory data that is currently not in the ANLN. One approach could be to conduct a national audit of all available Australian levelling data, with a view to a national program to fully update the ANLN. This is necessary regardless of whether levelling or geoid-only vertical datums are adopted as the official new AVD. An audit could also determine the feasibility of including all two-way levelling observations (rather than just averaged height differences currently in the ANLN) and additional information such as time and date of observation and weather conditions (if ever recorded) to the upgraded ANLN. In addition, BM positions (ϕ, λ) need upgrading to an uncertainty of <10 m (an automated method should be investigated, but further re-observation is probably required).

2. **Australian tide-gauge records:** A complete record of all Australian tide-gauges is required (PSMSL lists 211 Australian tide-gauges, although this includes many duplicate and some offshore records). Levelling connections to the ANLN are needed for all tide-gauges, along with MSL estimates (with epoch stated), and GNSS observations at tide-gauges, so that the accurate geodetic position (ϕ, λ, h) of each tide-gauge is known.

3. **ANGD:** The terrestrial gravity coverage needs extending in the Australian Alps and other rugged mountainous regions. Infill and densification of gravity observations in areas where only the original reconnaissance helicopter surveys exist is required. Terrestrial gravity observations should be transformed/corrected so that they all relate to the same height system (i.e., barometric, ellipsoid, ellipsoid + (unknown) geoid heights, AHD should all be in one system). However, this may not be possible if the necessary information is no longer available. Alternatively, correctly identifying the different methods of height observation in the

database could allow weighting of the gravity observations to reflect their height precision and possibly result in the development of a gravity error map of the ANGD.

4. **GNSS data:** GNSS h should be observed on ANLN junction points (JPs) rather than non-JP BMs, which are often located in the middle of the section. All GNSS outliers need to be found (whether blunders/typographic errors in GNSS h or discrete AHD height at the GNSS JP) and corrected or removed. Two-way levelling connections should be provided between ANLN and GNSS JPs, rather than derived AHD. The Australian GNSS network should continue to be densified, including repeat, or continuous observations to monitor vertical deformation.

The following recommendations relate to research areas that require further investigation prior to the final development of any new AVD:

1. **ANLN errors:** Outlier detection processes (Chapters 2 and 8) should be repeated during and following any ANLN upgrade, with all identified gross errors to be corrected. It is recommended that field books containing suspect sections are checked first for typographic/transcription error in ANLN. If the problem is not found and there is good evidence of a large error, then field work is required. To avoid large amounts of time-consuming levelling (of entire ANLN sections), it is recommended that GNSS and AGQG09 be used to identify the erroneous sub-section, which can then be re-levelled. Faster levelling methods such as motorised and/or total station levelling (as distinct from trigonometrical heighting) may have a role to play where additional re-levelling is needed. If the ANLN is fully upgraded, methods of identifying and treating systematic levelling errors should be implemented. In addition, improved *a priori* STD estimates for the different levelling types comprising the ANLN are recommended, possibly using variance component estimation (VCE).

2. **Levelling refraction:** It is suggested that the entire high-quality second-order network in WA (including two-way levelling and time and date of the surveys)

be entered into electronic file format, which can be used as a test area for retrospectively applying refraction corrections. Indeed, this test area (with all data available) could be used to test for numerous systematic errors/corrections (including GNSS and geoid testing).

3. **SSTM accuracy at tide-gauges:** Further research is required to fully evaluate the quality of different SSTM at tide-gauges and in coastal regions. Further tests to accurately determine error estimates at individual tide-gauges around Australia for SSTop + MSL constraints would improve combined adjustments of the ANLN.

4. **MSL estimates:** MSL estimates made from observations taken at different epochs require further examination. To incorporate large numbers of additional tide-gauges into the ANLN adjustment (up to 100 if the information is available), all MSL estimates need to be transformed to a common epoch to remove any temporal bias.

5. **Gravity errors:** Differences found between terrestrial- and EGM2008-derived gravity at BMs (particularly in mountainous regions) need further investigation. Further research into the effects of using 2D versus 3D interpolation of Bouguer anomalies is also warranted. Error estimates for gravity and geoid models across Australia (particularly in coastal and mountainous regions) are required.

6. **Rigorous orthometric heights:** Further research is required, particularly in mountainous regions. This could include tests to determine whether loop misclosure is reduced by the application of more rigorous (than Helmert) orthometric heights.

APPENDIX A: WEATHER STATIONS USED FOR SIMULATED APPLICATION OF REFRACTION CORRECTIONS TO THE ANLN

Data from the Australian Bureau of Meteorology

http://www.bom.gov.au/climate/averages/

Site	Label	State	Lat°	Lon°	Elev (m)
Canberra	CANB	ACT	-35.30	149.20	578
Armidale	ARMI	NSW	-30.52	151.67	980
Sydney	SYDN	NSW	-33.86	151.21	39
Bathurst	BATH	NSW	-33.43	149.56	713
Wagga	WAGG	NSW	-35.16	147.46	212
Dubbo	DUBB	NSW	-32.24	148.61	260
Cobar	COBA	NSW	-31.48	145.83	260
Broken Hill	BRHI	NSW	-31.98	141.47	315
Charlotte Pass	CHPA	NSW	-36.43	148.33	1755
Swan Hill	SWHI	Vic	-35.34	143.55	70
Corryong	CORR	Vic	-36.20	147.90	314
Sale	SALE	Vic	-38.12	147.13	5
Melbourne	MELB	Vic	-37.67	144.83	113
Hamilton	HAMI	Vic	-37.73	142.02	209
Alice Springs	ALSP	NT	-23.71	133.87	580
Tennant Creek	TNCR	NT	-19.65	134.19	377
Daly Waters	DAWT	NT	-16.26	133.38	210
Darwin	DARW	NT	-12.42	130.89	30
Brisbane	BRIS	Qld	-27.42	153.11	4
Emerald	EMER	Qld	-23.53	148.16	179
Mackay	MACK	Qld	-21.15	149.18	11
Charters Towers	CHTO	Qld	-20.08	146.26	310
Cunnamulla	CUNN	Qld	-28.07	145.68	189

Site	Label	State	Lat°	Lon°	Elev (m)
Julia Creek	JUCR	Qld	-20.66	141.75	123
Karumba	KARU	Qld	-17.46	140.83	2
Birdsville	BIRD	Qld	-25.90	139.35	47
Cairns	CAIR	Qld	-16.93	145.78	2
Weipa	WEIP	Qld	-12.63	141.88	11
Mt Barker	MTBA	SA	-35.06	138.85	360
Keith	KEIT	SA	-36.10	140.36	29
Loxton	LOXT	SA	-34.44	140.60	30
Hawker	HAWK	SA	-31.88	138.44	315
Warooka	WARO	SA	-34.99	137.40	53
Port Lincoln	PLIN	SA	-34.72	135.86	4
Kyancutta	KYAN	SA	-33.13	135.56	57
Tarcoola	TARC	SA	-30.71	134.57	120
Ernabella	ERNA	SA	-26.29	132.13	676
Preolenna	PREO	Tas	-41.09	145.55	260
Launceston	LAUN	Tas	-41.54	147.20	166
Hobart	HOBA	Tas	-42.83	147.50	4
Forrest	FORR	WA	-30.84	128.11	156
Southern Cross	SOCR	WA	-31.23	119.33	355
Norseman	NRSM	WA	-32.20	121.78	277
Northam	NRTM	WA	-31.65	116.66	170
Lake Grace	LAGR	WA	-33.10	118.46	286
Esperence	ESPE	WA	-33.85	121.88	4
Bridgetown	BRID	WA	-33.96	116.14	150
Carnamah	CARH	WA	-29.69	115.89	268
Carnarvon	CAVN	WA	-24.89	113.67	4
Wittenoom	WITT	WA	-22.24	118.34	463
Carnegie	CRNG	WA	-25.80	122.98	448
Telfer	TELF	WA	-21.71	122.23	292
Fitzroy Crossing	FITZ	WA	-18.19	125.56	114

APPENDIX B: JULY METEOROLOGICAL DATA USED FOR C_F AND W_F ESTIMATES USED IN CHAPTER 4

CODE: MT is average daily maximum temperature for July; MP is daily average maximum air pressure at MSL for July; CLR is average number of clear days for July; CDY is average number of cloudy days for July; PREC is average precipitation for July; WS is average wind speed for July; met1 is meteorological data set 1; met2 is meteorological data set 2; C_f and W_f are factors accounting for cloud cover and surface wetness respectively in the Angus-Leppan (1979) refraction correction. Data from the Australian Bureau of Meteorology, http://www.bom.gov.au/climate/averages/

Site	MT	MP	CLR	CDY	PREC	WS	met1		met2	
	(°C)	(mb)			(mm)	kph	C_f	W_f	C_f	W_f
CANB	12	1018	8	12	41	11	0.7	0.5	0.5	0.4
ARMI	12	1018	10	10	49	12	0.6	0.6	0.5	0.5
SYDN	16	1017	13	8	80	12	0.7	0.5	0.6	0.4
BATH	12	1017	6	11	44	6	0.5	0.5	0.4	0.4
WAGG	13	1019	7	15	55	11	0.6	0.5	0.4	0.4
DUBB	15	1020	11	10	45	11	0.7	0.6	0.5	0.5
COBA	16	1022	11	10	26	12	0.8	0.8	0.6	0.7
BRHI	16	1021	9	9	22	12	0.7	0.8	0.6	0.6
CHPA	3	1020	6	12	189	11	0.3	0.1	0.3	0.1
SWHI	14	1020	6	12	36	8	0.7	0.7	0.5	0.5
CORR	11	1020	3	18	81	4	0.3	0.4	0.2	0.3
SALE	14	1019	5	15	41	15	0.5	0.4	0.3	0.3
MELB	13	1020	3	15	36	23	0.4	0.4	0.2	0.3
HAMI	13	1021	3	17	72	14	0.2	0.1	0.2	0.2
ALSP	20	1021	15	4	15	8	1.0	1.0	0.8	0.8
TNCR	24	1018	24	1	5	10	1.0	1.0	0.9	0.9
DAWT	29	1015	18	3	1	12	1.0	0.8	0.8	0.7
DARW	30	1012	18	4	3	17	1.0	0.9	0.9	0.9

Site	MT	MP	CLR	CDY	PREC	WS	met1		met2	
	(°C)	(mb)			(mm)	kph	C_f	W_f	C_f	W_f
BRIS	20	1018	17	6	42	15	0.8	0.7	0.7	0.6
EMER	22	1020	18	4	21	7	1.0	0.9	0.8	0.8
MACK	22	1018	15	4	40	11	0.8	0.6	0.7	0.5
CHTO	25	1018	18	3	15	7	1.0	0.8	0.8	0.8
CUNN	19	1021	19	4	17	10	1.0	1.0	0.9	0.9
JUCR	27	1019	20	1	5	10	1.0	0.9	0.9	0.9
KARU	27	1014	21	3	2	14	1.0	0.8	0.9	0.9
BIRD	22	1020	21	4	10	8	1.0	1.0	0.8	0.9
CAIR	26	1017	10	5	40	7	0.7	0.6	0.6	0.5
WEIP	31	1014	5	7	2	9	1.0	0.7	0.4	0.6
MTBA	14	1022	4	14	100	12	0.5	0.3	0.3	0.2
KEIT	15	1021	5	13	57	12	0.5	0.5	0.3	0.4
LOXT	16	1021	5	13	28	14	0.6	0.7	0.4	0.6
HAWK	16	1022	8	9	35	11	0.7	0.7	0.6	0.6
WARO	15	1022	3	13	66	15	0.4	0.4	0.2	0.3
PLIN	16	1022	3	13	78	16	0.3	0.3	0.2	0.3
KYAN	17	1021	7	11	40	14	0.7	0.6	0.5	0.5
TARC	18	1024	9	8	17	9	0.9	1.0	0.7	0.8
ERNA	18	1022	15	4	12	13	1.0	1.0	0.8	0.9
PREO	10	1026	2	21	205	7	0.2	0.1	0.1	0.1
LAUN	11	1020	5	15	62	12	0.4	0.3	0.3	0.3
HOBA	12	1026	4	15	45	14	0.4	0.6	0.3	0.3
FORR	18	1022	11	7	17	20	0.9	1.0	0.7	0.8
SOCR	16	1020	7	12	40	14	0.7	0.7	0.5	0.6
NRSM	17	1020	9	9	30	14	0.7	0.8	0.5	0.6
NRTM	17	1019	7	11	82	11	0.5	0.5	0.4	0.4
LAGR	15	1020	5	12	50	10	0.5	0.6	0.4	0.4
ESPE	17	1021	6	11	107	15	0.5	0.5	0.4	0.3
BRID	17	1021	3	14	146	6	0.2	0.1	0.2	0.2
CARH	18	1020	8	7	70	14	0.7	0.6	0.5	0.5
CAVN	22	1017	19	4	47	20	1.0	0.9	0.9	0.7

Site	MT	MP	CLR	CDY	PREC	WS	met1		met2	
	(°C)	(mb)			(mm)	kph	C_f	W_f	C_f	W_f
WITT	24	1016	22	3	9	8	1.0	0.9	0.8	0.8
CRNG	21	1020	22	3	12	15	1.0	1.0	0.9	0.9
TELF	25	1016	13	5	14	17	1.0	1.0	0.7	0.8
FITZ	30	1015	23	2	2	10	1.0	0.9	0.8	0.9

REFERENCES

Abeyratne, P. G. V. and W. E. Featherstone. 2008. Assessment of EGM2008 over Sri Lanka, an area where fill-in data were used in EGM2008. *Newton's Bulletin*, 4:284–316.

Abeyratne, P. G. V., W. E. Featherstone, and D. A. Tantrigoda. 2010. On the geodetic datums in Sri Lanka. *Survey Review*, 42(317):229–239. doi:10.1179/003962610X12572516251880.

Ahmad, Z., A. H. W. Kearsley, and B. R. Harvey. 1993. Optimising GPS, geoid and tide gauge heights in vertical control networks. In *UNISURV S43*, ed. A. H. W. Kearsley, 127–209. Sydney, Australia: University of New South Wales.

Allister, N. A. and W. E. Featherstone. 2001. Estimation of Helmert orthometric heights using digital barcode levelling, observed gravity and topographic mass-density data over part of the Darling Scarp, Western Australia. *Geomatics Research Australasia*, 75:25–52.

Altamimi, Z., X. Collileux, J. Legrand, B. Garayt, and C. Boucher. 2007. ITRF2005: A new release of the International Terrestrial Reference Frame based on time series of station positions and Earth Orientation Parameters. *Journal of Geophysical Research*, 112:B09401. doi:10.1029/2007JB004949.

Altamimi, Z., P. Sillard, and C. Boucher. 2002. ITRF2000: A new release of the International Terrestrial Reference Frame for Earth science applications. *Journal of Geophysical Research*, 107(B10):2214. doi:10.1029/2001JB000561.

Amin, M. 1993. Changing mean sea level and tidal constants on the west coast of Australia. *Australian Journal of Marine and Freshwater Research*, 44(6):911–925. doi:10.1071/MF9930911.

Amos, M. J. 2007. *Quasigeoid modelling in New Zealand to unify multiple local vertical datums*. Ph.D. diss., Curtin University of Technology, Perth, Aus-

tralia.

Amos, M. J. and W. E. Featherstone. 2009. Unification of New Zealand's local vertical datums: iterative gravimetric quasigeoid computations. *Journal of Geodesy*, 83(1):57–68. doi:10.1007/s00190-008-0232-y.

Andersen, O. B. 1999. Shallow water tides in the northwest European shelf region from TOPEX/Poseidon altimetry. *Journal of Geophysical Research*, 104(C4):7729–7741. doi:10.1029/1998JC900112.

Andersen, O. B. and P. Knudsen. 2009. DNSC08 mean sea surface and mean dynamic topography models. *Journal of Geophysical Research*, 114:C11001. doi:10.1029/2008JC005179.

Angus-Leppan, P. V. 1975. An investigation of possible systematic errors in levelling along the eastern coast of Australia. In *UNISURV G23*, 80–91. Sydney, Australia: University of New South Wales.

Angus-Leppan, P. V. 1979. Refraction in levelling - its variation with ground slope and meteorlogical conditions. *Australian Journal of Geodesy, Photogrammetry and Surveying*, 31:27–41.

Angus-Leppan, P. V. 1980. Refraction in levelling: extension to stable and neutral atmospheric conditions. In *Second International Symposium on Problems Related to the Redefinition of the North American Vertical Geodetic Networks: NAD Symposium 1980*, ed. G. Lachapelle, 677–689. Ottawa, Canada: Canadian Institute of Surveying.

Angus-Leppan, P. V. 1982. The required frequency of gravity measurements for levelling reduction. *Australian Journal of Geodesy, Photogrammetry and Surveying*, 36:65–82.

Angus-Leppan, P. V. 1984. Refraction in geodetic levelling. In *Geodetic Refraction*, ed. F. Brunner, 163–180. Berlin, Germany: Springer.

Arabelos, D. and C. C. Tscherning. 2001. Improvements in height datum transfer expected from the GOCE mission. *Journal of Geodesy*, 75(5-6):308–312. doi:10.1007/s001900100187.

Ardalan, A. A., R. Karimi, and M. Poutanen. 2010. A bias-free geodetic boundary value problem approach to height datum unification. *Journal of Geodesy*, 84(2):123–134. doi:10.1007/s00190-009-0348-8.

Ardalan, A. A. and A. Safari. 2005. Global height datum unification: a new approach in gravity potential space. *Journal of Geodesy*, 79(9):512–523. doi:10.1007/s00190-005-0001-0.

Baarda, W. 1968. A testing procedure for use in geodetic networks. New Series Report 2(5), Netherlands Geodetic Comission, Delft, The Netherlands.

Balasubramania, N. 1994. Definition and realization of a global vertical datum. Report 427, The Ohio State University, Columbus, USA.

Balasz, E. I. and B. C. Douglas. 1979. Geodetic leveling and the sea level slope along the California coast. *Journal of Geophysical Research*, 84(B11):6195–6206. doi:10.1029/JB084iB11p06195.

Balazs, E. I. and G. M. Young. 1982. Corrections applied by the National Geodetic Survey to precise leveling observations. National Oceanic Atmospheric Administration Technical Memorandum 34, National Geodetic Survey, Rockville, USA.

Barlow, B. C. 1977. Data limitations on model complexity; 2-D gravity modelling with desk-top calculators. *Bulletin of the Australian Society of Exploration Geophysics*, 8(4):139–143. doi:10.1071/EG977139.

Bellamy, C. J. and G. D. Lodwick. 1968. The reduction of barometric networks and field gravity surveys. *Survey Review*, 19(147):216–227. doi:10.1071/EG977139.

Belperio, A. P. 1993. Land subsidence and sea-level rise in the Port Adelaide estuary: Implications for monitoring the greenhouse effect. *Australian Journal of Earth Sciences*, 40(4):359–368. doi:10.1080/08120099308728087.

Best, A. C. 1935. Transfer of heat and momentum in the lowest layers of the atmosphere. Geophysical Memoirs 65-8(VII), Air Ministry, Meteorological Office, His Majesty's Stationary Office. London, UK.

Bingham, R. J. and K. Haines. 2006. Mean dynamic topography: intercomparisons and errors. *Philosophical Transactions of the Royal Society A*, 364(1841):903–916. doi:10.1098/rsta.2006.1745.

Biró, P. 1983. *Time variation of height and gravity*. Karlsruhe, Germany: Wichmann.

Boal, D., R. Gareau, and F. Young. 1985. Status of vertical control networks in Canada. In *Proceedings of the Third International Symposium on the North American Vertical Datum - NAVD Symposium '85*, 1–10. Rockville, USA: National Oceanic and Atmospheric Administration.

Bomford, G. 1971. *Geodesy*. 3rd ed. Oxford, UK: Oxford University Press.

Bouin, M. N. and G. Wöppelmann. 2010. Land motion estimates from GPS at tide gauges: a geophysical evaluation. *Geophysical Journal International*, 180(1):193–209. doi:10.1111/j.1365-246X.2009.04411.x.

Bretreger, K. 1986. Tidal effects on geodetic levelling. *Australian Journal of Geodesy, Photogrammetry and Surveying*, 45:37–54.

Brocks, K. 1948. Über den täglichen und jährlichen Gang der Temperatur in den unteren 300 m der Atmosphäre und ihren Zusammenhang mit der Konvenktion. Technical Report Nr. 5, Berichte des Deutschen Wetterdienstes in der U.S.-Zone.

Brooks, B. A., M. A. Merrifield, J. Foster, C. L. Werner, F. Gomez, M. Bevis, and S. Gill. 2007. Space geodetic determination of spatial variability in relative sea level change, Los Angeles basin. *Geophysical Research Letters*, 34:L01611. doi:10.1029/2006GL028171.

Buble, G., R. A. Bennett, and S. Hreinsdóttir. 2010. Tide gauge and GPS measurements of crustal motion and sea level rise along the eastern margin of Adria. *Journal of Geophysical Research*, 115:B02404. doi:10.1029/2008JB006155.

Buckley, S. M., P. A. Rosen, S. Hensley, and B. D. Tapley. 2003. Land subsidence in Houston, Texas, measured by radar interferometry and constrained by extensometers. *Journal of Geophysical Research*, 108(B11):2542.

doi:10.1029/2002JB001848.

Burša, M., S. Kenyon, J. Kouba, K. Raděj, V. Vatrt, M. Vojtíšková, and J. Šimek. 2002. World height system specified by geopotential at tide-gauge stations. In *Vertical Reference Systems*, eds. H. Drewes, A. Dodson, L. P. S. Fortes, L. Sánchez, and P. Sandoval, 291–296. Berlin, Germany: Springer.

Burša, M., S. Kenyon, J. Kouba, Z. Šima, V. Vatrt, and M. Vojtíšková. 2004. A global vertical reference frame based on four regional vertical frames. *Studia Geophysica et Geodaetica*, 48(3):493–502. doi:10.1023/B:SGEG.0000037468.48585.e6.

Burša, M., J. Kouba, M. Kumar, A. Müller, K. Raděj, S. A. True, V. Vatrt, and M. Vojtíšková. 1999a. Geoidal geopotential and World Height System. *Studia Geophysica et Geodaetica*, 43(4):327–337. doi:10.1023/A:1023273416512.

Burša, M., J. Kouba, A. Müller, K. Raděj, S. A. True, and V. Vatrt. 2001. Determination of geopotential differences between local vertical datums and realization of a World Height System. *Studia Geophysica et Geodaetica*, 45(2):127–132. doi:10.1023/A:1021860126850.

Burša, M., J. Kouba, A. Müller, K. Raděj, V. Vatrt, M. Vojtíšková, and S. A. True. 1999b. Determination of the geopotential at the tide-gauge defining the North American Vertical Datum 1988 (NAVD1988). *Geomatica*, 53(3):291–296.

Calvert, C. E. and A. H. Dodson. 1985. A comparison of approaches to the levelling refraction problem. In *Third International Symposium on the North American Vertical Datum - NAVD Symposium '85*, 301–309. Rockville, USA: National Oceanic and Atmospheric Administration.

Carrera, G. H. 1984. Heights on a deforming Earth. Technical Report 107, University of New Brunswick, Fredricton, Canada.

Cassinis, G. 1930. Sur l'adoption d'une formule internationale pour la pesanteur normale (On the adoption of an international formula for normal gravity). *Bulletin Géodésique*, 26(1):40–49. doi:10.1007/BF03030025.

Castle, R. O., J. P. Church, and M. R. Elliot. 1976. Aseismic uplift in southern

California. *Science*, 192(4236):251–253. doi:10.1126/science.192.4236.251.

Castle, R. O., J. P. Church, M. R. Elliot, T. D. Gilmore, R. K. Mark, E. B. Newman, and J. C. I. Tinsley. 1983. Comment on 'The impact of refraction correction on leveling interpretations in southern California' by William E. Strange. *Journal of Geophysical Research*, 88(B3):2508–2512. doi:10.1029/JB088iB03p02508.

Castle, R. O. and M. R. Elliot. 1982. The sea slope problem revisited. *Journal of Geophysical Research*, 87(B8):6989–7024. doi:10.1029/JB087iB08p06989.

Chambers, D. 2008. DOT_DNSCMSS08-EGM08_gau_ave_111km_dpc.txt. Technical details in file header, Jet Propulsion Laboratory, California Institute of Technology. Online [accessed 13 November 2008] http://grace.jpl.nasa.gov/data/dot.

Chi, S. C. and R. E. Reilinger. 1984. Geodetic evidence for subsidence due to groundwater withdrawal in many parts of the United States of America. *Journal of Hydrology*, 67(1-4):155–182. doi:10.1016/0022-1694(84)90239-7.

Christie, R. R. 1994. A new geodetic heighting strategy for Great Britain. *Survey Review*, 32(252):328–343.

Church, J. A. and N. J. White. 2006. A 20th century acceleration in global sea-level rise. *Geophysical Research Letters*, 33:L01602. doi:10.1029/2005GL024826.

Church, J. A., N. J. White, A. Thorkild, W. S. Wilson, P. L. Woodworth, C. M. Domingues, J. R. Hunter, and K. Lambeck. 2008. Understanding global sea levels: past, present and future. *Sustainability Science*, 3(1):9–22. doi:10.1007/s11625-008-0042-4.

Claessens, S. J. 2006. *Solutions to ellipsoidal boundary value problems for gravity field modelling*. Ph.D. diss., Curtin University of Technology, Perth, Australia.

Claessens, S. J., W. E. Featherstone, I. M. Anjasmara, and M. S. Filmer. 2009. Is Australian data really validating EGM2008, or is EGM2008 just in/validating Australian data? *Newton's Bulletin*, 4:207–251.

Claessens, S. J., C. Hirt, M. J. Amos, W. E. Featherstone, and J. F. Kirby. 2011. The NZGEOID09 model of New Zealand. *Survey Review*, 43(319):2–15. doi:10.1179/003962610X12747001420780.

Clendinning, J. and J. G. Olliver. 1969. *Principles and use of surveying instruments*. 3rd ed. London, UK: Van Nostrand Reinhold.

Cleveland, W. S. and S. J. Devlin. 1988. Locally weighted regression: An approach to regression analysis by local fitting. *Journal of the American Statistical Association*, 83(403):596–610.

Coleman, R., C. Rizos, E. G. Masters, and B. Hirsch. 1979. The investigation of the sea surface slope along the north eastern coast of Australia. *Australian Journal of Geodesy, Photogrammetry and Surveying*, 31:686–99.

Collier, P. A. and M. J. Croft. 1997a. Heights from GPS in an engineering environment (part 1). *Survey Review*, 34(263):11–18.

Collier, P. A. and M. J. Croft. 1997b. Heights from GPS in an engineering environment (part 2). *Survey Review*, 34(264):76–85.

Colombo, O. L. 1980. A world vertical network. Report 296, The Ohio State University, Columbus, USA.

Comerlati, A., M. Ferronato, G. Gambolati, M. Putti, and P. Teatini. 2006. Fluid-dynamic and geomechanical effects of CO_2 sequestration below the Venice Lagoon. *Environmental and Engineering Geoscience*, 12(3):211–226. doi:10.2113/gseegeosci.12.3.211.

Craymer, M. R. and P. Vaníček. 1986. Further analysis of the 1981 Southern California field test for levelling refraction. *Journal of Geophysical Research*, 91(B9):9045–9055. doi:10.1029/JB091iB09p09045.

Craymer, M. R. and P. Vaníček. 1989. Comment on "Saugus-Palmdale, California, field test for refraction error in historical levelling surveys" by R.S. Stein, C.T. Whalen, S.R. Holdahl, W.E. Strange, and W. Thatcher, and Reply to "Comment on 'Further analysis of the 1981 Southern California field test for levelling refraction by M.R. Craymer and P. Vaníček by R.S Stein, C.T. Whalen, S.R. Holdahl, W.E. Strange, and W. Thatcher' ". *Journal of*

Geophysical Research, 94(B6):7667–7672. doi:10.1029/JB094iB06p07667.

Craymer, M. R., P. Vaníček, and R. O. Castle. 1995. Estimation of rod scale errors in geodetic levelling. *Journal of Geophysical Research*, 100(B8):15,129–15,145. doi:10.1029/95JB00614.

Currie, R. G. 1975. Period, Q_p and the amplitude of the pole tide. *Geophysical Journal of the Royal Astronomical Society*, 43(1):73–86. doi:10.1111/j.1365-246X.1975.tb00628.x.

Dach, R., U. Hugentobler, P. Fridez, and M. Meindl. 2007. *Bernese GPS Software Version 5.0*. Astronomical Institute, University of Bern, Switzerland.

de Freitas, S. R. C., S. H. S. Schwab, E. Marone, A. O. Pires, and R. Dalazoana. 2002. Local effects in the Brazilian vertical datum. In *Vistas for Geodesy in the New Millenium*, eds. J. Ádám and K.-P. Schwarz, 102–107. Berlin, Germany: Springer.

Deng, X. and W. E. Featherstone. 2006. A coastal retracking system for satellite radar altimeter waveforms: Application to ERS-2 around Australia. *Journal of Geophysical Research*, 111:C06012. doi:10.1029/2005JC003039.

Deng, X., W. E. Featherstone, C. Hwang, and P. A. M. Berry. 2002. Estimation of contamination of ERS-2 and Poseidon satellite radar altimetry close to the coasts of Australia. *Marine Geodesy*, 25(4):249–271. doi:10.1080/01490410214990.

Dennis, M. L. and W. E. Featherstone. 2003. Evaluation of orthometric and related height systems using a simulated mountain gravity field. In *Gravity and Geoid 2002*, ed. I. N. Tziavos, 389–394. Thessaloniki, Greece: Ziti Editions.

Dentith, M. C. and W. E. Featherstone. 2003. Controls on intra-plate seismicity in southwestern Australia. *Tectonophysics*, 376(3-4):167–184. doi:10.1016/j.tecto.2003.10.002.

Ding, X. and R. Coleman. 1996. Multiple outlier detection by evaluating redundancy contributions of observations. *Journal of Geodesy*, 70(8):489–498. doi:10.1007/s001900050037.

Drinkwater, M. R., R. Floberghagen, R. Haagmans, D. Muzi, and A. Popescu. 2003. GOCE: ESA's first Earth explorer core mission. *Space Science Reviews*, 108(1-2):419–432. doi:10.1023/A:1026104216284.

Dunn, J. 2006. CSIRO Atlas of Regional Seas: CARS2006. Online [accessed 23 September 2008], Website last updated 22 July 2006, http://www.marine.csiro.au/ dunn/cars2006/.

Dunn, J. 2008. BlueLink Ocean Archive - BOA. Online [accessed 23 September 2008], Website last updated 7 April 2008, http://www.marine.csiro.au/ dunn/BOA.html.

Dunn, J. R. and K. R. Ridgway. 2002. Mapping ocean properties in regions of complex topography. *Deep-Sea Research I*, 49(3):591–604. doi:10.1016/S0967-0637(01)00069-3.

Easton, A. K. 1968. A handbook of selected Australian tide gauges. Survey Paper 6, Horace Lamb Centre for Oceanographical Research, Flinders University, Adelaide, Australia.

Easton, A. K. and R. Radok. 1970. Tidal programme 1966-1967. Memorandum 5, Horace Lamb Centre for Oceanographical Research, Flinders University, Adelaide, Australia.

Ekman, M. 1989. Impacts of geodynamic phenomena on systems for height and gravity. *Bulletin Géodésique*, 63(3):281–296. doi:10.1007/BF02520477.

Entin, I. I. 1959. Main systematic errors in precise levelling. *Bulletin Géodésique*, 52(1):37–45. doi:10.1007/BF02526861.

Fawaz, E. 1981. *Beurtelung von Nivellementsnetzen auf der Grundlage der Theorie der stochastischen Prozesse*. Ph.D. diss., Arbeiten der Fachrichtung Vermessungswesen, der Universität Hannover, Hannover, Germany.

Featherstone, W. E. 1995. On the use of Australian geodetic datums in gravity field determination. *Geomatics Research Australasia*, 62:17–36.

Featherstone, W. E. 1998. Do we need a gravimetric geoid or a model of the Australian Height Datum to transform GPS heights in Australia? *The Australian Surveyor*, 43(4):273–280.

Featherstone, W. E. 2000. Towards the unification of the Australian Height Datum between mainland and Tasmania using GPS and AUSGeoid98. *Geomatics Research Australasia*, 73:33–54.

Featherstone, W. E. 2001. Absolute and relative testing of gravimetric geoid models using Global Positiong System and orthometric height data. *Computers and Geosciences*, 27(7):807–814. doi:10.1016/S0098-3004(00)00169-2.

Featherstone, W. E. 2002a. Attempts to unify the Australian Height Datum between the mainland and Tasmania. In *Vertical Reference Systems*, eds. H. Drewes, A. Dodson, L. Fortes, L. Sánchez, and P. Sandoval, 328–333. Berlin, Germany: Springer.

Featherstone, W. E. 2002b. Prospects for the Australian Height Datum and geoid model. In *Vistas for Geodesy in the New Millenium*, eds. J. Ádám and K.-P. Schwarz, 96–101. Berlin, Germany: Springer.

Featherstone, W. E. 2003. Improvement to long-wavelength Australian gravity anomalies expected from the GRACE, CHAMP and GOCE dedicated satellite gravimetry missions. *Exploration Geophysics*, 34(1-2):69–76. doi:10.1071/EG03069.

Featherstone, W. E. 2004. Evidence of a north-south trend between AUSGeoid98 and the AHD in southwest Australia. *Survey Review*, 37(291):334–343.

Featherstone, W. E. 2005. Long-wavelength discrepancies between the Australian gravity field and EIGEN-2 CHAMP data. In *A Window on the Future of Geodesy*, ed. F. Sansò, 300–305. Berlin, Germany: Springer.

Featherstone, W. E. 2006. Yet more evidence for a north-south slope in the AHD. *Journal of Spatial Science*, 51(2):1–6.

Featherstone, W. E. 2008. GNSS-heighting in Australia: current and emerging issues. *Journal of Spatial Science*, 53(2):115–133.

Featherstone, W. E. and V. Dent. 2002. Transfer of vertical control using only one GPS receiver: a case study. *The Australian Surveyor*, 47(1):31–37.

Featherstone, W. E. and M. C. Dentith. 1997. A geodetic approach to gravity data reduction for geophysics. *Computers and Geosciences*, 23(10):1063–1070.

doi:10.1016/S0098-3004(97)00092-7.

Featherstone, W. E., M. C. Dentith, and J. F. Kirby. 1998. Strategies for the accurate determination of orthometric heights from GPS. *Survey Review*, 34(267):278–296.

Featherstone, W. E. and M. S. Filmer. 2008. A new GPS-quasigeoid-based evaluation of distortions in the Australian Height Datum in Western Australia. *Journal of the Royal Society of Western Australia*, 91(2):199–206.

Featherstone, W. E. and W. Guo. 2001. Evaluations of the precision of AUSGeoid98 versus AUSGeoid93 using GPS and Australian height datum data. *Geomatics Research Australasia*, 74:75–102.

Featherstone, W. E. and J. F. Kirby. 1998. Estimates of the separation between the geoid and the quasigeoid over Australia. *Geomatics Research Australasia*, 68:79–90.

Featherstone, W. E. and J. F. Kirby. 2000. The reduction of aliasing in gravity anomalies and geoid heights using digital terrain data. *Geophysical Journal International*, 141(1):204–212. doi:10.1046/j.1365-246X.2000.00082.x.

Featherstone, W. E. and J. F. Kirby. 2002. New high-resolution grid of gravimetric terrain corrections over Australia. *Australian Journal of Earth Sciences*, 49(5):733–734. doi:10.1046/j.1440-0952.2002.00952.x.

Featherstone, W. E., J. F. Kirby, C. Hirt, M. S. Filmer, S. J. Claessens, N. Brown, G. Hu, and G. M. Johnston. 2011. The AUSGeoid09 model of the Australian Height Datum. *Journal of Geodesy*, 85(3):133–150. doi:10.1007/s00190-010-0422-2.

Featherstone, W. E., J. F. Kirby, A. H. W. Kearsley, J. R. Gilliland, G. M. Johnston, J. Steed, R. Forsberg, and M. G. Sideris. 2001. The AUSGeoid98 geoid model of Australia: data treatment, computations and comparisons with GPS-levelling data. *Journal of Geodesy*, 75(5-6):313–330. doi:10.1007/s001900100177.

Featherstone, W. E. and M. Kuhn. 2006. Height systems and vertical datums: a review in the Australian context. *Journal of Spatial Sciences*, 51(1):21–42.

Featherstone, W. E. and L. Morgan. 2007. Validation of the AUSGeoid98 model in Western Australia using historic astrogeodetically observed deviations of the vertical. *Journal of the Royal Society of Western Australia*, 90:143–150.

Featherstone, W. E. and D. M. Sproule. 2006. Fitting AUSGeoid98 to the Australian Height Datum using GPS-levelling and least squares collocation: application of a cross-validation technique. *Survey Review*, 38(301):573–582.

Featherstone, W. E. and M. P. Stewart. 1998. Possible evidence for distortions in the Australian Height Datum in Western Australia. *Geomatics Research Australasia*, 68:1–12.

Fenoglio-Marc, L. and E. Tel. 2010. Coastal and global sea level change. *Journal of Geodynamics*, 49(3-4):151–160. doi:10.1016/j.jog.2009.12003.

Fielding, E. J., R. G. Blom, and R. M. Goldstein. 1998. Rapid subsidence over oil fields measured by SAR. *Geophysical Research Letters*, 25(17):3215–3218. doi:10.1029/98GL52260.

Filmer, M. S. and W. E. Featherstone. 2009. Detecting spirit-levelling errors in the AHD: recent findings and some issues for any new Australian height datum. *Australian Journal of Earth Sciences*, 56(4):559–569. doi:10.1080/08120090902806305.

Filmer, M. S., W. E. Featherstone, and M. Kuhn. 2010. The effect of EGM2008-based normal, normal-orthometric and Helmert orthometric height systems on the Australian levelling network. *Journal of Geodesy*, 84(8):501–513. doi:10.1007/s00190-010-0388-0.

Filmer, M. S., M. Kuhn, and W. E. Featherstone. 2009. Correction to Angus-Leppan, P. V. (1979) Refraction in levelling - its variation with ground slope and meteorological conditions, Australian Journal of Geodesy, Photogrammetry and Surveying, no. 31, pp. 27-41. *Journal of Spatial Science*, 54(1):105–107.

Fischer, I. 1975. Does mean sea level slope up or down toward north? *Bulletin Géodésique*, 49(1):17–26. doi:10.1007/BF02523939.

Flury, J. and R. Rummel. 2009. On the geoid-quasigeoid separation in mountain

areas. *Journal of Geodesy*, 83(9):829–847. doi:10.1007/s00190-009-0302-9.

Forbes, A. M. G. and J. A. Church. 1983. Circulation in the Gulf of Carpentaria. II. Residual currents and mean sea level. *Australian Journal of Marine and Freshwater Research*, 34(1):11–22. doi:10.1071/MF9830011.

Forsberg, R. 1984. A study of terrain reductions, density anomalies and geophysical inversion methods in gravity field modelling. Report 355, The Ohio State University, Columbus, USA.

Forsberg, R. 1985. Gravity field terrain effect computations by FFT. *Bulletin Géodésique*, 59(4):342–360. doi:10.1007/BF02521068.

Forsberg, R. and C. C. Tscherning. 1981. The use of height data in gravity field approximation by collocation. *Journal of Geophysical Research*, 86(B9):7843–7854. doi:10.1029/JB086iB09p07843.

Fotopolous, G. 2005. Calibration of geoid error models via a combined adjustment of ellipsoidal, orthometric and gravimetric geoid height data. *Journal of Geodesy*, 79(1-3):111–123. doi:10.1007/s00190-005-0449-y.

Fraser, A. R., F. J. Moss, and A. Turpie. 1976. Reconnaissance gravity survey of Australia. *Geophysics*, 41(6):1337–1345. doi:10.1190/1.1440683.

Fuchs, H. 1982. Contribution to the adjustment by minimizing the sum of absolute residuals. *manuscripta geodaetica*, 7(3):151–207.

Gao, Y., E. J. Krakiwsky, and J. Czompo. 1992. Robust testing procedure for detection of multiple blunders. *Journal of Surveying Engineering*, 118(1):11–23. doi:10.1061/(ASCE)0733-9453.

Gareau, R. M. 1986. History of precise levelling in Canada and the North American Vertical Datum readjustment. UCSE Report 20018, The University of Calgary, Calgary, Canada.

Garfinkel, B. 1978. On the theory of terrestrial refraction. First quarterly report Contract no. 78-40065, Yale University Observatory, USA.

Garfinkel, B. 1979. On the theory of terrestrial refraction. Fourth quarterly report Contract no. 78-40065, Yale University Observatory, USA.

Gilliland, J. R. 1986. Heights and GPS. *The Australian Surveyor*, 33(4):277–283.

Godfrey, J. S. 1973. Mean sea level: the oceanographer's point of view. In *Proceedings of the Symposium on Earth's Gravitational Field & Secular Variations in Position*, eds. R. S. Mather and P. V. Angus-Leppan, 560–564. Sydney, Australia: University of New South Wales.

Goos, J. M., W. E. Featherstone, J. F. Kirby, and S. A. Holmes. 2003. Experiments with two different approaches to gridding terrestrial gravity anomalies and their effect on regional geoid computation. *Survey Review*, 37(288):92–112.

Granger, H. W. 1972. The Australian Height Datum. *The Australian Surveyor*, 24(4):228–237.

Hackney, R. I. and W. E. Featherstone. 2003. Geodetic versus geophysical perspectives of the 'gravity anomaly'. *Geophysical Journal International*, 154(1):35–43. doi:10.1046/j.1365-246X.2003.01941.x, Erratum 154(2):596; Corrigendum 167(2):585.

Hamon, B. V. and M. A. Greig. 1972. Mean sea level in relation to geodetic land levelling around Australia. *Journal of Geophysical Research*, 77(36):7157–7162. doi:10.1029/JC077i036p07157.

Harvey, B. R. 2006. Practical Least Squares and Statistics for Surveyors, 3rd ed. Monograph 13, University of New South Wales, Sydney, Australia.

Hayford, J. F. 1909. The figure of the Earth and isostasy, from measurements in the United States. Technical Report, U.S. Coast and Geodetic Survey, USA.

Heck, B. 1990. An evaluation of some systematic error sources affecting terrestrial gravity anomalies. *Bulletin Géodésique*, 64(1):88–108. doi:10.1007/BF02530617.

Heck, B. 1993. Tidal corrections in geodetic height determination. In *Applications of Geodesy to Engineering*, ed. Linkwitz, K. and Eisele, V. and Mönicke, H.-J. Berlin, Germany: Springer.

Heck, B. 1995. *Rechenverfahren und Auswertemodelle der Landesvermessung (Computational methods and models in surveying)*. Heidelberg, Germany:

Wichmann.

Heer, R. 1984. Refraktionsuntersuchungen auf der Nivellementsschleife Koblenz. Bericht zur 10.AG - Sitzung 'Haupthöhennetz' in Emden (unpublished).

Heer, R. and W. Neimeier. 1985. Theoretical models, practical experiments and the numerical evaluation of refraction effects in geodetic leveling. In *Proceedings of the Third International Symposium on the North American Vertical Datum - NAVD Symposium '85*, 321–342. Rockville, USA: National Oceanic and Atmospheric Administration.

Heiskanen, W. A. and H. Moritz. 1967. *Physical Geodesy*. San Francisco, USA: Freeman.

Hekimoğlu, S. 1997. Finite sample breakdown points of outlier detection procedures. *Journal of Surveying Engineering*, 123(1):15–31. doi:10.1061/(ASCE)0733-9453.

Hekimoğlu, S. and M. Berber. 2003. Effectiveness of robust methods in heterogeneous linear models. *Journal of Geodesy*, 76(11-12):706–713. doi:10.1007/s00190-002-0289-y.

Helmert, F. R. 1890. Die Schwerkraft im Hochgebirge, Insbesondere in den Tyroler Alpen (Gravity in high mountains with focus on the Tyrol Alps). No. 1, Veröff. Königl. Preuss. Geod. Inst.

Hernandez, F., M. H. Calvez, J. Dorandeu, Y. Faugre, F. Mertz, and P. Schaeffer. 2001. Surface Moyenne Oceanique: Support scientifique à la mission altimétrique Jason-1, et à une mission micro-satellite altimé trique. Contrat SSALTO 2945 - Lot2 - A.1 Rapport d'avancement Rapport no. Final CLS/DOS/NT/00.341, Collecte Localisation Satellites, Ramonville, France.

Heroux, P., W. Gale, and F. Faucher. 1985. Field test report on the systematic effect of refraction in precise levelling. In *Proceedings of the Third International Symposium on the North American Vertical Datum - NAVD Symposium '85*, 311–320. Rockville, USA: National Oceanic and Atmospheric Administration.

Hill, E. M., J. L. Davis, M. E. Tamisiea, and M. Lidberg. 2010. Combination of geodetic observations and models for glacial isostatic adjust-

ment fields in Fennoscandia. *Journal of Geophysical Research*, 115:B07403. doi:10.1029/2009JB006967.

Hipkin, R. 2000. Modelling the geoid and sea-surface topography in coastal areas. *Physics and Chemistry of the Earth (A)*, 25(1):9–16. doi:10.1016/S1464-1895(00)00003-X.

Hipkin, R., K. Haines, C. Beggan, R. Bingley, F. Hernandez, J. Holt, and T. Baker. 2004. The geoid EDIN2000 and the mean sea surface topography around the British Isles. *Geophysical Journal International*, 157(2):565–577. doi:10.1111/j.1365-246X.2004.01989.x.

Hirt, C. 2010. Prediction of vertical deflections from high-degree spherical harmonic synthesis and residual terrain model data. *Journal of Geodesy*, 84(3):179–190. doi:10.1007/s00190-009-0354-x.

Hirt, C., W. E. Featherstone, and U. Marti. 2010a. Combining EGM2008 and SRTM/DTM2006.0 residual terrain model data to improve quasigeoid computations in mountainous areas devoid of gravity data. *Journal of Geodesy*, 84(9):557–567. doi:10.1007/s00190-010-0395-1.

Hirt, C., M. S. Filmer, and W. E. Featherstone. 2010b. Comparison and validation of recent freely-available digital elevation models ASTER-GDEM ver1, SRTM ver4.1 and GEODATA DEM-9S ver3 digital elevation models over Australia. *Australian Journal of Earth Sciences*, 57(3):337–347. doi:10.1080/08120091003677553.

Hirt, C. and J. Flury. 2008. Astronomical-topographic levelling using high-precision astrogeodetic vertical deflections and digital terrain model data. *Journal of Geodesy*, 82(4-5):231–248. doi:10.1007/s00190-007-0173-x.

Hirt, C., U. Marti, B. Bürki, and W. E. Featherstone. 2010c. Assessment of EGM2008 in Europe using accurate astrogeodetic vertical deflections and omission error estimates from SRTM/DTM2006.0 residual terrain model data. *Journal of Geophysical Research*, 115:B10404. doi:10.1029/2009JB007057.

Holdahl, S. R. 1980. A model of temperature stratification for correction of levelling refraction. In *Second International Symposium on Problems Related to*

the Redefinition of the North American Vertical Geodetic Networks: NAD Symposium 1980, ed. G. Lachapelle, 647–676. Ottawa, Canada: Canadian Institute of Surveying.

Holdahl, S. R. 1981. A model of temperature stratification for correction of levelling refraction. *Bulletin Géodésique*, 55(3):231–249. doi:10.1007/BF02530864.

Holdahl, S. R. 1982. Recomputation of vertical crustal motions near Palmdale, California, 1959-1975. *Journal of Geophysical Research*, 87(B11):9374–9388. doi:10.1029/JB087iB11p09374.

Holgate, S. J. and P. L. Woodworth. 2004. Evidence for enhanced coastal sea level rise during the 1990s. *Geophysical Research Letters*, 31:L07305. doi:10.1029/2004GL019626.

Holloway, R. D. 1988. The integration of GPS heights into the Australian Height Datum. UNISURV S-33, University of New South Wales, Sydney, Australia.

Holmes, S. A. and N. K. Pavlis. 2008. A Fortran program for very-high-degree harmonic synthesis. Technical report for harmonic_synth version 05/01/2006, National Geospatial-Intelligence Agency, http://earth-info.nga.mil/GandG/wgs84/gravitymod/egm2008/egm08_wgs84.html.

Hu, G. 2007. Data analysis of the 1995-2007 GPS data for height modernisation in Western Australia. Technical Report, Geoscience Australia, Canberra, Australia.

Hu, G. 2009. Analysis of Regional GPS campaigns and their alignment to the International Terrestrial Reference Frame (ITRF). *Journal of Spatial Science*, 54(1):15–22.

Hutchinson, M. F. 2001. *GEODATA 9 Second DEM (Version 2): Data Users Guide*. Geoscience Australia, Canberra, Australia.

Hwang, C. 1997. Height system of Taiwan from satellite and terrestrial data. *Journal of Surveying Engineering*, 123(4):162–180. doi:10.1061/(ASCE)0733-9453.

Hwang, C. and Y. S. Hsiao. 2003. Orthometric corrections from levelling, gravity,

density and elevation data: a case study in Taiwan. *Journal of Geodesy*, 77(5-6):279–291. doi:10.1007/s00190-003-0325-6.

Hwang, C., Y. S. Hsiao, H. C. Shih, M. Yang, K. H. Chen, R. Forsberg, and A. V. Olesan. 2007. Geodetic and geophysical results from a Taiwan airborne gravity survey: Data reduction and accuracy assessment. *Journal of Geophysical Research*, 112:B04407. doi:10.1029/2005JB004220.

ICSM. 2006. Geocentric Datum of Australia Technical Manual. Version 2.3, Inter-Governmental Committee on Surveying and Mapping, Canberra, Australia. http://www.icsm.gov.au/icsm/gda/gdatm/gdav2.3.pdf.

ICSM. 2007. Standards and practices for control surveys V1.7. Special Publication 1, Inter-Governmental Committee on Surveying and Mapping, Canberra, Australia. http://www.icsm.gov.au/icsm/publications/sp1/sp1v1-7.pdf.

Ihde, J., W. Augath, and M. Sacher. 2002. The vertical reference system for Europe. In *Vertical Reference Systems*, eds. H. Drewes, A. H. Dodson, L. P. S. Fortes, L. Sánchez, and P. Sandoval, 345–350. Berlin, Germany: Springer.

Ihde, J. and L. Sánchez. 2005. A unified global height reference system as a basis for IGGOS. *Journal of Geodynamics*, 40(4-5):400–413. doi:10.1016/j.jog.2005.06.015.

Iliffe, J., M. Ziebart, P. Cross, R. Forsberg, G. Strykowski, and C. Tscherning. 2003. OGSM02: a new model for converting GPS-derived heights to local height datums in Great Britain and Ireland. *Survey Review*, 37(290):276–293.

International Association of Geodesy. 1971. Geodetic Reference System 1967. Special Publication 3, Bulletin Géodésique, Paris, France.

IOC. 2006. Manual on sea level measurement and interpretation, Volume IV: An update to 2006. Manuals and Guides No. 14, Intergovernmental Oceanographic Commission, Paris, France.

Jekeli, C. 2000. Heights, the Geopotential and Vertical Datums. Report 459, The Ohio State University, Columbus, USA.

Jiang, Z. and H. Duquenne. 1996. On the combined adjustment of a gravimetrically determined geoid and GPS levelling stations. *Journal of Geodesy*,

70(8):505–514. doi:10.1007/s001900050039.

Johannessen, J. A., G. Balmino, C. Le Provost, R. Rummel, R. Sabadini, H. Sünkel, C. C. Tscherning, P. Visser, P. Woodworth, C. W. Hughes, P. Legrand, N. Sneeuw, F. Perosanz, M. Aguirre-Martinez, H. Rebhan, and M. Drinkwater. 2003. The European gravity field and steady-state ocean circulation explorer satellite mission: its impact on geophysics. *Surveys in Geophysics*, 24(4):339–386. doi:10.1023/B:GEOP.0000004264.04667.5e.

Johnson, D. 2009. *The Geology of Australia*. 2nd ed. Cambridge, UK: Cambridge University Press.

Johnston, G., B. Twilley, and S. Yates. 2002. Total station levelling. In *Proceedings of the 26th National Surveying Conference of the Institution of Engineering and Surveying*, 4–8. Darwin, Australia.

Kao, S. P., R. Hsu, and F. S. Ning. 2000. Results of field test for computing orthometric correction based on measured gravity. *Geomatics Research Australasia*, 72:43–60.

Kearsley, A. H. W. 1986. Data requirements for determining precise relative geoid heights from gravimetry. *Journal of Geophysical Research*, 91(B9):9193–9201. doi:10.1029/JB091iB09p09193.

Kearsley, A. H. W. 1988. The determination of the geoid ellipsoid separation for GPS levelling. *The Australian Surveyor*, 34(1):11–18.

Kearsley, A. H. W. and Z. Ahmad. 1993. Algorithms for geodetic corrections for the tide gauge monitoring project. Report for the Australian Surveying and Land Information Group, University of New South Wales, Sydney, Australia.

Kearsley, A. H. W., Z. Ahmad, and A. Chan. 1993a. National height datums, levelling, GPS heights and geoids. *Australian Journal of Geodesy, Photogrammetry and Surveying*, 59:53–88.

Kearsley, A. H. W., Z. Ahmad, and G. Luton. 1993b. Error sources in tide gauge monitoring surveys. Report for the Australian Surveying and Land Information Group, University of New South Wales, Sydney, Australia.

Kearsley, A. H. W., G. J. Rush, and P. W. O'Donnell. 1988. The Australian Height Datum - problems and proposals. *The Australian Surveyor*, 34(4):363–380.

Kerr, R. A. 1981. Palmdale bulge doubts now taken seriously. *Science*, 214(4527):1331–1333.

Kharaghani, G. A. 1987. Propagation of refraction errors in trigonometric height traversing and geodetic levelling. Technical Report 132, University of New Brunswick, Fredricton, Canada.

Kingdon, R., P. Vaníček, M. Santos, A. Ellman, and R. Tenzer. 2005. Toward an improved orthometric height system for Canada. *Geomatica*, 59(3):241–249.

Kirby, J. F. and W. E. Featherstone. 1999. Terrain correcting Australian gravity observations using the national digital elevation model and the fast Fourier transform. *Australian Journal of Earth Sciences*, 46(4):555–562. doi:10.1046/j.1440-0952.1999.00731.x.

Knight, N. L., J. Wang, and C. Rizos. 2010. Generalised measures of reliability for multiple outliers. *Journal of Geodesy*, 84(10):625–635. doi:10.1007/s00190-010-0392-4.

Koch, K. R. 1988. *Parameter Estimation and Hypothesis Testing in Linear Models*. Berlin, Germany: Springer.

Kotsakis, C., G. Fotopoulos, and M. G. Sideris. 2002. A study on the effects of data accuracy and datum inconsistencies on relative GPS levelling. In *Vertical Reference Systems*, eds. P. Drewes, A. Dodson, L. Fortes, L. Sánchez, and P. Sandoval, 113–118. Berlin, Germany: Springer.

Kotsakis, C. and M. G. Sideris. 1999. On the adjustment of combined GPS/levelling/geoid networks. *Journal of Geodesy*, 73(8):412–421. doi:10.1007/s001900050261.

Kuhn, M., W. E. Featherstone, and J. F. Kirby. 2009. Complete spherical Bouguer gravity anomalies over Australia. *Australian Journal of Earth Sciences*, 56(2):213–223. doi:10.1080/08120090802547041.

Kukkamäki, T. J. 1938. Über die nivellitische Refraktion (On the refraction in levelling). Technical Report 25, Finnish Geodetic Institute, Helsinki, Finland.

Kukkamäki, T. J. 1939. Formeln und Tabellen zur Berechnurg der nivellitischen Refraktion (Formulae and tables for the computation of refraction in levelling). Technical Report 27, Finnish Geodetic Institute, Helsinki, Finland.

Kung, E. C., R. A. Bryson, and D. H. Lenschow. 1964. Study of a continental albedo on the basis of flight measurements and structure of the Earth's surface cover over North America. *Monthly Weather Review*, 92(12):543–564.

Lachapelle, G. and R. Gareau. 1980. Status of geodetic vertical networks in Canada. In *Second International Symposium on Problems Related to the Redefinition of the North American Vertical Geodetic Networks: NAD Symposium 1980*, ed. G. Lachapelle, 49–71. Ottawa, Canada: Canadian Institute of Surveying.

Lambert, B. P. and K. Leppert. 1975. A study of the Australian national levelling survey. In *Commonwealth Survey Officers Conference*. Cambridge, UK. Paper No. C5.

Lemoine, F. G., S. C. Kenyon, J. K. Factor, R. G. Trimmer, N. K. Pavlis, D. S. Chinn, C. M. Cox, S. M. Klosko, S. B. Luthcke, M. H. Torrence, Y. M. Wang, R. G. Williamson, E. C. Pavlis, R. H. Rapp, and T. R. Olson. 1998. The development of the joint NASA GSFC and the National Imagery and Mapping Agency (NIMA) geopotential model EGM96. Technical Report NASA/TP-1998-206861, National Aeronautics and Space Administration, Maryland, USA.

Leppert, K., B. V. Hamon, and R. S. Mather. 1975. A status report on investigations of sea surface slope along the eastern coast of Australia. In *UNISURV G23*, 60–67. Sydney, Australia: University of New South Wales.

Lines, J. D. 1992. *Australia on Paper: the Story of Australian Mapping*. Box Hill, Australia: Fortune Publications.

Lucht, H. 1971. Correlation in levellings of high precision. In *XV General Assembly of the International Union of Geodesy and Geophysics - International*

Assosciation of Geodesy. Moscow, USSR.

Luton, G. 2000. Report on processing and analysis of the 1999/2000 AHD tide-gauge GPS survey data set - preliminary results at August 2000. Report, Geoscience Australia, Canberra, Australia.

Luz, R. T., L. P. S. Fortes, M. Hoyer, and H. Drewes. 2002a. The vertical reference frame for the Americas - The SIRGAS 2000 GPS campaign. In *Vertical Reference Systems*, eds. H. Drewes, A. H. Dodson, L. P. S. Fortes, L. Sánchez, and P. Sandoval, 302–305. Berlin, Germany: Springer.

Luz, R. T., V. M. Guimarães, A. C. Rodrigues, and J. D. Correia. 2002b. Brazilian first order levelling network. In *Vertical Reference Systems*, eds. H. Drewes, A. H. Dodson, L. P. S. Fortes, L. Sánchez, and P. Sandoval, 20–22. Berlin, Germany: Springer.

Lyons, L. 1991. *Data Analysis for Physical Science Students*. 1st ed. Cambridge, UK: Cambridge University Press.

Macleod, R. T., A. H. W. Kearsley, and C. Rizos. 1988. GPS surveys of mean sea-level along the New South Wales coastline. *Australian Journal of Geodesy, Photogrammetry and Surveying*, 49:39–53.

Mader, K. 1954. Die orthometrische Schwerekorrektion des Präzisions Nivellements in den Hohen Tauern (The orthometric gravity correction of the precise levelling in the Hohen Tauern). *Österreichische Zeitschrift für Vermessungswesen*, Sonderheft 15.

Madsen, K. S., J. L. Høyer, and C. C. Tscherning. 2007. Near-coastal satellite altimetry: Sea surface height variability in the North Sea-Baltic Sea area. *Geophysical Research Letters*, 34:L14601. doi:10.1029/2007GL029965.

Mark, R. K., T. D. Gilmore, and R. O. Castle. 1987. Evidence of suppression of the unequal refraction error in geodetic levelling. *Journal of Geophysical Research*, 92(B3):2767–2790. doi:10.1029/JB092iB03p02767.

Marti, U. and A. Schlatter. 2002. The new height system in Switzerland. In *Vertical Reference Systems*, eds. H. Drewes, A. H. Dodson, L. P. S. Fortes, L. Sánchez, and P. Sandoval, 50–55. Berlin, Germany: Springer.

Mather, R. S. 1974. On the solution of the geodetic boundary value problem for the definition of sea surface topography. *Geophysical Journal of the Royal Astronomical Society*, 39(1):87–109. doi:10.1111/j.1365-246X.1974.tb05441.x.

Mather, R. S. 1975. On the evaluation of sea surface topography using geodetic techniques. *Bulletin Géodésique*, 115(1):65–82. doi:10.1007/BF02523944.

Mather, R. S. 1979. The analysis of Geos 3 altimeter data in the Tasman and Coral Seas. *Journal of Geophysical Research*, 84(B8):3853–3866. doi:10.1029/JB084iB08p03853.

Mather, R. S., C. Rizos, and R. Coleman. 1979. Remote sensing of surface ocean circulation with satellite altimetry. *Science*, 205(4401):11–17. doi:10.1126/science.205.4401.11.

Mather, R. S., C. Rizos, B. Hirsch, and B. C. Barlow. 1976. An Australian gravity data bank for sea surface topography determinations (AUSGAD 76). In *UNISURV G25*, 54–84. Sydney, Australia: University of New South Wales.

Melchior, P. 1978. *The Tides of the Planet Earth*. Oxford, UK: Pergamon.

Mellors, R. J. and A. Boisvert. 2003. Deformation near the Coyote Creek fault, Imperial County, California: tectonic or groundwater-related? *Geochemistry, Geophysics, Geosystems*, 4(2):1012. doi:10.1029/2001GC000254.

Merry, C. L. 2003. The African geoid project and its relevance to the unification of African vertical reference frames. In *Proceedings of the 2nd. FIG Regional Conference, Marrekech, Morocco*. Online: accessed 18 November 2010, www.fig.net/pub/morocco/proceedings/TS9/TS9_3_merry.pdf.

Merry, C. L. and P. Vaníček. 1983. Investigation of local variations of sea-surface topography. *Marine Geodesy*, 7(1-4):101–126. doi:10.1080/15210608309379477.

Milbert, D. G. 1988. Treatment of geodetic levelling in the integrated geodesy approach. Report 396, The Ohio State University, Columbus, USA.

Milbert, D. G. 1995. Improvement of a high resolution geoid height model in the United States by GPS height on NAVD 88 benchmarks. New geoids in the world, *IGes Bulletin* 4:13-36.

Mitchell, H. L. 1973a. An Australian geopotential network based on observed gravity. In *UNISURV G18*, 32–50. Sydney, Australia: University of New South Wales.

Mitchell, H. L. 1973b. Relations between mean sea level and geodetic levelling in Australia. UNISURV S-9, University of New South Wales, Sydney, Australia.

Mitchell, H. L. 1973c. Sea-surface topography in geodesy with particular reference to Australia. In *Proceedings of the Symposium on the Earth's Gravitational Field & Secular Variations in Position*, eds. R. S. Mather and P. V. Angus-Leppan, 573– 584. Sydney, Australia: University of New South Wales.

Mitchell, H. L. 1988. GPS heighting in Australia: an introduction. *The Australian Surveyor*, 34(1):5–10.

Mitchell, H. L. 1990. GPS heighting and the AHD. Technical Report, GPS heighting study group.

Mohr, P. J. and B. N. Taylor. 2005. CODATA recommended values of the fundamental physical constants: 2002. *Reviews of Modern Physics*, 77(1):1–107. doi:10.1103/RevModPhys.77.1.

Molodensky, M., V. Yeremeyev, and M. Yurkina. 1962. *Methods for Study of the External Gravitational field and Figure of the Earth*. Jerusalem: Israeli Program for Scientific Translations.

Morgan, P. 1992. An analysis of the Australian Height Datum: 1971. *The Australian Surveyor*, 37(1):46–63.

Moritz, H. 1980. Geodetic reference system 1980. *Bulletin Géodésique*, 54(3):395–405. doi:10.1007/BF02521480.

Mozzuchin, O. A. 1977. Die nivellitische Refraktion und die Methoden ihrer Berücksichtigung (Refraction in levelling and their treatment). *Vermessungstechnik*, 25(10):335–338.

Murray, A. S. 1997. The Australian National Gravity Database. *AGSO Journal of Australian Geology and Geophysics*, 17(1):145–155.

Nerem, R. S., F. J. Lerch, J. A. Marshall, E. C. Pavlis, B. H. Putney, B. D. Tapley, R. J. Eanes, J. C. Ries, B. E. Schutz, C. K. Shum, M. M. Watkins,

S. M. Klosko, J. C. Chan, S. B. Luthcke, G. B. Patel, N. K. Pavlis, R. G. Williamson, R. H. Rapp, R. Biancale, and F. Nouel. 1994. Gravity model development for TOPEX/POSEIDON: Joint Gravity Models 1 and 2. *Journal of Geophysical Research*, 99(C12):24,421–24,447. doi:10.1029/94JC01376.

NGS. 2007. The GRAV-D project: gravity for the redefinition of the American vertical datum. Report, National Geodetic Survey, http://www.ngs.noaa.gov/GRAV-D/pubs/GRAV-D_v2007_12_19.pdf.

Niethammer, T. 1932. *Nivellement und Schwere als Mittel zur Berechnung wahrer Meereshöhen (Levelling and gravity as a means to derive true heights above mean sea level)*. Schweizerische Geodätische Kommission, Bern, Switzerland.

NMC. 1966. Standard specifications and recommended practices for horizontal and vertical control surveys. Special Publication 1, 1st ed., National Mapping Council, Canberra, Australia.

NMC. 1979. The Australian Height Datum (AHD). Special Publication 8, National Mapping Council, Canberra, Australia.

NMC. 1981. Standard specifications and recommended practices for horizontal and vertical control surveys. Special Publication 1, 3rd ed., National Mapping Council, Canberra, Australia.

NOAA, NASA, and USAF. 1976. U.S. Standard Atmosphere, 1976. Technical report, National Oceanic and Atmospheric Administration, National Aeronautics and Space Administration and United States Air Force, Washington, USA.

Obukhov, A. M. 1971. Turbulence in an atmosphere with a non-uniform temperature. *Boundary-Layer Meteorology*, 2(1):7–29. doi:10.1007/BF00718085.

Panet, I., V. Mikhailov, M. Diament, F. Pollitz, G. King, O. De Viron, M. Holschneider, R. Biancale, and J.-M. Lemoine. 2007. Coseismic and post-seismic signatures of the Sumatra 2004 December and 2005 March earthquakes in GRACE satellite gravity. *Geophysical Journal International*, 171(1):177–190. doi:10.1111/j.1365-246X.2007.03525.x.

Papp, G., E. Szeghy, and J. Benedek. 2009. The determination of potential differ-

ence by the joint application of measured and synthetical gravity data: a case study in Hungary. *Journal of Geodesy*, 83(6):509–521. doi:10.1007/s00190-008-0257-2.

Pavlis, N. K., S. A. Holmes, S. C. Kenyon, and J. K. Factor. 2008. An Earth gravitational model to degree 2160: EGM2008. Presented at EGU-2008, Vienna, Austria, April 13-18. http://earth-info.nga.mil/GandG/wgs84/gravitymod/egm2008/egm08_wgs84.html.

Pelzer, H. 1982. Error propagation in levelling. In *International Symposium on Geodetic Networks and Computations*, 258. München: IAG, DGK, Reihe B.

Pope, A. J. 1976. The statistics of residuals and the detection of outliers. Technical Report NOS 65 NGS 1, National Oceanic and Atmospheric Atmospheric, Rockville, USA.

Poutanen, M. 1999. Use of GPS in unification of vertical datums and detection of levelling network errors. In *Geodesy and surveying in the future - The Importance of Heights*, ed. M. Lilje, 301–312. Gävle, Sweden.

Priestley, C. H. B. 1959. *Turbulent transfer in the lower atmosphere*. Chicago, USA: University of Chicago Press.

Prószyñski, W. 2000. On outlier-hiding effects in specific Gauss-Markov models: geodetic examples. *Journal of Geodesy*, 74(7-8):581–589. doi:10.1007/s001900000121.

PSMSL. 2003. The Permanent Service for Mean Sea Level: further information. Online [accessed 5 August 2008], http://www.pol.ac.uk/psmsl/datainfo/psmsl.hel.

Pugh, D. 1987. *Tides, Surges and Mean Sea-level*. Chichester, UK: John Wiley.

Ramsayer, K. 1959. Report about gravity reduction of the levelling network in Baden-Württemberg (summary). *Bulletin Géodésique*, 52(1):76–79. doi:10.1007/BF02526868.

Rangelova, E., M. G. Sideris, and G. Fotopoulos. 2009. A dynamic reference surface for heights in Canada. *Geomatica*, 63(4):333–340.

Rao, C. R. 1971. Estimation of variance and covariance components - MINQUE theory. *Journal of Multivariate Analysis*, 1(3):257–275. doi:10.1016/0047-259X(71)90001-7.

Rapp, R. H. 1961. *The orthometric height*. Master's thesis, The Ohio State University, Columbus, USA.

Rapp, R. H. 1989. The treatment of permanent tidal effects in the analysis of satellite altimeter data for sea surface topography. *manuscripta geodaetica*, 14(6):368–372.

Rapp, R. H. 1994. Separation between reference surfaces of selected vertical datums. *Bulletin Géodésique*, 69(1):26–31. doi:10.1007/BF00807989.

Rapp, R. H. 1997. Use of potential coefficient models for geoid undulation determinations using a spherical harmonic representation of the height anomaly/geoid undulation difference. *Journal of Geodesy*, 71(5):282–289. doi:10.1007/s001900050096.

Rapp, R. H. and N. Balasubramania. 1992. A conceptual formulation of a world height system. Report 427, The Ohio State University, Columbus, USA.

Rapp, R. H. and N. K. Pavlis. 1990. The development and analysis of geopotential coefficient models to spherical harmonic degree 360. *Journal of Geophysical Research*, 95(B13):21885–21911. doi:10.1029/JB095iB13p21885.

Rapp, R. H., Y. M. Wang, and N. K. Pavlis. 1991. The Ohio State 1991 geopotential and sea surface topography harmonic coefficient models. Report 410, The Ohio State University, Columbus, USA.

Rappleye, H. S. 1948. Manual of geodetic levelling. Special Publication 239, Coast and Geodetic Survey, Washington, USA.

Reigber, C., H. Jochmann, J. Wünsch, S. Petrovic, P. Schwintzer, F. Barthelmes, K.-H. Neumayer, R. König, C. Förste, G. Balmino, R. Biancale, J. M. Lemoine, S. Loyer, and F. Perosanz. 2004. Earth gravity field and seasonal variability from CHAMP. In *Earth Observation with CHAMP - Results From Three Years in Orbit*, eds. C. Reigber, H. Lühr, P. Schwintzer, and J. Wickert, 25–30. Berlin, Germany: Springer.

Reigber, C., P. Schwintzer, K.-H. Neumayer, F. Barthelmes, R. König, C. Förste, G. Balmino, R. Biancale, J. M. Lemoine, S. Loyer, S. Bruinsma, F. Perosanz, and T. Fayard. 2003. The CHAMP-only Earth gravity field model EIGEN-2. *Advances in Space Research*, 31(8):1883–1888. doi:10.1016/S0273-117(03)00162-5.

Reilly, W. I. 1972. New Zealand gravity map series. *New Zealand Journal of Geology and Geophysics*, 15(1):3–15.

Reissman, G. 1954. Untersuchungen zur ausschaktung des einflusses der vertikalrefraktion beim präzisionsnivellement. *Vermessung*, 5(2).

Remmer, O. 1980. An analysis of the second precise levelling of Finland and the proper use of Kukkamäki's correction. In *Second International Symposium on Problems Related to the Redefinition of the North American Vertical Geodetic Networks: NAD Symposium 1980*, ed. G. Lachapelle, 623–646. Ottawa, Canada: Canadian Institute of Surveying.

Remmer, O. 1994. Refraction studies in the North American levelling datum. *Bulletin Géodésique*, 69(1):21–25. doi:10.1007/BF00807988.

Ridgway, K. R. and J. R. Dunn. 2003. Mesoscale structure of the mean East Australian Current System and its relationship with topography. *Progress in Oceanography*, 56:189–222. doi:1016/S0079-6611(03)00004-1.

Ridgway, K. R., J. R. Dunn, and J. L. Wilkin. 2002. Ocean interpolation by four-dimensional weighted least squares-application to the waters around Australasia. *Journal of Atmospheric and Oceanic Technology*, 19(9):1357–1375.

Rio, M. H. and F. Hernandez. 2004. A mean dynamic topography computed over the world ocean from altimetry, in situ measurements, and a geoid model. *Journal of Geophysical Research*, 109:C12032. doi:10.1029/2003JC002226.

Rizos, C., R. Coleman, and N. Ananga. 1991. The Bass Strait GPS survey: preliminary results of an experiment to connect Australian Height Datums. *Australian Journal of Geodesy, Photogrammetry and Surveying*, 55:1–25.

Robertson, A. 2003. First order total station levelling. Honours thesis, Curtin University of Technology, Perth, Australia.

Robertson, A. and A. Snow. 2005. First order total station levelling - is it possible? In *Proceedings of SSC Spatial Intelligence, Innovation and Praxis: The National Biennial Conference of the Spatial Sciences Institute*. Melbourne, Australia: Spatial Sciences Institute. CD ROM.

Roelse, A., H. W. Granger, and J. W. Graham. 1971. The adjustment of the Australian levelling survey 1970-1971. Technical Report 12, Division of National Mapping, Canberra, Australia.

Roelse, A., H. W. Granger, and J. W. Graham. 1975. The adjustment of the Australian levelling survey 1970-1971, 2nd ed. Technical Report 12, Division of National Mapping, Canberra, Australia.

Rott, H. 2009. Advances in interferometric synthetic aperture radar (InSAR) in Earth system science. *Progress in Physical Geography*, 33(6):769–791. doi:10.1177/0309133309350263.

Rüeger, J. M. 1997. Staff errors in and the adjustment of ordinary levelling runs. *The Australian Surveyor*, 42(1):16–24.

Rüeger, J. M. 2003. Electronic surveying instruments: a review of principles, problems and procedures. Monograph 18, University of New South Wales, Sydney, Australia.

Rummel, R. and P. Teunissen. 1988. Height datum definition, height datum connection and the role of the geodetic boundary value problem. *Bulletin Géodésique*, 62(4):477–498. doi:10.1007/BF02520239.

Sánchez, L. 2002. A reference surface for the unified height system in the northern part of South America. In *Vistas for Geodesy in the New Millenium*, eds. J. Ádám and K.-P. Schwarz, 84–89. Berlin, Germany: Springer.

Sansò, F. and P. Vaníček. 2006. The orthometric height and the holonomity problem. *Journal of Geodesy*, 80(5):225–232. doi:10.1007/s00190-005-0015-7.

Santos, M. C., P. Vaníček, W. E. Featherstone, R. Kingdon, B. A. Ellmann, A. Martin, M. Kuhn, and R. Tenzer. 2006. The relation between rigorous and Helmert's definitions of orthometric heights. *Journal of Geodesy*, 80(12):691–704. doi:10.1007/s00190-006-0086-0.

Schlemmer, H. 1985. Advanced technology for a new precise levelling rod. In *Third International Symposium on the North American Vertical Datum - NAVD Symposium '85*, 471–476. Rockville, USA: National Oceanic and Atmospheric Administration.

Schomaker, M. C. and R. M. Berry. 1981. Geodetic levelling. National Oceanic and Atmospheric Administration Manual NOS NGS 3, National Geodetic Survey, Rockville, USA.

Schwarz, C. R. and J. J. Kok. 1993. Blunder detection and data snooping in LS and robust adjustments. *Journal of Surveying Engineering*, 119(4):127–136. doi:10.1061/(ASCE)0733-9453.

Seeber, G. 2003. *Satellite Geodesy*. 2nd ed. Berlin, Germany: Walter de Gruyter.

Serpas, J. G. and C. Jekeli. 2005. Local geoid determination from airborne vector gravimetry. *Journal of Geodesy*, 78:577–587. doi:10.1007/s00190-004-0416-z.

Ses, S. and A. Mohamed. 2009. The second precise levelling network of peninsular Malaysia. *Survey Review*, 41(314):384–394. doi:10.1179/003962609X451627.

Shaw, A. G. P. and M. N. Tsimplis. 2010. The 18.6 yr nodal modulation in the tides of Southern European coasts. *Continental Shelf Research*, 30(2):138–151. doi:10.1016/j.csr.2009.10.006.

Shaw, R. H. and P. J. Smietana. 1983. Temperature stratification and refraction errors in geodetic leveling. *Journal of Geophysical Research*, 88(B12):10485–10494. doi:10.1029/JB088iB12p10485.

Sjöberg, L. E. 1995. On the quasigeoid to geoid separation. *manuscripta geodaetica*, 20(3):182–192.

Sjöberg, L. E. 2006. A refined conversion from normal to orthometric height. *Studia Geophysica et Geodetica*, 50(4):595–606. doi:10.1007/s11200-006-0037-5.

Sjöberg, L. E. 2010. A strict formula for geoid-to quasigeoid separation. *Journal of Geodesy*, 84(11):699–702. doi:10.1007/s00190-010-0407-1.

Skeivalas, J. 2005. Determination of the refraction influence in precision levelling. *Optical Engineering*, 44(1):013603. doi:10.1117/1.1827224.

Smith, D. A. and K. Edwards. 2010. Taking the "Boulder" step from static to dynamic geoid. *Eos*, 91(5):46.

Smith, D. A. and D. G. Milbert. 1999. The GEOID96 high-resolution geoid height model for the United States. *Journal of Geodesy*, 73(5):219–236. doi:10.1007/s001900050239.

Smith, D. A. and D. R. Roman. 2001. GEOID99 and G99SSS: 1-arc-minute geoid models for the United States. *Journal of Geodesy*, 75(9-10):469–490. doi:10.1007/s001900100200.

Smith, W. H. F. and P. Wessel. 1990. Gridding with continuous curvature splines in tension. *Geophysics*, 55(3):293–305. doi:10.1190/1.1442837.

Sproule, D. M., W. E. Featherstone, and J. F. Kirby. 2006. Localised gross-error detection in the Australian land gravity database. *Exploration Geophysics*, 37(2):175–179. doi:10.1071/EG06175.

Steed, J. 2006. Height Modernisation - Data Cleaning and Adjustment (unpublished). Report for Geoscience Australia, Canberra, Australia.

Stein, R. S., C. T. Whalen, S. R. Holdahl, W. E. Strange, and W. Thatcher. 1986. Saugus-Palmdale, California, field test for refraction error in historical leveling surveys. *Journal of Geophysical Research*, 91(B9):9031–9044. doi:10.1029/JB091iB09p09031.

Stein, R. S., C. T. Whalen, S. R. Holdahl, W. E. Strange, and W. Thatcher. 1989. Reply to "Comment on 'Saugus-Palmdale, California, field test for refraction error in historical leveling surveys' by R.S. Stein, C.T. Whalen, S.R. Holdahl, W. Strange, and W. Thatcher" by Michael R. Craymer and Peter Vaníček and Comment on "Further analysis of the 1981 Southern California field test for leveling refraction" by M.R. Cramer and P. Vaníček. *Journal of Geophysical Research*, 94(B6):7673–7677. doi:10.1029/JB094iB06p07673.

Stewart, M. P. 1998. How accurate is the Australian National GPS Network as a framework for GPS heighting. *The Australian Surveyor*, 43(1):53–61.

Stewart, M. P., X. L. Ding, M. Tsakiri, and W. E. Featherstone. 1997. The 1996 STATEFIX project. Report for the Department of Land Administration,

Curtin University of Technology, Perth, Australia.

Strang van Hees, G. L. 1992. Practical formulas for the computation of the orthometric, dynamic and normal heights. *Zeitschrift für Vermessungswesen*, 117(11):727–734.

Strange, W. E. 1981. The impact of refraction corrections on levelling interpretations in Southern California. *Journal of Geophysical Research*, 86(B4):2809–2824. doi:10.1029/JB086iB04p02809.

Strange, W. E. 1982. An evaluation of orthometric height accuracy using bore hole gravimetry. *Bulletin Géodésique*, 56(4):300–311. doi:10.1007/BF02525730.

Strange, W. E. 1983. Reply. *Journal of Geophysical Research*, 88(B3):2513–2519. doi:10.1029/JB088iB03p02513.

Strange, W. E. 1985. Empirical determination of magnetic corrections for Ni 1 level. In *Third International Symposium on the North American Vertical Datum - NAVD Symposium '85*, 363–374. Rockville, USA: National Oceanic and Atmospheric Administration.

Sturges, W. 1967. Sea slope along the Pacific Coast of the United States. *Journal of Geophysical Research*, 72(14):3627–3637. doi:10.1029/JZ072i014p03627.

Sturges, W. 1974. Sea level slope along continental boundaries. *Journal of Geophysical Research*, 79(6):825–830. doi:10.1029/JC079i006p00825.

Sünkel, H. 1983. The geoid in Austria. In *Proceedings of the International Association of Geodesy (IAG) Symposia, XVIII General Assembly, Hamburg, Federal Republic of Germany*, eds. E. Groten and R. H. Rapp, 348–364.

Tapley, B. and D. Kim. 2001. Applications to Geodesy. In *Satellite Altimetry and Earth Sciences: A Handbook of Techniques and Applications*, eds. L.-L. Fu and A. Cazenave, 371–406. San Diego, USA: Academic Press.

Tapley, B., J. Ries, S. Bettadpur, D. Chambers, M. Cheng, F. Condi, B. Gunter, Z. Kang, P. Nagel, R. Pastor, T. Pekker, S. Poole, and F. Wang. 2005. GGM02 - An improved Earth gravity field model from GRACE. *Journal of Geodesy*, 79(8):467–478. doi:10.1007/s00190-005-0480-z.

Tapley, B. D., S. Bettadpur, J. C. Ries, P. F. Thompson, and M. M. Watkins. 2004a. GRACE measurements of mass variability in the Earth system. *Science*, 305(5683):503–505. doi:10.1126/science.1099192.

Tapley, B. D., S. Bettadpur, M. Watkins, and C. Reigber. 2004b. The gravity recovery and climate experiment: Mission overview and early results. *Geophysical Research Letters*, 31:L09607. doi:10.1029/2004GL019920.

Tapley, B. D., D. P. Chambers, S. Bettadpur, and J. C. Ries. 2003. Large scale ocean circulation from the GRACE GGM01 geoid. *Geophysical Research Letters*, 30(22):2163–2166. doi:10.1029/2003GL018622.

Tenzer, R., P. Novak, P. Moore, M. Kuhn, and P. Vaníček. 2006. Explicit formula for the geoid-quasigeoid separation. *Studia Geophysica et Geodaetica*, 50(4):607–618. doi:10.1007/s11200-006-0038-4.

Tenzer, R., P. Vaníček, M. Santos, W. E. Featherstone, and M. Kuhn. 2005. Rigorous determination of the orthometric height. *Journal of Geodesy*, 79(1-3):82–92. doi:10.1007/s00190-005-0445-2.

Teunissen, P. J. G. 2006a. *Adjustment theory*. 1st ed. Delft, The Netherlands: Vereniging voor Studie - en Studentbelangen te Delft.

Teunissen, P. J. G. 2006b. *Network quality control*. 1st ed. Delft, The Netherlands: Vereniging voor Studie - en Studentbelangen te Delft.

Teunissen, P. J. G. 2006c. *Testing theory*. 2nd ed. Delft, The Netherlands: Vereniging voor Studie - en Studentbelangen te Delft.

Thomas, C. M. and W. E. Featherstone. 2005. Validation of Vincenty's formulas for the geodesic using a new fourth-order extension of Kivioja's formula. *Journal of Surveying Engineering*, 131(1):20–26. doi:10.1061/(ASCE)0733-9453.

Thwait, E. 1966. *Accuracy of staff calibration to meet National Mapping Council requirements*. National Standards Laboratory, Commonwealth Organisation.

Torge, W. 1989. *Gravimetry*. Berlin, Germany: Walter de Gruyter.

Torge, W. 2001. *Geodesy*. 3rd ed. Berlin, Germany: Walter de Gruyter.

Tracey, R., M. Bacchin, and P. Wynne. 2007. AAGD07: A new absolute gravity datum for Australian gravity and new standards for the Australian National

Gravity Database. *ASEG Extended Abstracts, 19th Geophysical Conference*, 2007(1):241–244. doi:10.1071/ASEG2007ab149.

Tregoning, P., K. Lambeck, and G. Ramillien. 2008. GRACE estimates of sea surface height anomalies in the Gulf of Carpentaria, Australia. *Earth and Planetary Science Letters*, 271(1-4):241–244. doi:10.1016/j.epsl.2008.04.018.

Vaníček, P. 1978. To the problem of noise reduction in sea-level records used in vertical crustal movement detection. *Physics of the Earth and Planetary Interiors*, 17(3):265–280. doi:10.1016/0031-9201(78)90041-9.

Vaníček, P. 1988. The height of reason. *GPS World*, 9(4):14.

Vaníček, P. 1991. Vertical datum and NAVD 88. *Surveying and Land Information Systems*, 51(2):83–86.

Vaníček, P., G. H. Carrera, and M. R. Craymer. 1985. Corrections for systematic errors in the Canadian levelling network. Contract Report 85-001, Geodetic Survey of Canada.

Vaníček, P., R. O. Castle, and E. I. Balazs. 1980. Geodetic leveling and its applications. *Reviews of Geophysics and Space Physics*, 18(2):505–524. doi:10.1029/RG018i002p00505.

Vaníček, P. and E. J. Krakiwsky. 1982. *Geodesy : the Concepts*. 1st ed. Amsterdam, The Netherlands: North-Holland.

Vaníček, P., R. Tenzer, L. E. Sjöberg, Z. Martinec, and W. E. Featherstone. 2004. New views of the spherical Bouguer gravity anomaly. *Geophysical Journal International*, 159(2):460–472. doi:10.1111/j.1365-246X.2004.02435.x.

Vermeer, M. 1998. The geoid as a product. Report 98(4):63-69, Finnish Geodetic Institute, Helsinki, Finland.

Véronneau, M., R. Duval, and J. Huang. 2006. A gravimetric geoid model as a vertical datum in Canada. *Geomatica*, 60(2):165–172.

Vincenty, T. 1975. Direct and inverse solutions of geodesics on the ellipsoid with application of nested equations. *Survey Review*, 22(176):88–93.

Volkov, D. L., G. Larnicol, and J. Dorandeu. 2007. Improving the quality of satellite altimetry data over continental shelves. *Journal of Geophysical Research*,

112:C06020. doi:10.1029/2006JC003765.

Vossepoel, F. C. 2007. Uncertainties in the mean ocean dynamic topography before the launch of the Gravity Field and Steady-State Ocean Circulation Explorer (GOCE). *Journal of Geophysical Research*, 112:C05010. doi:10.1029/2006JC003891.

Webb, E. K. 1965. Aerial Microclimate. *Meterological Monographs*, 6(28):27–58.

Webb, E. K. 1968. The temperature structure of the lower atmosphere. In *Conference on Refraction Effects in Geodesy, 5-8 Nov. 1968*, ed. P. V. Angus-Leppan, 1–9. Sydney, Australia: University of New South Wales.

Weibull, W. 1951. A statistical distribution function of wide applicability. *Journal of Applied Mechanical Transactions*, 18(3):293–297.

Wellman, P. and R. Tracey. 1987. Southwest seismic zone of Western Australia: measurement of vertical ground movements by repeat levelling and gravity measurements. *BMR Journal of Australian Geology and Geophysics*, 10:225–232.

Wessel, P. and W. H. F. Smith. 2007. *The Generic Mapping Tools, GMT, version 4.2.0*. http://www.soest.hawaii.edu/gmt/.

Whalen, C. T. 1980a. Refraction errors in levelling - NGS test results. In *Second International Symposium on Problems Related to the Redefinition of the North American Vertical Geodetic Networks: NAD Symposium 1980*, ed. G. Lachapelle, 757–782. Ottawa, Canada: Canadian Institute of Surveying.

Whalen, C. T. 1980b. Status of the national geodetic vertical control network in the United States. In *Second International Symposium on Problems Related to the Redefinition of the North American Vertical Geodetic Networks: NAD Symposium 1980*, ed. G. Lachapelle, 11–24. Ottawa, Canada: Canadian Institute of Surveying.

White, N. J., J. A. Church, and J. M. Gregory. 2005. Coastal and global averaged sea level rise for 1950 to 2000. *Geophysical Research Letters*, 32:L01601. doi:10.1029/2004GL021391.

Woodworth, P. L. and R. Player. 2003. The Permanent Service for Mean Sea Level: an update to the 21st century. *Journal of Coastal Research*, 19(2):287–295.

Wöppelmann, G., S. Zerbini, and M. Marcos. 2006. Tide gauges and geodesy: a secular synergy illustrated by three present-day case studies. *Comptes Rendus Geoscience*, 338(14-15):980–991. doi:10.1016/j.crte.2006.07.006.

Wynne, P. 2007. Australian National Gravity Data. Data description with 2007 release of Australian National Gravity Database.

Xu, P. 1992. A quality investigation of global vertical datum connection. *Geophysical Journal International*, 110(2):361–370. doi:10.1111/j.1365-246X.1992.tb00880.x.

Xu, P. and R. Rummel. 1991. A quality investigation of global vertical datum connection. New Series Report 34, Netherlands Geodetic Commission, Delft, The Netherlands.

Yang, M., K. H. Chen, and S. W. Shiao. 2003. A new height reference network in Taiwan. *Survey Review*, 37(290):260–268.

Zhang, K. F. and W. E. Featherstone. 2004. Investigation of the roughness of the Australian gravity field using statistical, graphical, fractal and Fourier power spectrum techniques. *Survey Review*, 37(293):520–530.

Zhang, L., F. Li, W. Chen, and C. Zhang. 2009. Height datum unification between Shenzhen and Hong Kong using the solution of the linearized fixed-gravimetric boundary value problem. *Journal of Geodesy*, 83(5):411–417. doi:10.1007/s00190-008-0234-9.

Ziebart, M. K., J. C. Iliffe, R. Forsberg, and G. Strykowski. 2008. Convergence of the UK OSGM05 GRACE-based geoid and the UK fundamental benchmark network. *Journal of Geophysical Research*, 113:B12401. doi:10.1029/2007JB004959.

Zilkoski, D. B., J. H. Richards, and G. M. Young. 1992. Results of the general adjustment of the North American Vertical Datum of 1988. *Surveying and Land Information Systems*, 52(3):133–149.